Investigating the Chemistry and Biomechanical Strength of Stalks for Understanding Lodging

A Dissertation
Presented in Partial Fulfillment of the Requirements for the
Degree of Doctor of Philosophy
with a
Major in Environmental Science
in the
College of Graduate Studies
University of Idaho
by
Endalkachew Mengistie

Approved by:
Major Professor: Armando McDonald, Ph.D.
Committee Members: Daniel Robertson, PhD., P.E.; Lili Cai, PhD.; and Andrew Nelson PhD.
Department Administrator: Charles Goebel, Ph.D.

December 2022

Abstract

Sorghum is an important crop mainly grown for food, animal feed, bioenergy, and fiber requirements. The production of a higher yield is compromised by its stalk lodging. Stalk lodging, the permanent displacement and mechanical failure of stems from their natural position prior to harvesting, poses a serious agronomic challenge leading to substantial yield losses annually. Despite its enormous economic impact on commercial crops, stalk lodging mechanisms are not clearly understood. Previous studies used methods such as bending tests, histochemical methods, rind penetrometer, and crushing strength measurements to understand stem biomechanical behavior. However, these approaches are inadequate to fully understand lodging, as the structural composition of the stalks was not considered. Approaches involving compositional analysis together with biomechanical behavior will improve our understanding of lodging mechanisms. This study evaluated stem biomechanical, compositional, and microstructural traits to assess their relationship with mechanical strength and/or loading. The whole biomass composition of Della (D) and its mutant *REDforGREEN* (RG) sweet sorghum stalks grown in 2018 (D1, RG1) and 2019 (D2, RG2) were examined employing different analytical instruments. Noticeable changes in the composition of fatty acids, structural carbohydrates (glucan, and xylan), and lignin content and structure were found, attributable to growing season and mutation factors. The results revealed that D2 had the highest lignin content, while RG1 had the lowest lignin content. Particularly in RG1, Klason lignin reduction by 16-44 % at the internode was detected. Lignin from the sorghum stalks were enriched in guaiacyl units and syringyl/guaiacyl ratio was increased in RG1 and RG2 respectively by 96% and more than two-fold at IN. In addition, the chemical composition, biomechanical properties of rinds, and the microfibril angle (MFA) of the S2 cell wall were determined. The flexural modulus (FM) and flexural strength (FS) showed a significant reduction for RG. Particularly, a reduction of FS by (16-37%) and FM (22-41%) were detected for RG1. Changes in the stalk rind biomechanical properties were found positively correlated with total lignin and glucan/cellulose contents, and inversely proportional to MFA. However, the contents of xylan/hemicellulose in the rinds were not significant for the strength. The result suggested that the lodging resistance of sorghum stalk would be improved by increasing the amount of cellulose and lignin. The results can also provide biotechnological targets in breeding programs aimed at improving lodging resistance in sorghum.

Acknowledgments

First and foremost, I would like to praise and thank God, the Almighty, who has given me the strength and encouragement to pass through the challenging moments of completing this dissertation. I am extremely grateful to my supervisor, Prof. Armando McDonald, whose insight, experience, and knowledge of the subject matter steered me through this research. His continuous support, invaluable advice, and guidance during my Ph.D. were immense. I would like to extend my deepest gratitude and appreciation to Drs. Daniel Robertson, Lili Cai, and Andrew Nelson for serving on my graduate committee and for their valuable feedback and suggestions. I would also like to thank Dr. Thomas Williams for training me on SEM, XRD, and TEM; Dr. Alexander Blumenfeld for helping on NMR experiment and Dr. Joseph Jakes on nanoindentation. I am also grateful to my colleagues and lab mates at the Forest and Sustainable Products Lab, who have made this journey easy. Dr. Farid Sotoudehnia, your professional and moral support was wonderful. I owe a debt of gratitude to my family and friends for their constant support to keep me energized and motivated.

Dedication

This work is dedicated to my family. Tremendous gratitude to my dad and mom, Yaya and Tatey. Although you are no longer in this world, Yaya, your exemplary hard-working character, self-discipline, and words of encouragement to go to the end of academia are with me now and forever. I wish I shared with you this adventure. Tatey, this would have been impossible without your prayers. I love you and appreciate everything that you have done for me. My sisters Abiti, Assegedech, Misir, and Tiruye have been constantly supporting and inspiring me during this journey, your motivation was indispensable. I also dedicate this dissertation to my wife Emaye, who was always with me. I am so blessed to have you in my life.

Table of Contents

List of Tables

List of Figures

Chapter 1: Introduction

1.1 Background

Lodging is the permanent displacement and mechanical failure of crops from their upright position before harvesting [1]. There are two types of lodging; namely stalk lodging and root lodging [2]. Root lodging happens when the mechanical failure occurs at the root-soil interface while stalk lodging occurs when the structural stability of the plant is lost by the structural or material failure of the stalk [3]. Lodging severely reduces grain production, and quality of the major cereal crops; subsequently leading to substantial economic losses worldwide. Annual crop yield losses because of lodging is estimated from 5 to 43% [4], [5]. Lodging is caused by external factors (wind, rain, topography, soil, etc.), field management practices, plant characters (morphology, anatomical traits, and cell wall composition), and by the interactions of these factors [6], [7]. Lodging-inducing external factors might be uncontrollable as they could be related to geographical and meteorological conditions [3], while plant characters (anatomical, morphological, and compositional) are genetic controllable traits of the plant associated with material properties. Lodging occurs when externally applied loads surpass the maximum load that the stalks can withstand. The mechanical failure of crop is a multiscale phenomenon that starts at the cellular level, and propagates ultimately to the whole plant [8]. The structural rigidity and flexibility of stalks and the roots are vital for providing frameworks to support the aboveground components and retain their vertical position, otherwise, the crops may fail by buckling and/or breakage of the lower internodes or roots [9]. Differences in the cell wall microstructure and cellular structure can give rise to a wide range of plant mechanical properties [10]. It is thus important to understand compositional, molecular, and microstructural attributes affecting the mechanical response of plant tissues, thereby the stalk lodging.

1.2 Stalk lodging

Late stalk lodging refers to breakage/buckling of plant stem prior to harvest at late plant stages [11]. Distinct failure patterns and mechanisms are typically obscured in different crops [7]. Stalk lodging is caused by the breaking of internodes and occurs when the stem bending moment exceeds the strength of the stem base [2]. For crops to be lodging resistant, their stalks need to be not only biomechanically rigid enough to support their own weight but also be resilient enough to resist external forces [7]. Biomechanical rigidity-flexibility trade-offs are dependent on the cell wall composition and the structural properties of its building polymers. The structural integrity and biomechanical properties of plants arise from the physico-chemical features of the cell wall building polymers and the complex interactions among those components.

The growth of plant cells requires the synthesis and deposition of structural multilayers surrounding the cell. These protective extracellular matrixes are called cell walls [12]. The biomechanical properties of the cell wall are of special interest in plant biomechanics, and changes in cell wall building materials are influencing the stalk biomechanical properties and ultimately its failure [13]. The cell walls are predominantly composed of structural polymers (cellulose, hemicellulose, and lignin), which are woven into an organized and highly cross-linked network allowing them providing mechanical support to the plant [14]. Cell walls constitute the majority of plant biomass and significantly vary in their composition, architecture and microstructure depending on the species of origin, tissue type, and stage of development [15]. They play a crucial role in determining the mechanical strength of plants. The composition, integrity, and architecture of the macromolecular matrix of cell walls and distinctions in their physico-chemical, mechanical, rheological, and structural features are largely governed by the organization and relative proportion of cell wall main polymeric components as well as their interactions [16].

1.3 Chemistry of stalk lodging

The stalk is one of the most important parts of crops performing multiple architectural and physiological functions that encompasses complex structural, compositional heterogeneity and anisotropy, viscoelasticity, and rheology [17]. Stalk strength is an important agronomic trait in determining the resistance against lodging, which is a well-known factor in affecting harvesting efficiency, yield, and quality. In line with cell wall composition, the biomechanical strength of stalks arises from (1) metabolic factors such as lignin, cellulose, and hemicelluloses contents, (2) structural and supramolecular factors such as cellulose crystallinity index (CI), degree of polymerization (DP), microfibril angle (MFA), and lignin structure and syringyl/guaiacyl (S/G) composition, and (3) component interactions such as lignin-carbohydrates complexes. Stalks endowed with biomechanically stiff character can prevent crops from breaking. Thus, knowing the role of cell wall compositions and structural features on stalk lodging might lead to comprehensive understanding about the phenomena.

Stalks should be strong enough to maintain the crop's upright position as well as flexible to bend without breaking to withstand strong winds and other loads [18]. These range of properties are conferred by three main molecular components – cellulose, hemicelluloses and lignin which are arranged by an exquisite hierarchical organization in the plant cell walls from the nanoscale to the macroscopic scale [19]. Cellulose constitutes the main structural component of plant fibers and is formed by long linear polymeric chains of glucose units linked by β-(1→4) glycosidic linkages. This linear conformation of the cellulose chains enables their arrangement in semicrystalline microfibrils

during biosynthesis. Lignin, on the other hand, is a complex three-dimensional amorphous, heteroaromatic and branched biopolymer composed of monolignols mainly coniferyl, sinapyl and *p*-coumaryl alcohols, which are respectively polymerized to guaiacyl (G), syringyl (S) and hydroxyphenyl (H) units through dehydrogenative polymerization reactions [20]. Hemicelluloses are similar in some ways to cellulose linked by β-(1→4) glycosidic linkages consisting of arabinose, mannose, galactose, glucose, and xylose. Thus, cell wall materials are conceptualized as a fiber reinforced composite structure, where cellulose fibrils act as stiff fibers, while hemicellulose and lignin molecules act as soft matrix. The angle between the fiber direction and the loading direction (microfibril angle, MFA) has been found to be the key factor controlling the mechanical properties [21]. It is thus important to evaluate the influence of molecular scale arrangement and composition on macroscale biomechanical properties of the stalk. These include lignin content and its monomer composition (S/G ratio, H/G/S/), glucan content, MFA of cellulose, and hemicellulose/xylan content.

Sorghum stems have sclerenchyma tissue (rinds with many sub-epidermal cell layers) as well as parenchyma tissue (pith, consisting of vascular bundles and soft tissues) [22]. Although pith parenchyma cells play a vital role in stabilizing the stem and reducing the risk of local buckling and collapse, up to 80% of the biomechanical strength of a stalk comes from the rind [13], [23]. Thus, the mechanical strength of stalks primarily depends on the cell wall of the rinds. The rinds are dense and fibrous tissue having higher mechanical strength. The rind provides the principal structure supporting plants against tension and bending loads. Studies based on dissection of stalk strength into its constituent features showed that the structural composition of the rind, not the pith or total girth, appears to be the most important stalk strength determining component [24]. Therefore, it is necessary to evaluate the biomechanical and viscoelastic nature of sorghum rinds to reveal macromolecular and lodging variation of stems. Cell wall layers are considered as a nanofiber-reinforced composite material consisting of helically wound cellulose microfibrils embedded in a matrix of amorphous cellulose, hemicelluloses, and lignin [25]. Dynamic mechanical analysis (DMA) can be used to examine composite properties and the response of individual cell wall components in situ and enlightens the individual cell wall polymer contributions as well as their interactions. For example, DMA has been applied to investigate the viscoelastic and mechanical properties of barley stems [26].

Despite the significant body of literature on stalk lodging [3], [6], [7], a detailed compositional investigation of sorghum stalks has not been reported. This research involves evaluating the cell wall chemistry of the sorghum stalk, investigating the biomechanical and viscoelastic behavior of the stalk's main structural component (rind), developing strength ─ composition correlations, and

identifying key structural elements of cell walls with a high impact on strength of sorghum stalks. Cellulose, lignin, and hemicelluloses are essential constituents of plant cell walls, but their individual roles on the biomechanical strength of sorghum remain not fully understood. Even though the microfibril angle of the main secondary cell wall (SCW) S2 layer has been highly associated with the mechanical properties of wood [27], it remains uninvestigated in crop stalks. Thus, this research aims to investigate the cell wall chemistry of the sorghum stalks, microfibril angle and correlate to the biomechanical property of rinds, which is the main structural component of the stalk, contributing about 80% of the strength [28].

1.4 Objectives

Stalk biomechanical properties determine the structural stability of crops. To understand physical failure mechanisms of sorghum stalks at macroscale, evaluation of cell wall chemistry and correlating with their corresponding biomechanical properties is selected. Identifying the key contributing parameters for structural integrity and biomechanical stiffness of the stalks, besides to creating comprehensive insight to the phenomena of lodging, are crucial for the development of robust cultivars with higher lodging resistance capability. The objectives of this research are compositional analysis of sorghum stalks to gain a better understanding of the relationships between cell wall components and stalk lodging. The specific objectives include:

I. Statistical analysis of fatty acid-based chemometrics for predicting compositional and metabolic variations in sorghum varieties
II. Evaluation of compositional and cell wall structural analysis of whole sorghum stalks of different lodging-behaviors using ranges of analytical tools
III. Investigation of cell wall compositions, rheological and biomechanical strength based on the main structural components of stalks and evaluating composition-mechanical property performance correlation
IV. Evaluating the molecular, supramolecular, and microstructural attributes of cell walls influencing strength

Chapter 1 provides a general background of stalk lodging, chemistry of lodging, and the objectives of the research. Chapter 2 reviews the current body of literature and analysis of the effect of cell wall composition on the lodging resistance of different cereal crops. It also presents the effect of chemistry of cell wall polymers on the mechanical strength of different cereal stalks. The chapters thereafter are entirely based on experiments and findings of sorghum stalks grown in 2018 and 2019. Chapter 3 discusses the application of fatty acid compositions as fingerprints to assess the compositional and metabolic variations associated with the mutation and growing season. Fatty acid-based

chemometrics was conducted using different statistical analyses. Chapter 4 covers the comprehensive chemical compositional analysis and evaluation of molecular structural attributes pertaining to the main polymers of the cell walls in whole stalks. Chapter 5 discusses the biomechanical strength, rheological properties, and composition-biomechanical property performance relation to identify key cell wall polymers influencing the strength of the stalk rind. Chapter 6 outlines microstructural properties and nanoindentation results to explore the effect of cell wall organization on nano-mechanical properties. Chapter 7 summarizes the conclusions and potential further work beyond this dissertation. Chapters 2 through 5 were written as separate journal manuscripts.

1.5 References

[1] C. J. Stubbs, C. McMahan, W. Seegmiller, D. D. Cook, and D. J. Robertson, "Integrated Puncture Score: Force-displacement weighted rind penetration tests improve stalk lodging resistance estimations in maize," *Plant Methods*, vol. 16, no. 1, pp. 1–12, Aug. 2020, doi: 10.1186/S13007-020-00654-W/TABLES/4.

[2] P. M. Berry *et al.*, "Understanding and Reducing Lodging in Cereals," *Adv. Agron.*, vol. 84, pp. 217–271, 2004, doi: 10.1016/S0065-2113(04)84005-7.

[3] C. Stubbs, C. McMahan, R. S. Sekhon, and D. J. Robertson, "Diverse maize hybrids are structurally inefficient at resisting wind induced bending forces that cause stalk lodging," *Plant Methods*, vol. 16, no. 1, pp. 1–15, May 2020, doi: 10.1186/S13007-020-00608-2/FIGURES/12.

[4] S. A. Flint-Garcia, C. Jampatong, L. L. Darrah, and M. D. McMullen, "Quantitative Trait Locus Analysis of Stalk Strength in Four Maize Populations," *Crop Sci.*, vol. 43, no. 1, pp. 13–22, Jan. 2003, doi: 10.2135/CROPSCI2003.1300A.

[5] A. J. Lindsey, P. R. Carter, and P. R. Thomison, "Impact of imposed root lodging on corn growth and yield," *Agron. J.*, vol. 113, no. 6, pp. 5054–5062, Nov. 2021, doi: 10.1002/AGJ2.20848.

[6] L. Shah *et al.*, "Improving Lodging Resistance: Using Wheat and Rice as Classical Examples," *Int. J. Mol. Sci.*, vol. 20, no. 17, Sep. 2019, doi: 10.3390/IJMS20174211.

[7] L. Erndwein, D. D. Cook, D. J. Robertson, and E. E. Sparks, "Field-based mechanical phenotyping of cereal crops to assess lodging resistance," *Appl. Plant Sci.*, vol. 8, no. 8, p. e11382, Aug. 2020, doi: 10.1002/APS3.11382.

[8] Q. Li *et al.*, "Crop Lodging and The Roles of Lignin, Cellulose, and Hemicellulose in Lodging Resistance," *Agron. 2022, Vol. 12, Page 1795*, vol. 12, no. 8, p. 1795, Jul. 2022, doi: 10.3390/AGRONOMY12081795.

[9] M. Neenan and J. L. Spencer-Smith, "An analysis of the problem of lodging with particular reference to wheat and barley," *J. Agric. Sci.*, vol. 85, no. 3, pp. 495–507, 1975, doi: 10.1017/S0021859600062377.

[10] L. J. Gibson, "The hierarchical structure and mechanics of plant materials," *J. R. Soc. Interface*, vol. 9, no. 76, pp. 2749–2766, Nov. 2012, doi: 10.1098/rsif.2012.0341.

[11] D. D. Cook, W. De La Chapelle, T. C. Lin, S. Y. Lee, W. Sun, and D. J. Robertson, "DARLING: a device for assessing resistance to lodging in grain crops," *Plant Methods*, vol. 15, no. 1, Sep. 2019, doi: 10.1186/S13007-019-0488-7.

[12] P. Sarkar, E. Bosneaga, and M. Auer, "Plant cell walls throughout evolution: towards a molecular understanding of their design principles," *J. Exp. Bot.*, vol. 60, no. 13, pp. 3615–3635, Sep. 2009, doi: 10.1093/jxb/erp245.

[13] Shah D, T. P. S. Reynolds, and M. H. Ramage, "The strength of plants: Theory and experimental methods to measure the mechanical properties of stems," *J. Exp. Bot.*, vol. 68, no. 16, pp. 4497–4516, Oct. 2017, doi: 10.1093/jxb/erx245.

[14] B. Zhang, Y. Gao, L. Zhang, and Y. Zhou, "The plant cell wall: Biosynthesis, construction, and functions," *J. Integr. Plant Biol.*, vol. 63, no. 1, pp. 251–272, Jan. 2021, doi: /10.1111/jipb.13055.

[15] S. Pattathil *et al.*, "Cell Wall Ultrastructure of Stem Wood, Roots, and Needles of a Conifer Varies in Response to Moisture Availability," *Front. Plant Sci.*, vol. 0, p. 882, Jun. 2016, doi: 10.3389/FPLS.2016.00882.

[16] S. Pattathil, M. G. Hahn, B. E. Dale, and S. P. S. Chundawat, "Insights into plant cell wall structure, architecture, and integrity using glycome profiling of native and AFEXTM-pre-treated biomass," *J. Exp. Bot.*, vol. 66, no. 14, pp. 4279–4294, Jul. 2015, doi: 10.1093/jxb/erv107.

[17] D. Dongdong and W. Jun, “Research on mechanics properties of crop stalks: A review,” *Int. J. Agric. Biol. Eng.*, vol. 9, no. 6, pp. 10–19, Dec. 2016, doi: 10.25165/IJABE.V9I6.1499.

[18] Berry P.M, “Lodging Resistance in Cereals,” in *Sustainable Food Production*, W. C. B. . Christou P., Savin R., Costa-Pierce B.A., Misztal I., Ed. Springer, New York, NY, 2013, pp. 1096–1110.

[19] J. Keckes *et al.*, “Cell-wall recovery after irreversible deformation of wood,” *Nat. Mater. 2003 212*, vol. 2, no. 12, pp. 810–813, Nov. 2003, doi: 10.1038/nmat1019.

[20] L. Qingquan, L. L, and Z. L, “Lignins: Biosynthesis and Biological Functions in Plants,” *Int. J. Mol. Sci.*, vol. 19, no. 2, Feb. 2018, doi: 10.3390/ijms19020335.

[21] K. Jin, Z. Qin, and M. J. Buehler, “Molecular deformation mechanisms of the wood cell wall material,” *J. Mech. Behav. Biomed. Mater.*, vol. 42, pp. 198–206, Feb. 2015, doi: 10.1016/j.jmbbm.2014.11.010.

[22] S. Lee *et al.*, “Time-dependent mechanical behavior of sweet sorghum stems,” *J. Mech. Behav. Biomed. Mater.*, vol. 106, p. 103731, Jun. 2020, doi: 10.1016/J.JMBBM.2020.103731.

[23] T. R. Colbert, L. L. Darrah, and M. S. Zuber, “Effect of Recurrent Selection for Stalk Crushing Strength on Agronomic Characteristics and Soluble Stalk Solids in Maize,” *Crop Sci.*, vol. 24, no. 3, pp. 473–478, May 1984, doi: 10.2135/CROPSCI1984.0011183X002400030010X.

[24] J. A. Peiffer, S. A. Flint-Garcia, N. De Leon, M. D. McMullen, S. M. Kaeppler, and E. S. Buckler, “The Genetic Architecture of Maize Stalk Strength,” *PLoS One*, vol. 8, no. 6, p. e67066, Jun. 2013, doi: 10.1371/JOURNAL.PONE.0067066.

[25] X. Arzola-Villegas, R. Lakes, N. Z. Plaza, and J. E. Jakes, “Wood Moisture-Induced Swelling at the Cellular Scale—Ab Intra,” *For. 2019, Vol. 10, Page 996*, vol. 10, no. 11, p. 996, Nov. 2019, doi: 10.3390/F10110996.

[26] H. Chen, N. Zhao, N. Fu, D. Li, L. J. Wang, and X. D. Chen, “Mechanical Properties of Hulless Barley Stem with Different Moisture Contents,” *Int. J. Food Eng.*, vol. 15, no. 1–2, Feb. 2019, doi: 10.1515/IJFE-2018-0033/MACHINEREADABLECITATION/RIS.

[27] Y. Yin, M. Bian, K. Song, F. Xiao, and J. Xiaomei, “Influence of Microfibril angle on within-tree variations in the Mechanical properties of chinese fir (Cunninghamia Lanceolata),” *IAWA J.*, vol. 32, no. 4, pp. 431–442, Jan. 2011, doi: 10.1163/22941932-90000069.

[28] M. S. Zuber and M. S. Kang, “Corn lodging slowed by sturdier stalks,” *Crop. Soils Mag.*, vol. 30, no. 5, pp. 1–32, Jul. 1978.

Chapter 2: Effect of Cell Wall Compositions on Lodging Resistance of Cereal Crops: Review

"Effect of Cell Wall Compositions on Lodging Resistance of Cereal Crops: Review", Submitted to *Journal of Agricultural Science*

2.1 Abstract

Lodging is the permanent displacement of stalks due to disrupted secondary cell walls caused by external factors, plant characters, and their interaction. Anatomical, morphological, and compositional traits are among lodging-inducing plant traits. Compared with morphological and anatomical features, the correlation between lodging resistance and cell wall compositions is not frequently reviewed. The relationship between cell wall chemical components and the lodging resistance of cereal stalks were summarized comprehensively based on previous reports. The results demonstrated that stalk lodging resistance was correlated with cell wall composition, among which lignin and cellulose were found the key cell wall components enhancing the lodging resistance of cereal crops. Trace minerals and metals were found to have minimal influence on lodging in most of the cereals. In relation to lodging, supramolecular and structural features of cellulose and lignin were not extensively studied. This review also highlights the importance of biomass recalcitrance and lodging resistance trade-offs in the spectrum of genetic cell wall modifications.

2.2 Introduction

The structural rigidity and flexibility of stems (also known as the stalk or culm and these terms will be used interchangeably throughout this review) and roots in cereal crops are vital to providing frameworks to support aboveground plant components and retain their vertical position [1], [2]. The structure of the crops may fail by either stem buckling or failure of root-soil anchorage, respectively called stalk lodging and root lodging [3]; consequently leading to substantial agronomic losses. Stem lodging is caused by the breaking of internodes and occurs when the stem bending moment exceeds the strength of the stem, while root lodging is caused by disturbance to the root-soil interaction and occurs when the total bending moment of a plant exceeds the strength of the root-soil interface [4]. Lodging is a multi-factor and complex phenomenon caused by external factors (wind, rain, topography, soil, etc.), plant characters (stalk morphology, anatomical traits, and chemical composition), and their synergistic interactions. Lodging resistance, on the other hand, is the structural ability to withstand against lodging [5]. Morphological, anatomical, and composition trait-associated factors influencing stem lodging in cereals are shown in Figure 2.1. Crop stems can be considered slender cylindrical columns that are loaded by both self-weight and external loads [6]. Thus, for crops to be lodging resistant their stalks need to be not only structurally rigid enough to

support their weight but also flexible to be resilient to resist external forces [7]. If the stems are too stiff, stem deformation may not occur, but will transfer the force to the underground parts and may cause root lodging [8], subsequently leading to failure. On the other hand, extreme stalk flexibility can also result in stalk lodging because the stalk is not rigid enough to provide sufficient support.

The stalk is one of the most important parts of crops performing multiple architectural and physiological functions. It encompasses complex structural, compositional heterogeneity and anisotropy, viscoelasticity, and rheology, where its mechanical and viscoelastic response under different conditions significantly vary from crop to crop [9]. Differences in the cell wall microstructure and cellular structure give rise to a wide range of mechanical properties [10]. Lodging in cereal crops is the result of mainly the interaction between plant character and external force, among which wind pressure and rain constitute the main variables of the external forces. External factors are uncontrollable, while plant characters are genetic controllable traits associated with material properties of the plant. Furthermore, the proportionality between mechanical strength of the lower internodes and the weight of upper parts of the stem determines a plant's vulnerability to lodging. As a result, plant lodging resistance is also determined by the weight of its upper portion (upper leaves, stems, and seeds) and the pushing resistance of the lower portion [11]. Thus, the biomechanical properties of the stem in cereals play an important role in its lodging resistance

The literature on lodging has mainly focused on the morphological and anatomical characteristics of the crop, including plant height, internode length, and culm diameter (Figure 2.1). This review aims to provide an up-to-date survey of the role of chemical composition, structural, and supramolecular features that strengthen the cereal crops, thus contributing to lodging resistance. The impact of cell wall composition on lodging resistance has not been comprehensively reviewed. The general classification of lodging-inducing plant characters is given (Figure 2.1) and the associated glossary of terminologies are summarized (Table 2.1).

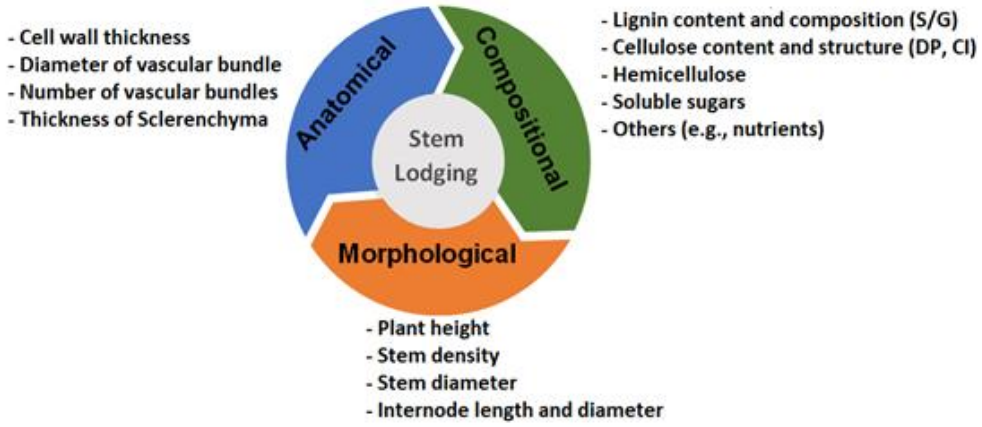

Figure 2.1. Lodging-inducing plant characters: anatomical, compositional, and morphological traits associated with stem lodging ; S/G- syringyl/guaiacyl ratio, DP-degree of polymerization, CI- crystallinity index.

Table 2.1. Glossary of terminologies in reference to the plant stems.

Terms	Definition
Morphological	The physical appearance of a stem, describing features related to the form and external structure of plant (e.g., height, diameter etc.)
Anatomical	Traits related to the internal structures, mostly at the cellular/microscopic level. Cells are basic units of plants, organized into tissues and in turn tissues are organized into organs. In plants, different organs show differences in their internal structure.
Compositional	The chemical constituents/components of the stem, referring both structural (cellulose, lignin hemicellulose, protein) and non-structural components of cell wall
Microstructures	Structural inhomogeneities consist of spatially distributed phases of different structures, grains of different orientations, structural defects, and porosity. The geometric arrangement of cells and their intercellular spaces.
Supramolecular	Structures attributed to the arrangement and stacking state of the cellulose molecular chains by intermolecular hydrogen bond

2.3 Plant cell walls

The growth of plant cells requires synthesis and deposition of dynamic structural multilayers called cell walls [12]. Cell walls are composed of structural polymers (cellulose, hemicellulose, and lignin) that are woven into an organized and highly cross-linked network allowing them to perform various functions such as; providing mechanical support to the plant body, providing a physical barrier to harsh biotic and environmental conditions, conducting water and nutrients, and signal transduction in response to pathogen attack, and environmental stresses [12], [13]. Cell walls constitute the majority of plant biomass and significantly vary in their composition, architecture and microstructure depending on the species of origin, tissue type, stage of development, and environmental conditions [14]. The composition, integrity, and architecture of the macromolecular matrix of cell walls, collectively referred to as cell wall ultrastructure, exhibit variation across species [15]. The physicochemical, biomechanical, rheological, and structural features of cell walls are largely

governed by the organization, relative proportion and interaction among cell wall polymeric components [14],[16]. Generally, plant cell wall components with significant contribution to the structural integrity of stems are cellulose, lignin, and hemicellulose. Non-covalent interactions such as hydrogen bonding and van der Waals forces are primarily responsible for the integrity of cellulose microfibrils and the cellulose–hemicellulose associations and networks within plant cell walls [17]. On the other hand, covalent cross-links and ionic interactions play major roles in the formation and integrity of pectic matrices. Lignin–carbohydrate complexes that are held together via ester and ether linkages between lignin and hemicelluloses can further strengthen wall integrity [18]. Interactions between various cell wall components, especially the connections of non-cellulosic components such as hemicelluloses with the cellulosic core and lignin, are subject to significant variation [14].

2.3.1 Cell wall organization

The plant cell walls (CW) are organized from three compositionally and structurally distinctive layers: middle lamella (ML), primary cell walls (PCW), and secondary cell walls (SCW) [19]. The cell plate formed during cell division develops into the ML─ a thin layer that connects two plant cells and is mainly composed of pectins [20], shown in Figure 2.2d. PCW is then deposited on each side during cell expansion. PCW is composed of carbohydrate-based polymers such as cellulose, hemicelluloses, pectin, and structural glycoproteins [21] and contains cellulose microfibrils with a dispersed orientation and some degree of microfibril alignment. After cessation of cell growth, the SCW is deposited inside PCW, thus making the walls thicker, and rigid, subsequently determining the mechanical characteristics of plants. SCW is composed of cellulose, hemicellulose, and lignin in varying proportions. The SCW is further organized into three layers: an outer layer (S1), a middle layer (S2), and the innermost layer (S3). The S2 layers constitute the highest proportion of the CW thickness endowed with smaller microfibril angles, whereas S1 and S3 have transversely oriented microfibrils with higher angles [22]. The mechanical properties of a plant mainly depend on the architecture of the secondary cell walls and structural parameters like microfibril angles, dictate its stiffness. Plant cell wall structure consisting of ML, PCW, and SCW is shown in Figure 2.2d.

2.3.2 Function

ML and PCW play an indispensable role in cell-to-cell adhesion, cell expansion, and the determination of cell shape [23]. ML glues cells together [20] while PCW is elastic to allow cell wall expansion during growth [24]. After cell expansion the SCW forms provide axial stiffness, collapse, and burst resistance. The S2 layer comprises approximately 80-90% of the cell wall [25], thus it has a profound effect on the properties of the plant. The low microfibril angle, higher thickness, and high cellulose content are important characteristics of the S2 layer for better mechanical stiffness [23].

Compared to S2, S1 and S3 layers are relatively thin but play a critical role in increasing the elastic modulus of the cell in the transverse plane [26]. The S1 layer acts as a reinforcing layer preventing excessive radial expansion and rotation of the cell, while the S3 layer helps to avoid sideway collapse when under hydrostatic tension forces [23]. The fibers will slightly rotate under stress because of the microfibril angle arrangement of the S2 layer. Because of the thickness, the high-volume fraction, and the alignment of cellulose fibrils, the mechanical properties of the CW in the longitudinal direction are largely dependent on the S2 layer [10].

2.4 Plant cell wall and mechanical strength

In this review, mechanical strength is mainly ascribed to measures of resistance to deformations and distortions (elastic properties), and measures of failure-related (strength) properties, as described in [30]. The mechanical strength of plants arises from (1) metabolic factors such as lignin, cellulose, and hemicelluloses contents, (2) structural factors such as cellulose crystallinity index (CI), degree of polymerization (DP), lignin structure and composition (S/G ratio), and (3) component interactions such as lignin-carbohydrates complexes.

2.4.1 Cellulose

Cellulose is the primary structural framework of plant cell walls consisting of a linear D-glucosyl repeat unit linked via β-(1,4) glycosidic bonds [31]. Cellulose is a main load-bearing structural component due to its higher DP and linear orientation [30]. It is a long-chain polysaccharide made up of 7,000–15,000 D-glucose monomer units, where the molecules align to form microfibrils 3–5 nm wide [10], [20]. Supramolecular properties of cellulose contributing to mechanical stiffness include the degree of crystallinity, microfibril angle (MFA), and DP [31]. Each glucose contains three free hydroxyl moieties that can interact to form hydrogen bonds, which play a crucial role in the aggregation of cellulose chains and determine the crystal structure of the cellulose [23]. Long-chain cellulose contains more hydrogen bonds and is difficult to break, while short-chain cellulose contains a weaker hydrogen-bonding system, and thus is easier to deform. Cellulose contains both crystalline and non-crystalline regions embedded in a lignocellulosic matrix [32]. Crystallinity index (CI) refers to the relative proportion of crystalline to amorphous regions and is among one of the supramolecular properties influencing mechanical properties such as strength and stiffness [31]. [32] The cellulose microfibrils are aligned into fibrils of about 10–25 nm diameter within the lignin and hemicellulose matrix [33][10]. The orientation of the cellulose microfibrils in the S2 layers of the CW has a significant influence on the mechanical properties of the plant. The angle between cellulose fibrils and the longitudinal axis (MFA, Figure 1.2d & g) is a critical factor in controlling physical and mechanical properties [34]. The variation of MFA in the S1, S2, and S3 layers in the cell wall give

rise to anisotropy in the mechanical properties of the cell wall. The DP of cellulose, the number of glucose units in the polymer, is another superstructural feature affecting the stiffness (flexural modulus) of the plant CW. The cellulose DP varies between 2000–6000 in PCW and about 10,000 in SCW [23].

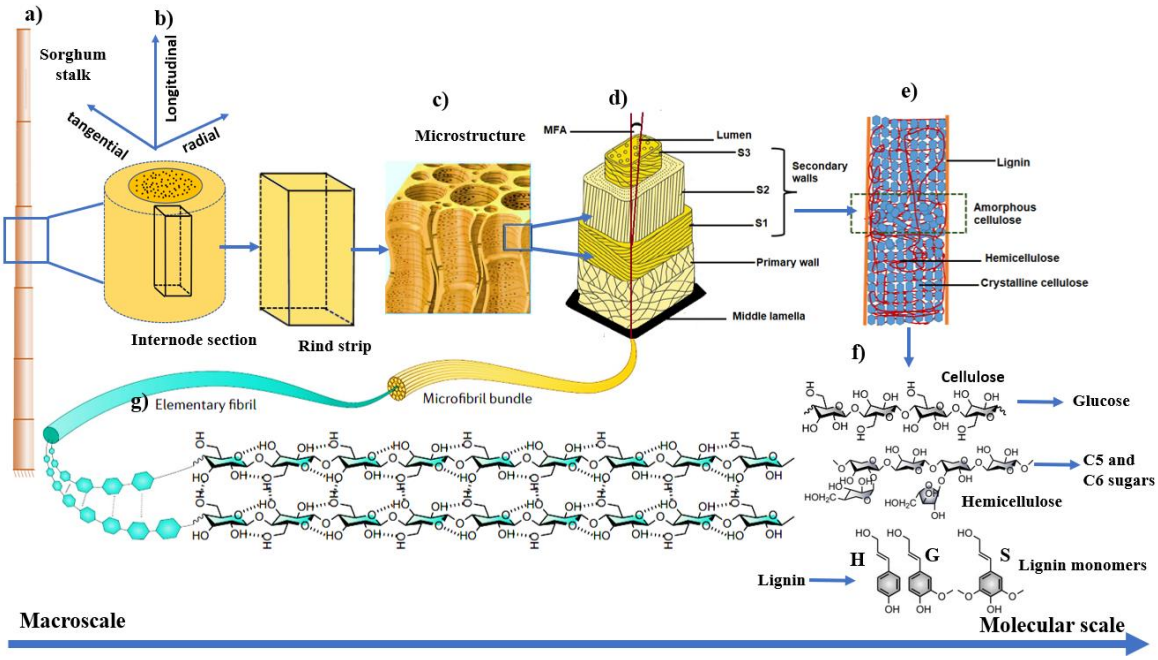

Figure 2.2. Conceptualization of top-down (macroscale-to-molecular scale) arrangement based on sorghum stalk ; a) Schematic depiction of the stalk; b) Sections and strips of the stalk; c) Hierarchical cellular microstructure of plant, adapted from [27] ; d) Individual cells organized from middle lamella (ML), primary cell walls layer (PCW) and secondary cell walls (SCW) layers, which is further divided into S1, S2, and S3 layers, adapted from [28]; e) Representation of lignocellulose arrangement: composed of three major components, cellulose (crystalline and amorphous), hemicellulose and lignin; f) Major cell wall components are decomposing into their respective monomers, monomer structures are adapted from [29]; g) Cellulose is oriented into elementary fibrils and ultimately arranged to microfibril bundles to resist the major load during cell wall deformations, adapted from [29].

2.4.2 Lignin

Lignin is a complex three-dimensional amorphous, heteroaromatic, and branched biopolymer composed of monolignols mainly coniferyl, sinapyl, and p-coumaryl alcohols [35], which are respectively polymerized to guaiacyl (G), syringyl (S) and hydroxyphenyl (H) units through a dehydrogenative polymerization reaction. The monolignols differ in their degree of methoxylation and are coupled by C-C or ether interunit linkages, such as arylglycerol-β-ether dimer, resinols, phenylcoumaran, spirodienone, and dibenzodioxin [36] (as shown in Figure 2.3), leading to the irregular three-dimensional structures. Lignin gives structural rigidity and mechanical strength to the cell walls via covalent linkage with hemicellulose, and by occupying the voids between carbohydrate polymers [37]. There are van der Waal interactions between lignin and cellulose microfibrils, which

create cohesion between the lignin/hemicellulose matrix and the crystalline cellulose. The weakest interactions are found between the amorphous cellulose and the lignin/hemicellulose matrix [23]. Thus, lignin binds carbohydrate molecules together and acts as a stiffening agent for the cellulose molecules within the cell wall [30]. Factors such as total lignin content and lignin composition (S/G ratio) can influence the mechanical property of the cell wall [38]. The S/G ratio indicates the ratio of different monolignols present in lignin and influences the linkage distribution (β-O-4, β-β, etc.) within the lignin. G-rich lignin is highly cross-linked due to a greater proportion of biphenyl and other carbon-carbon bonds, whereas S-rich lignin is less condensed, linked by more labile ether bonds at the 4-hydroxyl position [39]. Furthermore, S-rich lignin is more easily depolymerized than G-rich lignin, due to the fact that an additional methoxy group at position 5 on a lignin monomer results in reduced available reactive sites for coupling and less possible combinations during polymerization [40].

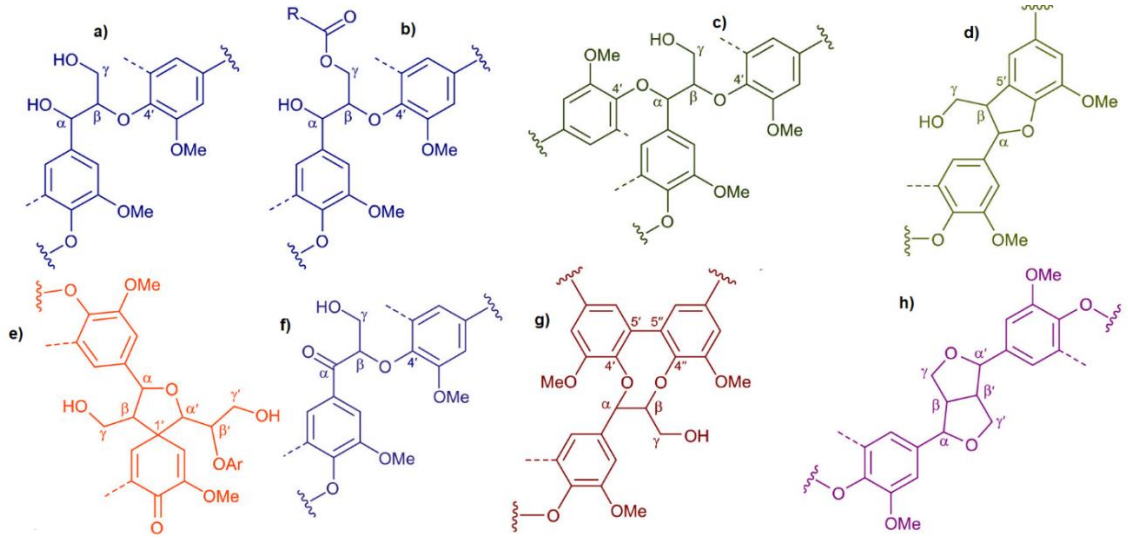

Figure 2.3. Lignin interunit linkages a) β-O-4 alkyl-aryl ethers; b) β-O-4 alkyl-aryl ethers with acylated γ-OH; c) α,β-diaryl ethers; d) phenylcoumarans; e) spirodienones; f) Cα-oxidized β-O-4 structures; g) dibenzodioxocins; h) resinols [41]

2.4.3 Hemicelluloses

Hemicelluloses are heteropolysaccharides containing C5 (xylose, arabinose), C6 (mannose, glucose, galactose) monosaccharides, uronic acids, and acetyl groups [42]. The heterogeneous nature of hemicelluloses is a crucial factor for molecular interactions with cellulose microfibrils and the occurrence of covalent linkages with lignin [43]. Hemicelluloses are highly branched (Figure 2.2f) and amorphous polysaccharides with 500–3000 monomer units [10] with an average DP of 100–200 units [44], which is lower compared to cellulose DP. Hemicellulose links the fibrous cellulose and the amorphous lignin serves as a matrix for the cellulose and increases the packing density of the cell

wall [30]. The impact of hemicelluloses on biomechanical strength cell walls in wood showed distinct biomechanical contributions: glucomannans increasing the elastic modulus in compression, and xylans contributing to a significant increase of the elongation at break under tension [43].

2.4.4 Interactions between CW polymers

Plant CW consists of a network of interlinked polymers with distinct mechanical properties. Attributed to its complex structural behavior, CW has been compared with a composite material, emphasizing CW polymers play different roles in the overall mechanical behavior of the structure [16]. Because of the CW's intricate interwoven nature, studying the behavior of individual polymer components may have the limited predictive potential for the biomechanical property of the heterogeneous structure. Hence, cross-links and other interactions between biopolymers are crucial for a comprehensive understanding of the mechanical property of CW. The biomechanical integrity of secondary cell walls is controlled by the molecular interactions between cellulosic microfibrils, hemicelluloses, and lignin [43]. Thus, strong interactions between the CW components may increase their biomechanical property. Cellulose and hemicelluloses are linked by hydrogen bonds, whereas lignin is covalently bounded to hemicelluloses to create the lignin-carbohydrate complex (LCC) [45]. A computational cell wall network model study on PCW showed that stiffness is most sensitive to the cellulose microfibril-hemicellulose interaction in which Young's (tensile) modulus increases with the interaction [46]. Although considering the whole CW polymer network is crucial, general principles can be decoded by characterizing the properties of individual components [16].

2.5 Composition and strength of cereal stems

The CW structural compositions are not uniformly distributed within the cell walls of cereal stalks. The structure and the quantity of these CW components vary according to species, tissues, and maturity of the plant cell wall [47]. As shown in Table 2.2, the CW compositions of cereals stems are fundamentally different: generally consisting of 32–53% cellulose, 12–37% hemicellulose, and 16–31% lignin, whereas extractives, ash, and proteins make up the remaining fraction. Because of the heterogeneity in the composition, structure, and CW interaction with other external lodging-inducing factors, the response and mechanism of each crop against lodging might be different. Stems resist the forces of gravity and powerful lateral wind forces through the cumulative strength of the CW surrounding each cell. These walls consist mainly of lignin, cellulose, and non-cellulosic polysaccharides in proportions that depend on the type of cereal and stage of development.

Table 2.2. Summary of literature for cell wall composition of some cereal crop stalks (%, dry mass)

Cereal	Cellulose	Hemicellulose	Lignin	Extractives	Ash	CI (%)	Ref.
Wheat	32.0-46.4	18.0-29.3	18.0-25.1	–	9.7	43-58	[48], [49]
Rice	37.0	22.7	13.6	13.1	19.8	–	[50]
Millet	41.0	20.9	18.3	–	6.0	–	[51]
Sorghum	36.1-39.4	26.9-29.2	20.8-22.1	1.5-2.2	–	45.5	[52]
Rye	37.9	36.9	17.6	–	3.0	–	[53]
Oat	39.6	22.6	18.2	10.1	1.4	–	[54]
Barley	30.0-31.0	27.0	16.0-19.0	13.37	3.9	–	[55]
Corn	42.4	11.8	30.62	8.2	7.0	57.0-65.0	[56]
Soybean	52.6	28.9	21.6	–	1.4	–	[57]

Stalk strength in cereal crops is closely associated with the structure and composition of the CW. In most cereal crops, stem strength is the main determinant of resistance to lodging. For example, in barely [58], the breaking strength of brittle culms was found significantly lower than nonbrittle culms. The association of brittleness with lower bending strength implied that stems with lower bending stress are prone to structural falling and stalk lodging. Although lodging resistance varies among different genotypes, it is still selected primarily based on mechanical phenotyping. For instance, Chuanren D. et al. [59] recommended the selection of high-yield and lodging resistance rice species based on the 'middle stem' and 'rigid stem' traits, which are not explicitly defined in terms of composition or other parameters. The rigidity, length of plants, and other anatomical and morphological features are genetically controlled traits, thus we might not be entirely relying on the evaluation of the complicated lodging trait based on such factors. Thus, knowing the role of CW composition in relation to structural features and stalk lodging might lead to a comprehensive understanding of the phenomena. Stems endowed with lodging resistance and mechanically stiff character can prevent crops from breaking. There are no standardized approaches for quantitative measurement of stalk lodging resistance, but biomechanical properties such as bending (flexural) strength [60], and rind penetration [7] are indicators of its strength, and thus can be associated with lodging resistance. But single measurement entities may not sufficiently define lodging resistance due to the complex and multivariate nature of lodging traits. General methods to measure the biomechanical properties of stems are discussed and reviewed elsewhere [1].

2.5.1 Macroscopic lodging mechanisms

Lodging is the state of permanent and irreversible displacement of the stems from their upright position [8]. Macroscopically, stalk lodging generally arises from three distinct types of failure mechanisms: bending-type, breaking-type, and root lodging. The bending type lodging occurs when the stem fails to resist bending pressure and is commonly observed in the upper internodes affected by strong winds and rain [61]. Semi-dwarfism of the cereals improved such lodging by lowering the "center of gravity" of the plant. Even if the introduction of the semi-dwarf trait has improved lodging,

it remains a challenge for high-yield cereals. Thus, improving lodging resistance by semi-dwarf trait alone is possible only up to a certain limit, beyond which other traits may be needed for enhancement [62]. On the other hand, breaking-type lodging usually occurs at the lower internodes due to excessive wind forces at the upper internodes [61], [62]. This type of lodging is mainly affected by the morphology and quality of the stem [63]. Lastly, root lodging happens when the stem remains intact, and failure occurs at the root-soil anchorage due to the low bending moment of roots than the above-ground parts. In wheat, barley, and oats, stem lodging is usually caused by one of the bottom two internodes buckling [4], whereas, in corn, it occurs primarily due to the stalk buckling below the ear and usually occurs in the middle of the third internode below the ear [64]. Yield was found to be considerably decreasing with an increase in stalk breakage (Figure 2.4). It has been reported in wheat that during the grain filling stage, lodging between 25–90° angle from the perpendicular could result in lodging-induced grain yield reduction of 20–61% [65], [66]. Annual yield loss of 5-35% in corn [67] and barley by 28–65% [65] has been reported.

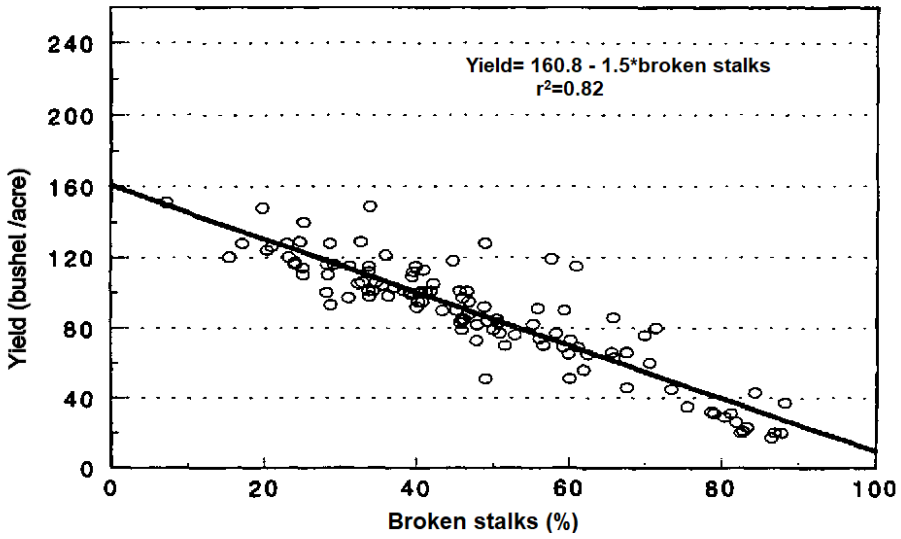

Figure 2.4. The effect of stalk breakage on grain yield of different corn hybrids. In 1993, stalk breakage in Nebraska ranged from 7 to 88% at 100 mph wind speed, and grain yield was reduced by 1.5 bu/acre for every 1% increase in stalk breakage, adapted from [68].

2.5.2 Microscopic lodging mechanisms

Apart from the macroscopic failure mechanisms, what happens at the microscopic scale during lodging is yet unknow and unexplored. The nanomechanical properties of various crop stalks [69], [70] confirm the elastic nature of stems. Thus, failure of stalks (stalk lodging) in response to certain loads can be explained in terms of molecular phenomena in the stress-strain relationship. Failure is the result of the rupture of bonds at the molecular level. Upon loading, stresses are created in the cell wall of the stalks and spread throughout the material, resulting in a different extent of strain. In crops,

lodging occurs when the bending moment caused by a combination of external loading such as wind, and loading from the plant's weight exceeds the bending strength of stems [4], [71]. What happens at the molecular and cellular level in situations below and beyond the proportionality limit of the strength of the stem remains unclear. According to Winandy et al. [30], below the proportionality limit, the hydrogen bonds (H-bonds) between and within individual polymer chains are breaking, sliding, and uncoiling during the loading of materials. Consequently, the covalent bonds (C–C and C–O) start to distort within the cell wall and the H-bonds connecting microfibrils are breaking and reforming, causing the microfibrils to slide by one another upon the disruption of the reformed H-bonds. Stresses are uniformly distributed between individual cells and insufficient to cause permanent translocation and deformation, thus only temporary distortion occurs [30]. Below the proportionality limit, all molecular and macromolecular deformations arising from stress buildup are recoverable to their original position after unloading.

Progressive bending and buckling of cell walls were reported [72] for balsa upon loading. The stress-strain relationship is no longer linear above the proportionate limit of materials strength, and the limit of recoverable hydrogen bonding is exceeded, thus loads are sufficient to cause covalent bond rupture and permanent dislocation at all structural levels. Nonrecoverable covalent bond (C–C and C–O) scission in carbohydrates and lignin leads to lignin-hemicellulose copolymer separation, hemicellulose depolymerization, and amorphous cellulose depolymerization [30]. The accumulation of stress within the crystalline region of the cellulose trigger failure and disorientation of microfibrils, covalent bond rupture, and CW layers distortion, ultimately causing micro-cracks and separation of the layers. The fibers distort to an extent that recovery to an original position is impossible thereby failing either by scission of the cell (cells tear into two parts) or by middle lamella failure (cells detach from one another). Even if the stress is released, there is no back-flowing but a lock-in at the new position and the bonds reform immediately in the new position of the fibrils [73]. Close to the ultimate strength, even if CW continues to deform and absorb strain energy, stress redistribution within the individual polymers eventually becomes impossible and cannot withstand extra stress any longer, thus will be torn apart. Due to the disintegration of the crystalline cellulose framework of the material, failure is related to CW scission or cell-to-cell withdrawal [30].

Fractures of the tracheids under flexural loading were observed, which explains the tracheid failure mechanism under bending load [74]. When wooden material is loaded, fractures start and propagate throughout the cellular system in all directions. Since each cell is tightly aligned with the next cell, the material can elastically transfer stress until an induced crack or a natural growth defect or an abrupt change in CW thickness interrupts the cellular arrangement. The stress buildup within the

wood material initiates cracks in regions where stress transfer is interrupted and propagates until either energy from the crack is transferred to the structural elements, or by ultimate failures. At the cellular level below the proportional limit, stresses are transferred between S1/S2/S3 cell wall layers. Because of its larger proportion, the highest stress concentration regions of the wood cell wall occur in the S2 layer and become the center of fracture initiation in the CW. The MFA has a substantial impact on the resistance to deformation [75]. The S1 and S3 layer fibrils are oriented at larger MFA angles compared to the S2 layers, thus are more perpendicular to the cellulose chain length direction, causing greater slippage deformation than the S2 layer [76]. The larger degree of deformation on the S1 and S3 layers leads to higher stress concentration in the S2 layer [74]. Therefore, CW might initially fail by S1/S2 layer interface debonding, resulting in the S2/S3 layers to withstand stress buildup. Consequently, carbohydrate covalent bond failure or ultimate stress yielding to a phenolic covalent bond failure occurs. It was suggested that [77] shear deformation is initially generated on the lignin-hemicellulose matrix, and the authors explained that the cellulose layers stick with each other firmly during deformation. On the other hand, beyond the proportionality limit, even if there is stress transfer between S1/S2/S3 cell wall layers, the S1/S2 interface debonding and separation causes the transfer of stresses to the S2/S3 layers [78]. Before the eventual failure of the S2 layer, the ultimate strength of the cell wall is thus dictated by the S2/S3 cell wall layer's capability to withstand further stress.

2.6 Composition-lodging correlations

From a materials property perspective, the mechanical strength of materials is determined by their chemical composition and microstructures. The composition and interaction between individual biopolymers of cell walls affect stem mechanical strength [79], yet little is known about the role of the major CW polymers (cellulose, hemicelluloses, and lignin), and other nonstructural components in lodging resistance in crops. Thus, understanding and evaluating the resistivity of stems against lodging from a CW composition standpoint is crucial, particularly for research aimed at genetic engineering of the CW to improve lodging resistance.

2.6.1 Lignin for lodging resistance

Lignin plays a vital role in the survival of terrestrial plants as it provides mechanical support, water transport, and defense against pathogens in plants [80]. For instance, it provides strength and rigidity to plant structures such as the xylem, sclerenchyma, and bundle sheath cells. The impact of lignin content reduction on plant fitness has been reviewed elsewhere [81]. Lignin forms a highly cross-linked network with other cell wall components and thus can be regarded as the "cellular glue" giving strength to the fibers and stiffness to the CW [82]. As a result, the deposition of lignin significantly

enhances the mechanical strength of CW [35]. There is a body of knowledge corroborating the contribution of lignin to the mechanical strength of plant CW. In relation to this, a study on biomechanics of plant stems revealed that lignin reduction results in a significant reduction in flexural modulus of elasticity (MOE) and modulus of rupture, (MOR) [83]. Gui et al. [84] found that the lodging resistance was significantly and positively correlated with lignin content. Moreover, Liu et al. [85] also studied 56 rice varieties with distinct cell wall compositions and reported that lignin was the predominant biopolymer that enhances lodging resistance. The authors also reported that lignin was directly correlated with the breaking force and stem wall thickness thereby improving rice lodging resistance by increasing the mechanical strength but negatively correlated with plant height. On the other hand, a recent study by Heuschele et al. [86] showed no correlation between lodging and cell wall components at the nodes and internodes of oat, wheat, and barley. Because of the complex nature and mode of loading variation from crop to crop, correlational analysis of cereal's CW composition with lodging for all cereals at the same time may not be viable option.

The glass transition (T_g) temperature and viscoelastic properties of lignin were reported to have a relation with composition and p-hydroxyphenyl to guaiacyl to syringyl (H/G/S) ratio [87]. The softening temperature of wood was found to decrease with the methoxyl content of lignin [88], suggesting that a high amount of methoxyl groups (higher S/G ratio) would decrease lignin glass transition temperature. As more methoxyl groups prevent covalent crosslinking, the polymer formed primarily from H monomers has a reduced tendency to react and forms more condensed C–C bonds [89] and is stiffer. Following this S-rich lignin (higher S/G ratio) would limit C–C cross-links, increase molecular mobility, and be expected to lower T_g. Biomasses with higher S/G ratio yield more depolymerization monomers [90] revealing easy depolymerization of S lignin. Horvath et al. reported that [91] reduced lignin content of different transgenic aspen exhibited lower T_g, but the S/G ratio did not change it. Li and McDonald [92] showed T_g was decreased with the S/G ratio of corn stover lignin. The inference that lignin with a condensed structure has higher glass transition suggests the lodging resistance could be impacted by the lignin composition. In this regard, Muhammad et al. [49] correlated lignin content and monomers composition to the breaking strength of wheat stems, and reported that stronger breaking strength was related to higher lignin content. Furthermore, a significant variation in lignin monomer composition (H, S, and G) was found between high and low-breaking strength stalks, whereby a reduction of S units by 27.6% was detected for the stronger stems. Concomitantly, H and G monomers for the stronger stalks were significantly increased respectively by 19.7% and 11.7%, causing a reduction of the S/G ratio by 16.8%. Another study by Li et al. [93] demonstrated that lignin content positively impacted lodging resistance in rice, where the G monomer had a predominant impact on loading resistant over S and H monomers. Similarly, Wei et al. [94]

demonstrated that lodging was significantly and positively correlated to the S/G ratio in rapeseed, suggesting that a smaller amount of S monomers (lower S/G ratio) and the greater amount of G monomers may play important roles in the determination of the breaking force, subsequently the lodging resistance. Another study in maize [95] revealed that H lignin and high ferulic acid content increase maize stalk strength and lodging resistance. The literature indicates that the lodging susceptibility of stalks may also be conditioned by the structural features of the cell wall. Although the mechanism underlying this correlation remains poorly understood and needs future elucidation, the positive impact of G and H monomers on lodging resistance and breaking strength could be associated with its inherent inter-unit linkage structures. It is known that G monomer-rich lignin is structurally more condensed than S lignin, due to C–C linkages (β-5 and 5–5), which are absent in S lignin due to the unavailability and occupation of 5 position with methoxyl (─OCH_3) group [96]. S lignin oxidizes more easily than G lignin due to the presence of more susceptible β-O-4 linkages. Contrary to this, G monolignol can be more easily polymerized than S as it can form more diverse cross-linkages. This property might influence its role in lodging. However, further investigation is needed for the relation between mechanical strength and lignin monomer composition and condensed C-C lignin linkages such as β-5 and 5–5.

Ahmad et al. [97] also reported that lignin content was positively associated with breaking strength, and negatively correlated with lodging rate, whereby the higher lignin content considerably enhanced the lodging resistance in the internode of wheat. It was also pointed out that activities of lignin biosynthesis enzymes such as phenylalanine ammonial-yase (PAL), peroxidase (POD), tyrosine ammonialyase (TAL), 4-coumarate: CoA ligase (4CL), and cinnamyl alcohol dehydrogenase (CAD) had a positive relationship with lignin content and lodging resistance at the basal internodes of maize [98], [99]. Another study on winter wheat by Zheng et al. [100] reported a positive significant correlation ($r = 0.97$) between lignin content and culm-breaking strength. Recently, Li et al. [101] demonstrated stalk lodging resistance, mechanical strength, and lignin accumulation were found to increase significantly with lignin synthesis-related enzyme activities (PAL, POD, 4CL, and CAD). In the same report, lignin monomers (H, G, and S) were reported to have significant contributions to lodging resistance. The enzymes PAL, TAL, CAD, POD, and 4CL are key enzymes involved in the lignin biosynthesis pathway. This suggests that lignin biosynthesis enzyme activities have imperative roles in dictating the lignin content and structures, which implies their contribution to enhancing the lodging resistance of stalks [102]. Even though the correlation between lignin S/G ratio and stalk lodging of the cereal stalks is not extensively studied, some studies (shown in Table 2.3) showed that cereal stalks with higher S/G ratio are found to be more susceptible to lodging. This could be

attributed to the higher binding capacity of G (with a branched structure) over S (with a low degree of polymerization) to cellulose.

2.6.2 Structural carbohydrates and lodging resistance

Cellulose is the major load-bearing constituent polymer for the CW [31], as verified by the association of the brittleness of stalks with a lower cellulose content of the cell wall [58]. Cellulose content, MFA, and CI are the most important structural parameters that influence the mechanical properties of plant fibers [103], which in turn can affect the load-bearing and lodging properties of the cereal stalks. Crystalline cellulose has significantly better stiffness than amorphous constituents, thus stalks with high cellulose content and crystallinity are supposed to be mechanically strong. However, there is a trade-off between rigidity and flexibility; where the rigidity of cellulose fibers improves with increasing crystallinity, whereas their flexibility decreases. Cereal stalks need to be stiffer and flexible at the same time to be lodging resistant, thus, the role of cellulose crystallinity on the lodging resistance of stalks is confusing and open for further investigation.

In barley, the cellulose content of the “nonbrittle” strain was significantly higher than the “brittle” strain [58], suggesting the contribution of cellulose to the mechanical strength of the culm. Besides, the maximum bending stress, at which the culm was broken, was significantly and positively correlated with the cellulose content. A study by Tan et al. [104] also supports the role of cellulose in enhancing stem strength, where low cellulose content displayed a significant reduction in stem strength. A study [60] reported that stalk bending strength was strongly associated with lodging incidence, which implies the influence of cellulose on lodging resistance. A recent study on maize also shows [105] internode breaking resistance increases with cellulose content. A study on soybean [106] also revealed that lower cellulose content exacerbated lodging thus resulting in a higher rate of lodging. Similarly to this, cellulose content was reported to have a positive relationship with the breaking strength of wheat stalks [49], contrarily the same study showed that hemicellulose content was reported to hurt the cell wall breaking strength. Kokubo et al. [58] stressed the role of cellulose content in the mechanical properties of the cell walls of barley culms. However, the result failed to show if the significant strength variations are associated with the structure of cellulose, such as CI and MFA, as low cellulose contents in the culm might indicate a low level of crystallinity or higher MFA. For pure cellulose fibers, increasing crystallinity is related to greater strength, whereas decreasing crystallinity means increasing elongation.

However, some results regarding the role of cellulose and hemicellulose are inconsistent and contradictory. It was reported [85] that cellulose and hemicellulose contents were not correlated with lodging resistance in rice. A recent study [107] also reported that none of the major CW structural

carbohydrates (cellulose and hemicellulose) in maize has an impact on lodging. Likewise, among four genotypes of wheat studied by Kong and co-workers [108], lodging resistance was not significantly correlated to cellulose contents in three of the cultivars, while other morphological characteristics such as stem width, were reported to have a significant impact on lodging. These inconsistent results might be due to the inherent genetic differences between the genotypes used in different studies.

The DP of cellulose, molar mass, plays a crucial role in the mechanical properties of the cell wall. It was found that [109], mutation of wild-type rice resulted in a significant reduction of cellulose DP and crystallinity, and an improved lodging resistance character. It is possible that cellulose synthesis and/or biosynthesis of a direct substrate for cellulose synthesis could be impaired during mutation. However, it is not clear how the disordered orientation of cellulose fibrils improves lodging resistance, or possibly the flexibility of stalks is more important than their stiffness for short stalks like rice. Furthermore, the impact of crystallinity on lodging resistance is not clearly understood and extensively studied in cereal stalks. For example research on rice [93] showed that lodging increases with the crystallinity index of cellulose fibers, but another study reported that crystallinity correlated positively with the stalk strength of wheat [49]. The results summarized in Table 2.3 show this gap. Generally, the association of mechanical strength and lodging resistance to cellulose structural features is not yet extensively elucidated and open for further investigation.

2.6.3 Other contributing factors

In addition to the major cell wall components, the effect of other minor chemical constituents on lodging resistance has been appraised. Esechie et al. [110] studied the relationship of stalk chemical composition to lodging resistance in maize and reported that lodging was negatively correlated with total non-structural carbohydrate (TNC), protein, and potassium, revealing that maize stalks with higher TNC, protein, and potassium are lodging resistant. Similar reports were indicated for TNC in sorghum, but protein and potassium were not significantly affecting the lodging resistance of the stalk [111]. However, TNC content could be an indication of the healthiness and vigor of the stalk than defining lodging resistance. The cell wall of rice [112] was investigated and reported that silica content was found to be significantly higher in lodging resistant than lodging susceptible types. The same study also showed that ash content was positively correlated to the lodging resistance of the rice stalks. Yet, the use of higher nitrogen fertilizer in rice and wheat significantly reduced the mechanical strengths (breaking strength and bending stress) of stalks and the lodging resistance by reducing lignin biosynthesis [97], [113]. It was reported that the application of higher nitrogen fertilizer decreased lignin deposition in the SCW of the sclerenchyma cells and vascular bundle cells compared to low nitrogen treatments, whereas cellulose deposition was not significantly altered [113]. As

nutrients are essential for the growth and development of plants, this finding could be an indication of how trace nutrients are affecting lignin and carbohydrate biosynthesis. Therefore, the impacts of trace nutrients on lodging are possibly related to their enhancement/inhibition of lignin and carbohydrate accumulation in the secondary cell walls than their direct effect on lodging.

Table 2.3. Summary of literature on the correlation of cell wall compositions, structural features, nutrient elements, and minerals to the stalk lodging resistance of different cereal crops. The correlations are significantly positive (Positive), significantly negative (Negative), Not significant (NS), and uninvestigated (—) to lodging resistance

Cereal	Cultivar Name	Country	Cel.	Lignin	Hemi.	TNC	CI	MFA	S/G	Others	Ref.
Sorghum	Sorghum	US	NS	Positive	NS	Positive	—	—	—	—	[114]
	Bmr-12	China	—	NS	—	—	—	—	—	—	[115]
	BMR, and others	US	—	NS	—	—	—	—	—	—	[116]
	LR, LS	US	—	—	—	Positive	—	—	—	Positive (K)	[111]
Oat	Brisasu and 7 others	Brazil	NS	NS	NS	—	—	—	—	—	[117]
	LENA and others	China	Positive	Positive	Positive	Positive	—	—	—	—	[118]
Maize or Corn	LI68, Q1261, others	China	NS	NS	NS	—	—	—	—	—	[107]
	Gibberella & Diplodia	US	Negative	NS	—	—	—	—	—	Negative (ash)	[119]
	Exotic	Oman	—	Positive	—	Positive	—	—	—	NS (K)	[120]
	ZD958 and XY335	China	Positive	Positive	—	—	—	—	—	—	[121]
	—	Greek	NS	NS	NS	—	—	—	—	NS (N, K, Na)	[122]
	Dongnong 253	China	Positive	Positive	Positive	—	—	—	—	—	[123]
	LR and LS	US	—	—	—	—	—	—	—	Negative (ash & K)	[124]
	Maize		Positive	Positive	Positive	Negative	—	—	—	—	[125]
	B73 and 11 others	Spain	NS	Positive (H lignin)	NS	—	—	—	Negative	—	[95]
	B14A/H95 and others	US	NS	Negative	NS	—	—	—	—	—	[60]
	DH605 and XD20	China	—	Positive & also (H, G, S)	—	—	—	—	Negative	Positive (PAL, CAD, 4CL, POD)	[101]

Table 2.3 (continued).

Rice	KongYu131 & others	China	None	Positive	None	–	–	–	–	–	**[85]**
	bp1		Positive	–	Negative	–	–	–	–	–	**[126]**
	fc17	China	Negative	Positive	–	–	Negative	–	–	–	**[127]**
	DSRAL	Philippines	–	NS	–	–	–	–	–	–	**[128]**
	Osfc16		Negative	–	–	–	Negative	–	–	–	**[109]**
	Ben 250 and 4 others	China	–	–	–	–	–	Negative	–	–	**[129]**
	S1 and Koshihikari	Japan	NS	NS	–	–	–	–	–	NS (Si), Positive (Starch)	**[130]**
	indica LY084 and japonica WYJ23	China	–	NS	–	–	–	–	–	Positive (Sta) NS (P, K), negative (Si)	**[131]**
	OsSUS3 and others	China	Positive	NS	Positive	–	Negative	–	–	–	**[132]**
Wheat	HC and WH	China	Positive	Positive (H, G contents)	Negative	–	Positive	–	Negative	Positive (Si)	**[49]**
	Pastor and others	Mexico	Positive	Positive	–	–	–	–	–	NS(K)	**[133]**
	BN AK58	China	–	–	–	–	Positive	–	–	–	**[134]**
	HD-2329, Raj-4014 &C-306	India	Positive	Positive	Positive	–	–	–	–	Positive (K, Ca, Mg, Si)	**[135]**
	XNSX**,** CS	China	NS	NS	–	–	–	–	–	–	**[108]**
	CK and PB	China	–	Positive	–	–	–	–	–	Positive (PAL, TAL, CAD, 4CL)	**[102]**
	Tartary buckwheat	China	–	Positive	–	–	–	–	–	–	**[136]**
	JM22 and SN16	China	–	Positive	–	–	–	–	–	Positive (PAL, TAl, POD)	**[137]**
	Yangmai 20	China	Positive	Positive	–	–	–	–	–	NS (Si), Positive (WSC/N ratio)	**[138]**

Table 2.3 (continued).

Millet	Yugu 18 and others	China	Positive	None	–	–	–	–	–	–	**[139]**
	FC1 (Paspalum scrobiculatum L.)	India	Positive	Positive	Positive	–	–	–	–	–	**[140]**
Barley	Astor, Scarlett and Jaran	Croatia	–	Positive	–	–	–	–	–	–	**[141]**
	Brittle and non-brittle	Japan	Positive	–	NS	–	–	–	–	–	**[58]**
	T1, S1 and others	China	–	Positive (H, G, S contents)	–	–	–	–	–	–	**[142]**

H, G & S are respectively p-hydroxyphenyl, Guacyl, and Syringyl.; Cel. –Cellulose content; Hemi. – Hemicellulose content; TNC– non-structural carbohydrate; CI– crystallinity index; MFA– microfibril angle; PAL – phenylalanine ammonialyase; CAD– cinnamyl alcohol dehydrogenase; 4CL– 4-coumarate-CoA ligase; POD– peroxidase; TAL – tyrosine ammonia-lyase; WSC– water soluble carbohydrate; N–Nitrogen; Ca–Calcium; K– Potassium; Mg – magnesium; P – Phosphorus and Na– Sodium; Si– Silicon; Sta–starch.

The relationship between lodging resistance and constituents of the CW in cereal crops has been extensively investigated, summarized in Table 2.3. In one way or the other, the CW components affect the lodging of stalks. Significant compositional differences between lodging-resistant and susceptible varieties have been found in most of the cereal crop stalks. However, consistent relationships with CW composition, relevant to a complete array of varieties differing in lodging resistance, have not been discovered (Table 2.3). The most marked and significant CW component related to lodging resistance is lignin. The results regarding the lignin content of the cereal stalks are mostly corroborating that lignin significantly enhanced lodging resistance. Especially in wheat and corn, the literature points to a significant positive correlation with lodging resistance, which is ascribed to its molecular and physiological function to stiffen the cell wall. Cellulose is the main load-bearing component of the CW and was comprehensively studied in most cereals, except in sorghum and barley. The notion that cellulose content enhances lodging resistance is well supported by the cereal literature. Among the main CW components, the role of hemicellulose on lodging resistance remains little explored. Consequently, the relationship between hemicellulose contents and lodging resistance of stalks is still unclear as consistent correlations were not reported. Meanwhile, there are only a few trials aimed at correlating the strength of the stalk with the CW composition in cereals like barely, millet, and sorghum. The development of a lodging-resistant cultivar requires a comprehensive understanding of the role of enzyme activities, which dictates the lignin and structural carbohydrate biosynthesis pathway. However, only a few literatures related to lignin enzymatic activities are reported (Table 2.3). The relationships between lodging with cellulose (structural and supramolecular features), and lignin (structural, compositional, linkage, and enzymatic activities) in the basal internodes remained unexplored. Nutrient and mineral contents in the basal internodes have been found to be associated with lodging resistance in certain cases, nevertheless, the results are inconsistent and sometimes even contradictory.

It is reported that MFA is one of the main supramolecular parameters defining the mechanical properties such as MOE and MOR, in the wood [143]. For instance, Huang et al. [129] investigated the correlation of the mechanical properties of rice stem to its cellulose MFA and found that the tensile modulus and strength of rice stem were decreasing with an increase in MFA. As the mechanical property of the stalks is an indicator of lodging behavior, the ultrastructural parameters of cellulose in the cell wall might be an important factor affecting the lodging resistance of cereal crops. However, as can be seen in Table 2.3, structural features of cellulose (MFA, CI) and lignin (Monomer’s composition, polydispersity, S/G, linkages) are the least investigated parameters affecting the mechanical strength of stalks. Thus, in connection with lodging, exploring the effect of supramolecular parameter of cellulose and structural features of lignin should be paid attention.

Practically, studying the effect of structural polymer interactions on lodging is quite challenging. However, molecular simulations and models developed for composite materials could help to understand the synergistic effect of lignin-cellulose-hemicellulose interactions.

2.7 Lodging and digestibility paradigm

Biomass recalcitrance and plant lodging are two complex traits that tightly associate with plant cell wall structure and features [132]. The recalcitrance of biomass in broader terms is defined as "those features of biomass which disproportionately increase energy requirements in conversion processes, increase the cost and complexity of operations in the biorefinery, and/or reduce the recovery of biomass carbon into desired products" [144]. Biomass recalcitrance to enzymatic hydrolysis due to the heterogeneous and multi-scale structure of plant cell walls is the major obstacle to the efficient valorization of biomass to biofuels [145]. Enhanced enzymatic digestibility of the lignocellulosic biomass on the other hand is a requirement for reducing the cost of pretreatment. Engineering and modifying plant cell walls by altering the major CW constituents and features (lignin, cellulose, hemicelluloses, and cellulose microfibrils) and molecular interactions between them; have been suggested as a strategy to overcome the enzymatic digestibility problem [146]. This strategy is mainly focused on changing lignin content and structure, lignin–carbohydrate complexes, and cellulose-related supramolecular properties. As a result, the modification of plant cell walls to reduce lignocellulose recalcitrance and enhance biomass saccharification has been a hot research area aimed at developing reliable and digestible lignocellulosic biomass for biofuel production. In line with this, lignin reduction and/or structural alteration has been shown to reduce biomass recalcitrance and improve cell wall digestibility [147]. In connection with this, lignin and cellulose reduction of crop stalks are likely to become susceptible to lodging, thus the lodging-digestibility trade-off is a great challenge for developing dual-purpose crops. For instance, the reduction of two features of cellulose (DP and crystallinity) in rice [109] through mutation have significantly increased enzymatic saccharification. As stem-based lodging is a crucial yield-limiting factor for cereal crops [139], digestible stems might suffer from low yield. On the other hand, systematic attention has been given to the development of dual-purpose crops recently: high-yielding grain, and digestible forage (i.e., easily digestible by enzymes and converted to biofuel) through breeding. Crops grown for dual-purpose applications should endow simultaneously high grain and stalk yields, low lodging susceptibility, and high conversion efficiency [148]. But increased digestibility is characteristically associated with low structural strength and a tendency for lodging [149]. There is a wide perception that as digestibility is negatively correlated with lodging resistance, breeding to reduce stem lodging through greater stem stiffness could result in modified anatomical features of the stem that reduce

biomass digestibility [150]. The digestibility of stalks can be influenced by varying the composition of lignin, cellulose, and hemicellulose in the cell wall. Related to this, breeding with reduced lignin content has been suggested for enhanced digestibility. The lignin content modification and its effect on forage digestibility have been summarized by Li et al. [151]. On the other hand, lignin content reduction has been strongly associated with a reduction in the mechanical stiffness of crop stalks. The trade-off between lodging resistance and digestibility has been noted in the literature [150]. Since susceptibility to lodging is highly related to grain yield and quality reduction [4], the development of dual food-bioenergy crops with higher grain yield and digestibility seemed challenging.

As lodging affects not only the grain yield but also stalk quality, research on genetic modification of plant cell walls, to enhance biomass digestibility/reduce recalcitrance for optimized biofuels production, should focus on identifying key genomic factors altering the plant cell wall without compromising the strength of the plant. Even though genetic modification of plant cell walls can potentially reduce recalcitrance and enhance biomass saccharification, it could be challenging to sustain both reduced recalcitrance and enhanced lodging resistance traits at the same time.

2.8 Summary and perspectives

This review aimed to evaluate the effect of CW composition on stalk lodging and highlight the key CW entities that contribute to the structural integrity of the stalk. Developing lodging-resistant and high-yielding crops is challenging and a comprehensive understanding of the biochemical and physiological pathways behind the development of stronger plant phenotypes is needed. However, the molecular mechanisms of plant lodging resistance remain largely uninvestigated. Lodging-inducing factors such as meteorological, pathological/biological, nutrient levels, morphological, anatomical, and biochemical composition of the CW and the interactions of all these factors make lodging one of the complex multi-scale phenomena in the sphere of agronomy. Thus, lodging cannot simply be assayed by one single or few factors due to the complex and still unknown interactions between these parameters. The complexity of the plant cell wall and the exact effects of its polymers on crop lodging resistance remain subtle. However, genetic analysis combined with compositional and environmental factors could help to better understand lodging traits. The materials property concept “structure determines the properties” can be applied to the lodging susceptibility of crop cell walls to investigate the structure-property relationships of the stalks and develop governing models and principles. Hence for future developments, the integration and analysis of a large amount of data using different machine learning algorisms could assist in developing more complex models and predicting the behavior of lodging. In this context, different imaging techniques of cell walls, and an understanding of structural features at the cellular level might be essential to acquire the underlying

mechanisms of lodging at the molecular level. In addition, “bottom-up” or “top-down” mechanisms integrated with cell wall structure and organization could help to enlighten the lodging phenomenon. As one of the most complex natural nanostructures, employing all technological advancements can be an effective way of understanding the cell wall component interactions and their effect on the lodging mechanism.

Genetic modification of cell walls and breeding have been proposed and implemented as a mechanism to improve the digestibility of lignocellulosic biomasses. However, because of the complexity of the plant cell wall, the exact effect on lodging resistance is not yet studied in energy crops such as sorghum. Thus, the correlation between lodging resistance and biomass digestibility needs to be fully explored, otherwise, it could lead to counterproductive findings. In addition, the underlying mechanisms for the formation of strong cell walls of cereals have not been widely studied. Although the effect of lignin content and cellulose on lodging have relatively been extensively studied, the correlation of lodging to their structures, composition, and linkages remains unexplored in most cereal crops. For example, S/G ratio, DP, and CI are highly regarded as supramolecular parameters affecting the stalk stiffness. Nevertheless, the direct relationship between their interaction with the strength of the stalk and lodging is virtually uninvestigated. The other limitation frequently observed in the literature is that identification of lodging-prone varieties is relayed on the assessment of mechanical properties conducted in laboratories. Such assessments may not provide a clear picture, thus evaluation of lodging based on direct field observations is suggested.

2.9 Reference

[1] D. U. Shah, T. P. Reynolds, and M. H. Ramage, “The strength of plants: theory and experimental methods to measure the mechanical properties of stems,” Journal of Experimental Botany, vol. 68, no. 16, pp. 4497–4516, Oct. 2017.

[2] M. E. Gáspár and P. Csermely, “Rigidity and flexibility of biological networks,” Briefings in Functional Genomics, vol. 11, no. 6, pp. 443–456, Nov. 2012.

[3] M. Neenan and J. L. Spencer-Smith, “An analysis of the problem of lodging with particular reference to wheat and barley,” The Journal of Agricultural Science, vol. 85, no. 3, pp. 495–507, 1975.

[4] P. M. Berry et al., “Understanding and Reducing Lodging in Cereals,” Advances in Agronomy, vol. 84, pp. 217–271, 2004.

[5] W. Long et al., “Deciphering the Genetic Basis of Lodging Resistance in Wild Rice Oryza longistaminata,” Frontiers in Plant Science, vol. 0, p. 628, May 2020.

[6] J. Huang, W. Liu, F. Zhou, Y. Peng, and N. Wang, “Mechanical properties of maize fibre bundles and their contribution to lodging resistance,” Biosystems Engineering, vol. 151, pp. 298–307, Nov. 2016.

[7] L. Erndwein, D. D. Cook, D. J. Robertson, and E. E. Sparks, “Field-based mechanical phenotyping of cereal crops to assess lodging resistance,” Applications in Plant Sciences, vol. 8, no. 8, Aug. 2020.

[8] M. J. Pinthus, “Lodging in Wheat, Barley, and Oats: The Phenomenon, its Causes, and Preventive Measures,” Advances in Agronomy, vol. 25, no. C, pp. 209–263, Jan. 1974.

[9] D. D. Du and J. Wang, “Research on mechanics properties of crop stalks: A review,” International Journal of Agricultural and Biological Engineering, vol. 9, no. 6, pp. 10–19, 2016.

[10] L. J. Gibson, “The hierarchical structure and mechanics of plant materials,” Journal of The Royal Society Interface, vol. 9, no. 76, pp. 2749–2766, Nov. 2012.

[11] C. Fan et al., “Ectopic expression of a novel OsExtensin-like gene consistently enhances plant lodging resistance by regulating cell elongation and cell wall thickening in rice,” Plant Biotechnology Journal, vol. 16, no. 1, pp. 254–263, Jan. 2018.

[12] P. Sarkar, E. Bosneaga, and M. Auer, “Plant cell walls throughout evolution: towards a molecular understanding of their design principles,” Journal of Experimental Botany, vol. 60, no. 13, pp. 3615–3635, Sep. 2009.

[13] B. Zhang, Y. Gao, L. Zhang, and Y. Zhou, “The plant cell wall: Biosynthesis, construction, and functions,” Journal of Integrative Plant Biology, vol. 63, no. 1, pp. 251–272, Jan. 2021.

[14] S. Pattathil, M. G. Hahn, B. E. Dale, and S. P. S. Chundawat, “Insights into plant cell wall structure, architecture, and integrity using glycome profiling of native and AFEXTM-pre-treated biomass,” Journal of Experimental Botany, vol. 66, no. 14, pp. 4279–4294, Jul. 2015.

[15] S. Pattathil et al., “Cell Wall Ultrastructure of Stem Wood, Roots, and Needles of a Conifer Varies in Response to Moisture Availability,” Frontiers in Plant Science, vol. 0, p. 882, Jun. 2016, doi: 10.3389/FPLS.2016.00882.

[16] A. J. Bidhendi and A. Geitmann, “Relating the mechanics of the primary plant cell wall to morphogenesis,” Journal of Experimental Botany, vol. 67, no. 2, pp. 449–461, Jan. 2016, doi: c.

[17] A. C. O’Sullivan, “Cellulose: the structure slowly unravels,” Cellulose 1997 4:3, vol. 4, no. 3, pp. 173–207, Jun. 1997.

[18] R. L. Silveira, S. R. Stoyanov, S. Gusarov, M. S. Skaf, and A. Kovalenko, “Plant biomass recalcitrance: Effect of hemicellulose composition on nanoscale forces that control cell wall strength,” Journal of the American Chemical Society, vol. 135, no. 51, pp. 19048–19051, Dec. 2013.

[19] K. Nishitani and T. Demura, “An Emerging View of Plant Cell Walls as an Apoplastic Intelligent System,” Plant and Cell Physiology, vol. 56, no. 2, pp. 177–179, Feb. 2015.

[20] D. J. Cosgrove, “Growth of the plant cell wall,” Nature Reviews Molecular Cell Biology 2005 6:11, vol. 6, no. 11, pp. 850–861, Nov. 2005.

[21] A. Endler and S. Persson, “Cellulose Synthases and Synthesis in Arabidopsis,” Molecular Plant, vol. 4, no. 2, pp. 199–211, Mar. 2011.

[22] J. R. Barnett and V. A. Bonham, “Cellulose microfibril angle in the cell wall of wood fibres,” Biological reviews of the Cambridge Philosophical Society, vol. 79, no. 2, pp. 461–472, May 2004.

[23] M. Sorieul, A. Dickson, S. J. Hill, and H. Pearson, “Plant Fibre: Molecular Structure and Biomechanical Properties, of a Complex Living Material, Influencing Its Deconstruction towards a Biobased Composite,” Materials, vol. 9, no. 8, pp. 1–36, Jul. 2016.

[24] I. Burgert, “Exploring the micromechanical design of plant cell walls,” American journal of botany, vol. 93, no. 10, pp. 1391–1401, 2006.

[25] R. E. Booker and J. Sell, “The nanostructure of the cell wall of softwoods and its functions in a living tree,” Holz als Roh- und Werkstoff 1998 56:1, vol. 56, no. 1, pp. 1–8, 1998.

[26] L. Donaldson, “Microfibril angle: Measurement, variation and relationships - A review,” IAWA Journal, vol. 29, no. 4, pp. 345–386, 2008.

[27] C. Chen and L. Hu, “Nanoscale Ion Regulation in Wood-Based Structures and Their Device Applications,” Advanced Materials, vol. 33, no. 28, p. 2002890, 2021, doi: 10.1002/adma.202002890.

[28] U. P. Agarwal, “Raman imaging to investigate ultrastructure and composition of plant cell walls: Distribution of lignin and cellulose in black spruce wood (Picea mariana),” Planta, vol. 224, no. 5, pp. 1141–1153, Oct. 2006.

[29] C. Chen et al., “Structure–property–function relationships of natural and engineered wood,” Nat Rev Mater, vol. 5, no. 9, Art. no. 9, Sep. 2020, doi: 10.1038/s41578-020-0195-z.

[30] J. E. WINANDY and R. M. ROWELL, “The Chemistry of Wood Strength,” in The Chemistry of Solid Wood, vol. 207, Advances in Chemistry, 1984, pp. 211–255. doi: 10.1021/BA-1984-0207.CH005.

[31] S. Rongpipi, D. Ye, E. D. Gomez, and E. W. Gomez, “Progress and Opportunities in the Characterization of Cellulose – An Important Regulator of Cell Wall Growth and Mechanics,” Frontiers in Plant Science, vol. 0, p. 1894, Mar. 2019.

[32] C. M. Lee, J. D. Kubicki, B. Fan, L. Zhong, M. C. Jarvis, and S. H. Kim, “Hydrogen-Bonding Network and OH Stretch Vibration of Cellulose: Comparison of Computational Modeling with Polarized IR and SFG Spectra,” Journal of Physical Chemistry B, vol. 119, no. 49, pp. 15138–15149, Dec. 2015.

[33] L. Donaldson, “Cellulose microfibril aggregates and their size variation with cell wall type,” Wood Science and Technology, vol. 41, no. 5, pp. 443–460, Jun. 2007.

[34] T. A. Tabet and F. A. Aziz, “Cellulose Microfibril Angle in Wood and Its Dynamic Mechanical Significance,” Cellulose - Fundamental Aspects, Aug. 2013.

[35] L. Q, L. L, and Z. L, “Lignins: Biosynthesis and Biological Functions in Plants,” International journal of molecular sciences, vol. 19, no. 2, Feb. 2018.

[36] J. C. Del Río, J. Rencoret, A. Gutiérrez, T. Elder, H. Kim, and J. Ralph, “Lignin Monomers from beyond the Canonical Monolignol Biosynthetic Pathway: Another Brick in the Wall,” ACS Sustainable Chemistry & Engineering, vol. 8, no. 13, pp. 4997–5012, Apr. 2020.

[37] X. Kang, A. Kirui, M. C. Dickwella Widanage, F. Mentink-Vigier, D. J. Cosgrove, and T. Wang, “Lignin-polysaccharide interactions in plant secondary cell walls revealed by solid-state NMR,” Nature Communications 2019 10:1, vol. 10, no. 1, pp. 1–9, Jan. 2019.

[38] M. Özparpucu, N. Gierlinger, I. Cesarino, I. Burgert, W. Boerjan, and M. Rüggeberg, “Significant influence of lignin on axial elastic modulus of poplar wood at low microfibril angles under wet conditions,” Journal of Experimental Botany, vol. 70, no. 15, pp. 4039–4047, Aug. 2019.

[39] J. L. Ferrer, M. B. Austin, C. Stewart, and J. P. Noel, “Structure and function of enzymes involved in the biosynthesis of phenylpropanoids,” Plant Physiology and Biochemistry, vol. 46, no. 3, pp. 356–370, Mar. 2008.

[40] S. R. Verma and U. N. Dwivedi, “Lignin genetic engineering for improvement of wood quality: Applications in paper and textile industries, fodder and bioenergy production,” South African Journal of Botany, vol. 91, pp. 107–125, Mar. 2014.

[41] J. C. Del Río, J. Rencoret, P. Prinsen, Á. T. Martínez, J. Ralph, and A. Gutiérrez, “Structural characterization of wheat straw lignin as revealed by analytical pyrolysis, 2D-NMR, and reductive cleavage methods,” Journal of Agricultural and Food Chemistry, vol. 60, no. 23, pp. 5922–5935, Jun. 2012.

[42] L. Z. Huang, M. G. Ma, X. X. Ji, S. E. Choi, and C. Si, “Recent Developments and Applications of Hemicellulose From Wheat Straw: A Review,” Frontiers in Bioengineering and Biotechnology, vol. 9, p. 440, Jun. 2021.

[43] J. Berglund et al., “Wood hemicelluloses exert distinct biomechanical contributions to cellulose fibrillar networks,” Nature Communications 2020 11:1, vol. 11, no. 1, pp. 1–16, Sep. 2020.

[44] R. M. Rowell, R. Pettersen, J. S. Han, J. S. Rowell, and M. A. Tshabalala, “Cell wall chemistry,” Handbook of wood chemistry and wood composites. Boca Raton, Fla. : CRC Press, 2005: pages 35-74., 2005.

[45] N. Giummarella, Y. Pu, A. J. Ragauskas, and M. Lawoko, “A critical review on the analysis of lignin carbohydrate bonds,” Green Chemistry, vol. 21, no. 7, pp. 1573–1595, Apr. 2019.

[46] H. Yi and V. M. Puri, “Contributions of the mechanical properties of major structural polysaccharides to the stiffness of a cell wall network model,” American Journal of Botany, vol. 101, no. 2, pp. 244–254, Feb. 2014.

[47] K. Houston, M. R. Tucker, J. Chowdhury, N. Shirley, and A. Little, “The Plant Cell Wall: A Complex and Dynamic Structure As Revealed by the Responses of Genes under Stress Conditions,” Frontiers in Plant Science, vol. 0, no. AUG2016, p. 984, Aug. 2016.

[48] Q. Zheng et al., “Pretreatment of wheat straw leads to structural changes and improved enzymatic hydrolysis,” Scientific Reports 2018 8:1, vol. 8, no. 1, pp. 1–9, Jan. 2018.

[49] A. Muhammad et al., “Survey of wheat straw stem characteristics for enhanced resistance to lodging,” Cellulose, vol. 27, no. 5, pp. 2469–2484, Mar. 2020.

[50] K. Raveendran, A. Ganesh, and K. C. Khilar, “Influence of mineral matter on biomass pyrolysis characteristics,” Fuel, vol. 74, no. 12, pp. 1812–1822, Dec. 1995.

[51] H. A. M. Saeed, Y. Liu, L. A. Lucia, and H. Chen, “Sudanese agro-residue as a novel furnish for pulp and paper manufacturing,” BioResources, vol. 12, no. 2, pp. 4166–4176, May 2017.

[52] M. Dong et al., “Pretreatment of sweet sorghum straw and its enzymatic digestion: insight into the structural changes and visualization of hydrolysis process,” Biotechnology for Biofuels 2019 12:1, vol. 12, no. 1, pp. 1–11, Nov. 2019.

[53] R. C. Sun, J. M. Fang, and J. Tomkinson, “Delignification of rye straw using hydrogen peroxide,” Industrial Crops and Products, vol. 12, no. 2, pp. 71–83, Aug. 2000.

[54] Y. Tamaki and G. Mazza, “Measurement of structural carbohydrates, lignins, and micro-components of straw and shives: Effects of extractives, particle size and crop species,” Industrial Crops and Products, vol. 31, no. 3, pp. 534–541, May 2010.

[55] M. Lara-Serrano, S. Morales-delaRosa, J. M. Campos-Martín, and J. L. G. Fierro, “Fractionation of lignocellulosic biomass by selective precipitation from ionic liquid dissolution,” Applied Sciences (Switzerland), vol. 9, no. 9, May 2019.

[56] X. Zhao, J. Chen, F. Chen, X. Wang, Q. Zhu, and Q. Ao, “Surface characterization of corn stalk superfine powder studied by FTIR and XRD,” Colloids and Surfaces B: Biointerfaces, vol. 104, pp. 207–212, Apr. 2013.

[57] J. M.-F. Johnson, N. W. Barbour, and S. L. Weyers, “Chemical Composition of Crop Biomass Impacts Its Decomposition,” Soil Science Society of America Journal, vol. 71, no. 1, pp. 155–162, Jan. 2007.

[58] K. A, K. S, and S. N, “Culm strength of barley : correlation among maximum bending stress, cell wall dimensions, and cellulose content,” Plant physiology, vol. 91, no. 3, pp. 876–882, Nov. 1989.

[59] D. Chuanren, W. Bochu, W. Pingqing, W. Daohong, and C. Shaoxi, “Relationship between the minute structure and the lodging resistance of rice stems,” Colloids and Surfaces B: Biointerfaces, vol. 35, no. 3–4, 2004.

[60] R. S. Sekhon, C. N. Joyner, A. J. Ackerman, C. S. McMahan, D. D. Cook, and D. J. Robertson, “Stalk Bending Strength is Strongly Associated with Maize Stalk Lodging Incidence Across Multiple Environments,” Field Crops Research, vol. 249, Apr. 2020, doi: 10.1016/J.FCR.2020.107737.

[61] K. HIRANO, R. L. ORDONIO, and M. MATSUOKA, “Engineering the lodging resistance mechanism of post-Green Revolution rice to meet future demands,” Proceedings of the Japan Academy. Series B, Physical and Biological Sciences, vol. 93, no. 4, p. 220, 2017.

[62] K. Hirano et al., “Utilization of stiff culm trait of rice smos1 mutant for increased lodging resistance,” PLoS ONE, vol. 9, no. 7, Jul. 2014.

[63] M. S. Islam, S. Peng, R. M. Visperas, N. Ereful, M. S. U. Bhuiya, and A. W. Julfiquar, “Lodging-related morphological traits of hybrid rice in a tropical irrigated ecosystem,” Field Crops Research, vol. 101, no. 2, pp. 240–248, Mar. 2007.

[64] L. Gou, J. Huang, R. Sun, Z. Ding, Z. Dong, and M. Zhao, “Variation characteristic of stalk penetration strength of maize with different density-tolerance varieties,” Nongye Gongcheng Xuebao/Transactions of the Chinese Society of Agricultural Engineering, vol. 26, no. 11, pp. 156–162, Nov. 2010.

[65] Berry P.M, “Lodging Resistance in Cereals,” in Sustainable Food Production, W. C. B. A. Christou P., Savin R., Costa-Pierce B.A., Misztal I., Ed. Springer, New York, NY, 2013, pp. 1096–1110.

[66] P. M. Berry and J. Spink, “Predicting yield losses caused by lodging in wheat,” Field Crops Research, vol. 137, pp. 19–26, Oct. 2012.

[67] M. S. Zuber and M. S. Kang, “Corn lodging slowed by sturdier stalks,” Crops and Soils Magazine, vol. 30, no. 5, pp. 1–32, Jul. 1978.

[68] R. W. Elmore and R. B. Ferguson, “Mid-season stalk breakage in corn: Hybrid and environmental factors,” Journal of Production Agriculture, vol. 12, no. 2, pp. 293–299, 1999.

[69] Y. Wu, S. Wang, D. Zhou, C. Xing, Y. Zhang, and Z. Cai, “Evaluation of elastic modulus and hardness of crop stalks cell walls by nano-indentation,” Bioresource Technology, vol. 101, pp. 2867–2871, 2010.

[70] L. Al-Zube, W. Sun, D. Robertson, and D. Cook, “The elastic modulus for maize stems,” Plant Methods 2018 14:1, vol. 14, no. 1, pp. 1–12, Feb. 2018.

[71] C. J. Stubbs, Y. A. Oduntan, T. R. Keep, S. D. Noble, and D. J. Robertson, “The effect of plant weight on estimations of stalk lodging resistance,” Plant Methods, vol. 16, no. 1, pp. 1–18, Sep. 2020.

[72] K. E. Easterling, R. Harrysson, L. J. Gibson, and M. F. Ashby, “On the Mechanics of Balsa and Other Woods,” Source: Proceedings of the Royal Society of London. Series A, Mathematical and Physical Sciences, vol. 383, no. 1784, pp. 31–41, 1982.

[73] J. Keckes et al., “Cell-wall recovery after irreversible deformation of wood,” Nature Materials 2003 2:12, vol. 2, no. 12, pp. 810–813, Nov. 2003.

[74] D. Wang, L. Lin, F. Fu, and M. Fan, “The fracture mechanism of softwood via hierarchical modelling analysis,” Journal of Wood Science, vol. 65, no. 1, pp. 1–11, Dec. 2019.

[75] D. C. Adler and M. J. Buehler, “Mesoscale mechanics of wood cell walls under axial strain,” Soft Matter, vol. 9, no. 29, pp. 7138–7144, Jul. 2013.

[76] D. Wang, L. Lin, and F. Fu, “Deformation mechanisms of wood cell walls under tensile loading: a comparative study of compression wood (CW) and normal wood (NW),” Cellulose, vol. 27, no. 8, pp. 4161–4172, May 2020.

[77] K. Jin, Z. Qin, and M. J. Buehler, “Molecular deformation mechanisms of the wood cell wall material,” Journal of the Mechanical Behavior of Biomedical Materials, vol. 42, pp. 198–206, Feb. 2015.

[78] Khan Sbabeed, “Failure of Aspen Wood/Resorcinol-formaldehyde Adhesive Bond,” The University of New Brunswick, 2000.

[79] H. Vogler, D. Felekis, B. J. Nelson, and U. Grossniklaus, “Measuring the Mechanical Properties of Plant Cell Walls,” Plants, vol. 4, no. 2, p. 167, Jun. 2015.

[80] M. M. Campbell and R. R. Sederoff, “Variation in Lignin Content and Composition (Mechanisms of Control and Implications for the Genetic Improvement of Plants),” Plant Physiology, vol. 110, no. 1, pp. 3–13, Jan. 1996.

[81] J. F. Pedersen, K. P. Vogel, and D. L. Funnell, “Impact of reduced lignin on plant fitness,” Crop Science, vol. 45, no. 3, pp. 812–819, May 2005.

[82] E. M. Rubin, “Genomics of cellulosic biofuels,” Nature 2008 454:7206, vol. 454, no. 7206, pp. 841–845, Aug. 2008.

[83] S. L. Voelker, B. Lachenbruch, F. C. Meinzer, and S. H. Strauss, “Reduced wood stiffness and strength, and altered stem form, in young antisense 4CL transgenic poplars with reduced lignin contents,” New Phytologist, vol. 189, no. 4, pp. 1096–1109, Mar. 2011.

[84] M. Y. Gui et al., “Studies of the relationship between rice stem composition and lodging resistance,” Journal of Agricultural Science, vol. 156, no. 3, pp. 387–395, Apr. 2018.

[85] S. Liu, Y. Huang, H. Xu, M. Zhao, Q. Xu, and F. Li, “Genetic enhancement of lodging resistance in rice due to the key cell wall polymer lignin, which affects stem characteristics,” Breeding Science, vol. 68, no. 5, p. 508, 2018.

[86] D. J. Heuschele, K. P. Smith, and G. A. Annor, “Variation in Lignin, Cell Wall-Bound p-Coumaric, and Ferulic Acid in the Nodes and Internodes of Cereals and Their Impact on Lodging,” Journal of Agricultural and Food Chemistry, vol. 68, no. 45, pp. 12569–12576, Nov. 2020.

[87] A. G. M. Stephen Carter Fox, “CHEMICAL AND THERMAL CHARACTERIZATION OF THREE INDUSTRIAL LIGNINS AND THEIR CORRESPONDING LIGNIN ESTERS | Fox | BioResources,” BioResources, vol. 5, no. 2, 2010.

[88] A. M. Olsson and L. Salmén, “The effect of lignin composition on the viscoelastic properties of wood,” Nordic Pulp and Paper Research Journal, vol. 12, no. 3, pp. 140–144, Aug. 1997, doi: 10.3183/NPPRJ-1997-12-03-P140-144/HTML.

[89] A. Ziebell et al., “Increase in 4-Coumaryl Alcohol Units during Lignification in Alfalfa (Medicago sativa) Alters the Extractability and Molecular Weight of Lignin,” Journal of Biological Chemistry, vol. 285, no. 50, pp. 38961–38968, Dec. 2010, doi: 10.1074/JBC.M110.137315.

[90] E. M. Anderson et al., “Differences in S/G ratio in natural poplar variants do not predict catalytic depolymerization monomer yields,” Nature Communications 2019 10:1, vol. 10, no. 1, pp. 1–10, May 2019, doi: 10.1038/s41467-019-09986-1.

[91] P. P. Bbalazs Horvath and I. P. Charles Frazier, “Thermal softening of transgenic aspen ,” BioResources, vol. 6, no. 2, pp. 2125–2134, 2011.

[92] H. Li and A. G. McDonald, “Fractionation and characterization of industrial lignins,” Industrial Crops and Products, vol. 62, pp. 67–76, Dec. 2014, doi: 10.1016/J.INDCROP.2014.08.013.

[93] F. Li et al., “High-level hemicellulosic arabinose predominately affects lignocellulose crystallinity for genetically enhancing both plant lodging resistance and biomass enzymatic digestibility in rice mutants,” Plant Biotechnology Journal, vol. 13, no. 4, pp. 514–525, May 2015.

[94] L. Wei et al., “Genetic and transcriptomic analyses of lignin- and lodging-related traits in Brassica napus,” Theoretical and Applied Genetics 2017 130:9, vol. 130, no. 9, pp. 1961–1973, Jun. 2017.

[95] A. Manga-Robles et al., “Elucidating compositional factors of maize cell walls contributing to stalk strength and lodging resistance,” Plant Science, vol. 307, p. 110882, Jun. 2021.

[96] Y. Mottiar, R. Vanholme, W. Boerjan, J. Ralph, and S. D. Mansfield, “Designer lignins: harnessing the plasticity of lignification,” Current Opinion in Biotechnology, vol. 37, pp. 190–200, Feb. 2016.

[97] I. Ahmad et al., “Effects of uniconazole or ethephon foliar application on culm mechanical strength and lignin metabolism, and their relationship with lodging resistance in winter wheat,” Crop and Pasture Science, vol. 71, no. 1, pp. 12–22, Jan. 2020.

[98] I. Ahmad et al., “Uniconazole application strategies to improve lignin biosynthesis, lodging resistance and production of maize in semiarid regions,” Field Crops Research, vol. 222, pp. 66–77, Jun. 2018.

[99] M. Kamran et al., “Effect of paclobutrazol, a potential growth regulator on stalk mechanical strength, lignin accumulation and its relation with lodging resistance of maize,” Plant Growth Regulation 2017 84:2, vol. 84, no. 2, pp. 317–332, Nov. 2017.

[100] M. Zheng et al., “Manipulation of lignin metabolism by plant densities and its relationship with lodging resistance in wheat,” Scientific Reports 2017 7:1, vol. 7, no. 1, pp. 1–12, Feb. 2017.

[101] B. LI et al., “Lignin metabolism regulates lodging resistance of maize hybrids under varying planting density,” Journal of Integrative Agriculture, vol. 20, no. 8, pp. 2077–2089, Aug. 2021.

[102] M. Kamran, I. Ahmad, X. Wu, T. Liu, R. Ding, and Q. Han, “Application of paclobutrazol: a strategy for inducing lodging resistance of wheat through mediation of plant height, stem physical strength, and lignin biosynthesis,” Environmental Science and Pollution Research 2018 25:29, vol. 25, no. 29, pp. 29366–29378, Aug. 2018.

[103] S. R. Djafari Petroudy, “Physical and mechanical properties of natural fibers,” Advanced High Strength Natural Fibre Composites in Construction, pp. 59–83, Jan. 2017.

[104] H.-T. Tan et al., “Powerful regulatory systems and post-transcriptional gene silencing resist increases in cellulose content in cell walls of barley,” BMC Plant Biology 2015 15:1, vol. 15, no. 1, pp. 1–16, Feb. 2015.

[105] Y. Zhang et al., “Ethephon Improved Stalk Strength of Maize (Zea Mays L.) Mainly through Altering Internode Morphological Traits to Modulate Mechanical Properties under Field Conditions,” Agronomy 2019, Vol. 9, Page 186, vol. 9, no. 4, p. 186, Apr. 2019.

[106] W. Liu et al., “Relationship between cellulose accumulation and lodging resistance in the stem of relay intercropped soybean [Glycine max (L.) Merr.],” Field Crops Research, vol. 196, pp. 261–267, Sep. 2016.

[107] Y. Guo et al., “Identification of traits and genes associated with lodging resistance in maize,” The Crop Journal, Feb. 2021.

[108] E. Kong et al., “Anatomical and chemical characteristics associated with lodging resistance in wheat,” The Crop Journal, vol. 1, no. 1, pp. 43–49, Oct. 2013.

[109] F. Li et al., “OsCESA9 conserved-site mutation leads to largely enhanced plant lodging resistance and biomass enzymatic saccharification by reducing cellulose DP and crystallinity in rice,” Plant Biotechnology Journal, vol. 15, no. 9, p. 1093, Sep. 2017.

[110] H. A. Esechie, “Relationship of stalk morphology and chemical composition to lodging resistance in maize (Zea mays L.) in a rainforest zone,” J. agric. Sci., Camb, vol. 104, pp. 429–433, 1985.

[111] H. A. Esechie, J. W. Maranville, and W. M. Ross, “Relationship of Stalk Morphology and Chemical Composition to Lodging Resistance in Sorghum,” Crop Science, vol. 17, no. 4, pp. 609–612, Jul. 1977.

[112] S. Hasan, M. Shimojo, and I. Goto, “Chemical components influencing lodging resistance of rice plant and its straw digestibility in vitro,” Asian-Australasian Journal of Animal Sciences, vol. 6, no. 1, pp. 41–44, Mar. 1993.

[113] W. Zhang et al., “Nitrogen fertilizer application affects lodging resistance by altering secondary cell wall synthesis in japonica rice (Oryza sativa),” Journal of Plant Research, vol. 130, no. 5, pp. 859–871, Sep. 2017.

[114] V. R. Isbell, “The lodging complex in sorghum [Sorghum bicolor(L.) Moench] : morphological, chemical, and anatomical stem features associated with lodging in sorghum,” Texas A&M University. Libraries, 1992.

[115] Y. Li et al., “Acid detergent lignin, lodging resistance index, and expression of the caffeic acid O-methyltransferase gene in brown midrib-12 sudangrass,” Breeding Science, vol. 65, no. 4, pp. 291–297, Sep. 2015.

[116] B. W. Bean, R. L. Baumhardt, F. T. McCollum, and K. C. McCuistion, “Comparison of sorghum classes for grain and forage yield and forage nutritive value,” Field Crops Research, vol. 142, pp. 20–26, Feb. 2013.

[117] D. C. Silveira et al., “Anatomical traits and structural components of peduncle associated with lodging in Avena sativa L,” Agronomy Research, vol. 19, no. 1, pp. 250–264, 2021.

[118] R. Zhang, Z. Jia, X. Ma, H. Ma, and Y. Zhao, “Characterising the morphological characters and carbohydrate metabolism of oat culms and their association with lodging resistance,” Plant Biology, vol. 22, no. 2, 2020.

[119] M. S. Zuber, C. O. Grogan, M. E. Michaelson, C. W. Gehrke, and J. F. Monge, “Studies of the Interrelation of Field Stalk Lodging, Two Stalk Rotting Fungi, and Chemical Composition of Corn1,” Agronomy Journal, vol. 49, no. 6, pp. 328–331, Jun. 1957.

[120] H. A. Esechie, V. Rodriguez, and H. Al-Asmi, “Comparison of local and exotic maize varieties for stalk lodging components in a desert climate,” European Journal of Agronomy, vol. 21, pp. 21–30, Jun. 2004.

[121] Y. Yang et al., “Quantitative effects of solar radiation on maize lodging resistance mechanical properties,” Field Crops Research, vol. 255, p. 107906, Sep. 2020.

[122] E. Hondroyianni ; D.K. Papakosta; A.A. Gagianas; K.A. Tsatsarelis, “Corn stalk traits related to lodging resistance in two soils of differing salinity,” Maydica, vol. 45, no. 2, pp. 125–133, 2000.

[123] Fan HaiChao ; Gu WanRong ; Yang DeGuang ; Yu JuPing ; Piao Lin ; Zhang Qian ; Zhang LiGuo ; Yang XiuHong ; Wei Shi, “Effect of chemical regulators on physical and chemical properties and lodging resistance of spring maize stem in northeast China.,” Acta Agronomica Sinica, vol. 44, no. 6, pp. 909–919, 2018.

[124] M. S. Zuber and P. J. Loesch, “Total Ash and Potassium Content of Stalks as Related to Stalk Strength in Corn (Zea mays L.)1,” Agronomy Journal, vol. 58, no. 4, pp. 426–428, Jul. 1966.

[125] X. Wang et al., “Stalk architecture, cell wall composition, and QTL underlying high stalk flexibility for improved lodging resistance in maize,” BMC Plant Biology 2020 20:1, vol. 20, no. 1, pp. 1–12, Nov. 2020.

[126] Y. Zhang et al., “BRITTLE PLANT1 is required for normal cell wall composition and mechanical strength in rice,” Journal of Integrative Plant Biology, vol. 63, no. 5, pp. 865–877, May 2021.

[127] F. Li, S. Liu, H. Xu, and Q. Xu, “A novel FC17/CESA4 mutation causes increased biomass saccharification and lodging resistance by remodeling cell wall in rice,” Biotechnology for Biofuels 2018 11:1, vol. 11, no. 1, pp. 1–13, Nov. 2018.

[128] P. M. Nathaniel Marcelo, R. T. Tapic, and O. E. Manangkil, “Relationship of Culm Anatomy and Lodging Resistance in Rice (Oryza sativa L.) Genotypes under Direct-Seeded System,” International Journal of Agricultural Technology, vol. 13, no. 3, pp. 2367–2385, 2017.

[129] J. Huang, W. Liu, F. Zhou, and Y. Peng, “Effect of multiscale structural parameters on the mechanical properties of rice stems,” Journal of the Mechanical Behavior of Biomedical Materials, vol. 82, pp. 239–247, Jun. 2018.

[130] K. Ishimaru, E. Togawa, T. Ookawa, T. Kashiwagi, Y. Madoka, and N. Hirotsu, “New target for rice lodging resistance and its effect in a typhoon,” Planta 2007 227:3, vol. 227, no. 3, pp. 601–609, Oct. 2007.

[131] X. Zhao, N. Zhou, S. Lai, M. Frei, Y. Wang, and L. Yang, “Elevated CO2 improves lodging resistance of rice by changing physicochemical properties of the basal internodes,” Science of The Total Environment, vol. 647, pp. 223–231, Jan. 2019.

[132] C. Fan et al., “AtCesA8-driven OsSUS3 expression leads to largely enhanced biomass saccharification and lodging resistance by distinctively altering lignocellulose features in rice,” Biotechnology for Biofuels 2017 10:1, vol. 10, no. 1, pp. 1–12, Sep. 2017.

[133] S. C. Tripathi, K. D. Sayre, and J. N. Kaul, “Fibre Analysis of Wheat Genotypes and its Association with Lodging: Effects of Nitrogen Levels and Ethephon,” Cereal Research Communications 2003 31:3, vol. 31, no. 3, pp. 429–436, Dec. 2003.

[134] Fan WenXiu ; Hou YuXia ; Feng SuWei ; Zhu FangKun ; Ru ZhenGang, “Study on cellulose and lodging resistance of wheat straw,” Journal of Henan Agricultural Sciences, vol. 41, no. 9, pp. 31–34, 2012.

[135] S. R. Bhagat, K. P. ; Sairam, R. K. ; Deshmukh, P. S. ; Kushwaha, “Biochemical analysis of stem in lodging tolerant and susceptible wheat (Triticum aestivum L.) genotypes under normal and late sown conditions.,” Indian Journal of Plant Physiology, vol. 16, no. 1, pp. 68–74, 2011.

[136] D. Xiang et al., “Relationship between stem characteristics and lodging resistance of Tartary buckwheat (Fagopyrum tataricum),” Plant Production Science, vol. 22, no. 2, 2019.

[137] D. Peng et al., “Lodging resistance of winter wheat (Triticum aestivum L.): Lignin accumulation and its related enzymes activities due to the application of paclobutrazol or gibberellin acid,” Field Crops Research, vol. 157, pp. 1–7, Feb. 2014.

[138] M. Zhang et al., “Effect of nitrogen levels and nitrogen ratios on lodging resistance and yield potential of winter wheat (Triticum aestivum L.),” PLOS ONE, vol. 12, no. 11, Nov. 2017.

[139] B. H. Tian et al., “Characterization of culm morphology, anatomy and chemical composition of foxtail millet cultivars differing in lodging resistance,” Journal of Agricultural Science, vol. 153, no. 8, pp. 1437–1448, Nov. 2015.

[140] R. Sreeja, S. Balaji, L. Arul, A. Nirmala Kumari, J. R. Kannan Bapu, and A. Subramanian, “Association of lignin and FLEXIBLE CULM 1 (FC1) ortholog in imparting culm strength and lodging resistance in kodo millet (Paspalum scrobiculatum L.),” Molecular Breeding, vol. 36, no. 11, 2016.

[141] L. Begović, I. Abičić, A. Lalić, H. Lepeduš, V. Cesar, and D. Leljak-Levanić, “Lignin synthesis and accumulation in barley cultivars differing in their resistance to lodging,” Plant Physiology and Biochemistry, vol. 133, 2018.

[142] M. Yu, M. Wang, T. Gyalpo, and Y. Basang, “Stem lodging resistance in hulless barley: Transcriptome and metabolome analysis of lignin biosynthesis pathways in contrasting genotypes,” Genomics, vol. 113, no. 1, pp. 935–943, Jan. 2021.

[143] J. E. M. Treacy; A.N. Dhubháin, “The influence of microfibril angle on modulus of elasticity and modulus of rupture in four provenances of Irish grown Sitka spruce (Picea sitchensis (Bong.) Carr),” Journal of the Institute of Wood Science, vol. 15, no. 4, pp. 211–220, Dec. 2000.

[144] M. C. McCann and N. C. Carpita, “Biomass recalcitrance: A multi-scale, multi-factor, and conversion-specific property,” Journal of Experimental Botany, vol. 66, no. 14. 2015.

[145] A. Zoghlami and G. Paës, “Lignocellulosic Biomass: Understanding Recalcitrance and Predicting Hydrolysis,” Frontiers in Chemistry, vol. 7. 2019. doi: 10.3389/fchem.2019.00874.

[146] M. E. Himmel et al., “Biomass recalcitrance: Engineering plants and enzymes for biofuels production,” Science, vol. 315, no. 5813. 2007.

[147] M. Li, Y. Pu, and A. J. Ragauskas, “Current understanding of the correlation of lignin structure with biomass recalcitrance,” Frontiers in Chemistry, vol. 4, no. NOV. 2016.

[148] N. Gabbanelli et al., “Towards an ideotype for food-fuel dual-purpose wheat in Argentina with focus on biogas production,” Biotechnol Biofuels, vol. 14, p. 85, 2021.

[149] G. Von Forell, D. Robertson, S. Y. Lee, and D. D. Cook, “Preventing lodging in bioenergy crops: a biomechanical analysis of maize stalks suggests a new approach,” Journal of Experimental Botany, vol. 66, no. 14, pp. 4367–4371, Jul. 2015.

[150] T. J. Townsend, D. L. Sparkes, and P. Wilson, “Food and bioenergy: reviewing the potential of dual-purpose wheat crops,” GCB Bioenergy, vol. 9, no. 3, pp. 525–540, Mar. 2017.

[151] X. Li, J.-K. Weng, and C. Chapple, “Improvement of biomass through lignin modification,” The Plant Journal, vol. 54, no. 4, pp. 569–581, May 2008.

Chapter 3: Fatty Acid Profiles-Based Chemometrics to Differentiate Metabolic Variations in Sorghum

"Fatty Acid Profiles-Based Chemometrics to Differentiate Metabolic Variations in Sorghum." ***ACS Food Science & Technology,*** **vol. 1, no. 11, 2021, pp. 2127–2134**

3.1 Abstract

The extractives content and fatty acid profiles of Della and *REDforGREEN* (RG) Sorghum varieties grown in two different seasons have been evaluated. The stalk internodes and nodes were quantitatively extracted with CH_2Cl_2. The extracts were converted to their fatty acid methyl ester (FAME) derivatives and analyzed by GCMS. The main fatty acids detected were azelaic (C9:0), lauric acid (C12:0), myristic (C14:0), palmitic (C16:0), palmitoleic (C16:1), stearic (C18:0), oleic (C18:1), linoleic (C18:2), and eicosenoic (C20:1) acids. Fatty acids were considered as chemical descriptors of varieties to evaluate metabolic variations, where principal component analysis (PCA) and linear discriminant analysis (LDA) multivariate analysis methods were applied. LDA allowed discrimination between Della and RG varieties with higher prediction accuracy, suggesting the metabolic variations between them. The high predictive power suggests the use of fatty acid composition as fingerprint to reveal metabolic variations.

3.2 Introduction

Sorghum is a commonly produced crop used for grain, forage, and bioenergy [1,2]. Sorghum stalks are an important part of the crop that provides mechanical support to the shoot components [3]. The cell-wall of lignocellulosic materials is mainly composed of structural biopolymer components such as cellulose, hemicellulose, and lignin [4]. The cell wall compositions may vary considerably between species with respect to cellulose, hemicellulose, and lignin. The mechanical strength and rigidity of the cell wall are mainly attributed to the supramolecular structure between lignin, cellulose, hemicellulose, and proteins [5]. Moreover, the composition, structure, and interactions of the biopolymers play several functions such as delivering nutrients, stabilizing the cell structure, and creating a protective environment [6]. Additionally, there are also minor nonstructural components within the cell wall, such as extractives, ashes, and pectin. These components vary with species, tissue, maturity of plants, harvest times, and storage times, and are primarily affected by environmental conditions [7]. In lignocellulosic materials, lipophilic extractives are extracted using organic solvents such as CH_2Cl_2, ethanol, or acetone. The nonpolar extractives are composed of mainly fatty acids, resin acids, fatty acid esters [8]. The variations of extractive content from species to species is the basis of chemotaxonomy [6].

Breeding of the Sorghum crops has produced varieties that are easily digestible and produce more bioethanol. To serve different end-uses, institutions have developed several Sorghum varieties. The *REDforGREEN* (RG) is a bioenergy Sorghum mutant developed by plant breeders [9] through ethyl methane sulfonate (EMS) mutagenesis of the Della variety. The Sorghum stalks (Figure 3.1) and RG varieties were screened through leaf color variation [9], which is apparent in the stalks as well (Figure 3.1). In relation to color variation, studies in the wood [10,11] show a strong association between color and lipophilic extractive contents. The chemical composition of Sorghum stalks has been used as a useful tool to characterize and differentiate varieties [9,12]. It has also been reported that EMS-based mutation has significantly changed the fatty acid composition of different seeds [13–15]. Despite fatty acids of extracts from stems of Sorghum varieties have been published [16,17] the effect of EMS-based mutation on the fatty acids biosynthesis and the use of fatty acids as a fingerprint to trace the metabolic variations in Sorghum stalks are limited. Therefore, analysis of lipid fractions of extracts can be used as an alternative approach to reveal metabolic differences in the two Sorghum lines.

Figure 3.1. Sorghum stalks from Della and RG varieties grown over two different seasons.

As the composition of fatty acids of extractives depends on several factors such as variety and environmental factors, the objectives of this study were investigating the extractives content variation due to EMS-based mutation and growing season, identifying, and quantifying fatty acid composition of Della and RG Sorghum stalk varieties grown in two different seasons. In addition, fatty acid profile-based chemometrics was applied using principal component and linear discriminant analysis to differentiate the metabolic variations among the two lines of Sorghum.

3.3 Materials and methods

3.3.1 Plant materials

Two varieties of sweet Sorghum, Della and RG were grown in Lexington, KY in 2018 and 2019 to characterize the ability of non-structural fatty acid extractives to differentiate between Sorghum stalk features. Della is a common mid-season cultivar of sweet Sorghum well-adapted for Kentucky growing conditions and displays excellent drought tolerance and disease resistance to anthracnose pathogens [18]. Chemical mutagenesis using ethyl methane sulfonate (EMS) was used to generate the previously characterized Della-derived RG mutant [9]. Standard cultivation conditions were used to grow either variety to full physiological maturity across both years. Mature stalks were harvested using garden shears by cutting below the first elongated internode. Leaves and leaf sheaths were stripped from individual plants and stalks were partitioned into subsets of nodes and internodes labelled sequentially starting from the base of a stalk; Figure 3.2a below denotes the labelling convention used. In order to accumulate enough dry matter for testing, stalk subsection from 4-5 individual plants was pooled for each variety in both years and ground using a Thomas–Wiley mill to pass through a 1 mm screen. Prior to sample testing, residual moisture contents were determined using a HB43-S Halogen moisture analyzer (Mettler Toledo) and all subsequent analyses were performed across two technical replicates to ensure data reliability.

3.3.2 Extractive content

Ground biomass samples at each N (4.0 g) and IN (4.0 g) were Soxhlet extracted using CH_2Cl_2 (150 mL) for 16-18 h, in duplicate, and the extractive content was determined gravimetrically according to ASTM D1108-96.

3.3.3 Fatty acid composition

The lipid extracts (2 mg, in duplicate) were trans-esterified into fatty acid methyl ester (FAME) derivatives by heating in a sealed 5 mL Reacti-vial for 90 min at 90°C in a mixture of $CH_3OH/H_2SO_4/CHCl_3$ (1.7:0.3:2.0 v/v/v, 2 mL) as outlined by Osman et al [19]. $CHCl_3$ contained 1-naphthaleneacetic acid as an internal standard (200 μg mL^{-1}). The FAME derivatives were analyzed by GCMS (ISQ-Trace1300, ThermoScientific) equipped with a ZB-5 (30 m x 0.25 mm Ø, 0.25 μm coating, Phenomenex) capillary column at a temperature gradient of 40°C (1 min) to 320°C at 5°C min^{-1}. The eluted compounds were identified with authentic saturated and unsaturated fatty acid standards along with spectral matching to the NIST-2017 library.

3.3.4 Multivariate analysis

To evaluate variation among two variety samples, analysis of variance (ANOVA) was performed using Microsoft Excel 2016 at a 95% confidence level. Pearson correlation, linear discriminant analysis (LDA) and principal component analysis (PCA) have been performed using R-4.1.0 software based on 64 observations, 9 variables, two varieties (Della and RG) and four groups (Della1, RG1, Della2 and RG2). For LDA, samples were divided into training (70%) and test (30%) sets and scaled. Unless stated, all statistical comparisons of RG1 and RG2 are performed from Della1 and Della 2, respectively. In order to maintain the natural variation of the fatty acids along the stalk, the multivariate analysis was performed directly from GCMS detected concentrations.

3.3.4.1 Principal component analysis (PCA)

PCA is a linear transformation method used for dimensional reduction, data visualization, and the exploration of multivariate data. As an unsupervised classification method, PCA is projecting multidimensional data into lower dimensions with a minimal loss of information and produces new orthogonal variables called principal components (PC) which are obtained as linear combinations of the descriptors. Thus, PCA was employed to understand fatty acid compositional variations in Sorghum stalks.

3.3.4.2 Linear discriminant analysis (LDA)

LDA is a supervised machine learning technique that uses linear combinations of variables to build a model to classify multivariate data. LDA is intended to determine vectors that produce the maximum separation between classes by the projection of points from an original space [20]. Therefore, LDA was applied mainly for the discrimination of fatty acid compositions for groups based on a combination of variety and growing seasons (Della1, RG1, Della2, and RG2).

3.4 Results and discussion

The RG and Della Sorghum stalk N and IN samples (Figure 3.2a) were characterized for extractives and their lipids content to observe differences between varieties and tissue types.

3.4.1 Extractives yields

Extractives are non-structural components such as lipids, tannins, waxes, and aromatics [7]. The CH2Cl2 extractives yield were Della1 (38.0-61.3 mg/g), RG1 (13.6-27.9 mg/g), Della2 (11.8-27.9 mg/g), and RG2 (39.3-53.6 mg/g). Sorghum stalk INs and Ns are represented in Figure 3.2a. The ANOVA test showed that extractive content variation between INs and Ns was not significant in all varieties. The extractive content of each internode (IN1-IN4 and node (N1-N4) is given in Appendix Figure A1. On the other hand, Della1 has significantly more extractives than both RG1 and Della2,

whereas Della2 and RG1 have similar contents (Figure 3.2b). The results also revealed that the extractive content of RG2 is (46-310 %) more than Della2, but RG1 has (36-70%) less than Della1. Across the growing seasons, notable variations have also been recorded; Della1 has 36-200% more than Della2, while RG1 has 40-63% less extractives than RG2. Combined analysis of variance for the entire stalk showed no significant difference between extractive contents of Della2 and RG1. Extractive content inhomogeneity of the stalks may suggest metabolic variations in the varieties [21]. The variation of extractives in the same growing season reveals the effect of EMS mutation, on the other hand, variation across the growing season demonstrates the effect of season of growth on extractives, verified by literature [22]. Even though extractives constitute a minor fraction of the cell wall composition, they may have a profound role in determining the surface property of the cell walls [23]. Studies showed that extractives provide diffusion resistance towards the pith through the blocking of miniature passages in cell walls, and have antifungal and antioxidant properties to protect the cell wall against fungi and insects [24]. These functions combined with the smaller variation and distribution of extractives within the stalk may result in unique stalk behavior by defining stalk-environmental interaction and indicate a disparity in cell wall chemistry [23].

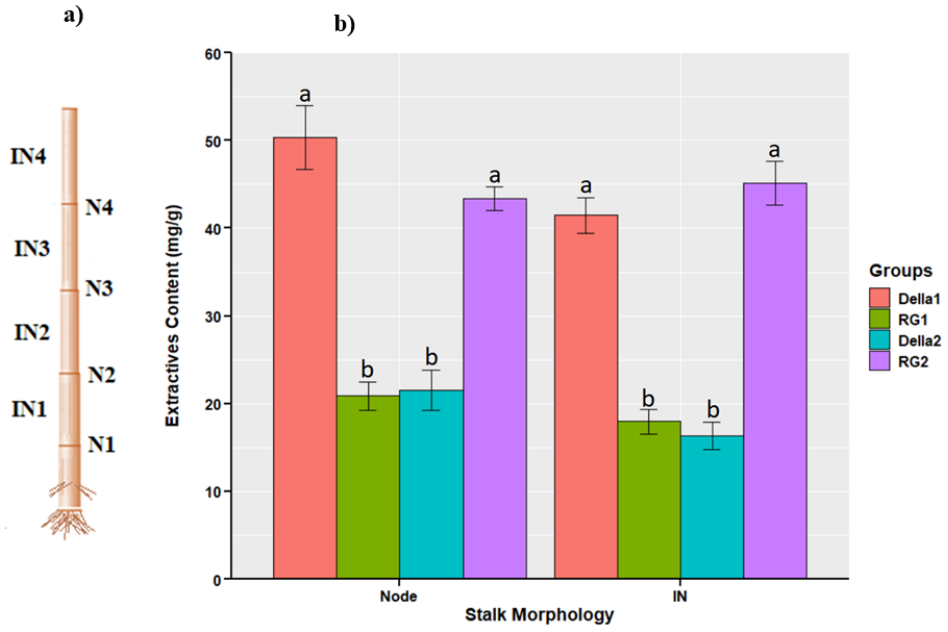

Figure 3.2. Sorghum stalk and extractive contents at Internodes and Nodes (a) Schematic depiction of Sorghum stalk and (b) average extractive content (mg/g dry biomass) for the Della1, RG1, Della2, and RG2 stalks at the nodes (N1-N4) and internodes (IN1-IN4. The same letters represent no significant difference.

3.4.2 Fatty acid composition analysis

Fatty acid profiles of Sorghum stalk tissue extracts were determined as FAME derivatives from stalk node and internode subsections; a representative chromatogram of a sample at IN3 is given in Figure 3.3. Retention times and detailed composition of the fatty acids at each node (N1-N4) and internode (IN1-IN4) for the two varieties in two different growing seasons are given in Appendix Table A1 and the averaged results are summarized and shown in Table 3.1. The main fatty acids identified were oleic (C18:1), linoleic (C18:2) and palmitic acids (C16:0). Trace amounts of azelaic (C9:0), lauric (C12:0), myristic (C14:0), palmitoleic (C16:1), stearic (C18:0) and eicosanoic (C20:0) acids were also detected. Azelaic acid is a di-acid.

The results were consistent with the literature [17], similar fatty acids were also detected in two different lines of Sorghum grains [25]. It was found that the axial concentration variation of fatty acids within the pool of stalks between the N and IN was not significant except for palmitoleic and linoleic acid. For palmitoleic acid, significant differences between N and IN were detected for Della1, Della2, and RG2. Similarly, linoleic acid variation across N and IN was significant for Della1. It is shown (Table 3.1) that fatty acids varied remarkably across varieties and growing seasons (Table 3.1), which could be an indication of metabolic variations.

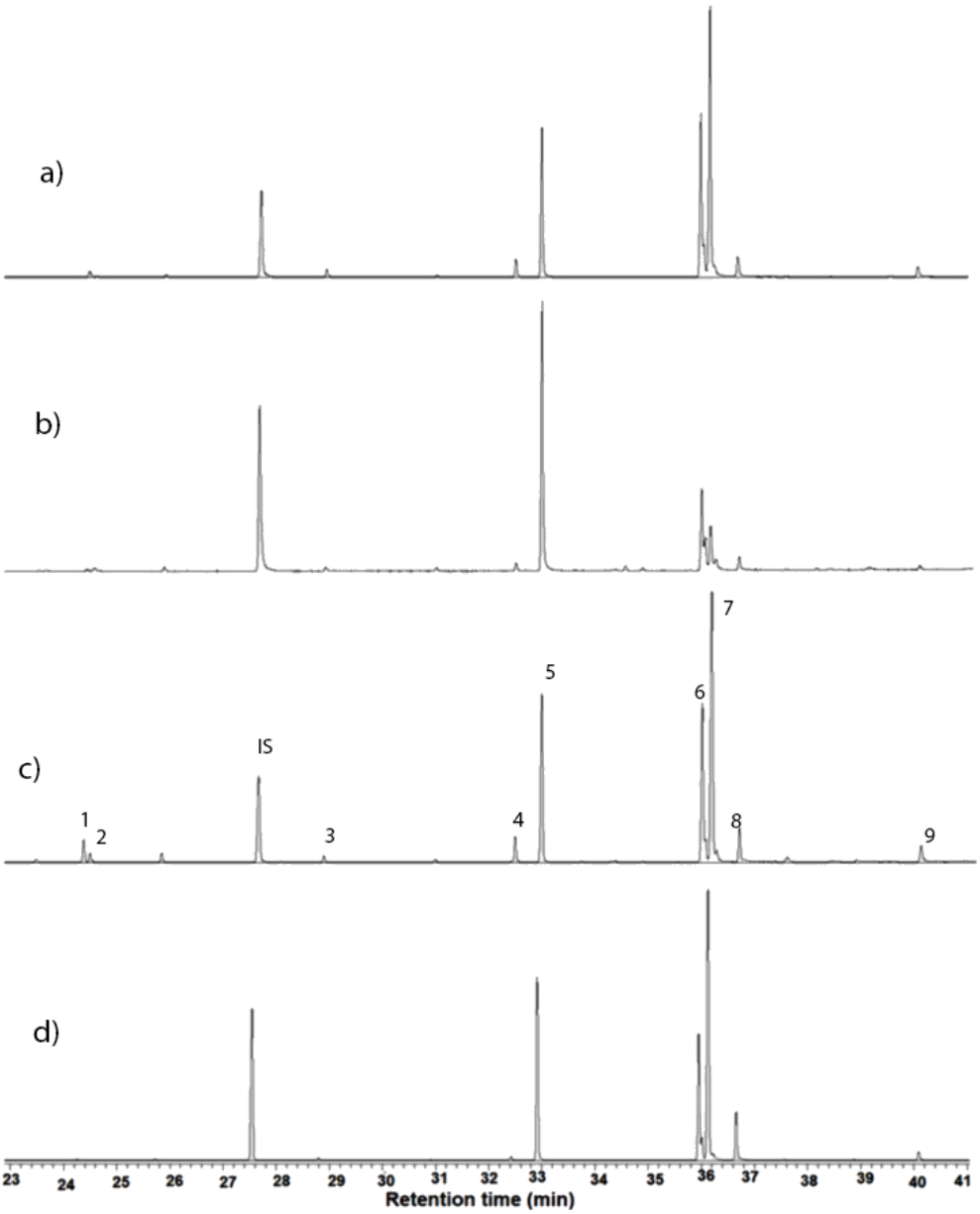

Figure 3.3. Representative of GC-MS chromatograms of fatty acid methyl esters from IN3 of a) Della 2, b) RG2, c) Della1 and d) RG1 Sorghum stalks. IS: internal standard, 1: lauric acid (C12:0), 2: azelaic acid (C9:0), 3: myristic acid (C14:0), 4: palmitoleic acid (C16:0), 6: linoleic acid (C18:2), 7: oleic acid (C18:1), 8: stearic acid (C18:0), and 9: eicosanoic acid (C20:0).

Table 3.1. Fatty acid concentrations of DCM extracts from Della1, RG1, Della2, and RG2 averaged at nodes (N1-N4) and internodes (IN1-IN4) in (mg/g of extract) determined by GCMS as FAME derivatives. Different letters represent significant differences in mean for each fatty acid at nodes and internodes for the varieties according to the Tukey HSD test from 8 samples.

Fatty Acid	M^+ (m/z)	RT (min)	Group	Internode (n=8)	Node (n=8)
			Della1	6.1±1.4^{a}	6.9±2.3^{a}
Lauric Acid	214	24.2	RG1	0.4± 0.0^{a}	1.0± 0.1^{a}
			Della2	20.0±6.0^{b}	3.0±1.0^{a}
			RG2	0.4±0.1^{a}	5.6±2.6^{a}
			Della1	3.3±0.4^{a}	4.1±0.5^{a}
Azelaic Acid	216	24.3	RG1	0.6±0.1^{bc}	1.2±0.2^{bc}
			Della2	0.8±0.3^{bc}	0.1±0.0^{c}
			RG2	0.7±0.2^{bc}	1.6±0.4^{b}
			Della1	1.7±0.2^{c}	2.2±0.2^{c}
Myristic Acid	242	28.7	RG1	1.3± 0.0^{c}	0.9± 0.1^{c}
			Della2	9.0±1.1^{a}	7.2±1.4^{ab}
			RG2	0.9±0.1^{c}	4.1±1.1^{bc}
			Della1	3.6±0.4^{cd}	9.4±1.5^{b}
Palmitoleic Acid	268	32.4	RG1	4.7±0.6^{bcd}	3.8±0.4^{cd}
			Della2	15.2±1.5^{a}	8.9±0.8^{b}
			RG2	1.6±0.1^{d}	8.1±2.0^{bc}
			Della1	54.4±2.3**c**	72.0±6.8^{c}
Palmitic Acid	270	32.8	RG1	62.8± 0.5**c**	81.9±8.6^{abc}
			Della2	112.2±9.4^{a}	108.7±10.9^{ab}
			RG2	73.6±2.8^{bc}	78.7±1.4^{abc}
			Della1	91.5±7.5^{cd}	154.7±15.7^{ab}
Linoleic Acid	294	34.7	RG1	48.7±1.0^{d}	51.1±8.6^{d}
			Della2	143.5±7.1^{ab}	172.6±15.8^{a}
			RG2	93.5±4.5^{cd}	120.4±16.9^{bc}
			Della1	151.4±5.7^{c}	250.7±19.5^{bc}
Oleic Acid	296	36.1	RG1	162.6±1.2^{c}	176.1±23.1^{c}
			Della2	404.3±27.1^{a}	423.1±55.6^{a}
			RG2	270.7±18.6^{bc}	335.4±43.7^{ab}
			Della1	10.3±0.7^{c}	14.9±1.3^{abc}
Stearic Acid	298	36.6	RG1	21.3±0.5^{bc}	13.9± 1.7^{bc}
			Della2	23.6±3.0^{ab}	26.5±3.2 ^{a}
			RG2	18.0±1.5^{ab}	22.7±3.9 ^{ab}
			Della1	9.2±0.8^{bc}	10.4±1.3^{bc}
Eicosanoic acid	326	40.0	RG1	5.4± 0.3^{c}	4.1± 0.7^{c}
			Della2	19.2±2.2^{a}	15.5±4.2^{ab}
			RG2	12.4±1.0^{abc}	8.5±1.6^{bc}

It is worth mentioning that oleic acid varied in concentration in Della1 (139-295 mg/g of extract), RG1(104-225 mg/g of extract), Della2 (298-537 mg/g of extract), and RG2 (233-449 mg/g of extract). Oleic acid is found in abundance in Sorghum grains [25]. Across the varieties, overall fatty acid concentration variations could be associated with a seasonal effect on the fatty acid composition [26] and/or the impact of the mutation on lipid biosynthesis [13,27].

For better visualization of the fatty acid compositional variation between N and IN within the same variety, axial variation along the stalk, and across the two varieties, mirror plots are given in Figure 3.4. It is shown that significant fatty acid compositional variation between Della and RG varieties within the same and different growing seasons have been detected. The C9:0 has significantly increased for Della in 2018 and Della varieties have more C14:0 and C18:2 than RG. The fatty acid compositional variation may be the metabolic differences between the two varieties and the impact of the growing seasons.

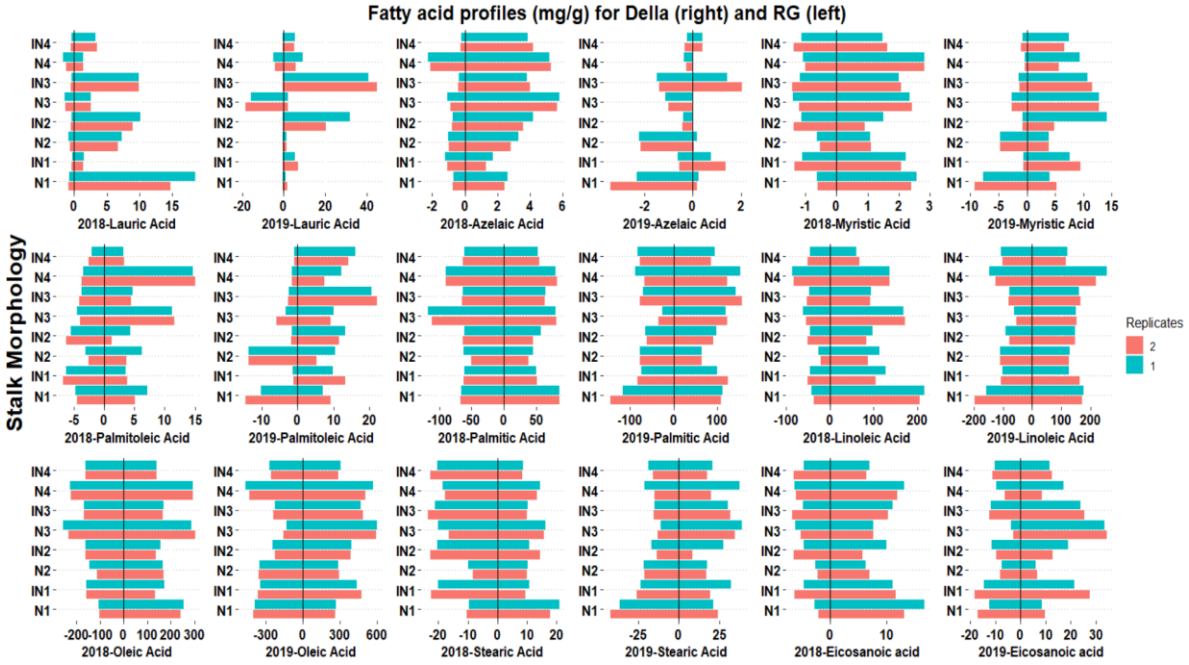

Figure 3.4. Mirror plots of fatty acid profiles for Della (right) and RG (left) varieties in mg/g at different internodes (IN) and nodes (N) across two growing seasons (2018 and 2019).

To understand the correlation of fatty acid accumulations in the stalks, Pearson correlational analysis was conducted, and the result is shown in Figure 3.5. The Pearson correlation coefficients between fatty acids showed that there was a better positive correlation between palmitic and oleic acids ($r = 0.82$, $p < 0.001$), myristic and eicosanoid acids ($r = 0.79$, $p < 0.001$), palmitic and stearic acids ($r = 0.75$, $p < 0.001$), oleic acid and linoleic acids ($r = 0.76$, $p < 0.001$) which reveals the increasing of one fatty acid with the other. Detailed correlation coefficient values are shown in Figure 3.5, and most of the fatty acid concentrations are positively correlated. However, no correlation was observed between azelaic and all other fatty acids, except with stearic acid as shown in Figure 3.5.

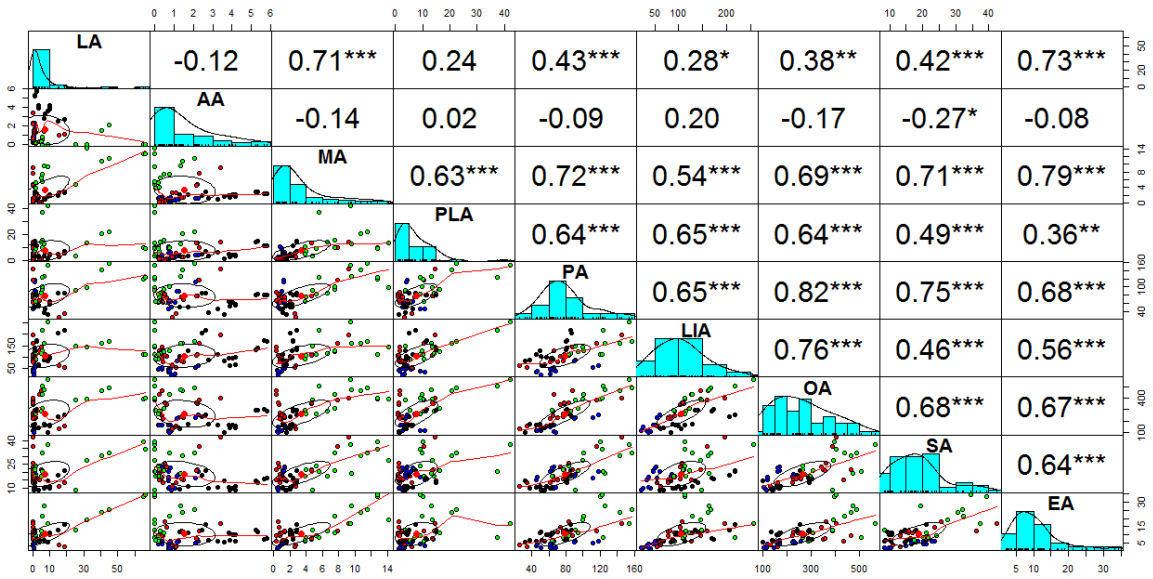

Figure 3.5. Scatter plots and Pearson correlation of fatty acid profiles from Sorghum stalks. LA: lauric acid, AA: azelaic acid, MA: myristic acid, PLA: palmitoleic acid, LIA: linoleic acid, OA: oleic acid, SA: stearic acid, and EA: eicosanoic acid. The symbols *, **, and *** correspond to significances at $p<0.05$, $p<0.01$, and $p<0.001$, respectively.

3.4.2.1 Principal component analysis (PCA)

PCA was applied to the data matrix generated from GC-MS of extracts from nodes (N1-N4) and internodes (IN1- IN4) in duplicates for Della 1, RG1, Della 2, and RG2 with a total of 64 observations with nine fatty acids (descriptors) and classed based on variety and groups (Figure 3.6). The analysis based on variety (Figure 3.6a, Della and RG) and groups (Figure 3.6b, Della1, RG1, Della2, RG2) showed that about 57.5% and 14.9% of the total metabolic variation was explained by the first and second principal components (PC1 and PC2) respectively, and 81.6% was explained by the first three components. The scores plot obtained from Eigen analysis of the covariance matrix of scaled data for the first two principal components demonstrates the data distribution of the two Sorghum varieties along the two axes.

It is shown (Figure 3.6a) that most RG varieties are contributing towards positive PC2 and negative PC1, which indicates the possibility of discriminating the Sorghum varieties based on their fatty acid compositions.

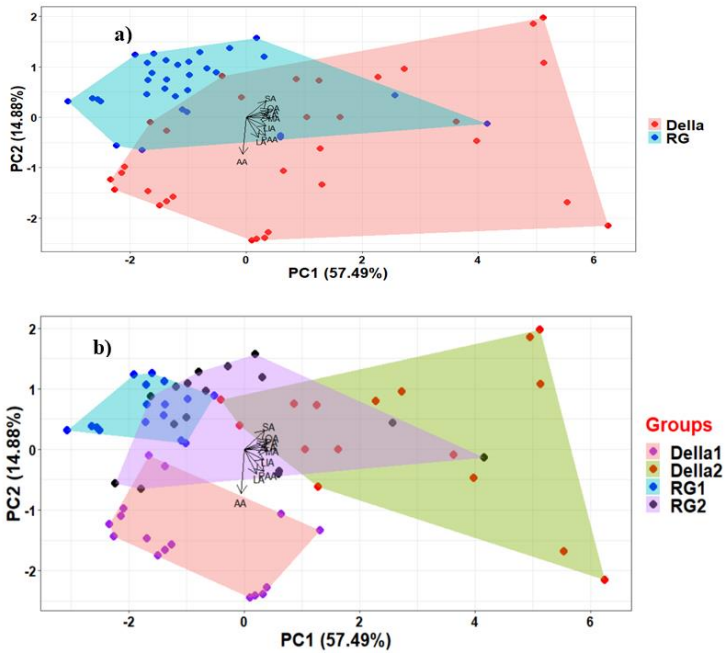

Figure 3.6. Principal components a) based on variety, b) based on groups

Table 3.2. Eigen analysis of the correlation matrix loadings of principal components (PC1 – PC4)

Fatty acid	PC1	PC2	PC3	PC4
LA	0.21	-0.41	0.74	-0.25
AA	-0.06	-0.73	-0.49	0.09
MA	0.40	-0.02	0.18	0.23
PAA	0.33	-0.36	0.07	0.56
PA	0.39	0.10	-0.14	0.11
LIA	0.34	-0.17	-0.32	-0.54
OA	0.39	0.16	-0.16	-0.25
SA	0.35	0.32	-0.15	0.35
EA	0.37	0.04	-0.01	-0.27

LA: lauric acid; AA: Azelaic acid; MA: Myristic acid; PLA: Palmitoleic acid; LIA: Linoleic acid; OA: Oleic acid; SA: Stearic acid; and EA: Eicosanoic acid.

3.4.2.2 Linear discriminant analysis (LDA)

The LDA model was developed using the training set consisting of 45 samples, while 19 samples were used for validating the predictive properties of the model. The biplot of the LDA model developed from the scaled data set of the fatty acid composition of Sorghum varieties is shown (Figure 3.7). It is shown that the model classified the groups with LD1 of about 64.4% and LD2 of 31.5%. The average accuracy for the prediction was found to be 97.6%. The high predictive power for the classification suggests the possibility of cultivar classification based on fatty acid profiles, which can be used to reveal metabolic variations in the stems. The LDA, besides corroborating the fatty acid compositional variation of each group, also indicates the possibility of classifying sorghum

stalks by fatty acid-based chemometrics. Findings showed the use of LDA of fatty acid composition as a fingerprint to identify among different cultivars [28]. The classification of groups with higher accuracy based on their fatty acid composition confirms the significant fatty acid profile variation between the varieties due to growing seasons and the mutational effect, which ultimately influences metabolic activities. Besides, the result also implies that the color variation on the stalks might associate with the variation in the extractives and their corresponding fatty acids. LDA has been applied to determine the geographical origin of hazelnuts based on their fatty acid compositions [29]. Fatty acids-based discrimination of the varieties also indicates the possibility of applying compositional chemometrics for evaluating metabolic variations.

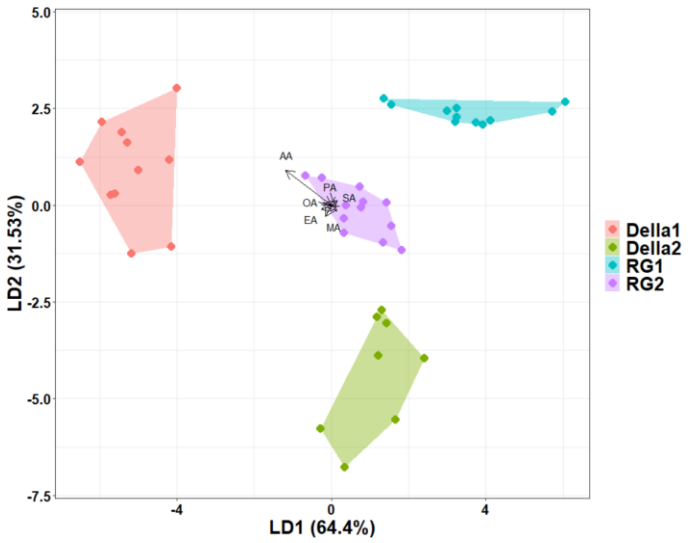

Figure 3.7. Biplot of linear discriminant analysis for the fatty acid composition from Della1, RG1, Della2, and RG2 stalks. AA: Azelaic acid, MA: Myristic acid, PLA: Palmitoleic acid, LIA: Linoleic acid, SA: Stearic acid, and EA: Eicosanoic acid.

3.5 Conclusions

The research result suggests that the analytical GC of fatty acid data combined with chemometric approaches can be employed to provide information on the anticipated metabolic and compositional differences among the Sorghum lines. The result also shows clear fatty acid compositional variation among the lines of the stalks which could be attributed to seasonal changes and chemical-induced mutation. The higher prediction accuracy of the LDA model also corroborates those fatty acids that can be used as fingerprints and descriptors to reveal metabolic changes, which could be associated with seasonal change and the impact of EMS-induced mutation.

3.6 References

[1] J. Mullet et al., “Energy Sorghum—a genetic model for the design of C4 grass bioenergy crops,” J. Exp. Bot., vol. 65, no. 13, pp. 3479–3489, Jul. 2014, doi: 10.1093/jxb/eru229.

[2] J. Xia, Y. Zhao, P. Burks, M. Pauly, and P. J. Brown, “A sorghum NAC gene is associated with variation in biomass properties and yield potential,” Plant Direct, vol. 2, no. 7, p. e00070, 2018, doi: 10.1002/pld3.70.

[3] B. Bakeer, I. Taha, H. El-Mously, and S. Shehata, “On the characterisation of structure and properties of sorghum stalks,” Ain Shams Eng. J., vol. 4, pp. 265–271, Jun. 2013, doi: 10.1016/j.asej.2012.08.001.

[4] M. Sorieul, A. Dickson, S. J. Hill, and H. Pearson, “Plant Fibre: Molecular Structure and Biomechanical Properties, of a Complex Living Material, Influencing Its Deconstruction towards a Biobased Composite,” Materials, vol. 9, no. 8, Jul. 2016, doi: 10.3390/ma9080618.

[5] Y. Zeng, M. E. Himmel, and S.-Y. Ding, “Visualizing chemical functionality in plant cell walls,” Biotechnol. Biofuels, vol. 10, Nov. 2017, doi: 10.1186/s13068-017-0953-3.

[6] R. M. Rowell, R. Pettersen, J. S. Han, J. S. Rowell, and M. A. Tshabalala, “Cell Wall Chemistry,” p. 42.

[7] B. H. Davison, J. Parks, M. F. Davis, and B. S. Donohoe, “Plant Cell Walls: Basics of Structure, Chemistry, Accessibility and the Influence on Conversion,” in Aqueous Pretreatment of Plant Biomass for Biological and Chemical Conversion to Fuels and Chemicals, C. E. Wyman, Ed. Chichester, UK: John Wiley & Sons, Ltd, 2013, pp. 23–38. doi: 10.1002/9780470975831.ch3.

[8] R. C. Sun and J. Tompkinson, “Comparative study of organic solvent and water-soluble lipophilic extractives from wheat straw I: yield and chemical composition,” J. Wood Sci., vol. 49, no. 1, pp. 0047–0052, Feb. 2003, doi: 10.1007/s100860300008.

[9] C. Petti et al., “Sorghum mutant RG displays antithetic leaf shoot lignin accumulation resulting in improved stem saccharification properties,” Biotechnol. Biofuels, vol. 6, no. 1, p. 146, Oct. 2013, doi: 10.1186/1754-6834-6-146.

[10] R. Moya, R. S. Fallas, P. J. Bonilla, and C. Tenorio, “Relationship Between Wood Color Parameters Measured by the CIELab System and Extractive and Phenol Content in Acacia mangium and Vochysia guatemalensis from Fast-Growth Plantations,” Molecules, vol. 17, no. 4, pp. 3639–3652, Mar. 2012, doi: 10.3390/molecules17043639.

[11] J. Klumpers, G. Janin, M. Becker, and G. Lévy, “The influences of age, extractive content and soil water on wood color in oak: the possible genetic determination of wood color,” Ann. Sci. For., vol. 50, no. Supplement, pp. 403s–409s, 1993, doi: 10.1051/forest:19930746.

[12] J. Wang, M. Wang, H. Spiertz, Z. Liu, L. Han, and G. Xie, “Genetic variation in yield and chemical composition of wide range of sorghum accessions grown in north-west China,” Res. Crops, vol. 14, pp. 95–105, Mar. 2013.

[13] D. W. James and H. K. Dooner, “Isolation of EMS-induced mutants in Arabidopsis altered in seed fatty acid composition,” Theor. Appl. Genet., vol. 80, no. 2, pp. 241–245, Aug. 1990, doi: 10.1007/BF00224393.

[14] S. Tang et al., “Development and screening of EMS mutants with altered seed oil content or fatty acid composition in Brassica napus,” Plant J., vol. 104, no. 5, pp. 1410–1422, 2020, doi: https://doi.org/10.1111/tpj.15003.

[15] S. Hadebe, A. T. Modi, A. Hugo, and H. A. Shimelis, “Seed oil content and fatty acid composition response to ethyl methanesulphonate mutagenesis in vernonia,” South Afr. J. Plant Soil, vol. 36, no. 5, pp. 375–380, Oct. 2019, doi: 10.1080/02571862.2019.1631399.

[16] K. L. Christiansen, C. L. Weller, V. L. Schlegel, S. L. Cuppett, and T. P. Carr, “Extraction and Characterization of Lipids from the Kernels, Leaves, and Stalks of Nine Grain Sorghum Parent Lines,” Cereal Chem., vol. 84, no. 5, pp. 463–470, 2007, doi: https://doi.org/10.1094/CCHEM-84-5-0463.

[17] M. C. Burnett and R. L. Lohmar, “Lipides in Feedstuffs, Fatty Acids of Sorghum Leaf and Stem,” May 01, 2002. https://pubs.acs.org/doi/pdf/10.1021/jf60100a012 (accessed Jul. 19, 2020).

[18] N. B. Osman, A. G. McDonald, and M.-P. G. Laborie, “Analysis of DCM extractable components from hot-pressed hybrid poplar,” Holzforschung, vol. 66, no. 8, pp. 927–934, Dec. 2012, doi: 10.1515/hf-2012-0011.

[19] L. A. Berrueta, R. M. Alonso-Salces, and K. Héberger, “Supervised pattern recognition in food analysis,” J. Chromatogr. A, vol. 1158, no. 1, pp. 196–214, Jul. 2007, doi: 10.1016/j.chroma.2007.05.024.

[20] C. L. Williams, T. L. Westover, R. M. Emerson, J. S. Tumuluru, and C. Li, “Sources of Biomass Feedstock Variability and the Potential Impact on Biofuels Production,” BioEnergy Res., vol. 9, no. 1, pp. 1–14, Mar. 2016, doi: 10.1007/s12155-015-9694-y.

[21] H. P. Dahm, “On the seasonal variation of the extractives content of Spruce.,” Sven. Papperstidning, vol. 73, no. 19, pp. 613–8, 1970.

[22] J. Routa, H. Brännström, P. Anttila, M. Mäkinen, J. Jänis, and A. Asikainen, “Wood extractives of Finnish pine, spruce and birch – availability and optimal sources of compounds,” p. 57.

[23] R. C. Pettersen, “The Chemical Composition of Wood,” in The Chemistry of Solid Wood, vol. 207, R. Rowell, Ed. Washington, DC: American Chemical Society, 1984, pp. 57–126. doi: 10.1021/ba-1984-0207.ch002.

[24] K. Liu, “Comparison of Lipid Content and Fatty Acid Composition and Their Distribution within Seeds of 5 Small Grain Species,” J. Food Sci., vol. 76, no. 2, pp. C334–C342, Mar. 2011, doi: 10.1111/j.1750-3841.2010.02038.x.

[25] R. Piispanen and P. Saranpaa, “Seasonal and within-steM variations of neutral lipids in silver birch (Betula pendula) wood,” Tree Physiol., vol. 24, pp. 991–9, Oct. 2004, doi: 10.1093/treephys/24.9.991.

[26] T. Vanhercke et al., “Up-regulation of lipid biosynthesis increases the oil content in leaves of Sorghum bicolor,” Plant Biotechnol. J., vol. 17, no. 1, pp. 220–232, 2019, doi: 10.1111/pbi.12959.

[27] M. J. Martín, F. Pablos, A. G. González, M. S. Valdenebro, and M. León-Camacho, “Fatty acid profiles as discriminant parameters for coffee varieties differentiation,” Talanta, vol. 54, no. 2, pp. 291–297, Apr. 2001, doi: 10.1016/S0039-9140(00)00647-0.

[28] E.-C. Shin et al., “Chemometric Approach to Fatty Acid Profiles in Soybean Cultivars by Principal Component Analysis (PCA),” Prev. Nutr. Food Sci., vol. 17, no. 3, pp. 184–191, Sep. 2012, doi: 10.3746/pnf.2012.17.3.184.

[29] M. Esteki, P. Ahmadi, Y. Vander Heyden, and J. Simal-Gandara, “Fatty Acids-Based Quality Index to Differentiate Worldwide Commercial Pistachio Cultivars,” Molecules, vol. 24, no. 1, Dec. 2018, doi: 10.3390/molecules24010058.

[30] F. Tüfekci and Ş. Karataş, “Determination of geographical origin Turkish hazelnuts according to fatty acid composition,” Food Sci. Nutr., vol. 6, no. 3, pp. 557–562, May 2018, doi: 10.1002/fsn3.595.

Chapter 4: Evaluation of Cell Wall Chemistry of Della and its Mutant Sorghum Stalks.

"Evaluation of Cell Wall Chemistry of Della and its Mutant Sorghum Stalks" ***Journal of Agricultural and Food Science,*** **vol. 70, no. 5, 2022, pp. 1689–1703**

4.1 Abstract

The cell wall compositional (lignin and polysaccharides) variation of two sweet sorghum varieties, Della (D) and its variant RG were evaluated at internodes (IN) and nodes (N) using HPLC, Py-GCMS, XRD, and 2D ^{1}H-^{13}C NMR. The stalks were grown in 2018 (D1 and RG1) and 2019 (D2 and RG2) seasons. In RG1, Klason lignin reduction by 16-44 % and 2-26 % was detected in IN and N, respectively. The analyses also revealed that lignin from the sorghum stalks were enriched in guaiacyl units and syringyl/guaiacyl ratio was increased in RG1 and RG2 respectively by 96% and more than two-fold at IN, and 61% and 23% at N. The glucan content was reduced by 23-27% (RG1) and 17-22% for RG2 at internodes. Structural variations due to changes in both cellulose and hemicellulose-based sugars were detected. The non-acylated and γ-acylated β–O–4 linkages were the main interunit linkages detected in lignin. These results indicate compositional variation of stalks due to the RG variation and growing season could influence its mechanical and lodging behavior.

4.2 Introduction

Sorghum is a versatile grass grown for grain, sugar, forage, and bioenergy applications [1]. Stalks of sorghums are load-bearing frameworks providing mechanical support to the aboveground shoot components [2]. Sorghum is one of the main crops that is highly affected by lodging. Lodging, the structural instability and failure of the stalk to support the shoot components before maturity and harvesting, is a major agronomic challenge leading to considerable yield losses, grain quality reductions and an increase in cost of harvesting [3]. It has been predicted that lodging-induced yield losses can reach to up to 60% in some crops [4]. One of the strategies of enhancing lodging resistance is by developing varieties having resilient mechanical property of cell walls, which plays an important role in defining the stalk strength. Especially in high yield sorghums (having greater load on the stem), strong mechanical properties of plant cell walls are vital to avoid product loss due to stalk lodging.

Plant cell wall structures are three-dimensional networks composed of primarily cellulose, hemicellulose and lignin [5,6]. Cell walls have different compositional, rheological, and mechanical properties [7] and provide strength, maintain rigidity, and protect cell structural integrity. Its composition mainly depends on the amount and distribution of constituents along the different

anatomical features of the stalks. Plant cell walls are further divided into primary and secondary walls. Primary cell walls are thinner and more flexible structures surrounding growing cells, mainly composed of cellulose, pectin, and xyloglucans with lesser amounts of arabinoxylans and structural proteins. Secondary cell walls are more rigid and stronger than primary cell walls, comprised of cellulose, lignin, xylan, and glucomannan [7,8]. The composition and the chemistry of the plant cell wall affect the mechanical behavior of the stalk [9].

Stalk lodging is a multidimensional phenomenon dependent on cell wall compositions, stalk morphology, anatomical, and metrological factors, biological factors, soil type, and inorganic nutrients [10,11]. Previously published literature has shown that stalk lodging incidence is highly related to the bending strength of the stalks [10], which suggests that the biomechanical properties of stalks largely determine their lodging resistance. Lignin, which is one of the major structural components of secondary cell walls, enhances plant growth and lodging resistance of the cell wall [12]. Furthermore, lignin plays an important role in cementing cellulose and hemicelluloses within the cell walls, thus aiding to improve the integrity and mechanical strength of the stalk. Lignin content was shown to be closely related to the lodging resistance behavior of the stem [9]. Studies have shown that low lignin content in crops resulted in weak mechanical strength of the stem [13].

On the other hand, the application of the sorghum for lignocellulosic biomass utilization has been highly limited by the recalcitrance of the cell wall, which is mainly attributed to lignin-carbohydrate complexes (LCC), and rigid lignin [14]. One of the promising approaches to mitigate cell wall recalcitrance and thereby improve sugar release and digestibility of sorghum stalks is by reducing lignin content through mutation [15], which can be achieved by reducing lignin content, modifying lignin composition, or both.

Breeding has a prospect of producing easily digestible sweet sorghum varieties with altered chemistry. The *REDforGREEN* (RG) sorghum variety was developed [16] through ethyl methane sulfonate (EMS) mutagenesis from Della (D) variety and has shown an increase in digestibility. However, increased digestibility is typically associated with lower stalk strength and a tendency for lodging. In relation to lodging, previous studies [3,10,17] have focused on macroscopic studies of stalk mechanical properties. Yet, understanding the biomechanical strength of stalks from the perspectives of their cell wall compositions is limited. Thus, for a comprehensive understanding of cell wall composition across growing seasons and the purpose of elucidating stalk biomechanical variations through chemical composition (which will be explored in future works), this study compares the cell wall composition of RG mutants with their corresponding Della variety at the nodes (N) and internodes (IN) across two growing seasons.

4.3 Materials and methods

4.3.1 Plant materials

Della (D) and RG sorghum varieties were grown in Lexington, KY in 2018 (D1 and RG1) and 2019 (D2 and RG2). The compositional variations of the varieties across two growing seasons were evaluated. Samples of 4-5 matured stalks were pooled for each variety in both years and ground using a Thomas–Wiley mill. The moisture contents were determined using a HB43-S Halogen moisture analyzer (Mettler Toledo). The extractives were previously removed by Soxhlet extraction and analyzed [18] and all subsequent structural carbohydrate analyses were performed using extractive-free biomass in duplicates to ensure data reliability.

4.3.2 Lignin and carbohydrate

Extractive-free biomass samples (200 mg), in duplicate, were hydrolyzed using sulphuric acid (2 ml, 72%) for 60 min at 30 °C in a water bath followed by secondary hydrolysis (4% sulfuric acid, 30 min, 20 psi) in an autoclave according to ASTM D 1106-96 with slight modification. Klason lignin (KL) content was determined gravimetrically after filtration, whereas acid-soluble lignin (ASL) was determined by UV spectroscopy (Genesys 50, ThermoScientific) at 205 nm [19] using an absorption coefficient of 110 L g-1 cm-1. Structural carbohydrate component analysis was performed on the hydrolyzed filtrate (5 mL), with the addition of mannitol as an internal standard, according to ASTM E 1758-01. The sugars were separated and quantified using high-performance liquid chromatography (HPLC, two Rezex RPM columns in series, 7.8 mm x 300 mm, Phenomenex) at 85 °C on elution with water (0.5 mL/min) using differential refractive index detection (Waters model 2414).

4.3.3 Fourier-Transform InfraRed (FTIR) spectroscopy

FTIR spectroscopy was performed on the biomass in triplicate using an iS5 spectrometer (Thermo-Nicolet) equipped with a ZnSe attenuated total reflection (iD5 ATR) accessory. The spectra were averaged, baseline corrected, and normalized using the Omnic v9 software. After spectral deconvolution using peak fitting, the syringyl/guaiacyl (S/G) [20] ratio was determined from the intensity ratio of 1325 cm^{-1} to 1235 cm^{-1}, whereas the cellulose total crystallinity index (TCI) and lateral order index (LOI) were estimated respectively from the normalized intensity ratio of 1370 cm^{-1} to 2920 cm^{-1} (I_{1370}/I_{2920}) [21] and 1427 cm^{-1} to 898 cm^{-1} (I_{1427}/I_{898}) [22]. As the TCI method was originally proposed for pure cellulose, the intensity of 1370 cm^{-1} might be influenced by the neighboring bands, when it is applied to the lignocellulosic sample.

4.3.4 Analytical Py-GCMS

The biomass S/G ratio was determined by pyrolysis–GCMS (Py-GCMS) using a Pyrojector II unit (SGE Analytical Science) at 500 ºC coupled to a GC-MS (ISQ-Trace1300). The compounds were separated using a ZB-5 capillary column (30 m × 0.25 mm Ø, 0.25 μm coating, Phenomenex) from 50 (1 min) to 250 °C (10 min) at 5 °C min^{-1}. Compounds were identified with authentic standards, by comparison with the literature [23,24] and NIST-2017 mass spectral library. The p-hydroxyphenyl/ guaiacyl/syringyl (H/G/S) was determined from peak areas of lignin monomer pyrolyzates selected by ion monitoring chromatogram for H between 7-15 min (m/z = 94, 107, 108, 120, 121, 134, 148), G between 18-23 min (m/z = 124, 135, 137, 138, 151, 164, 178) and S between 24-28 min (m/z = 154, 165, 167, 168, 181, 194, 208) [25].

4.3.5 Thermogravimetric analysis (TGA)

The thermal stability and decomposition behavior of the biomass samples was performed on a Perkin Elmer TGA-7 instrument (5-6 mg, in triplicate) from 30 to 800 °C at 20 °C min^{-1} under nitrogen (30 mL min^{-1}). The data was analyzed using Pyris v11 software.

4.3.6 X-Ray diffraction (XRD)

XRD analysis on biomass samples, in duplicate, was performed using Siemens D5000 diffractometer using Cu-Kα radiation (λ = 0.154 nm) from 2θ = 2 to 80o at 0.05o steps. The crystallinity index (CI) of cellulose was determined after peak fitting methods were applied to the amorphous and crystalline [(1-10), (110) and (200)] regions of diffractogram using two different methods: deconvolution method (equation 1) [26] and peak height method (equation 2) [27].

$$CI_d\ (\%) = \left(\frac{\sum A_{cry}}{\sum A_{cry} + \sum A_{am}}\right) x\ 100 \qquad \text{Eq. 1}$$

$$CI_h(\%) = \left(\frac{I_{200} - I_{am}}{I_{200}}\right) x\ 100 \qquad \text{Eq. 2}$$

Where, I_{200} and I_{am} are respectively the intensity of the main crystalline at (200) and amorphous. The mean width of crystallites of cellulose determines the broadness of XRD diffractograms and is inversely proportional to broadening. The size of the crystallite at the (200) plane was determined using the Scherrer formula in equation 3 [28].

$$L = \frac{57.3\ k\lambda}{\beta\ cos\theta} \qquad \text{Eq. 3}$$

Where, k is the shape factor of the crystal (0.91), λ is the wavelength of the X-ray, β is the full width at half maximum (FWHM) of the crystalline peak, θ is half of the Bragg angle corresponding to the (200) plane and factor of 57.3 was used to convert θ to radians. FWHM and peak position for the

(200) were determined from the diffractograms using Gaussian function peak fitting between 2θ of 18° and 29°.

4.3.7 NMR characterization of cell wall polymers

Solubilized whole-cell walls of N and IN were analyzed by ^{1}H-^{13}C Heteronuclear Single Quantum Coherence (HSQC) 2D-NMR spectroscopy (Bruker Avance III 500 MHz instrument). Extractive-free biomass (200 mg) was milled into fine powder using a planetary ball mill (Model: MPQ4X-V0.4L) using ZrO_2 50 mL jar and 3 mm and 6 mm Ø balls at 1000 rpm for 3 h [29]. The fine powder (50 mg) was transferred to a 5 mm NMR tube and DMSO-d6/pyridine-d5 (4:1, 0.7mL) added, sonicated for 30 min to form a gel. The spectra were collected at 30 °C with a Prodigy broadband cryo-probe and data processed using Topspin 3.62 software, and the structures were color coded using 3D paint.

4.3.8 Statistical analysis

To evaluate compositional variation among four samples, analysis of variance (ANOVA) was performed at a 95% confidence level. Unless stated, RG1 and RG2 are statistically compared with D1 and D2, respectively.

4.4 Results and discussion

The Della and RG sorghum stalk N and IN samples (depicted in Figure 3.1a) were systematically characterized to observe differences between varieties and tissue type.

4.4.1 Lignin and structural carbohydrate analysis

The KL, and ASL total lignin (TL) content analysis of the two varieties at different N and IN are shown (Figure 3.1b, c, d). The KL was found 15.5-21.6%, 9.4-16.3% 18.4-20.5 %, and 15.9-20.5 % of biomass, respectively for D1, RG1, D2 and RG2 (Figure 3.1b). The KL results for sorghum N and IN are consistent with the literature [30,31]. For D1, The KL at N1 and N2 was higher than the corresponding IN by 9.5 % and 9.7%, respectively. But KL at N3 was found to be less than its corresponding IN by 21.7%. Meanwhile, the variation of KL between N4 and IN4 within D1 stalks was not significant. The KL content of the N was 16.1-42.5% higher than IN in RG1. But, the KL content of N and IN was similar for D2, except at N2, 6.8% less than IN2. On the other hand, IN2-IN4 of RG2 contained 10.0-13.6% higher KL than Ns, while IN1 had 6.5% less than N1. The overall KL content of RG2 was considerably reduced; particularly notable reductions along stalks at N3 and N4 (18% and 12.4% respectively) were exhibited. RG1 displayed a significant reduction of KL: 16.5-44.3 % at IN and 2.0-25.6 % at Ns, shown in Figure 3.1e. Between Della, the KL of D1 was found reduced (1.4-20.2%), except at N1, which could be related to seasonal changes. Sattler et. al

[15] studied the KL of EMS induced sorghum mutant lines and found variations for one of the cultivar.

The ASL content (Figure 3.1c) constituted a small fraction of biomass, 2.0-3.4%, 2.9-4.2%, 2.4-3.0%, 2.1-3.1% for D1, RG1, D2 and RG2, respectively. The Ns had 14.6-37.0%, 7.0-27.2%, 13.8-20.4%, and 19.8-33.6% higher ASL than IN for D1, RG1, D2 and RG2, respectively. Among the stalks, the highest ASL was found in RG1, increased by 18.4 to 57.3% compared to its counterpart D1 (Figure 3.1e). Contrarily, ASL in RG2 was 4.7-18.3% lower than D2 at all IN, whereas discrepancies were observed at N2 and N3 (Figure 3.1e).

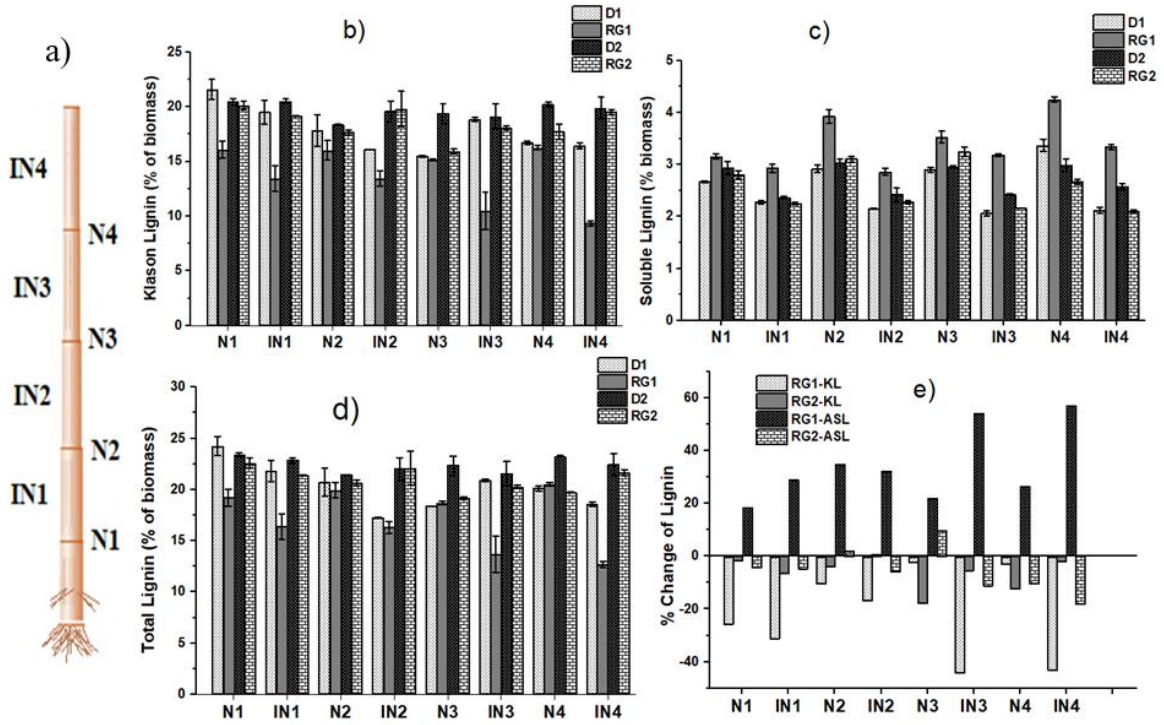

Figure 4.1. Schematic depiction, Klason lignin, acid soluble lignin and total lignin contents across nodes and internodes. (a) Schematic depiction of sorghum stalk, (b) Klason lignin (KL), (c) acid soluble lignin (ASL), (d) total lignin, and (e) % change in ASL and KL for, D1, RG1, D2 and, RG2 sorghum stalks (% of biomass) at nodes (N) and internodes (IN).

The TL contents (Figure 3.1d) were 17.3-24.2%, 12.7-20.5% , 22.0-23.4%, and 19.2-22.6% of biomass respectively for D1, RG1, D2, and RG2; consistent with reported values [32]. The TL content variations between IN and N of D2 were not significant, but IN of D1 had less lignin (7.7-12%) than N, except at IN3. The TL content of RG1-IN was significantly lower (14.7-38.2%) than corresponding N. On the other hand, RG2-IN has 5.6-9.7% more TL than its nodes, except at IN1. The TL of RG1was significantly reduced at the IN by 5.6-34.6%. Other than RG1-N1, which was reduced by 20.7%, the N of D1 and RG1 contained similar lignin content. The TL content of RG2 has

shown 6.4%, 6.0%, 14.3 % and 15.1% reduction respectively at IN1, IN3, N3 and N4. Interestingly, TL distribution of RG1 has shown a major shift towards the N, where greater amounts of lignin are stored. Between the Della, the TL of D1 was reduced by 3.2 to 21.6%, except at N1, which could be related to seasonal and climatic changes [33,34]. Across the mutants, the TL of RG1 has been significantly reduced by 2.4 to 41%, except at N4. The result reveals that combined effect of mutations and seasonal changes impaired the lignin content of RG1 than RG2. Moreover, the finding on prominent TL reduction (Figure 3.1d) of RG1-IN suggests that the mutant is markedly impacted by the mutagenesis and environmental changes, consequently leading to be more susceptible to the lignin reduction than the N. The limited lignin content variation at different morphologies between D2 and RG2 suggests that RG2 was not as equally impacted as RG1. The lignin content variation between D1 and D2 has also demonstrated the impact of growing seasons on lignin biosynthesis. Previous studies [35] showed that nodes are stronger, stiffer, and more rigid than internodes, hence greater lignin content at the nodes in RG1 could be related to nature's architectural design to avoid structural buckling of the cell wall of mutant [8]. Moreover, lignin is cross-linked with carbohydrates by covalent bonding to form LCC [36] and may play a role in maintaining the stiffness and mechanical recalcitrance of the cell wall. Thus, the stiffness of the RG1 stalk could be influenced by significant lignin reduction, subsequently, its lodging behavior could be likely impacted [14].

The architecture and biological function of N is different from IN and are under genetic control [37]. Structural carbohydrate analysis at both IN and N for the mutants was compared with their respective Della, and the results are shown in Figure 3.2. It was found in all varieties that glucan (cellulose) and xylan were the dominant polysaccharides and associated with the secondary cell wall of sorghum [38]. The glucan compositions were about 34-47%, 28-38% 37-47% and 32-42%, of biomass; and xylan 13-25%, 16-25% 11-26%, and 8-26% of biomass respectively, for D1, RG1 D2, and RG2. Minor amounts (< 3%) of galactan, mannan, and arabinan were also detected (Figure 3.2c, d, e). Along the stalks, N, and IN of D2 had similar glucan content (about 43.6%). However, glucan content between N and IN showed significant variation in D1, RG1, and RG2 stalks. The N of RG2 had a higher average glucan content (38.5%) than IN (35.2%). Contrarily, the IN of D1 and RG1 had higher average glucan content than their respective N: D1-IN (46.5%), D1-N (38.0%), RG1-IN (35%), and RG1-N (30%). This could be related to growth adaptation for more lignin repression at the IN [39]. The findings on sorghum stalk composition are consistent with the literature [30,40].

The glucan content of the Della variety was found to be significantly higher than their derivative mutants. In all N and IN analyzed, the glucan (Figure 3.2a) of RG2 was less than D2; giving a significant reduction of 17-22% for RG2-IN and 6-21% for RG2-N was recorded. Similarly, RG1 had

less glucan content than the control D1: a reduction of 23-27% at IN, and 11-28% at N was detected. Studies have shown a positive correlation between cellulose (glucan) deficiency and dwarfism in sorghum upon mutation [41]. Among Della stalks, an increase in glucan content of 3-9% at D1-IN and a decrease of 11-13% at D1-N were detected. RG-IN has similar glucan content, whereas a significant reduction (18-27%) at RG1-N was recorded. The glucan composition of sorghum stem tissues is influenced by environmental conditions and photoperiod sensitivity and varies among varieties and different stem tissues [30].

Xylan content analysis (Figure 3.2b) highlights that, within each RG1, D2, and RG2 stalks, the N contained significantly more xylan than the IN. The average xylan contents were RG1-IN (17.4%), RG1-N (22.7%), D2-IN (11.7%), D2-N (23.9%), RG2-IN (8.6%), and RG2-N (17.0%). However, D1-IN has more average xylan (22.4%) than N (17.2%). The results agree with the literature [16,42]. Across the varieties, 14-35% and 7-38% reduction respectively at RG2-IN and RG2-N was recorded. Meanwhile, a xylan reduction of 18-29% at RG1-IN and an increase of 11-60% at RG1-N were observed. Xylan variations at different sorghum stalk components have been reported [43]. Variation in galactan, arabinan, and mannan (Figure 3.2c, d, e) contents among varieties has also been detected.

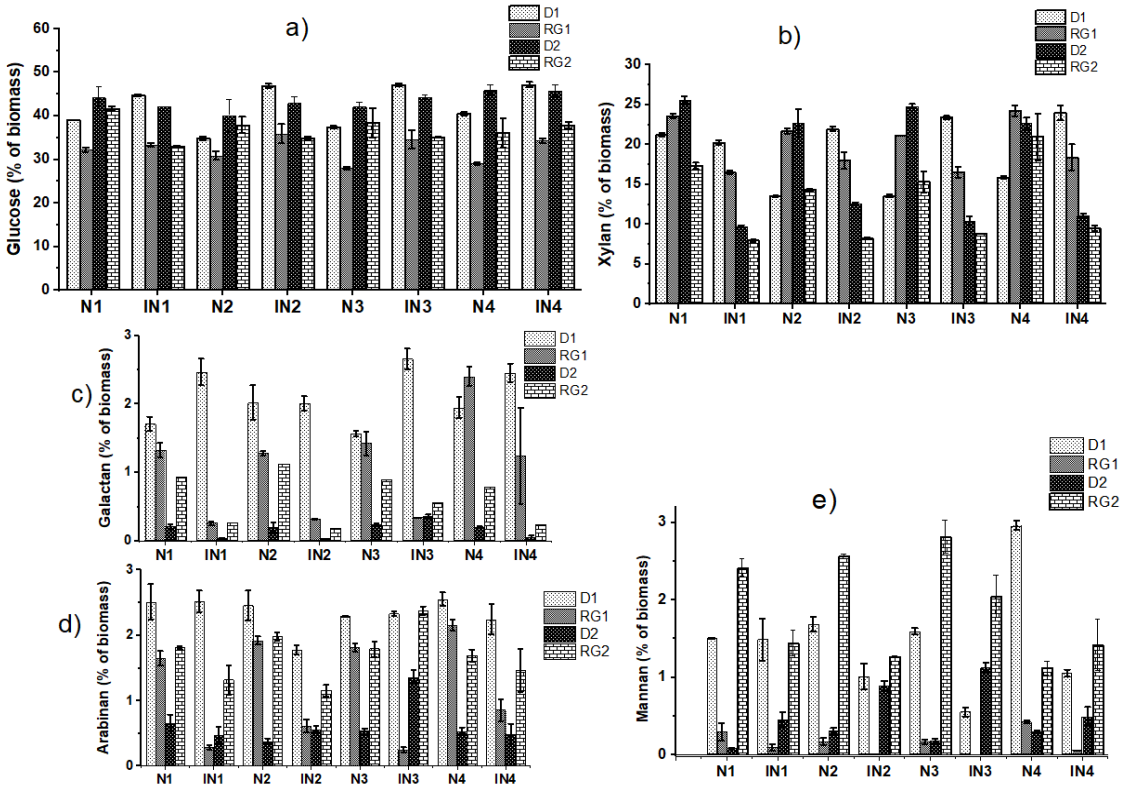

Figure 4.2. Structural carbohydrate contents across different morphologies of the stalk. (a) Glucan, (b) xylan, (c) galactan, (d) arabinan, and (e) mannan contents of sorghum stalk at nodes (N) and internodes (IN) for D1, RG1, D2, and RG2.

4.4.2 FTIR spectral analysis of biomass

FTIR spectroscopy has been used to investigate the functional groups of cellulose, hemicelluloses, and lignin of the IN for the sorghum varieties (Figure 3.3). Spectral assignments are given in Appendix Table B1. Analysis of the spectra of biomass samples shows that the fingerprint region of the IN (1800-900 cm^{-1}) contains important information pertaining to the functional groups of carbohydrates and lignin (Figure 3.3). The spectra of Della and RG varieties exhibited similar absorption bands. The strong absorbance band at 1034 cm^{-1} was attributed to glycosidic bonds (C–O–C) in carbohydrates [44]. Other polysaccharide bands include 1375 cm^{-1} attributed to C–H bending in cellulose and hemicellulose [45], and 898 cm^{-1} from the C–H deformation in cellulose were detected. For lignin, the band at 1165 cm^{-1} was assigned to C═O stretching from conjugated ketone, and ester groups [46], 1235 cm^{-1} from C═O, C–O, C–C bending in guaiacyl (G) units [47], 1325 cm^{-1} due to syringyl units (S) ring breathing, and 1515 cm^{-1} attributed to C═C stretch of the aromatic skeleton were all detected. The broad band centered at 1740 cm^{-1} was assigned to the C═O stretching of esters (acetyl groups), carboxylic acids, and unconjugated ketones in xylan and lignin. The conjugated C═O (1630 cm^{-1}) suggest the presence of noncanonical p-hydroxycinnamates (pCA and FA) in the stalks [48]. The band at 1460 cm^{-1} was assigned to the asymmetric bending of CH_2 in cellulose, and CH_3 in methoxy (CH3–O) groups [49]. The typical HGS band at 1160 and 835 cm^{-1} (C–H out-of-plane in syringyl and p-hydroxyphenyl units) confirms HGS-type lignin. The band at 1160 cm^{-1} corresponds to asymmetric C–O stretching of an ester and is most likely due to acetyl groups [19].

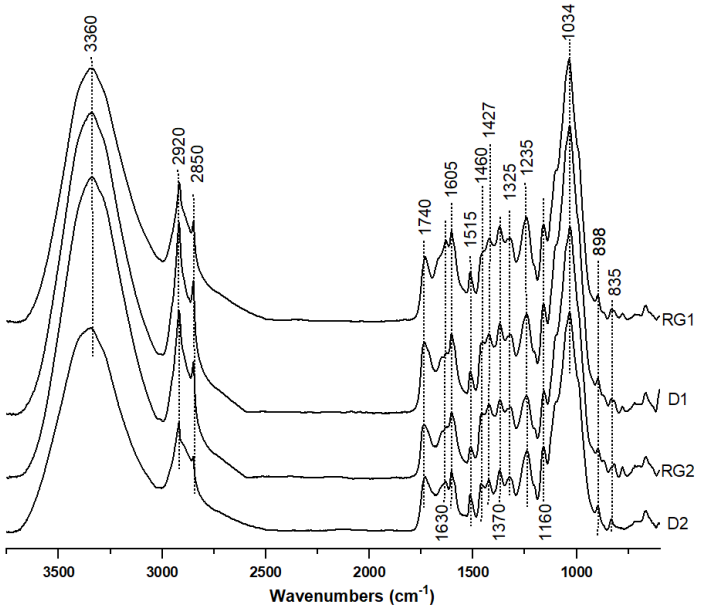

Figure 4.3. FTIR spectra of sorghum stalks for D2, RG2, D1 and RG1 at the internodes.

Features of cellulose (TCI and LOI) were determined from FTIR spectroscopy and summarized (Table 4.1). The TCI (I_{1370}/I_{2920}) values were 0.49, (0.62-0.71), (0.58-0.69), and (0.49-0.52), respectively for D1, RG1, D2, and RG2. The results are consistent with TCI values determined for sorghum bicolor [50]. The average TCI values for D2 were higher than for average RG2, which supports higher glucan/cellulose content in the structural carbohydrate analysis and crystallinity index by XRD (discussed later). Nevertheless, the TCI for RG1 was higher than that of D1. This suggests that D1 has more amorphous cellulose than RG1, while the XRD (discussed later) shows comparable crystallinity between the two varieties. As shown in Table 4.1, the LOI values for the Della variety were lower than their corresponding RG variety, which might arise from the cellulose structural difference in the varieties. Besides, the intensity at1370 cm^{-1} may be influenced by the neighboring lignin IR band at 1325 cm^{-1}. The LOI increased with the crystallinity of cellulose I [51]. FTIR spectra of the biomass also provided information on lignin composition (e.g., S/G ratio). The S/G ratio for D2, RG2, D1 and RG1 were 0.49-0.54, 0.62-0.66, 0.56-0.63, and 0.62-0.84, respectively. The S/G ratio (Table 4.1) of RG was significantly higher than Della. These S/G values are comparable to grass lignin [52]. FTIR spectroscopy has been employed to categorize lignin of different biomass origins [47] and detect S/G ratio variations of different biomass varieties [50].

Table 4.1. Total Crystallinity index (TCI), Lateral order index (LOI), and S/G ratio determined on sorghum biomass by FTIR spectral analysis.

Variety	TCI	LOI	S/G
D2-IN	57.9±2.0	2.14±0.11	0.49±0.01
RG2-IN	51.7±2.1	2.38±0.05	0.66±0.01
D1-IN	49.4±1.1	2.18±0.04	0.63±0.01
RG1-IN	64.1±1.9	3.05±0.14	0.77±0.03
D2-N	68.8±1.9	2.00±0.08	0.54±0.02
RG2-N	49.0±5.8	2.38±0.12	0.62±0.03
D1-N	49.5±2.2	2.66±0.09	0.56±0.01
RG1-N	62.0±3.2	3.38±0.21	0.62±0.01

4.4.3 Analytical Py-GCMS analysis

Analytical Py-GC-MS analysis was used to determine sorghum stalk compositional differences and the H/G/S ratio of lignin (Figure 3.4). The pyrograms showed the presence of carbohydrate and lignin thermal degradation products at the IN (Appendix Table B2) and N (Appendix Table B3). The pyrograms of RG1 both at IN and N were different (Appendix Figures B1 and B2) than those of D2, RG2, and D1. Despite the presence of common pyrolysate products and general pyrolysis trends, the

result revealed that the pyrolysis behavior of the varieties was different: resulting in distinct products likely due to differences in their compositional and structural variation. Most of these pyrolysis products have been detected in previous Py-GCMS studies of biomass in different abundances [50].

The S/G ratio is a crucial indicator of the degree and nature of cross-linking between lignin subunits. G-rich lignin is more cross-linked than S lignin [53]. The S/G ratio of D2, RG2, D1, and RG1 calculated from Py-GCMS chromatograms and FTIR spectra are given in (Figure 3.4a). The Py-GCMS result shows that the S/G ratio of mutants was significantly increased from their corresponding Della. The S/G ratio of D2 was about 0.32 (IN) and 0.33 (N), and for D1 was IN (0.25) and N (0.33), which are comparable to coconut shell powder (S/G = 0.27) and oats husks (S/G = 0.36) [54]. An S/G ratio increase of more than 2-fold at IN and 61% at N was recorded for RG2. Whereas in RG1, an S/G increase of about 96% at IN and 23% at N were observed (Figure 3.4a). An increase in the S/G ratio for RG1 stems have been reported by Petti et al [16]. The result shows that the G-type lignin in RG2 and RG1 was reduced while S lignin had increased resulting in a relatively higher S/G ratio. In Py-GCMS based determination of the S/G ratio, G-type lignin may be overestimated, as ferulates are also decarboxylated to 4-vinylguaiacol upon pyrolysis [55], which leads to underestimated S/G ratio. It is known that ferulates have been detected in 2D-NMR (discussed later) in the stalks. Even some studies [56,57] have suggested to ignore 4-vinylguaiacol and 4-vinylsyringol in wheat/grasses for determining S/G ratio, considering that the two lignin products are released primarily from non-canonical lignin monomers/cinnamtes. However, ignoring the two lignin products lead to significantly lower S/G ratio than reported for our samples. An increase in S/G may weaken the three-dimensional lignin structure and thus decrease lignin's glass transition temperature (and modulus) [58] and contribute to a reduced bending strength of the stalk, ultimately may influence resistance to lodging [59]. Considering the total lignin content analysis, RG2 has only shown lignin compositional change whereas RG1 showed both lignin content reduction as well as its composition. The results are consistent with previous studies [32]. The FTIR spectral S/G ratio analysis followed the same trend as Py-GCMS: has significantly increased by 10-22% and 16-32% for RG1 and RG2, respectively. Except at RG2-IN, the S/G ratio determined by FTIR was higher than by Py-GCMS as shown in Figure 3.4a at IN and N. By the same method, corn stover (S/G = 0.48) and switch grass lignin (S/G = 0.43) was reported [52]. The detection of a relatively higher S/G ratio by FTIR could be due to the complex nature of the cell wall and band interference/overlap from carbohydrates [60].

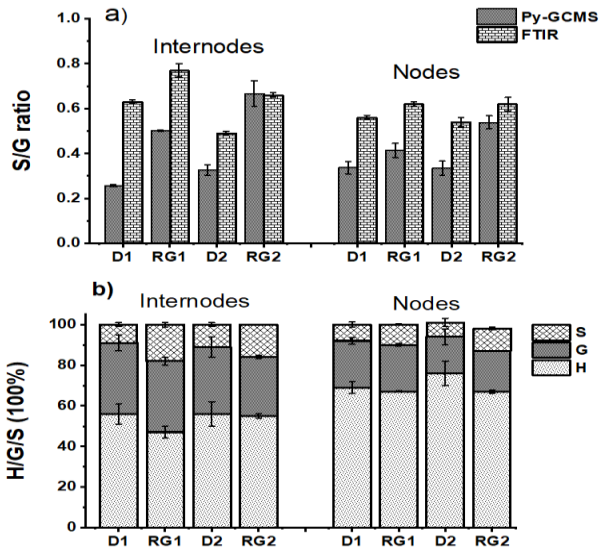

Figure 4.4. S/G ration and H/G/S distribution determined from Py-GCMS pyrograms. (a) S/G ratio comparison determined by Py-GCMS and FTIR at internodes (IN) and nodes (N) and (b) The distribution of p-hydroxyphenyl (H), guaiacyl (G), and syringyl (S) lignin from Py-GCMS (H/G/S in %) for D1, RG1, D2, and RG2, varieties at IN and N.

The relative H/G/S peak area distribution from the Py-GCMS (Figure 3.4b), confirms H/G/S type of lignin in sorghum. The presence of p-coumarates (confirmed by FTIR and 2D-NMR), which decarboxylate during pyrolysis, is primarily responsible for the detection of large amounts of 4-vinylphenol during pyrolysis [55]. Thus, 4-vinylphenol was ignored in H/G/S estimation. For the IN, the H/G/S ratios were found to be 56/33/11, 40/36/24, 56/35/9, and 47/35/18, respectively for D2, RG2, D1 and RG1. The H/G/S ratios for nodes were 76/18/7, 69/20/11, 69/23/8, and 67/23/10 for D2, RG2, D1 and RG1, respectively. H/G/S Ratios have been reported for different grass families: switchgrass (26/42/32) [61], miscanthus (4/44/54) [62], maize (9/58/33) [54] and wheat (6/58/36) [63]. As reactive sites for inter-unit linkages (H > G > S) [53], higher content of S lignin in RGs may lead to lower number of carbon-carbon and more β-O-4 ether linkages and lower lignin's glass transition temperature and modulus [64].

4.4.4 TGA analysis

The thermal decomposition behavior of the four sorghum stalks was investigated by TGA as a rapid method to distinguish between varieties (Figure 3.5). The thermogram shows different stages of weight loss in relation to the thermal stability of hemicellulose, cellulose, and lignin [65]. The first stage (40-120 ^{o}C) is associated with water loss. The second stage (180–340 °C) is attributed to the degradation of mainly hemicellulose (xylan) and shows distinct shoulders for D2 (340 °C) and RG1 (310 °C) and a peak for D1 (210 °C) varieties [66,67]. However, no shoulder/peak was detected in RG2. These variations are likely attributed to differences in hemicellulose structure [68]. The third

stage (340-400 °C) corresponds to cellulose decomposition. Lignin decomposes over a wide temperature range due to the dissimilar thermal stabilities of its functional groups [69]. It is believed that lignin pyrolysis starts at the third stage and continues to the final stage of degradation (long tail above 400 °C). These TGA findings are in agreement with sorghum [2] and corn stalk studies [70].

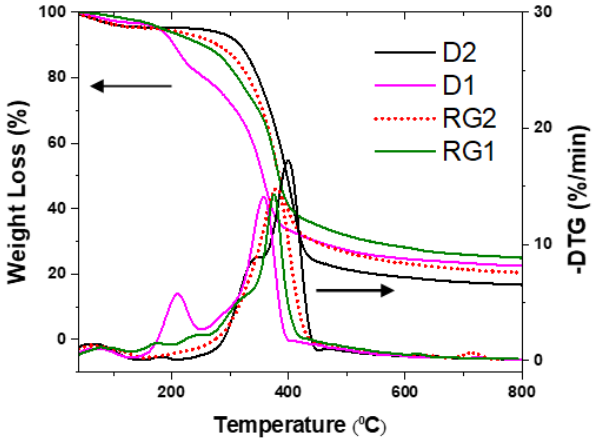

Figure 4.5. TGA thermograms of D2, D1, RG2 and RG1 sorghum biomass (y-axes on the right is differential thermogravimetric (DTG) of stalks).

Previous studies have shown that the TG curve varies with cellulose, hemicellulose and lignin content [68] and biomass type [71]. The residue char/ash left at 800 oC for, D1, RG1, D2, and RG2 was respectively 22.5, 24.9%, 16.6% and 19.9%, (Table 4.2). The onset temperature (T_{onset}) for the major weight loss transition varied for the different sorghum varieties (Table 4.2).

Table 4.2. Residual mass at 800 °C and major onset temperature (T_{onset}) of D2, RG2, D1 and RG1 stalks

Sorghum	Residual mass at 800 °C (%)	T_{onset} (°C)
D1	22.5±0.4	357±1
RG1	24.9±0.1	377±1
D2	16.6±0.2	403±1
RG2	19.9±0.5	385±5

4.4.5 XRD analysis

In plant cell walls, glucan chains of cellulose form long thread-like crystalline microfibrils which may be partly crystalline [72–74]. The crystallinity of the microfibrils in the sorghum samples has been evaluated by XRD (Figure 3.6a) and its pick fitting is shown in Figure 3.6b. The XRD analysis confirms the two-state structures: broad amorphous structure indicated at 2θ of about 18.5° (mainly from hemicellulose, lignin and amorphous cellulose) and distinct crystalline cellulose peaks at 2θ of 15.5 [Miller indices of (1-10) and (110) overlapped], and 21.9° assigned to (200) lattice indices [28].

The crystallinity indexes (CI_d and CI_h) for the IN were calculated from the XRD data and the results are given (Table 4.3). For D2 the CI_d and CI_h were 12 % and 6% higher than RG2, while the D1 and RG1 had similar crystallinity indexes for both methods. The CId values are comparable to the literature [45]. Petti et al. reported no variation between sorghum cultivars [16]. The cellulose microcrystalline grain size at (200) plane was comparable for all samples at about 3 nm (Table 4.3). The shape and crystallinity of microfibrils may impact the biomechanical properties of the stalks.

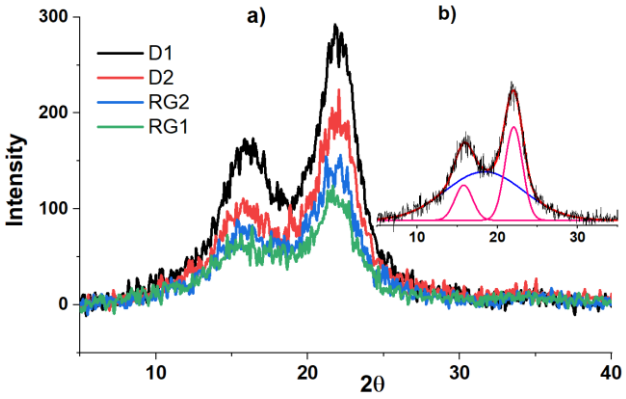

Figure 4.6. X-ray diffractogram of different sorghum stalks. (a) of D1, D2, RG2 and RG1 sorghum biomass at IN and (b) deconvolution of the peaks using peak fitting.

Table 4.3. Crystallinity index of D1, RG1 D2 and, RG2, at IN based on peak deconvolution (CI_d), peak height (CI_h) methods and average grain size (L) of cellulose at (200)

Sorghum	CI_d (%)	CI_h (%)	L (nm)
D1	32.0±1.3	58.2±1.9	3.3±0.0
RG1	31.8±0.9	58.1±1.0	3.2±0.1
D2	38.0±1.0	63.3±0.2	3.0±0.1
RG2	33.5±0.6	59.4±0.6	3.1±0.0

4.4.6 Nuclear magnetic resonance (NMR) spectroscopy of cell walls

Dissolved-gelatinized cell walls of N and IN sections from D2, RG2, D1 and RG1 sorghum stalks were analyzed by 2D $^{13}C–^{1}H$ HSQC NMR spectroscopy to elucidate lignin inter-unit linkages and structure. Spectral assignments were based on the works of Kim and Ralph [29,75], Yuan et al.[36], Balakshin et al.[76], and Komatsu and Kikuchi [77]. The types of inter-unit linkages in lignin monomers are found in the side-chain region (δC/δH 50-90/2.5-5.0 ppm) of the 2D HSQC spectra cross-peaks. The distribution of the lignin linkages in the side-chain regions of IN and N sections of the D1, RG1 D2, and RG2 are compared and shown (Figure 3.7). Polysaccharide associated signals are also observed in this spectra region. The characteristic signals at δC/δH 55.6/3.73 ppm and δC/δH 60.95/3.57 ppm corresponding respectively to methoxy groups and Cγ/Hγ units in G type β–O–4

linkages (Aγ) were observed in all samples [36]. For all varieties and N and IN sections, the β–O–4 aryl ether linkage was the major lignin linkage. An important feature observed in the HSQC spectra from the stalks was the occurrence of strong signals from γ-acylated β–O–4 alkyl aryl ethers. The occurrence of intense signals at around δC/δH 63.04/3.94 ppm assigned to the Cγ/Hγ correlations of γ-acylated β–O–4 (Aγ') substructures, revealed that a significant part of the lignin from stalks were acylated at the γ-position of the lignin sidechain. Other types of lignin linkages such as phenylcoumaran (β–5) units, resinol (β-β) units, and dibenzodioxocin (5–5/4–O–β) were not detected, consistent with reported results for corn stalks [29]. Complete cross peak assignments, and linkage (Appendix Table B4) and all possible lignin linkage structures (Figure B4) are provided in Appendix B.

The 2D-HSQC spectra of D1 (Figure 3.7a, e) show signals with relatively similar profile between the N and IN, except the detection of Xylp(3) at the N, whereas Xylp(2) was observed at IN. Among the lignin inter-unit linkages, signals for Aγ, Aγ' and methoxy were detected in both N and IN. The detection of cinnamyl acetate substructures Cγ/Hγ (66.63/4.48 ppm) [78] is a distinct feature of D1 than the other three sorghum samples. Other xylan and arabinan related substructures were also observed, as shown (Figure 3.7a, e). On the other hand, the spectra of RG1 stalks (Figure 3.7b, f) were also shown to be different from D1 in that; 2-O-acetyl-β-D-xylopyranosyl structural units were only observed in RG1. Like RG2 and D1, (1,3)-α-L-arabinofuranosyl, (1,2)-α-L-arabinofuranosyl, and C_4/H_4 in (1→4)-β-D-xylopyranosyl units with non-reducing ends were distinct structural features of RG1 than D2. The cross-peaks for (1,2)-α-L-arabinofuranosyl units in RG1 were shown to overlap with other unassigned cross-signals. On the other hand, structural features between the N and IN in RG1 were similar. Signals attributed to C_2/H_2 in (1→4)-β-D-xylopyranosyl, C_3/H_3 in (1→4)-β-D-xylopyranosyl, C_4/H_4 in (1→4)-β-D-xylopyranosyl, and C_5/H_5 in (1→4)-β-D-xylopyranosyl units together with lignin linkages of Aγ, Aγ' were detected [79]. However, signals for Cα/Hα in β–O–4 substructures were not observed in D1 and RG1.

For the D2, the HSQC spectra for the IN and N (Figure 3.7c, g) were similar, except that weaker signal at 61.71/4.16 ppm corresponding to Cγ/Hγ cinnamyl alcohol end group was detected in the N sample, which shows some structural variation between tissue type. Strong signals were observed for methoxy and Aγ. Furthermore, Cα/Hα correlations in β–O–4 (Aα) substructures were observed at δC/δH 72.23/4.96 ppm. In addition, the correlation at δC/δH 86.21/4.20 ppm was shown to corresponds to S-type β–O–4 (A-Sβ) substructures [80].

The hemicellulose (xylan) was identified in the D2 sorghum stalks by the presence of acetyl groups at δC/δH 73.51/4.61 ppm which is corresponding to C_2/H_2 in 2-O-acetyl-β-D-xylopyranosyl units and

δC/δH 75.00/4.91 ppm for C_3/H_3 in 3-O-acetyl-β-D-xylopyranosyl units [75]. These two signals for the acetylated structures were not detected in either the N or IN of RG2 and D1, while only 2-O-acetyl-β-D-xylopyranosyl structure was observed in RG1. The spectra also show δC/δH signals at 72.83/3.16 ppm for C_2/H_2 in (1→4)-β-D-xylopyranosyl, 74.04/3.35 ppm for C3/H3 in (1→4)-β-D-xylopyranosyl, 75.51/3.63 ppm for C_4/H_4 in (1→4)-β-D-xylopyranosyl, and 63.12/3.27 ppm for C5/H5 in (1→4)-β-D-xylopyranosyl.

In RG2, the N showed signals for the C_2/H_2 in (1→4)-β-D-xylopyranosyl units but were absent in the IN. In comparison with the D2, the RG2 was noticeably different. In terms of linkages, Aα substructures were not observed in RG2, whereas signals from Aγ, Aγ' and methoxy were detected (Figure 3.7d, h). Other distinct structures and signals for the RG2 samples in the side-chain region includes C2/H2 for (1,3)-α-L-arabinofuranosyl at δC/δH 80.81/3.86 ppm and 82.69/3.96 ppm and (1,2)-α-L-arabinofuranosyl units at δC/δH 81.73/3.69 ppm [81]. These results support relatively higher arabinan contents from carbohydrate analysis. Moreover, the C_4/H_4 in (1→4)-β-D-xylopyranosyl unit with a non-reducing end at δC/δH 76.82/3.22 ppm was also observed 29. Other carbohydrate signals attributed to C_2/H_2 in (1→4)-β-D-xylopyranoside, C_3/H_3 in (1→4)-β-D-xylopyranoside, C_4/H_4 in (1→4)-β-D-xylopyranoside, and C_5/H_5 in (1→4)-β-D-xylopyranoside units were also detected [82]. All these structural variations may contribute to property differences among the stalks of D1, RG1, D2 and RG2.

The main notable linkages detected were non-acylated β–O–4 and naturally γ-acylated β–O–4 (Appendix Figure B4). Thus, for the purpose of identifying their relative abundance and providing explicit information of structural difference among the samples, quantitative analysis as percentage of these chains was performed. The degree of γ-acylation of the lignin sidechains was estimated from the Cγ/Hγ correlation signals in β–O–4 and γ-acylated β–O–4 alkyl-aryl ethers. Accordingly, the percentage of acylation (Aγ/Aγ') was 79.0/21.0, 85.0/15.0, 83.0/17.0, 88.0/12.0 for IN of D1, RG1, D2 and RG2, respectively. The result shows significant variation in the degree of acylation between RG and Della variety, revealing more naturally γ-acylated β–O–4 linkages at IN of Della variety were identified than RG in both growing seasons, which shows the nature of lignin variation. Naturally occurring acylated lignin have been identified in different plants [83]. For the N, Aγ/Aγ' of D1 (90.0/10.0), RG1(88.0/12), D2(82.0/18.0), and RG2 (88.0/12.0) was detected.

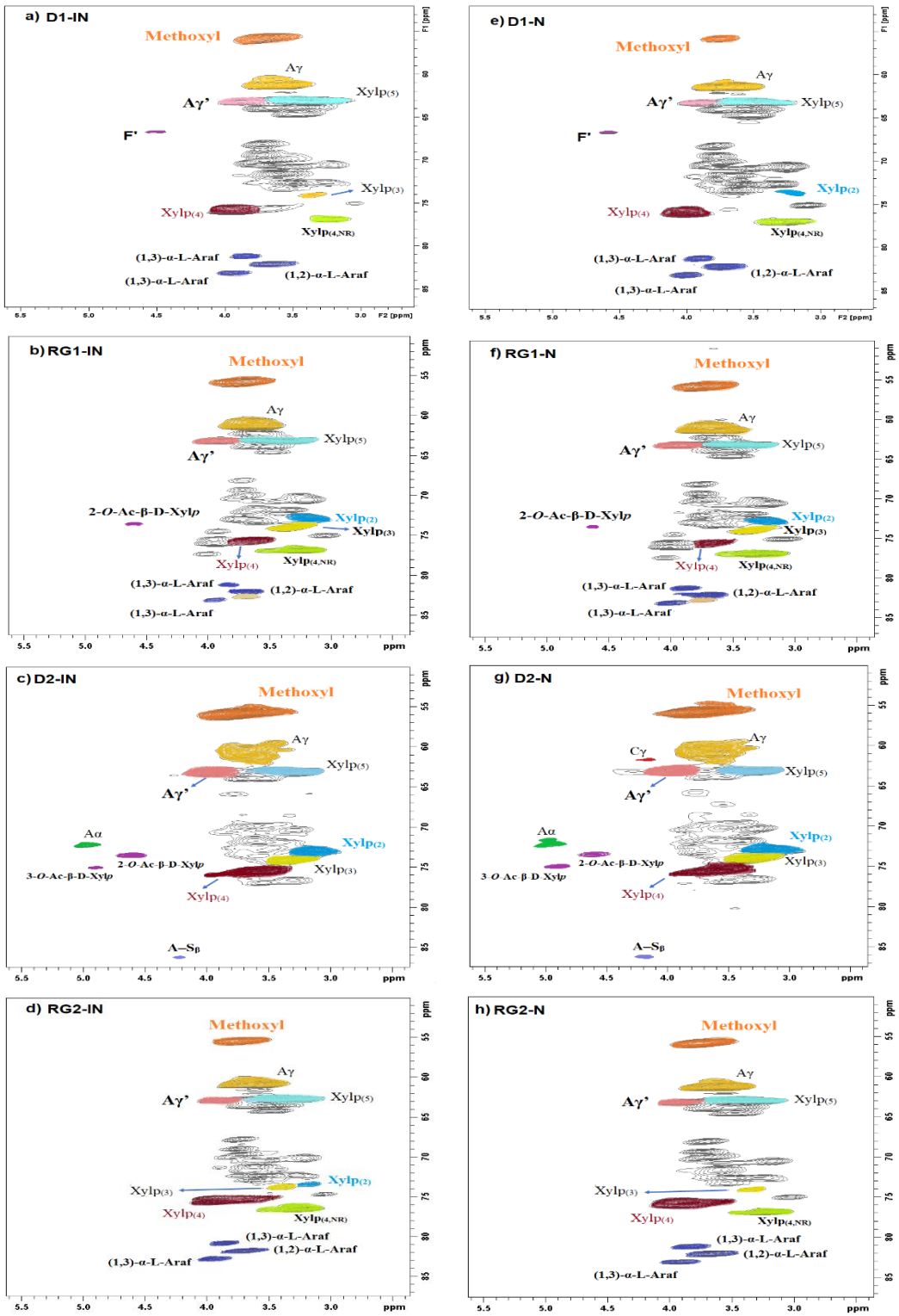

Figure 4.7. HSQC ^{1}H-^{13}C Spectra of aliphatic region of sorghum stalk cell wall a) D1-IN; b) RG1-IN; c) D2-IN, d) RG2-IN, e) D1-N, f) RG1-N, g) D2-N and h) RG2-N. Grey colors in the contours are either unassigned due to lack of reliable information or unresolved.

The polysaccharide anomeric region in the HSQC spectra (90–110/4.0–6.0 ppm) of the IN and N (Figure 3.8) provides key information to the composition of the various polysaccharides and their substituents [29,36,81]. Clearly resolved polysaccharide anomeric correlations were detected in all cell wall samples (Appendix Table B4).

The spectra of D1 in the anomeric region (Figure 3.8a, e) shows that strong signals attributed to (1→4)-β-D-glucopyranosyl units (103.15/4.34 ppm) were detected at both IN and N. Besides, (1→4)-α-D-glucopyranosyl (R), (1→4)-β-D-xylopyranosyl, 3-O-acetylated-β-D-xylopyranosyl, 2-O-acetylated-β-D-xylopyranosyl, and α-L-fucopyranosyl units were detected in both IN and N. In contrast to IN of D2, RG2 and RG1, the (1→4)-α-D-galactopyranosyl (R) units were weaker in D1-IN. Unlike the N of D2, RG2 and RG1, D1-N had distinct cross signals at 108.09/4.85 ppm and 106.3/4.60 ppm respectively from α-L-arabinofuranosyl and (1→4)-β-D-galactopyranosyl (not detected in D1-IN) units (Figure 3.8e). Moreover, a relatively weak signal of 3-O-acetylated-β-D-xylopyranosyl (101.86/4.34 ppm cross peak) was detected in the D1-N sample.

The HSQC spectra of RG1 in the anomeric region (Figure 3.8b, f) has shown a distinctive and prominent signal at 91.83/5.30 ppm, unassigned carbohydrate that makes RG1 different from D2, D1 and RG2. Like D2, RG2 and D1, prominent signals attributed to (1→4)-α-D-glucopyranosyl, (1→4)-β-D-glucopyranosyl, 3-O-acetylated-β-D-xylopyranosyl, and 2-O-acetylated-xylopyranosyl units were detected in RG1. Comparison of the anomeric features of IN and N of RG1 (Figure 3.8b, f) signaled the same profile, except slight differences in that weaker signal from nodes associated with (1→4)-α-D-galactopyranosyl units at 94.26/5.08 ppm.

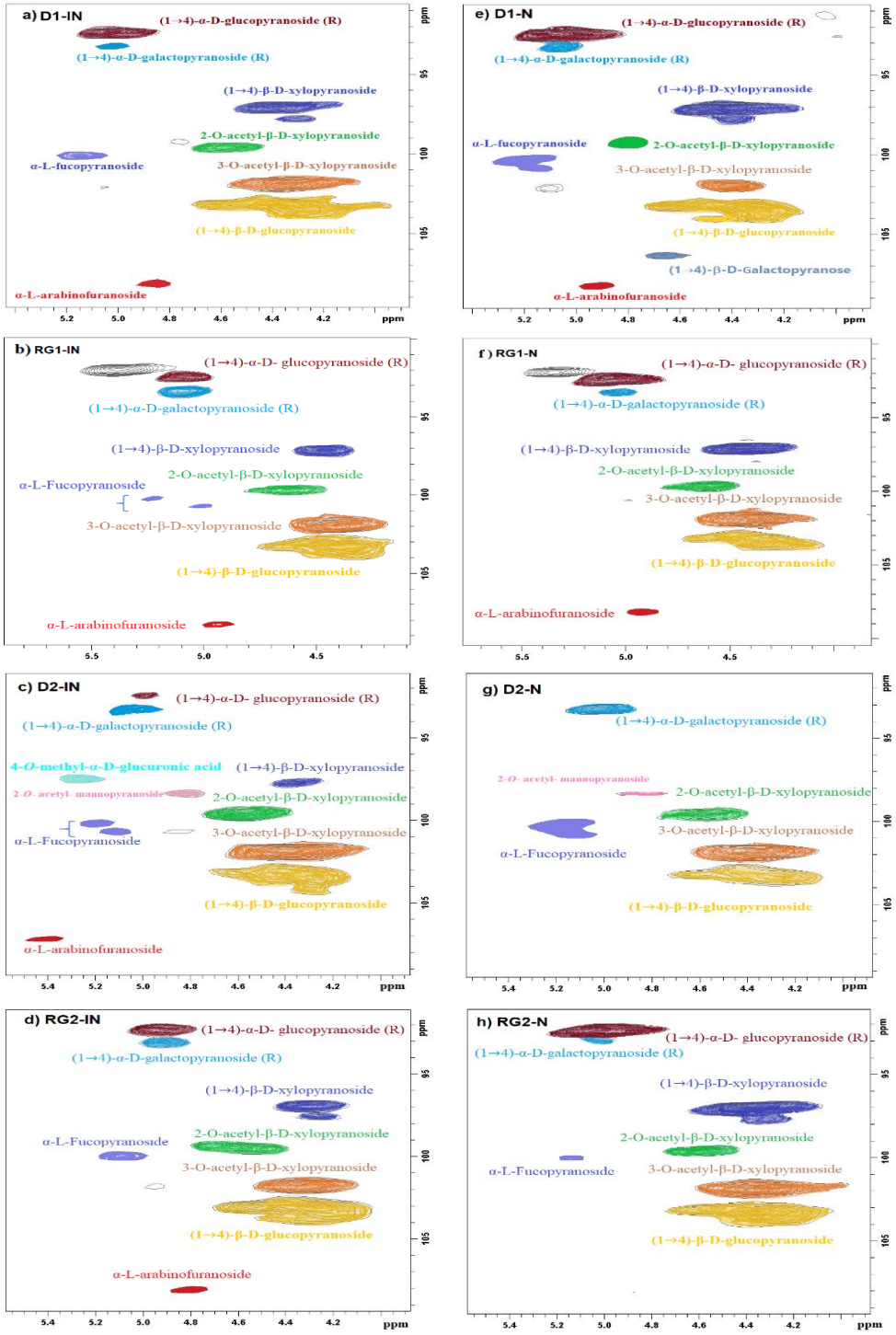

Figure 4.8. Polysaccharide anomeric regions from 2D ^{13}C– ^{1}H correlation (HSQC) spectra for the gel states of four sorghum whole-cell wall samples at the nodes (N) and internodes (IN) in DMSO-d_6/pyridine-d5 (4:1) solvent (a) D1-IN, (b) RG1-IN, (c) D2-IN, (d) RG2-IN, (e) D1-N, (f) RG1-N, (g) D2-N and (h) RG2-N. R refers to reducing end, grey cross-link in RG1 is unassigned carbohydrate.

The spectra of D2 (Figure 3.8c, g) anomeric region (C_1/H_1) show prominent signals for (1→4)-α-D-galactopyranosyl units (reducing end, R) at 93.29/5.04 ppm, 2-O-acetylated-β-D-xylopyranosyl units at 99.32/4.63 ppm, 3-O-acetylated-β-D-xylopyranosyl units at 101.56/4.38 ppm, (1→4)-β-D-glucopyranosyl units at 103.01/4.30 ppm. A strong signal from α-L-fucopyranosyl units at 100.72/5.12 ppm was detected in N and IN samples. On the other hand, comparison of the spectra between the IN and N (Figure 3.8c, g) revealed different signals for the IN material. Particularly, (1→4)-α-D-glucopyranosyl units (R) at 92.38/5.06 ppm, 4-O-methyl-α-D-glucuronic acid at 97.48/5.26 ppm, (1→4)-β-D-xylopyranosyl unit (R) at 97.10/4.40 ppm and α-L-arabinofuranosyl unit at 107.17/5.41 ppm were only detected at the IN. Similar findings were observed, by HSQC, on corn cell walls [29].

The anomeric positions (C_1/H_1) for RG2 samples for IN and N (Figure 3.8d, h) showed a similar spectrum, except for the α-L-arabinofuranosyl unit that was only detected at the IN and (1→4)-α-D-galactopyranosyl unit (R) at 93.29/5.04 ppm, and (1→4)-β-D-glucopyranosyl at about 103.01/4.30 ppm were not resolved well for the N. The signal strength of (1→4)-β-D-glucopyranosyl at the N was higher than at the IN. Contrarily, α-L-fucopyranosyl units at the N were of low intensity. In comparison with D2, signal strength of (1→4)-β-D-glucopyranosyl units of RG2 were strong. Moreover, unlike D2, signals of 4-O-methyl-α-D-glucuronic acid and 2-O-acetylated-mannopyranosyl units for RG2 were absent, revealing structural variations between the two. Unlike the N in the D2, (1→4)-β-D-xylopyranosyl units have been detected at the N of RG2. Likewise, notable anomeric signals associated with (1→4)-α-D-glucopyranosyl, 3-O-acetylated-β-D-xylopyranosyl, and 2-O-acetylated-xylopyranosyl units were also detected [75].

The aromatic region (δC/δH 100-150/6.0-8.0 ppm) of D1, RG1, D2 and RG2, samples in the 2D HSQC spectra at the IN and N are given respectively in Figure 3.9 and Appendix Figure B3. This region contains correlations of guaiacyl (G), syringyl (S), oxidized syringyl (S') units at Cα═O and hydroxycinnamates (ferulate, FA & *p*-coumaric acid, *p*CA) and limited p-hydroxyphenyl (H). Moreover, signals attributed to hydroxycinnamates were also detected in D1. The S units were detected in two forms: at correlations of δC/δH 103.48/6.75 ppm and δC/δH (104.12/7.43 ppm from ($C_{2/6}/H_{2/6}$), respectively for S units and an oxidized S lignin (S') at Cα-ketone. The S' units were minor, showing the possible oxidation of S units either during sample preparation or during lignification were limited.

The HSQC of D1 in the aromatic region for IN (Figure 3.9a) and N (Appendix Figure B3a) have similar spectra except relatively higher signal of H lignin at 127.92/7.26 ppm and detection of FA8 at the nodes. Correlation peak assignments are provided (Appendix Table B4). The signals from both

guaiacyl (G_2, G_5, G_6) and syringyl ($S_{2/6}$) units were readily observed from the signals respectively centered 111.18/7.10, 115.05/6.86, 119.30/6.88 and 03.6/6.8 ppm in both IN and N. On the other hand, the stalks of RG1 consisted of relatively strong signal correlations about 127.92/7.26 and 129.02/7.27 ppm from $C_{2/6}/H_{2/6}$ of H units at both the nodes (Appendix Figure B3b) and internodes (Figure 3.9b). Similar reports were found and published for Arabidopsis [84]. Like the control group (D1), G_2, G_5, G_6, and $S_{2/6}$ were also observed in RG1. A significant amount of *p*-coumarates in both control and mutant RG1 sample were observed at both N and IN. In addition, ferulate units were also detected for IN (Figure 3.9a, b), and N (Appendix Figure B3a, b) in both D1 and RG1 samples. Ferulate and *p*-coumarate units were detected in wild and transgenic switchgrasses [80] and forage sorghum [19]. Unlike N of D2, RG2 and D1, FA8 was not detected at both the N and IN of RG1 stalks.

The HSQC spectra of D2 whole-cell wall in the aromatic region (Figure 3.9c and Appendix Figure B3) shows that weaker signal corresponding to $H_{2/6}$ aromatic correlation from H units at 127.92/7.26 ppm was detected only at the N. Besides H units, the other distinct feature between the N and IN of D2 comes from ferulate units. Ferulates are involved in acylating arabinoxylans, lignification, cross coupling lignin monomers with oligomers forming lignin-carbohydrate complexes (LCC) [29]. Ferulate related signals were observed at 110.91/7.07, 115.19/6.5, 144.27/7.42 ppm, respectively for C_2/H_2, C_8/H_8 and C_7/H_7 of ferulic acid (FA) [85]. As it is seen in the spectra, FA_3 in the N (Appendix Figure B3) overlapped with $pCA_{3/5}$, whereas in the IN, it overlapped with G_5 and *p*CA8. Strong and well resolved signals attributed to $C_{2,6}/H_{2,6}$ of S units at δC/δH (103.48/6.75 ppm) were detected. Moreover, the aromatic region correlation was relatively dominated by signals associated with *p*CA at chemical environments 115.46/6.78 ppm from $C_{3/5}/H_{3/5}$ residues, 129.84/7.48 ppm for $C_{2/6}/H_{2/6}$, 113.54/6.31ppm for C_8/H_8 and 27/7.42 ppm. Moreover, G lignin associated contour signals were also detected at δC/δH (110.07/6.98 ppm, 114.59/6.79 ppm, 119.09/6.86 ppm), respectively for C_2/H_2, C_5/H_5 and C_6/H_6 residues of G units [79].

The HSQC correlations of aromatic region of RG2 revealed that FA8 and $H_{2/6}$ were not detected at the IN. Yet, like D2 nodes, FA8 were detected at the N. Ferulates, were also detected in previous studies [86]. The $H_{2/6}$ signals were able to be detected at both RG1-N and RG1-IN, but the FA_8 substructures were not observed.

To understand the lignin compositional variation across the variety and growing season, the volume integration was used to determine the relative abundances of the S and G lignin units (S/G ratio). Thus, the average S/G ratio in D1, RG1, D2, and RG2 was about 0.40, 0.51, 0.43, and 0.62, respectively. For energy sorghum S/G ratio of 0.53-0.58 by McKinley et.al [32] and 0.4 for sugarcane

straw was reported [87]. The S/G ratio for RG was significantly higher than Della in both growing seasons, which is consistent with the FTIR and Py-GCMS results. Besides demonstrating G-rich lignin in sorghum stalks, the result also indicates that the Della variety contains lower S lignin than RG, which reveals the alteration of lignin composition. Although HSQC NMR is entirely non-quantitative technique, the S/G ratio by this method is relatively considered reliable [88]. Contrarily, the *p*CA and FA units are significantly overestimated due to the longer relaxation of more mobile units than the backbone units in the cell wall [55]. Hence, the quantification of FA and *p*CA units from the volume integrals was not considered. Across the growing seasons, the S/G ratio of D1 and D2 was approximately equivalent, but RG2 contained higher than RG1.

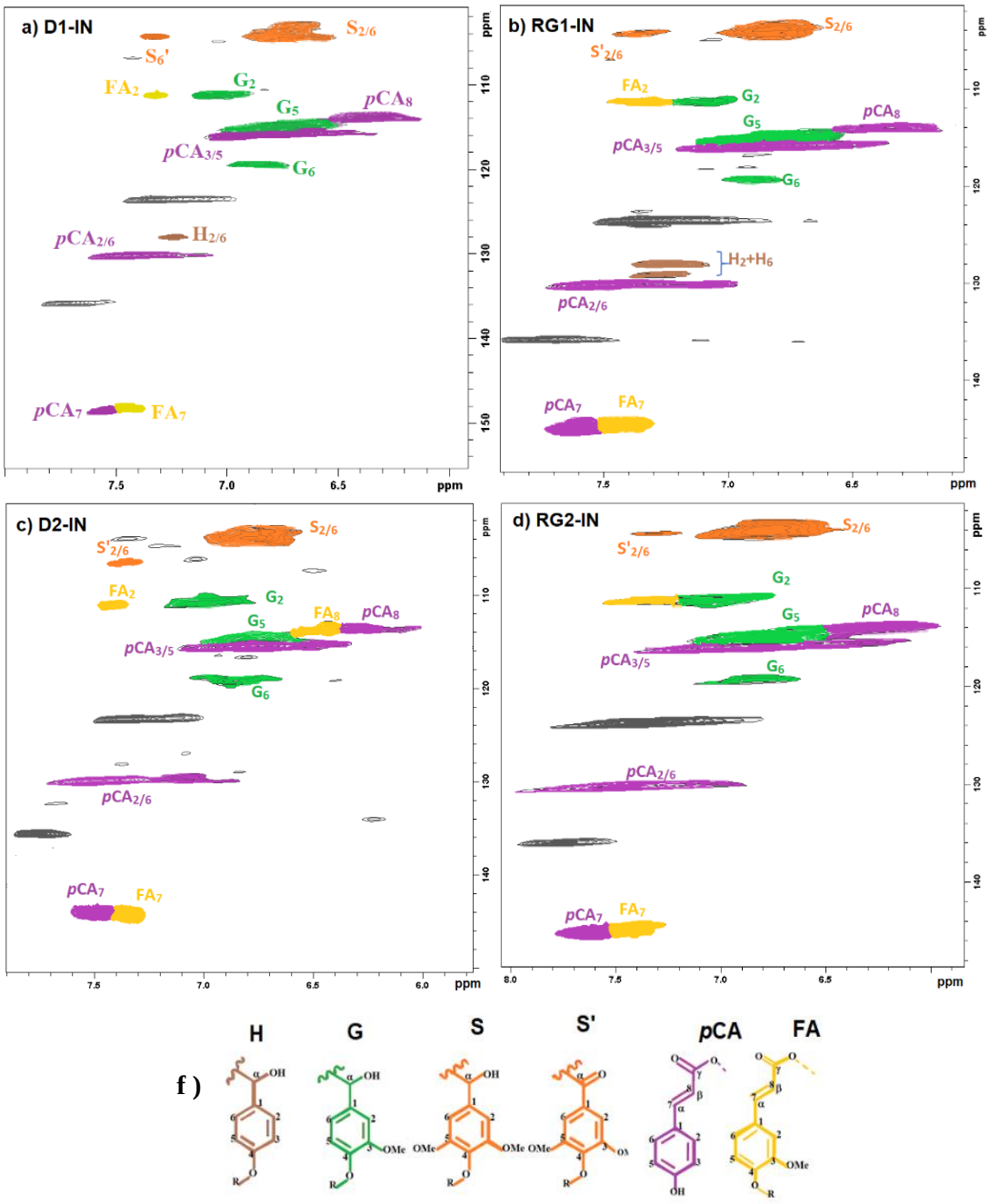

Figure 4.9. HSQC of sorghum whole-cell wall gels in DMSO-d_6/pyridine-d5 (4:1) solvent in the aromatic region at internodes (IN) (a) D1-IN, (b) RG1-IN, (c) D2-IN, (d) RG2-IN and (f) lignin structures: p-hydroxyphenyl units (H), guaiacyl units (G), syringyl units (S), oxidized syringyl units at Cα (S'), p-coumarate (*p*CA), and ferulate (FA). The signals in black/grey correspond to pyridine d_5.

In summary, the structural carbohydrate, lignin compositional, and structural variations in the cell wall of RG and Della sorghum stalks provide new opportunities for the investigation of their biomechanical strength, which could be enlightening about the lodging behavior. The significant variations in the glucan, xylan, and lignin content may result in disparity in the mechanical behavior

of the stalk. Furthermore, structural, and compositional features of cellulose and lignin (e.g., CI, S/G ratio) and the occurrence of different extents of non-acylated and naturally γ-acylated β–O–4 substructures may have different roles on the stiffness of the stalks. A future study will evaluate the impact of structural carbohydrates and lignin on the mechanical strength of the stalks and correlate cell wall compositional and structural differences in RG and Della with their corresponding biomechanical strength.

4.5 References

[1] Xia, J., Zhao, Y., Burks, P., Pauly, M. & Brown, P. J. A sorghum NAC gene is associated with variation in biomass properties and yield potential. Plant Direct 2, e00070 (2018).

[2] Bakeer, B., Taha, I., El-Mously, H. & Shehata, S. On the characterisation of structure and properties of sorghum stalks. Ain Shams Eng. J. 4, 265–271 (2013).

[3] Cook, D. D. et al. Stalk Lodging: A Portable Device for Phenotyping Stalk Bending Strength of Maize and Sorghum. bioRxiv (2019) doi:https://doi.org/10.1101/567578.

[4] Berry, P. & Spink, J. Predicting yield losses caused by lodging in wheat. Field Crops Res. 137, 19–26 (2012).

[5] Davison, B. H., Parks, J., Davis, M. F. & Donohoe, B. S. Plant Cell Walls: Basics of Structure, Chemistry, Accessibility and the Influence on Conversion. in Aqueous Pretreatment of Plant Biomass for Biological and Chemical Conversion to Fuels and Chemicals (ed. Wyman, C. E.) 23–38 (John Wiley & Sons, Ltd, 2013). doi:10.1002/9780470975831.ch3.

[6] Liao, J. J., Latif, N. H. A., Trache, D., Brosse, N. & Hussin, M. H. Current advancement on the isolation, characterization and application of lignin. Int. J. Biol. Macromol. 162, 985–1024 (2020).

[7] Rongpipi, S., Ye, D., Gomez, E. D. & Gomez, E. W. Progress and Opportunities in the Characterization of Cellulose – An Important Regulator of Cell Wall Growth and Mechanics. Front. Plant Sci. 9, (2019).

[8] Cosgrove, D. C. & Jarvis, M. Comparative structure and biomechanics of plant primary and secondary cell walls. Front. Plant Sci. 3, (2012).

[9] Wang, J., Zhu, J., Huang, R. & Yang, Y. Investigation of cell wall composition related to stem lodging resistance in wheat (Triticum aestivum L.) by FTIR spectroscopy. Plant Signal. Behav. 7, 856–863 (2012).

[10] Sekhon, R. S. et al. Stalk Bending Strength is Strongly Associated with Maize Stalk Lodging Incidence Across Multiple Environments. Field Crops Res. 249, 107737 (2020).

[11] Berry, P. et al. Understanding and Reducing Lodging in Cereals. Adv. Agron. 84, 217–271 (2004).

[12] Liu, Q., Luo, L. & Zheng, L. Lignins: Biosynthesis and Biological Functions in Plants. Int. J. Mol. Sci. 19, (2018).

[13] Xiang, D. et al. Relationship between stem characteristics and lodging resistance of Tartary buckwheat (Fagopyrum tataricum). Plant Prod. Sci. 22, 202–210 (2019).

[14] Li, M., Pu, Y. & Ragauskas, A. J. Current Understanding of the Correlation of Lignin Structure with Biomass Recalcitrance. Front. Chem. 4, (2016).

[15] Sattler, S. E. et al. Characterization of Novel Sorghum brown midrib Mutants from an EMS-Mutagenized Population. G3 GenesGenomesGenetics 4, 2115–2124 (2014).

[16] Petti, C. et al. Sorghum mutant RGdisplays antithetic leaf shoot lignin accumulation resulting in improved stem saccharification properties. Biotechnol. Biofuels 6, 146 (2013).

[17] Vogler, H., Felekis, D., Nelson, B. J. & Grossniklaus, U. Measuring the Mechanical Properties of Plant Cell Walls. Plants 4, 167–182 (2015).

18. Mengistie, E. et al. Fatty Acid Profile-Based Chemometrics to Differentiate Metabolic Variations in Sorghum. ACS Food Sci. Technol. 1, 2127–2134 (2021).

[19] Santos, J. et al. Lignin-enriched Fermentation Residues from Bioethanol Production of Fast-growing Poplar and Forage Sorghum. Bioresources 10, 5215–5232 (2015).

[20] Kline L., Hayes D, Womac A, Labbé N. Simplified determination of lignin content in hard and soft woods via UV-spectrophotometric analysis of biomass dissolved in ionic liquids. BioResources 5, 1366–1383 (2010).

[21] Balogun, A. O. & McDonald, A. G. Decomposition kinetic study, spectroscopic and pyrolytic analyses of Isoberlinia doka and Pinus ponderosa. Biomass Convers. Biorefinery 6, 315–324 (2016).

[22] Hurtubise, F. G. & Krassig, Hans. Classification of Fine Structural Characteristics in Cellulose by Infared Spectroscopy. Use of Potassium Bromide Pellet Technique. Anal. Chem. 32, 177–181 (1960).

[23] Faix, O., Meier, D. & Fortmann, I. Thermal degradation products of wood. Holz Als Roh- Werkst. 48, 351–354 (1990).

[24] Faix, O., Fortmann, I., Bremer, J. & Meier, D. Thermal degradation products of wood. Holz Als Roh-Werkst. 49, 213–219 (1991).

[25] Meier, D. & Faix, O. Pyrolysis-Gas Chromatography-Mass Spectrometry. in Methods in Lignin Chemistry (eds. Lin, S. Y. & Dence, C. W.) 177–199 (Springer, 1992). doi:10.1007/978-3-642-74065-7_13.

[26] Poletto, M., Ornaghi, H. & Zattera, A. Native Cellulose: Structure, Characterization and Thermal Properties. Materials 7, 6105–6119 (2014).

[27] Segal, L., Creely, J. J., Martin, A. E. & Conrad, C. M. An Empirical Method for Estimating the Degree of Crystallinity of Native Cellulose Using the X-Ray Diffractometer. Text. Res. J. 29, 786–794 (1959).

[28] French, A. D. & Santiago Cintrón, M. Cellulose polymorphy, crystallite size, and the Segal Crystallinity Index. Cellulose 20, 583–588 (2013).

[29] Kim, H. & Ralph, J. Solution-state 2D NMR of ball-milled plant cell wall gels in DMSO-d6 / pyridine-d5. Org. Biomol. Chem. 8, 576–591 (2010).

[30] Byrt, C. S. et al. Prospecting for Energy-Rich Renewable Raw Materials: Sorghum Stem Case Study. PLOS ONE 11, e0156638 (2016).

[31] Petti, C. et al. Comparative feedstock analysis in Setaria viridis L. as a model for C4 bioenergy grasses and Panicoid crop species. Front. Plant Sci. 4, 181 (2013).

[32] McKinley, B. A. et al. Variation in energy sorghum hybrid TX08001 biomass composition and lignin chemistry during development under irrigated and non-irrigated field conditions. PLOS ONE 13, e0195863 (2018).

[33] Patton, A. R. & Gieseker, L. Seasonal Changes in the Lignin and Cellulose Content of Some Montana Grasses. J. Anim. Sci. 1, 22–26 (1942).

[34] Mann, D. G. J. et al. Rapid Assessment of Lignin Content and Structure in Switchgrass (Panicum virgatum L.) Grown Under Different Environmental Conditions. BioEnergy Res. 2, 246–256 (2009).

[35] Gomez, F. E., Muliana, A. H., Niklas, K. J. & Rooney, W. L. Identifying Morphological and Mechanical Traits Associated with Stem Lodging in Bioenergy Sorghum (Sorghum bicolor). BioEnergy Res. 10, 635–647 (2017).

[36] Yuan, T.-Q., Sun, S.-N., Xu, F. & Sun, R.-C. Characterization of Lignin Structures and Lignin–Carbohydrate Complex (LCC) Linkages by Quantitative 13C and 2D HSQC NMR Spectroscopy. J. Agric. Food Chem. 59, 10604–10614 (2011).

[37] Wang, B., Smith, S. M. & Li, J. Genetic Regulation of Shoot Architecture. Annu. Rev. Plant Biol. 69, 437–468 (2018).

[38] Gao, Y., Lipton, A. S., Wittmer, Y., Murray, D. T. & Mortimer, J. C. A grass-specific cellulose–xylan interaction dominates in sorghum secondary cell walls. Nat. Commun. 11, 6081 (2020).

[39] Novaes, E., Kirst, M., Chiang, V., Winter-Sederoff, H. & Sederoff, R. Lignin and Biomass: A Negative Correlation for Wood Formation and Lignin Content in Trees1. Plant Physiol. 154, 555–561 (2010).

[40] Hatfield, R. D., Wilson, J. R. & Mertens, D. R. Composition of cell walls isolated from cell types of grain sorghum stems. J. Sci. Food Agric. 79, 891–899 (1999).

[41] Petti, C., Hirano, K., Stork, J. & DeBolt, S. Mapping of a Cellulose-Deficient Mutant Named dwarf1-1 in Sorghum bicolor to the Green Revolution Gene gibberellin20-oxidase Reveals a Positive Regulatory Association between Gibberellin and Cellulose Biosynthesis. Plant Physiol. 169, 705–716 (2015).

[42] Richie, W. R. & McBee, G. G. Structural components in Sorghum stem biomass. Bioresour. Technol. 38, 15–22 (1991).

[43] Billa, E., Koullas, D. P., Monties, B. & Koukios, E. G. Structure and composition of sweet sorghum stalk components. Ind. Crops Prod. 6, 297–302 (1997).

[44] Ghaffar, S. H. & Fan, M. Revealing the morphology and chemical distribution of nodes in wheat straw. Biomass Bioenergy 77, 123–134 (2015).

[45] Corredor, D. Y. et al. Evaluation and Characterization of Forage Sorghum as Feedstock for Fermentable Sugar Production. Appl. Biochem. Biotechnol. 158, 164–179 (2009).

[46] Stark, N. M., Yelle, D. J. & Agarwal, U. P. Techniques for Characterizing Lignin. in Lignin in Polymer Composites 49–66 (Elsevier, 2016). doi:10.1016/B978-0-323-35565-0.00004-7.

[47] Faix, O. Classification of Lignins from Different Botanical Origins by FT-IR Spectroscopy. Holzforschung 45, 21–28 (1991).

[48] Liu, C., Wang, X., Lin, F., Zhang, H. & Xiao, R. Structural elucidation of industrial bioethanol residual lignin from corn stalk: A potential source of vinyl phenolics. Fuel Process. Technol. 169, 50–57 (2018).

[49] Boukir, A., Fellak, S. & Doumenq, P. Structural characterization of Argania spinosa Moroccan wooden artifacts during natural degradation progress using infrared spectroscopy (ATR-FTIR) and X-Ray diffraction (XRD). Heliyon 5, e02477 (2019).

[50] Rodrigue, S.-T., Barhé, T., Souloungangа, P., Akagah, A. & Jeso, B. A comparative study of the syringyl, guaiacyl and hydroxyl groups units distribution in some African tropical hardwoods' lignin by Py-GC/MS and spectroscopic techniques. J. Mater. Environ. Sci. 8, 2530–2540 (2016).

[51] Nelson, M. L. & O'Connor, R. T. Relation of certain infrared bands to cellulose crystallinity and crystal latticed type. Part I. Spectra of lattice types I, II, III and of amorphous cellulose. J. Appl. Polym. Sci. 8, 1311–1324 (1964).

[52] Sammons, R. et al. Characterization of Organosolv Lignins using Thermal and FT-IR Spectroscopic Analysis. BioResources 8, (2013).

[53] Ziebell, A. et al. Increase in 4-Coumaryl Alcohol Units during Lignification in Alfalfa (Medicago sativa) Alters the Extractability and Molecular Weight of Lignin. J. Biol. Chem. 285, 38961–38968 (2010).

[54] Hoffmann, A., Bremer, M. & Fischer, S. Determination of Monomeric Building Blocks by Py-GC/MS of Lignins from Agricultural Residues. Austin Biomol. 3, (2019).

[55] Del Río, J. C. et al. Structural Characterization of Wheat Straw Lignin as Revealed by Analytical Pyrolysis, 2D-NMR, and Reductive Cleavage Methods. J. Agric. Food Chem. 60, 5922–5935 (2012).

[56] Del Río, J. C. et al. Structural Characterization of the Lignin in the Cortex and Pith of Elephant Grass (Pennisetum purpureum) Stems. J. Agric. Food Chem. 60, 3619–3634 (2012).

[57] Van Kuijk, S. J. A. et al. Selective ligninolysis of wheat straw and wood chips by the white-rot fungus Lentinula edodes and its influence on in vitro rumen degradability. J. Anim. Sci. Biotechnol. 7, 55 (2016).

[58] Olsson, A.-M. & Salmén, L. The effect of lignin structure on the viscoelastic properties of wood. Nord. Pulp Pap. Res. J. 12, 140–144 (1997).

[59] Wei, L. et al. Genetic and transcriptomic analyses of lignin- and lodging-related traits in Brassica napus. Theor. Appl. Genet. 130, 1961–1973 (2017).

[60] Lupoi, J. S., Singh, S., Simmons, B. A. & Henry, R. J. Assessment of Lignocellulosic Biomass Using Analytical Spectroscopy: an Evolution to High-Throughput Techniques. BioEnergy Res. 7, 1–23 (2014).

[61] Yan, J., Hu, Z., Pu, Y., Charles Brummer, E. & Ragauskas, A. J. Chemical compositions of four switchgrass populations. Biomass Bioenergy 34, 48–53 (2010).

62. El Hage, R. et al. Characterization of milled wood lignin and ethanol organosolv lignin from miscanthus. Polym. Degrad. Stab. 94, 1632–1638 (2009).

[63] Van Erven, G. et al. Quantification of Lignin and Its Structural Features in Plant Biomass Using 13C Lignin as Internal Standard for Pyrolysis-GC-SIM-MS. Anal. Chem. 89, 10907–10916 (2017).

[64] Lourenço, A. et al. Lignin Composition and Structure Differs between Xylem, Phloem and Phellem in Quercus suber L. Front. Plant Sci. 7, (2016).

[65] Carrier, M. et al. Thermogravimetric analysis as a new method to determine the lignocellulosic composition of biomass. Biomass Bioenergy 35, 298–307 (2011).

[66] Lv, G. & Wu, S. Analytical pyrolysis studies of corn stalk and its three main components by TG-MS and Py-GC/MS. J. Anal. Appl. Pyrolysis 97, 11–18 (2012).

[67] Wang, T., Yin, J., Liu, Y., Lu, Q. & Zheng, Z. Effects of chemical inhomogeneity on pyrolysis behaviors of corn stalk fractions. Fuel 129, 111–115 (2014).

[68] Burhenne, L., Messmer, J., Aicher, T. & Laborie, M.-P. The effect of the biomass components lignin, cellulose and hemicellulose on TGA and fixed bed pyrolysis. J. Anal. Appl. Pyrolysis 101, 177–184 (2013).

[69] Brebu, M. & Vasile, C. Thermal degradation of lignin – A Review. Cellul. Chem. Technol. 44, 353–363 (2010).

[70] Huang, S., Wu, Q., Zhou, D. & Huang, R. Thermal Decomposition Properties of Materials from Different Parts of Corn Stalk. BioResources 10, 2020–2031 (2015).

[71] Watkins, D., Nuruddin, Md., Hosur, M., Tcherbi-Narteh, A. & Jeelani, S. Extraction and characterization of lignin from different biomass resources. J. Mater. Res. Technol. 4, 26–32 (2015).

[72] Agarwal, U. P., Ralph, S. A., Reiner, R. S. & Baez, C. Probing crystallinity of never-dried wood cellulose with Raman spectroscopy. Cellulose 23, 125–144 (2016).

[73] Agarwal, U. P., Ralph, S. A., Reiner, R. S. & Baez, C. New cellulose crystallinity estimation method that differentiates between organized and crystalline phases. Carbohydr. Polym. 190, 262–270 (2018).

[74] Agarwal, U. P., Ralph, S. A., Baez, C. & Reiner, R. S. Contributions of Crystalline and Noncrystalline Cellulose Can Occur in the Same Spectral Regions: Evidence Based on Raman and IR and Its Implication for Crystallinity Measurements. Biomacromolecules 22, 1357–1373 (2021).

[75] Kim, H. & Ralph, J. A gel-state 2D-NMR method for plant cell wall profiling and analysis: a model study with the amorphous cellulose and xylan from ball-milled cotton linters. RSC Adv 4, 7549–7560 (2014).

[76] Balakshin, M., Capanema, E., Gracz, H., Chang, H. & Jameel, H. Quantification of lignin-carbohydrate linkages with high-resolution NMR spectroscopy. Planta 233, 1097–1110 (2011).

[77] Komatsu, T. & Kikuchi, J. Comprehensive Signal Assignment of 13 C-Labeled Lignocellulose Using Multidimensional Solution NMR and 13 C Chemical Shift Comparison with Solid-State NMR. Anal. Chem. 85, 8857–8865 (2013).

[78] Rencoret, J. et al. HSQC-NMR analysis of lignin in woody (Eucalyptus globulus and Picea abies) and non-woody (Agave sisalana) ball-milled plant materials at the gel state 10th EWLP, Stockholm, Sweden, August 25–28, 2008. Holzforschung 63, (2009).

[79] Mansfield, S. D., Kim, H., Lu, F. & Ralph, J. Whole plant cell wall characterization using solution-state 2D NMR. Nat. Protoc. 7, 1579–1589 (2012).

[80] Ragauskas, A. et al. Structural Characterization of Lignin in Wild-Type versus COMT Down-Regulated Switchgrass. Front. Energy Res. 1, (2014).

[81] Komatsu, T. & Kikuchi, J. Comprehensive Signal Assignment of 13C-Labeled Lignocellulose Using Multidimensional Solution NMR and 13C Chemical Shift Comparison with Solid-State NMR. Anal. Chem. 85, 8857–8865 (2013).

[82] Rencoret, J. et al. Variability in Lignin Composition and Structure in Cell Walls of Different Parts of Macaúba (Acrocomia aculeata) Palm Fruit. J. Agric. Food Chem. 66, 138–153 (2018).

[83] Del Río, J. C. et al. Highly Acylated (Acetylated and/or p-Coumaroylated) Native Lignins from Diverse Herbaceous Plants. J. Agric. Food Chem. 56, 9525–9534 (2008).

[84] Anderson, N. A. et al. Manipulation of Guaiacyl and Syringyl Monomer Biosynthesis in an Arabidopsis Cinnamyl Alcohol Dehydrogenase Mutant Results in Atypical Lignin Biosynthesis and Modified Cell Wall Structure. Plant Cell 27, 2195–2209 (2015).

[85] Fornalé, S. et al. Changes in Cell Wall Polymers and Degradability in Maize Mutants Lacking 3′- and 5′-O-Methyltransferases Involved in Lignin Biosynthesis. Plant Cell Physiol. 58, 240–255 (2017).

[86] Eudes, A. et al. SbCOMT (Bmr12) is involved in the biosynthesis of tricin-lignin in sorghum. PLOS ONE 12, e0178160 (2017).

[87] Del Río, J. C. et al. Differences in the chemical structure of the lignins from sugarcane bagasse and straw. Biomass Bioenergy 81, 322–338 (2015).

[88] Wen, J.-L., Sun, S.-L., Xue, B.-L. & Sun, R.-C. Recent Advances in Characterization of Lignin Polymer by Solution-State Nuclear Magnetic Resonance (NMR) Methodology. Materials 6, 359–391 (2013).

Chapter 5: Biomechanical and Viscoelastic Properties of Sorghum Stalk and its Correlation with Composition

"Biomechanical and Viscoelastic Properties of Sorghum Stalk and its Correlation with Composition", ***Submitted to the journal Cellulose***

5.1 Abstract

The biomechanical strength and structural rigidity of grain stalks are critical determinants of stalk lodging resistance. From the structural constituents of the stalk, the rind provides the principal structure supporting cells against tension and bending loads. In this work, the biomechanical and viscoelastic behavior of the rind from the internodes of two sorghum varieties (Della and RG), grown in two different growing seasons, were evaluated by three-point micro-bending tests using a dynamic mechanical analysis (DMA). In addition, the chemical composition of rinds and the microfibril angle (MFA) of the S2 cell wall were determined using XRD. The result revealed that the biomechanical behavior of Della varieties was stiffer and more resistant to loads than RG varieties. Two features of the rind biomechanical properties, flexural modulus (FM) and flexural strength (FS), showed a significant reduction for RG. Particularly, a reduction of FS by (16-37%) and FM (22-41%) were detected for RG1. Changes in the stalks rind biomechanical properties were attributed to cell wall components. Total lignin and glucan/cellulose contents were positively correlated to FM and FS of the rind and its viscoelastic behavior, subsequently, an increase in the two cell wall components drive an increase in stiffness. Furthermore, the MFA of the rind was also found to influence the rind's strength.

5.2 Introduction

Crops are widely grown across the globe, mainly for food, and crop yield can be reduced significantly by lodging. Lodging is defined as structural failure of the stem both at the microstructure and macrostructure level before harvesting [1]. Lodging causes dislocation leading to breakage of the stalk on the ground [2]. Lodging limits grain yield in cereal crops such as sorghum, maize, rice, and wheat [3]. Particularly in high-yielding cereal crops, lodging may result in global annual yield reductions from 2 to 30% [4], depending on the stage of growth. Biomechanical properties of stalks are important in determining their strength, which in turn impacts their resistance against lodging. Therefore, enhanced biomechanical strength of the stem is essential for lodging resistance and increasing annual yield. Despite its enormous economic impact on commercial crops, stem lodging mechanisms are not clearly understood. Previous studies used methods such as bending tests, histochemical methods, rind penetrometer, and crushing strength measurements to understand stem biomechanical behavior [5]. However, these approaches are inadequate to fully understand the

buckling of stem structures, as the chemical composition of the stalks was not considered. Thus, approaches involving chemical analysis together with the biomechanical behavior of the crops will improve our understanding to develop lodging-resistant varieties, enhancing agricultural productivity, and narrowing the knowledge gap in stalk lodging mechanisms.

The degree of lodging depends on many plant characteristics and other environmental aspects. Plant characteristics regulate its height and architecture, and thus contribute to lodging resistance [4]. Plants have adapted unique stem anatomical, morphological, and hierarchical architectures to maintain structural integrity when subjected to loads [6], [7]. Anatomical (e.g., vascular bundles, parenchyma, and sclerenchyma cells), morphological (e.g., plant height, internode length, stem diameter, rind thickness), biochemical (e.g., structural and nonstructural polymer composition), and genetic traits of the stalk contribute to lodging susceptibility [8]–[10]. Anatomical features of stems such as sclerenchyma tissue can impact lodging resistance. Cultivars with thicker sclerenchyma tissue with high content of cellulose and lignin scored lower lodging rates than cultivars with thin-layered mechanical tissues [11]. The biochemical traits of stems, such as lignin, cellulose, and hemicellulose play a major role in biomechanical strength and rigidity. Lignin is a dominant structural component of secondary cell walls and middle lamella that provides strength to plants and rigidity of basal stems [12], [13]. Higher lignin and cellulose contents in crop stems result in higher rigidity of culm [14], enhanced lodging resistance and stem strength [15].

Sorghum stalks fail structurally because of their weak biomechanical properties [16]. The biomechanical properties of sorghum internodes were found to exhibit significantly lower flexural modulus (FM), flexural strength (FS), and flexural rigidity than the nodes. Moreover, the study shows that nodes of sorghum were two to three-fold stronger, stiffer, and more rigid than the internodes, and are less liable to structural failure of the stalk [17]. Plant cell walls are microfibril-based nanocomposites with distinct polymer matrix arrangements and structures. The higher-order organization of cellulose microfibrils into bundles and discrete lamellae results in different rheological and biomechanical properties [18]. Therefore, investigation of stalk failure, beyond simply determining the elastic modulus and ultimate strength [16], needs to be correlated with structural compositions of the cell wall for a better understanding of the sorghum biomechanical and lodging behavior.

Stems provide physical support to the leaves, grain, and aid the transport of water and nutrients in crops [19]. Sorghum stems have sclerenchyma (epidermis and rind with many sub-epidermal cell layers) as well as parenchyma tissue (pith, consisting of vascular bundles and soft tissues) [16]. Because parenchyma cells can absorb the effects of environmental forces such as light, wind, and rain

without mechanical damage, stem standability increases with parenchyma layer thickness [12]. Although pith parenchyma cells play a vital role in stabilizing the stem and reducing the risk of local buckling and collapse, up to 80% of the mechanical strength of a stalk comes from the rind [10], [20]. Thus, the mechanical strength of stalks primarily depends on the rind of the internode. The rind is a dense and fibrous tissue having higher mechanical strength and provides the principal structure supporting cells against tension and bending loads [14]. Studies based on the dissection of stalk strength into its constituent features showed that the structural composition of the rind, not the pith or total girth, appears to be the most important stalk strength-determining component [21]. Cell wall chemical composition studies on corn stalks showed that the rind had higher lignin and cellulose content than other components [21]. Therefore, it is necessary to evaluate the biomechanical and viscoelastic nature of sorghum rinds to reveal the macromolecular and lodging variation of stems.

Plant cell wall layers are considered a nanofiber-reinforced composite material consisting of helically wound crystalline cellulose microfibrils embedded in a matrix of amorphous cellulose, hemicelluloses, and lignin [22]. Dynamic mechanical analysis (DMA) can be used to examine composite properties and the response of individual cell wall components in-situ and enlightens the individual cell wall polymer contributions as well as their interactions [23]. DMA has been applied to investigate the viscoelastic and mechanical properties of barley stems [24]. The present study aims to evaluate the rind biomechanical strength from two sorghum stalk varieties using DMA and correlate it with the accumulation of the main polymeric components of the cell wall (cellulose, hemicellulose, and lignin).

5.3 Materials and methods

5.3.1 Plant material

Sorghum stalks were collected from the University of Kentucky Horticulture Research Farm (Emmitt Road, Lexington, KY) during the 2018 (Della1, RG1) and 2019 (Della 2, RG2) growing seasons. The rind from the internodes was sectioned out using a razor blade and the residual pith on the inner surface was removed and smoothed (Figure 5.1a). The thickness and width of the rinds at internodes were measured using a micrometer and caliper, respectively.

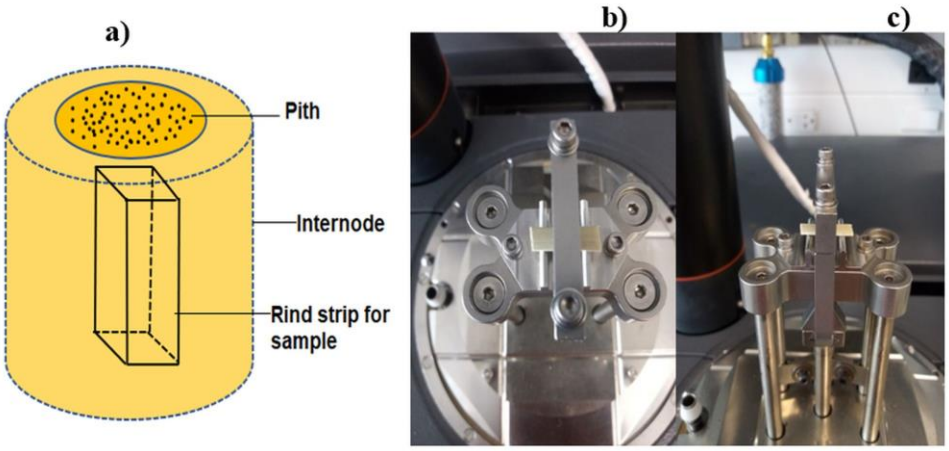

Figure 5.1. Experimental setup for DMA tests ; (a) depiction of rind specimen sectioned from stalk internodes; (b) rind specimen in the 3-point bending fixture - top view; and (c) rind specimen in the 3-point bending fixture - side view

5.3.2 Mechanical and viscoelastic properties

The viscoelastic and biomechanical properties of sectioned internode rind specimens were investigated using a Q800 DMA (TA Instruments) in three-point bending (10 mm span) (Figure 5.1b, c).

5.3.2.1 Micro-biomechanical bending tests

All micro-biomechanical bending tests were performed on rind tissues of stalk samples (at ambient conditions and ~4% moisture content). Two individual stalks from either genotype across both years were selected and rind tissues were sectioned from IN1-IN5 (Figure 5.2a). At each internode, at least 8 technical replicates of rind tissue (approximately 14 x 3.6 x 1.1 mm3) were collected and tested at a strain rate of 0.5 %·min-1 to the final strain of 6%, until failure was detected. Data were analyzed by TA analysis software and the stress-strain curves and flexural properties (FM and FS) were determined.

5.3.2.2 Viscoelastic properties response to relative humidity

The viscoelastic parameters (storage modulus (E'), loss modulus (E''), and tan δ)) of stalk rinds (approximately 10 × 4 × 1.5 mm^3), in triplicate, were also investigated using the DMA in 3-point bending mode (1 % strain). All samples were subjected to a relative humidity (RH) ramp (0 to 80%) at ambient temperature with the rate of 2%·min^{-1}. The viscoelastic properties of the sorghum rinds were evaluated as a function of RH.

5.3.2.3 Stress relaxation

The stress relaxation behavior of the specimen (approximately 12 × 4 × 1.5 mm^3 rinds) was determined using the DMA in 3-point bending mode by applying a constant strain of 5% throughout the experiment and measuring the corresponding stress required to maintain the deformation as a function of time for 15 min. At least 10 replicates were tested for each sample. The relaxation modulus E(t) was described according to the Generalized Maxwell model (GMM) as [25]:

$$E(t) = E_\infty + \sum_{i=1}^{n} E_i \exp\left(\frac{-E_i t}{\eta_i}\right) = E_\infty + \sum_{i=1}^{n} E_i \exp\left(\frac{-t}{\tau_i}\right) \quad \text{Eq. 1}$$

Where, E(t) is the relaxation modulus at time t. At long times the cell wall polymer molecules start to gradually accommodate the strain by conformational extension rather than bond distortion and the E(t) falls exponentially to a lower equilibrium modulus ($\lim_{t\to\infty} E(t) = E_\infty$). E_i are the relaxation modulus parameters and η_i is the viscosity of the dashpot for the ith series, n is the number of springs–dashpot, and $\tau_i = \eta_i / E_i$ is relaxation time.

5.3.2.4 Creep behavior

Creep is a slow continuous deformation of a material under constant stress. The creep behavior of the stalk rind (approximately 12 x 3.6 x 1.1 mm^3) was determined by DMA in 3-point bending mode with the constant stress of 40 MPa exerted for 15 min at ambient temperature and creep dynamical change was recorded. A preload force of 0.001 N was applied. At least 10 replicates were tested for each sample. The creep compliance C(t) was modeled according to the Generalized Kelvin model (GKM) [26] as:

$$C(t) = C_0 + C_1\left(1 - \exp\left(\frac{-t}{\tau_1}\right)\right) + C_2\left(1 - \exp\left(\frac{-t}{\tau_2}\right)\right) \quad \text{Eq. 2}$$

Where, C_0 is initial compliance; C_1 and C_2 are model coefficients, and τ_1 and τ_2 are retardation times.

5.3.2.5 Viscoelastic properties response to temperature

The viscoelastic properties of the stalk rind (approximately 12 x 4.0 x 1.6 mm^3), in triplicate, were determined using a temperature sweep (25 °C to 120 °C at 3 °C·min^{-1}) in 3-point bending mode with a constant strain of 1% and frequency of 1 Hz. Prior to the experiment, the rind specimen was equilibrated at 80% RH for 4 h. The softening temperature was measured from the peak of the loss modulus (E'') and *tan δ*.

5.3.3 Compositional analysis

After testing the biomechanical and viscoelastic properties, the rinds were collected for further compositional analysis using different analytical techniques.

5.3.3.1 Fourier-Transform InfraRed (FTIR) spectroscopy

FTIR spectra were obtained on previously 3-point bend tested specimens in triplicate using an iS5 spectrometer (Thermo-Nicolet) equipped with a ZnSe attenuated total reflection (iD5 ATR) accessory. The spectra were averaged, baseline corrected, and normalized to the highest band (1032 cm^{-1}, cellulose) using the Omnic v9 software.

5.3.3.2 Lignin and carbohydrate

Extractive-free samples (200 mg) were hydrolyzed using sulfuric acid (2 ml, 72%) for 60 min at 30 °C in a water bath followed by secondary hydrolysis (4% sulfuric acid, 30 min, 20 psi) in an autoclave according to a modified ASTM D 1106-96. The Klason lignin (KL) content was determined gravimetrically after filtration, whereas acid soluble lignin (ASL) was determined by UV/Vis spectroscopy (Genesys 50, ThermoScientific) at 205 nm using an absorption coefficient of 110 L g^{-1} cm^{-1} [27]. Structural carbohydrate analysis was performed on the hydrolyzed filtrate (5 mL), with the addition of mannitol as an internal standard, according to ASTM E 1758-01. The sugars were separated and quantified using high-performance liquid chromatography (HPLC, two Rezex RPM columns, 7.8 mm x 300 mm, Phenomenex) at 85 °C on elution with water (0.5 mL min^{-1}) using differential refractive index detection (Waters model 2414). Cellulose was estimated as the equivalent of glucose concentration, whereas hemicellulose was estimated from the summation of xylose, galactose, arabinose, and mannose monomers.

5.3.3.3 Microfibril angle by XRD

X-ray diffraction (XRD) analysis for crystallinity index (CI) was performed on milled 3-point bend tested specimens using a Siemens D5000 diffractometer using Cu Kα radiation (λ = 0.154 nm) from 2θ = 2 to 80° at 0.05° steps. After deconvolution of the amorphous and crystalline regions using Gaussian curve-fitting, the CI based on the area (CIA) and intensity (CII) methods, and the grain size of cellulose at (200) were determined [28]. MFA of cellulose on the exterior side of the 3-point bend tested rind specimen was determined using a Bruker D8 Discover XRD equipped with an array detector (GADDS). The data was collected using Cu-Kα radiation operating at 40 kV and 20 mA, and the area was integrated using the DIFFRAC.EVA software. MFA was determined according to the works of [29].

$$MFA = 1.575\times10{-}3\ T^3 - 1.431\times10{-}1\ T^2 + 4.693T - 36.19 \qquad \text{Eq. 3}$$

Where, parameter T was estimated from the curve fitted diffraction intensity of the (200) peak as described by [30] and shown in Figure 5.7a.

5.3.3.4 Analytical Py-GCMS

The p-hydroxyphenyl (H)/G/S ratio was determined by pyrolysis–GCMS (Py-GCMS) using a Pyrojector II unit (SGE Analytical Science) at 500oC coupled to a GC-MS (ISQ-Trace1300, ThermoScientific). The compounds were separated using ZB-5 capillary column (30 m × 0.25 mm Ø, 0.25 μm coating, Phenomenex) from 50 (1 min) to 250 °C (10 min) at 5 °C·min-1. Compounds were identified by comparison with standards, the literature [31] and NIST-2017 mass spectral library. The H/G/S ratio was determined from peak areas of lignin monomers by selective ion monitoring chromatogram for H between 7-15 min (m/z = 94, 107, 108, 120, 121, 134, 148), G between 18-23 min (m/z = 124, 135, 137, 138, 151, 164, 178) and S between 24-28 min (m/z = 154, 165, 167, 168, 181, 194, 208) [32].

5.3.3.5 Derivatization followed by reductive cleavage (DFRC)

The frequency of lignin β-ether bonds in the stalk rind was determined using the DFRC method according to the protocol [33] with slight modification. The sorghum rind sample (20 mg) was derivatized and solubilized with an acetic acid/acetyl bromide solution (4:1 v/v, 5 mL) upon stirring at 50 ^{o}C for 1 h, then acetyl bromide was removed under vacuum. The solid residue was dispersed in dioxane/acetic acid/water (5:4:1 v/v, 5 mL), zinc powder (50 mg) was added, and the mixture was stirred for 30 min at room temperature. The zinc powder was removed by filtration and tetracosane (10 mg in dichloromethane (CH_2Cl_2, 10 mL) was added as an internal standard to the filtrate. The organic layer was washed with saturated NH_4Cl, and recovered, then the aqueous layer was further extracted using CH_2Cl_2 (10 mL). The combined extracts were dried over anhydrous $NaSO_4$ and concentrated to dryness. Finally, the sample was acetylated with acetic acid/pyridine (1:1 v/v, 2 mL) at room temperature for 40 min, the reaction was quenched with ethanol, and excess reagents were removed under vacuum. The solid residue was dissolved in CH_2Cl_2 (1.5 mL) and analyzed by electron impact GC-MS (ISQ7000-Trace1300, ThermoScientific). Separation was achieved using a ZB-1ms capillary column (30 m x 0.25 mm i.d, Phenomenex) and temperature program of 100 ^{o}C (1 min) to 300 ^{o}C (10 min) at 5^{o}C·min^{-1}. Quantification and characterization of DFRC products were performed according to the literature and using response factors of 1.76, 1.85, and 2.06 respectively for H, G, and S [34].

5.3.4 Statistical analysis

The stalk rinds were not geometrically flawless due to their irregular shape. Thus, geometrically smoothed samples were taken at each internode (at least 8 replicates) and tested. The standard deviation was used to measure reproducibility for each specimen. One-way analysis of variance (ANOVA) was used to find differences in properties between the varieties at the internodes, where a 95% ($p = 0.05$) confidence level was used to assess statistical significance.

5.4 Results and Discussion

5.4.1 Micro-biomechanical bending tests

Bending test is a common mechanical phenotyping method to evaluate stalk strength and lodging, and can induce a similar failure pattern as observed in naturally lodged crops [35]. It was reported that the rind constitutes up to 80% of the strength of the stalk [20]. Thus, bending tests were performed on the rind to determine the FS and FM of the internodes from their stress-strain curves (Figure 5.2b). The FS describes the stress required to cause a rind to fail and can be taken as the ultimate resistance when the rind is exposed to bending stress [36]. Whereas the rind's stiffness is measured by the FM. Both FM and FS are the main indicators of lodging resistance of crop stalks [37].

It is shown (Figure 5.2c) that the FM of the rinds decreases towards the top section of the stem, which reveals the variation in physico-mechanical properties along the internodes. Consistent trends have been reported with axial flexural stiffness variation in maize [38] and rice stems [39]. The axial FM variation could be associated with morphological, anatomical, and compositional heterogeneity of the internodes [40]. The bottom basal internodes (IN1-IN2) were stiffer than the upper internodes (IN3-IN5), except for RG1 where IN2 and IN3 were similar (Figure 5.2c). The average FM values (Figure 5.2d) along the internodes for D1, RG1, D2, and RG2 were 2.1, 1.4, 2.7, and 2.3 GPa, respectively. This reveals that both RG1 and RG2 were significantly lower in FM than D1 and D2 varieties. In comparison to D1, a 33.2% reduction in FM was detected for RG1. Similarly, a 15.1% reduction in FM for RG2 was observed. The variations in FM for RG were likely from differences in their composition compared to the Della variety (discussed later). Differences between the two growing seasons were observed: the average FM of D1 was 25.7% lower than D2 while the average FM of RG1 was 59.8% lower than RG2. This observation reflects the pronounced impact of seasonal and environmental conditions on properties. Stem biomechanical property variations among different sorghum genotypes in terms of stem strength, rigidity, and stiffness have been reported [41]. Also, [42] had shown for barley that the biomechanical properties of wild-types were stiffer than their mutant varieties. In addition, the FM for wheat was 1.1-2.2 GPa and for barley was 1.1-1.3 GPa. Similar to fiber-reinforced composites, stem structures exhibit anisotropy (aligned fibers) in terms of

morphology, structure, stress distribution, growth, and development [14], which might lead to heterogeneity in the axial FM. It has been indicated that FM predicted 81% of the variation in maize stalk strength and is the predominant parameter in predicting maize stalk lodging [43]. Thus, considering the FM variations, Della could be regarded as a mechanically strong variant than the RG mutant within each growing season.

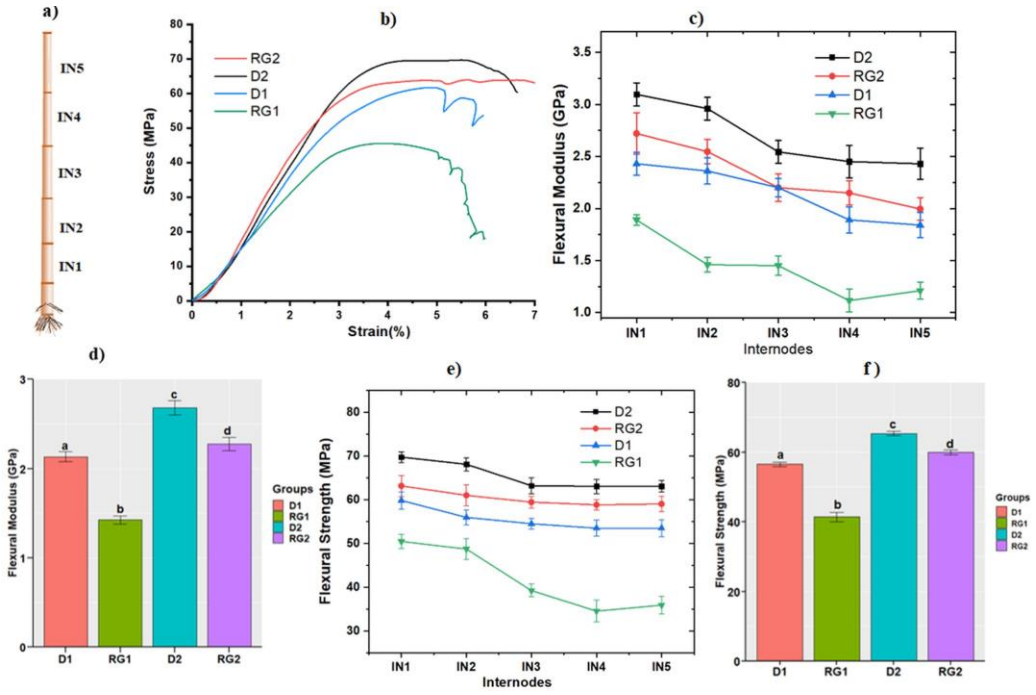

Figure 5.2. Flexural modulus and flexural stress across different morphologies determined by the DMA a) Schematics of stalks from internodes (IN1-IN5); b) representative flexural stress-strain curves of Della1 (D1), Della2 (D2), RG1, and RG2 stalk rinds; c) flexural modulus (FM) measured at various internodes (IN); d) averaged FM values for sorghum stalk rinds over IN1-IN5; e) flexural strength (FS) along the internodes (IN1-IN5); and f) averaged FS for D1, RG1, D2, and RG2. Different letters represent in (d and f) significant variations, and errors are standard error mean.

The FS of the D1, RG1, D2, and RG2 internode rinds ranged from 49.2-63.9, 30.9-58.1, 58.2-72.0, and 46.7-69.7 MPa, respectively (Figure 5.2e). Along the internodes, the results demonstrate (Figure 5.2e) a decrease in FS from the basal internode upwards and this trend has been previously reported [17]. Moreover, [44] demonstrated for maize stalk rinds that the lower internodes had higher FS than the upper internodes. Researchers have shown [45] that stalk lodging occurred in the upper basal internodes. As the rind constitutes the major structure of the stalk, this finding suggests that the upper internodes (IN3-IN5) might be highly vulnerable to lodging. Along the internodes within each stalk, ANOVA analysis shows that the FS of RG2 from IN1-IN5 was not statistically different. Similarly, the upper internodes (IN3-IN5) of D2, D1 and RG1 within each stalk rind were similar in FS. However, across the varieties, the FS of Della was found to be significantly higher than its

corresponding RG ($p < 0.001$) at all internodes, indicating its biomechanical property variation. The rinds of D2 and D1 were found to be 6.4-9.4% and 16-37% stronger than their respective RG1 and RG2 varieties. On an average basis (Figure 5.2f), the FS of D2 and D1 was about 8.2% and 27% higher, respectively than RG2 and RG1. These results suggest that the FS of RG1 was considerably reduced, which could be a combined effect of mutation and growing season. Moreover, this can also be explained by a significant reduction in lignin and glucan/cellulose content in RG1 (discussed later). Across the growing seasons, D1 and RG1 were 15-18% and 25-70% weaker, respectively than D2 and RG2. Surprisingly, D1 was 3.5-10% weaker than RG2. Stalk lodging was found highly associated with bending strength [46], thus according to FS values of stalk rinds, the RG variety could be structurally more lodging-susceptible. Sorghum rind thickness and strength were found to be highly correlated with lodging [47], which supports the lodging susceptibility of RG. Sclerenchyma cells around the vascular bundles of the stem are responsible for mechanical strength, thus a reduction of flexural properties in RG could be related to the reduction in lignin and carbohydrate accumulations in sclerenchyma cells, inducing stem lodging [10].

5.4.2 Viscoelastic properties

Viscoelastic properties of both Della (control group) and RG rinds were evaluated in terms of storage modulus (E'), loss modulus (E''), and dampening factor (tan δ) as a function of RH by DMA in 3-point bending mode. The E′ represents part of the deformation that can be recovered, thus characterizes the elastic component of the material. Whereas, E'' reflects the proportion of the deformation that cannot be recovered which is dissipated as heat due to viscous flow in a material [48]. The E' and E'' curves (Figure 5.3a and b, respectively) represent typical characteristics of wood's viscoelastic behavior [49]. The E' values of Della were higher than RG varieties, with D2 having the highest value of 3.6 GPa at 0% RH. The decreasing order of E' was D2 > RG2 > D1 > RG1. Generally, E' decreases with an increase in RH (Figure 5.3a) due to the plasticizing effect of water [49]. As RH increases moisture diffusion gradients are developed at the surface towards the center of the sample. Consequently, water can plasticize the cell wall matrix and decreases the rind E' [50]. A reduction in E′ of 11%, 9%, 14%, and 12%, was observed going from 0 to 80% RH respectively, for D2, RG2, D1, and RG1 samples. The water diffusion rate into the cell walls will depend on the structure and composition [51]. The viscoelastic behavior of the stalk rind will also be influenced by the hydroxyl groups (and other polar groups) present in amorphous zones of cellulose, hemicellulose, and lignin that interact with water [52]. Consequently, hydrogen bonds in the amorphous regions will be disrupted and new hydrogen bonds between water molecules and hydroxyl groups will be formed. This phenomenon leads to the expansion and swelling of the cell wall microstructures, which in turn

results in variation and decrease in E' [53]. The extent of change of E' was limited because of the low MC of the samples.

As relative humidity/moisture continues to increase, more energy is dissipated, and E'' increases (Figure 5.3b). D2 showed the highest E'' (177 MPa at 0%RH) compared to RG2, however, D1 was slightly greater than RG1 (lowest at 85 MPa at 0% RH). An increase in E'' was an indicator of enhanced plasticization [54]. The *tan δ* represents the damping or inner friction of a viscoelastic system. For the stalk rind, *tan δ* increased with RH which demonstrated that the absorbed water acted to increase energy dissipation (Figure 5.3c). Similar results have been reported in wood [55]. Going from 0 to 80% RH, *tan δ* was shown to increase by 114-120% for the stalk rind. The D2 samples have a higher *tan δ* compared to the other samples indicating a high non-elastic deformation. On the other hand, D1 and RG2 had relatively lower *tan* δ showing more elastic behavior. The clear variation of E'' and *tan δ* among varieties are shown in separate plots in Appendix Figure C1a and Figure C1b.

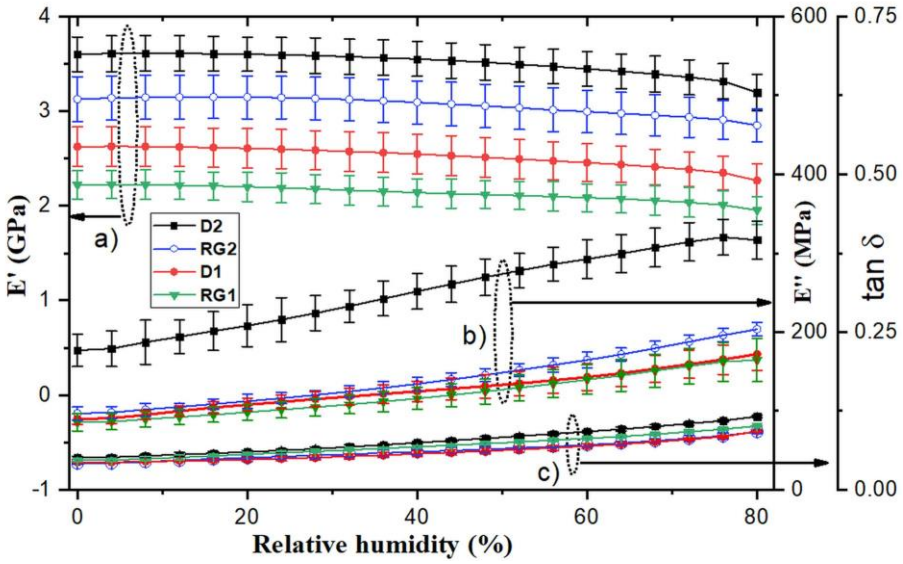

Figure 5.3. (a) Storage modulus (E'), (b) loss modulus (E'') and (c) damping factor (*tan δ*) as a function of relative humidity (RH) for sorghum stalk rind from Della and RG varieties (Whiskers represent the standard error mean).

In addition to moisture, viscoelastic properties of lignocellulosic materials are also influenced by temperature and were measured [24]. The E' was shown to decrease with temperature until ~70 °C and then started to increase to a peak maximum at about 88 °C (Figure 5.4a). Unlike polymers, the dynamic behavior of wood materials with temperature variation was not straightforward due to the coupling of thermal properties of three cell wall constituent polymers [56]. This peak at about 88 °C could be possibly due to aggregation and reformation of a network structure of lignin cross-linking at ~85 °C [57] and/or lignin relaxation [58]. Similar trends have been reported in polymers associated

with cold crystallization [59]. The *E′* values for the various stalk rinds were significantly different and decreased as follows D2 > RG2 > D1 > RG1, which was related to lignin content (discussed latter). These results agree with previous findings in transgenic aspen [60].

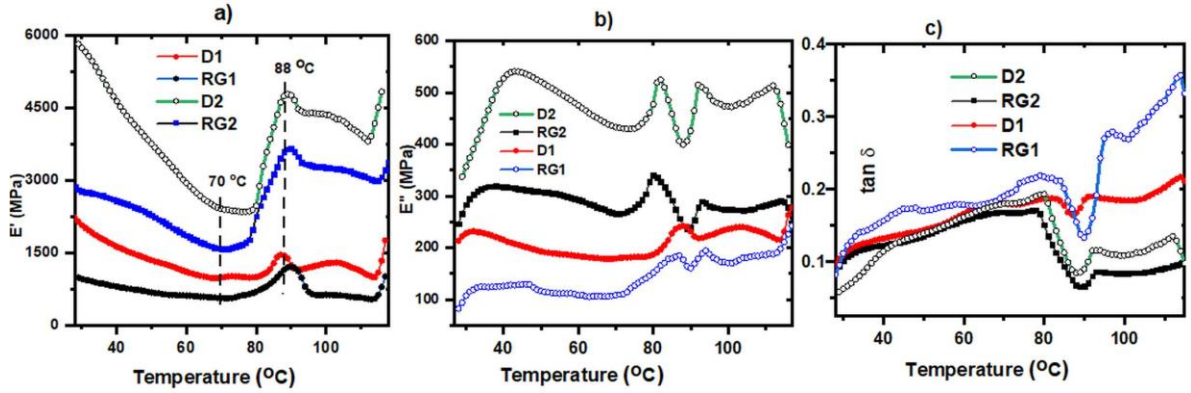

Figure 5.4. (a) Storage modulus (*E′*), (b) loss modulus (*E″*) and (c) *tan δ* thermograms of sorghum rind at IN3 for D1, RG1, D2, and RG2 samples.

The *in-situ* glass transition temperature (T_g) of lignin in the stalk was determined from the peaks of *E″* and *tan δ* [59], [60] (Figure 5.4b, c and Table 5.1). *In-situ* T_g values were consistent with the literature for wood [57]. Two distinct glass transitions (T_{g1} and T_{g2}) were observed in the rind samples (Figure 5.4b). For D2, T_{g1} was at 82 °C and T_{g2} at 92 °C, whereas for RG1 T_{g1} was at 80 °C and T_{g2} at 93 °C. For the D1 sample, only one T_g peak at 98 °C was observed (Table 5.1). Two minor peaks/shoulders at 87 °C and 94 °C were detected for RG1. Two-phase thermal transitions have been observed in wheat straw and spruce wood, in which α-transition (α_1) of 53 °C (straw), and 91 °C (spruce) associated with lignin was reported [61]. The observations of two transition peaks could be related to a less-rigid and high-rigid phase of lignin, which are interwoven respectively with amorphous and crystalline cellulose [62]. Furthermore, this can also reflect the supramolecular heterogeneity in the rind and *in-situ* thermo-rheological complexity of the lignocellulosic substrate [63]. The different thermo-rheological results revealed that lignin content, compositional, and structural variation within the varieties plays a role [60]. The T_g of lignin is dependent on moisture content [64]. Values for T_g of 72–88 °C for transgenic aspen lignin [60] and 80–95 °C for other woods [57], [65] have been reported.

The results also revealed that the first transition T_{g1} from tan δ peak slightly shifted towards lower temperatures as compared to T_{g1} from *E″* (Table 5.1). On the other hand, T_{g2} determined from *E″* and *tan δ* were only slightly different. The *tan δ* maximum at the distinct peak ($tan\ \delta_{max}$), which roughly reflects the quantity of the relaxing polymer [58], were different; (RG1 > D2 > D1 > RG2) at $tan\ \delta_{max1}$ and (RG1 >D1 > D2 > RG2) at $tan\ \delta_{max2}$ (Table 5.1). Given there was a significant difference in lignin

content and composition (discussed later) between the samples, the variation of *tan* δ_{max} between the varieties was expected. However, the correlation of lignin content and syringyl/guaiacyl (S/G ratio) with *in-situ* T_g (data not shown here) demonstrated that T_g was not significantly affected by both lignin content and composition. Unlike extracted lignin, the *in-situ* T_g might be highly impacted by molecular architecture and the lignin-carbohydrate complex in the cell wall [66].

Table 5.1. Glass transition temperatures (T_g) of stalk rind from D2, RG2, D1, and RG1 at IN3 determined by DMA

Sample	**E″**		**tan δ**		**tan $\delta_{maximum}$**	
	T_{g1} (°C)	T_{g2} (°C)	T_{g1} (°C)	T_{g2} (°C)	tan $_{\delta max1}$	tan δ_{max2}
D2	82	92	80	92	0.192	0.115
RG2	80	93	78	93	0.170	0.086
D1	88	—	83	91	0.186	0.188
RG1	87	94	79	97	0.218	0.280

5.4.3 Stress relaxation in stalk rind

Plant cell wall structural components (cellulose, lignin, and hemicellulose) behave as an anisotropic composite material [67]. As polymers, cell wall components exhibit time-dependent mechanical behavior representing the viscoelastic nature of plant material [68]. The viscoelastic nature of plant cell walls can be described by mechanical models consisting of both pure elastic springs and ideal viscous dashpots [69] and developed based on rheological principles [70]. The GMM was applied to fit the stress relaxation of the sorghum rind according to Eq. 1 for (n = 3). The experimental and fitted modulus of relaxation for D1, D2, RG1, and RG2 is shown in Figure 5.5a and the model parameters, equilibrium modulus of relaxation (E_∞), and coefficients (E_1 - E_3), are summarized in Table 5.2. The findings revealed that when the rind was exposed to constant strain and maintained over time, the internal stress developed decay exponentially from its initial maximum to an ultimate equilibrium state. Two distinct relaxation stages (regions i and ii, Figure 5.5a) were observed. Initially (t < 2 min), the modulus decreased exponentially due to a high rate of relaxation just after the application of maximum load, the curve flattens (t > 2 min) and approaches an equilibrium. Previous studies on the viscoelastic properties of barley stems [24] reported two stages of relaxation. The elastic deformation was due to bond distortion/breaking such as hydrogen bonds, van der Waals interactions, and electrostatic forces, which provide adhesion between the cellulose and hemicellulose–lignin matrix, which are likely responsible for the rapid relaxation [71]. The cellulose and hemicellulose–lignin matrix will become more mobile, and the loading stress will be released as these weak bonds break. On the other hand, the slow relaxation stage may be attributed to conformational changes and strong

covalent bonds. Significant variations in stress relaxation between rinds were observed (Figure 5.5a). This was consistent with the determined relaxation modulus from the GMM, shown by their equilibrium modulus (E_∞) (Table 5.2). It was shown that the modulus of relaxation (Table 5.2) of the Della varieties was considerably higher than their corresponding RG varieties. D2 had the highest E_∞ of 2.23 GPa, followed by RG2 (1.37 GPa), D1 (1.18 GPa) and RG1 (0.923 GPa). The model parameters (E_1-E_3) contribute to the initial modulus (E_0), which the samples had the following order of D2 > RG2 > D1 > RG1 (Table 5.2 and Figure 5.5a). On the other hand, the relaxation times (τ_1 - τ_3) determines the rate of change of the E_∞. The larger relaxation times, the smaller rate of change of E_∞ and vice versa. In this regard, D2 had significantly higher relaxation times (τ_1 - τ_3) than the other samples. The stress relaxation behavior of lignocellulosic material can significantly vary and was influenced by factors such as genetics and cell wall composition as seen in wheat straw cultivars [69]. The extent and the rate at which stress relaxation occurs is a critical factor in determining the effectiveness and performance of materials.

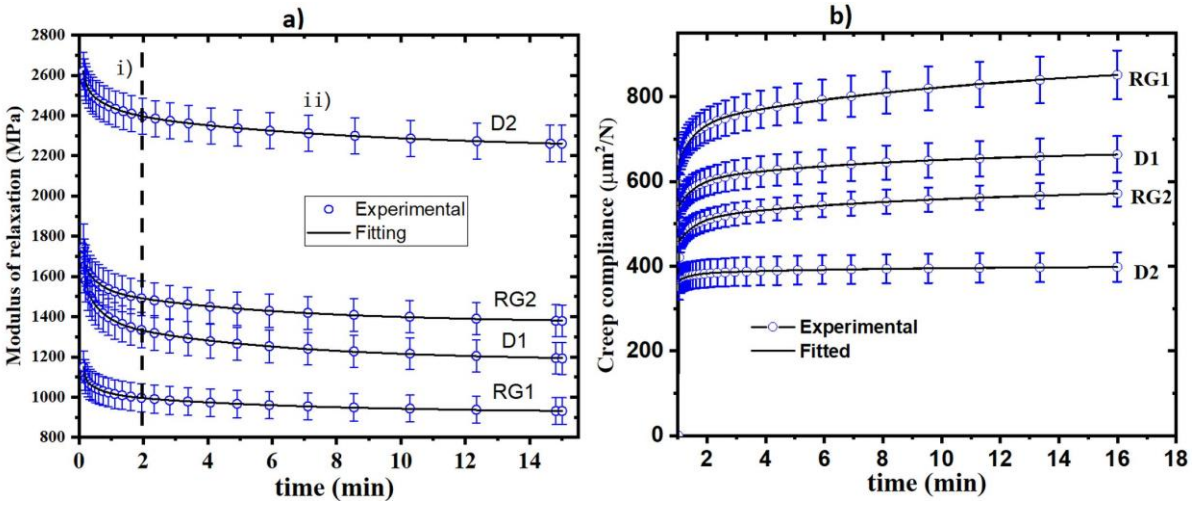

Figure 5.5. Modulus of relaxation and creep behavior a) Experimental and fitted modulus of relaxation; and b) creep behavior for stalk rinds of Della1 (D1), Della2 (D2), RG1, and RG2 samples. Whiskers represent the standard error mean, and each point represents the average value of several measurements.

Table 5.2. Stress relaxation generalized Maxwell model parameters for D1, RG1, D2, and RG2 sorghum rinds

Rind	E_∞ (MPa)	E_1 (MPa)	τ_1 (min)	E_2 (MPa)	τ_2 (min)	E_3 (MPa)	τ_3 (min)	E_0 (MPa)	R^2
D1	1180±21	421±57	0.054±0.003	205.1±2.1	0.52±0.04	206.7±4.7	5.6±0.4	2013	99.96
RG1	923±19	225±12	0.054±0.004	91.8±3.9	0.52±0.04	96.5±1.7	6.2±0.4	1336	99.96
D2	2231±66	291±16	0.103±0.006	133.2±4.2	0.76±0.06	198.7±2.4	7.9±0.5	2854	99.98
RG2	1368±14	567±25	0.033±0.004	168.6±7.7	0.46±0.04	168.4±3.6	5.7±0.4	2271	99.93

5.4.4 Creep behavior of rinds

Creep compliance measures the continuous deformation under constant stress over time [72]. The creep behavior of the rind was evaluated; experimental and fitted creep compliance is shown in Figure 5.5b and model parameters determined based on Eq.2 are summarized (Table 5.3). The creep behavior of the rinds (Figure 5.5b) showed an instantaneous deformation; elastic response; and viscous deformation, as verified by the literature [73]. The results (Figure 5.5b) revealed that the Della variety had significantly lower initial creep compliance (C_0) than its corresponding RG, which indicates an increase in deformation resistance. Initially, upon loading, the material has C_0 due to an instantaneous elastic deformation corresponding to bond distortion [74]. It is shown (Table 5.3) that C_0 of samples were significantly different and ranked in the following order: RG1 (372 $\mu m^2/N$) > D1 (356 $\mu m^2/N$) > RG2 (307 $\mu m^2/N$) > D2 (295 $\mu m^2/N$). The higher C_0 shows higher elastic deformation due to bond distortion, thereby RG1 showed the highest rate of deformation which was proven to have the lowest biomechanical strength (FM and FS). A larger instantaneous deformation in RG1 implies that biopolymers respond to the stress and orient along the stress direction in a short period, and the subsequent applied stress makes additional orientation and rearrangement of chains impossible [75], which results in greater deformation. The results were consistent with bending strength and stress relaxation behavior, which both showed higher deformation resistance of D2. Higher creep is associated with the poor performance of polymeric building blocks of the plant cell walls materials [14]. This suggests that the cell structure of Della was more resistant than RG, consequently enhancing the micromechanics of the cell wall which ultimately leads to improved macro-mechanical properties. Polymers with higher crystallinity, larger side groups, and higher molecular weight exhibit reduced polymer chain mobility, consequently, have higher resistance to creep and stress relaxation [76]. The C_0 of the varieties was found to be inversely proportional to lignin content.

Table 5.3. Creep compliance model parameters for D1, RG1, D2, and RG2 sorghum rinds

Sample	C_0 ($\mu m^2/N$)	C_1 ($\mu m^2/N$)	τ_1 (min)	C_2 ($\mu m^2/N$)	τ_2 (min)	R^2
D1	356±9	80.2±2.3	8.9±0.0	240±1	0.7±0.0	99.96
RG1	372±10	170±6	11.9±0.0	353±2	0.69±0.0	99.97
D2	296±8	74.7±1.2	0.61±0.4	19.3±1.2	7.9±0.02	99.97
RG2	307±5	210±5	0.7±0.0	80.5±0.4	9.6±0.5	99.98

The other model parameters (C_1 and C_2) contribute to the long-term compliance corresponding to the rubbery extension of the material [77] and the retardation times (τ_1 and τ_2) showed times required to change the compliance of each series in the model. Even though creep and relaxation were both

manifestations of the same molecular mechanisms and related, converting one into the other was not attempted. This was mainly because of different experimental conditions and the need for long times for attainment of equilibrium, which otherwise the model could result in an overestimated parameter.

5.4.5 Compositional Analysis

5.4.5.1 FTIR analysis

FTIR spectroscopy was performed to determine the chemical features of the rind samples (Figure 5.6). Band assignments are given in Appendix Table C1. Although the average spectral trends were similar, distinct absorption bands for RG1 were detected (Figure 5.6), likely related to cell wall compositional variability. A strong absorption band at 1030 cm^{-1} appeared from C–O–C glycosidic linkage [78]. Typical S and G lignin bands were observed at 1320 and 1230 cm^{-1}, respectively [79]. A lower spectral absorption intensity of RG1 relative to D1, D2, and RG2 was found (Figure 5.6) and most likely associated with its reduced glucan and lignin contents (discussed later). Similarly, the characteristic absorption band at 1370 cm^{-1} due to C─H bending from cellulose and hemicelluloses was also detected. A band intensity variation at 1605 cm^{-1}; attributed to skeletal C═C vibrations in S and G lignin coupled with C═O stretching, was also observed (Figure 5.6), which reveals the lignin content variation between samples [80].

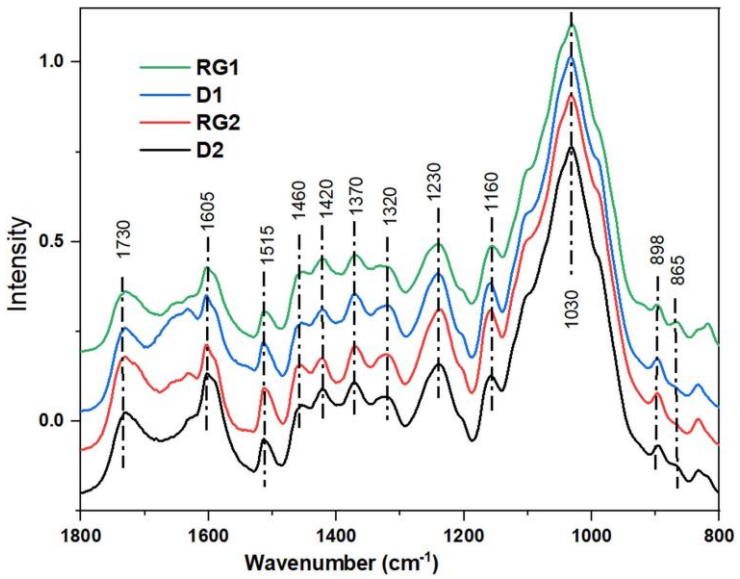

Figure 5.6. FTIR spectra of sorghum rinds from D1, RG1, D2, and RG2 varieties in the fingerprint region.

5.4.5.2 Crystallinity and MFA analysis

Cellulose crystallinity (CI) for the sorghum rinds was evaluated by XRD (Appendix Figure C2 and Table 5.4). The XRD diffractograms (Figure C2) confirm the presence of cellulose I crystals with peaks at 2θ of 15.5° and 21.9° which are respectively assigned to [(1-10) and (110) overlapped] and

(200) lattice indices [81]. A broad amorphous structure centered at 2θ of 18.5° was observed [82]. The CI of D2 (both in the area (CI_A) and intensity (CI_I) methods) was significantly higher than all samples. However, there was no difference between RG1 and D1, while RG2 was considerably more crystalline than D1 and RG1 (Table 5.4). The CI trends in both methods were consistent with reported values [83] and varies among varieties [84]. Sorghum stems have been reported to have a CI of 39% [85]. The crystallinity of cellulose in D2, by the CI_A method, was 13.1% higher than RG2, while using the CI_I method was 18.1% higher. The relatively higher crystallinity of D2 might contribute to its biomechanical stiffness. Regardless of season and variety, the grain size of cellulose I in all varieties was not significantly different. The CI_A calculation considers both (200) and (110) peaks with respect to the total area, while the CI_I calculation only considers the intensity of the larger peak (200) and, thus CI_I is higher than CI_A as expected (Table 5.4).

Table 5.4. Crystalline index (CI) based on the area (CI_A) and intensity (CI_I) methods, and grain size (L) of cellulose in sorghum stalk rinds

Rind	CI_A (%)	CI_I (%)	L (nm)
Della2	43.2	63.7	3.1
RG2	38.2	53.6	3.2
Della1	36.6	56.1	3.3
RG1	36.6	56.5	3.1

Cellulose microfibril angle (MFA), deviation of their orientation from the fiber axis highly affects the biomechanical properties of fibers and stalks. Thus, MFA was investigated to evaluate the S2 layer fibril orientation, which is the largest layer and has the most important role for mechanical properties. It was found that the mean MFA of rinds decreased in the order of RG1 > D1 > RG2 > D2, with values 30.6 ^{o}, 27.0 ^{o}, 23.3 ^{o} and 21^o, respectively. The results are comparable to the literature; 33-39^o [86] for corn stalk fibers, 20 ^{o} for sisal fibers [87], and 10-40^o [88] for sugarcane culms. The relation between MFA with FS and FM is presented in Figure 5.7b. The results demonstrated that both rind FS and FM properties decreased with MFA. It was reported that MFA affected both the rheological and mechanical properties of wood [89]. A larger MFA resulted in lower wood stiffness [90], which is consistent with our results. These results clearly show that MFA is an important supramolecular structure of cellulose affecting the biomechanical properties of lignocellulosic fibers.

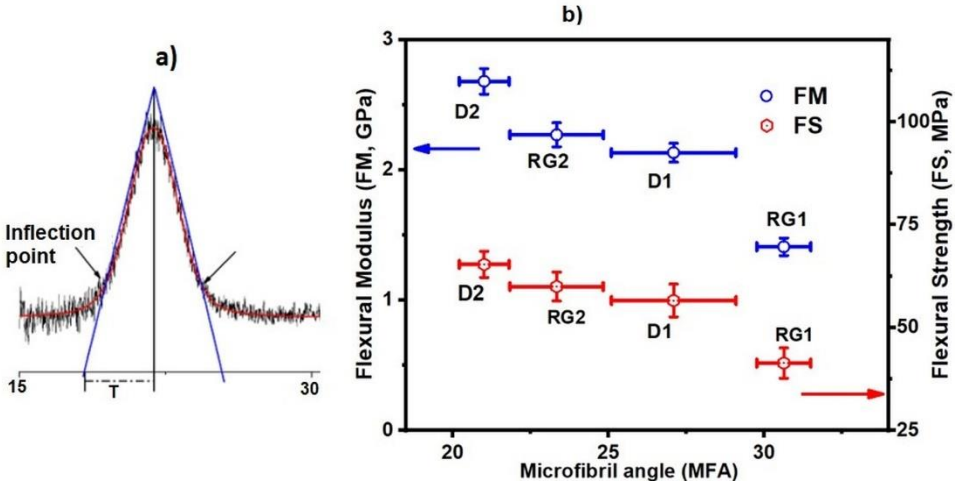

Figure 5.7. Schematics for determination of T parameter and correlation of biomechanical properties with MFA. a) Schematics for determination of parameter T; and b) relationship between MFA with the flexural modulus (FM) and flexural strength (FS) determined from three-point micro-bending.

5.4.5.3 Py-GCMS and DFRC analysis

Py-GCMS, a thermal degradation technique that provides rapid *in-situ* information on the cell wall constituents [91] was performed on the stalk rinds and the pyrograms are presented in Appendix Figure C3. The compositional variation of the rinds is revealed by the relative abundances of pyrolysis products, given in Appendix Table C2. The whole cell walls released carbohydrate-derived compounds as well as lignin and *p*-hydroxycinnamates-derived phenolic compounds [92]. The pyrolysis products were consistent with the literature [93].

The syringyl/guaiacyl (S/G) ratio of the internode rind was determined from Py-GCMS data (Figure 5.8a). The S/G ratios were 0.29, 0.36, 0.34, and 0.38, respectively for D1, RG1, D2 and RG2, which was consistent with previous work [28]. The S/G ratios of RG1 and RG2 were significantly increased respectively by 24.1% and 11.4%. This result was consistent with previous reports of transgenic plants having about 57 % higher S/G ratio than wild-type maize plants [94]. The relative percentage of monolignols (H/G/S ratio) determined from Py-GC/MS (Figure 5.8b) showed that H lignin was the dominant monolignol (70-79%), consistent with the fact that *p*-coumaryl alcohol (*p*-hydroxyphenyl) derived lignin was more common in grasses [95]. The H/G/S ratios were 71/22/7 for D1, 79/15/6 for RG1, 70/22/8 for D2, and 69/23/8 for RG2. The detection of higher amounts of H lignin-derived compounds could be due to the degradation of *p*-coumaric (*p*CA) and ferulic (FA) phenolic acids to 4-vinylphenol. Furthermore, aromatic amino acids constituents of proteins in the rind may also contribute to the phenol peak.

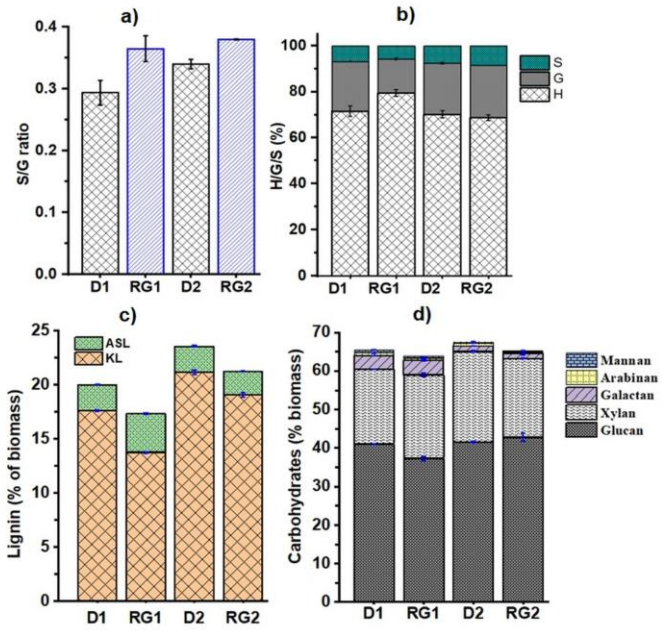

Figure 5.8. Lignin composition of rinds by Py-GCMS and acid hydrolysis a) S/G ratio comparison as determined by Py-GCMS; b) relative percentage of monolignols (H/G/S, %) at the internodes; c) lignin analysis: Klason Lignin (KL) and Acid Soluble Lignin (ASL); d) carbohydrate analysis based on % of biomass.

The relative abundance of monolignols, their inter-linkages, degree of polymerization, number of free phenolic groups, and degree of cross-linking with polysaccharides vary among different plant species, developmental stages, cell types, and plant tissue [96]. The S/G ratio determines the extent of crosslinking in lignin. Technically, the presence of an extra methoxy group in lignin monomers gives one less linkage site (S < G < H), consequently leading to fewer coupling combinations during the polymerization reaction [97]. As S lignin has no vacant 5-position, cross-linkages such as β-5, 5,5′, and 4-O-5 are not possible in S subunits. Thus, S-rich lignin was more easily depolymerized than G-rich lignin [97], [98] and yields a less crosslinked lignin, more linear β-O-4 linkages [99]. The correlation between the bending properties (FM, FS) and lignin composition (Table 5.5) revealed that FS (r = 0.67) and FM (r = 0.73) were significantly and positively correlated with G lignin. This finding demonstrates that G lignin plays a significant role in enhancing the biomechanical properties and possible resistance against lodging. G-lignin was reported to have a positive impact on lodging resistance in buckwheat [100]. Moreover, [101] and [102] also reported that G monolignol played an important role in lodging resistance. This could be likely related to the fact that greater G content leads to highly crosslinked lignin due to the presence of a larger number of biphenyl and C-C linkages [99]. Contrarily, S lignin was not correlated with bending properties (Table 5.5). This result contradicts the literature [103], where S monomers were suggested to be the predominant structural lignin subunit for strength and rigidity in wheat plants. On the other hand, the pairwise correlation

analysis shows that H-lignin was negatively correlated (Table 5.5) with FS (r = -0.68) and FM (r = -0.72). It was reported that H-type lignin is deposited at an earlier stage, followed by G and then S-type lignin units during lignification [104]. The higher H-lignin in RG variety suggests that the deposition of G-type and S-type lignin at later stages of lignification might be impaired by the mutation. Higher H-lignin was associated with reduced molecular weight and the biomass less recalcitrant [105]. However, according to [103], higher proportion of H monomers were not important to the lodging resistance of wheat stems. On the other hand, a recent study [106] highlighted the importance of H lignin subunits in strengthening the maize stalk. One possible explanation is that H lignin detected in Py-GCMS could be both canonical and non-canonical H-lignin (*p*CA and FA). Thus, the exact effect of canonical H-lignin on biomechanical properties might be interfered with by the presence of phenolic acids. It was also shown (Table 5.5) that the S/G ratio was not correlated to either FM or FS. As the concentration of S lignin was variable across the varieties and growing season, thus the S/G ratio will undoubtedly not affect stalk strength. A study in buckwheat demonstrated that the S/G ratio was not relevant for lodging resistance in different cultivars [100]. However, [39] reported that S/G was positively related to the flexural rigidity of rice stems. On the other hand, [101] reported that the S/G ratio exhibited a significant negative correlation with lodging resistance in oilseed crops. The limitation and inconsistency of the literature on the impact of lignin composition and cross-linkages on the biomechanical and lodging resistance properties of stalks has indicated that further investigations are needed using more varieties in future study.

Table 5.5. Pearson's correlation coefficients between lignin composition determined by Py-GCMS and bending properties of sorghum rinds

	FM	H	G	S	S/G
FS	0.96***	-0.68*	0.67*	0.62	-0.17
FM		-0.72*	0.73*	0.66	-0.20
H			-0.99**	-0.94***	0.16
G				0.89**	-0.28
S					0.19

*H: p-hydroxyphenyl; G: guaiacyl; S: syringyl; S/G: syringyl-to-guaiacyl ratio; FS: Flexural strength; FM: flexural modulus. Symbols ***, ** and * respectively represents significant correlation at p < 0.001, p <0.01, and p < 0.05.*

A DFRC is a degradation method that selectively cleaves α- and β-ether linkages in lignin and releases the lignin monomers involved in those linkages [107]. A characteristic and distinctive feature of the DFRC method in comparison with other degradative methods is that it leaves γ-esters intact,

thus allowing the release of γ-acylated monolignols [91]. DFRC was performed on milled sorghum rind and chromatograms of the degradation products are shown in Appendix Figure C4. The results show that the lignin released both cis- and trans-isomers of *p*-hydroxyphenyl (cH and tH), guaiacyl (cG and tG), and syringyl (cS and tS) lignin monomers. The levels of monomers arising from the uncondensed arylglycerol-β-aryl (β-O-4) ether linkages is given in Table 5.6. The results revealed that sorghum rind had HGS-type lignin with a dominant G monolignol (Table 5.6). Significant variations in the β-ether linkage contents between the samples were found. Given that D2 had the highest lignin content, D2 also had the highest total uncondensed monomer released (4.25 mmol/g of lignin) followed by RG2 (3.44 mmol/g of lignin). D1 and RG1 had respectively 2.00 and 1.87 mmol/g of uncondensed monomer released. The total content of β-O-4-ethers for palm kernel lignin was reported at 2.29 mmol/g [108]. β-O-4 lignin linkages were the main linkage detected by 2D-NMR in sorghum stalks [28]. The data (Table 5.6) also indicated that 63-71 % of β-O-4 were released as G monomer. A comparable S/G ratio for wheat straw has been reported [107].

Table 5.6. Relative molar abundance (mmol/g of lignin) of the DFRC degradation monomers of the MWL isolated from D2, RG2, D1, and RG1 sorghum stalks

Rind	H	G	S	S/G	H/G/S	Total yield (mmol/g)
D2	0.39±0.04	2.68±0.06	1.18±0.04	0.44	9/63/28	4.25
RG2	0.37±0.02	2.25±0.02	0.81±0.05	0.36	11/65/24	3.44
D1	0.23±0.04	1.44±0.01	0.34 ±0.04	0.24	12/71/17	2.00
RG1	0.24±0.02	1.26±0.02	0.36±0.04	0.29	13/68/19	1.87

5.4.5.4 Lignin and carbohydrate analysis

Lignin and carbohydrate analyses were performed on rinds after 3-point bending tests and the results are given in Figure 5.8c and d, respectively. The KL content of the rinds (Figure 5.8c) was found to be 17.6%, 13.8%, 21.2%, and 19.1% respectively for D1, RG1, D2, and RG2. Meanwhile, the ASL contents were 2.40% for D1, 3.54% for RG1, 2.42% for D2 and 2.18% for RG2. The results were in close agreement with the whole cell wall of sorghum stalks previously reported [28]. Comparison of the results revealed that KL lignin was found to be significantly reduced by about 22.0 and 9.9% in RG1 and RG2 relative to D1 and D2, respectively. On the other hand, the ASL lignin was 47.7% higher in RG1 relative to D1 but decreased by 10.0% in RG2 relative to D2. In comparison to Della, the total lignin content (KL+ASL) was significantly reduced by 13.6%. and 9.9%, respectively for RG1 and RG2. Considering the significant reduction of the mechanical properties of RG1, this result suggests that lignin content may have a profound impact on mechanical properties. Across the

growing season, the total lignin content of D2 and RG2 was about 17.9% and 22.9% higher than D1 and RG1, respectively. RG2 contained 6% higher total lignin than D1.

Carbohydrate analysis (Figure 5.8d) showed that glucan and xylan were the predominant components of the rind. The glucan/cellulose was 41.0%, 37.2%, 41.5% and 42.8%, respectively for D1, RG1, D2 and RG2. Similarly, the xylan/hemicellulose content for D1 was 19.5%, for RG1 21.8%, for D2 23.6% and RG2 20.5%. Significant variations were particularly detected between D1 and RG1 with a 9.0% glucan reduction and a 11.8% increase in xylan. On the other hand, the glucan content of D2 and RG2 was similar, however, a 13.1% reduction in xylan was detected in RG2. It was reported that cellulose and lignin concentration in sorghum was highly affected by growing seasons and environmental factors [109], which corroborates that changes in lignin and carbohydrate content were likely related to seasonal variations. Other minor components like mannan, arabinan and galactan were also detected as shown in Figure 5.8d. Previous studies [110], [111] have shown that the biomechanical properties of the biomass tissues are highly correlated with composition. Significant reduction of lignin and glucan in RG could be due to reduced lignin and cellulose deposition in the sclerenchyma and vascular bundle cells [112]. This may consequently lead to weak tissue and low stem strength, causing a higher degree of lodging incidence.

5.4.5.5 Correlations of chemical compositions with flexural properties

The cell wall composition of lignocellulosic material has a large effect on its macro-scale mechanical behavior [36], which can be attributed to the cell wall microstructure and chemical differences. The effect of chemical composition on the bending properties of the stalks has been evaluated and Pearson's correlation coefficients are shown (Table 5.7). It was found that FS and FM have been significantly correlated with KL, ASL, and glucan/cellulose content. The results revealed that FS had a strong positive correlation with KL (r = 0.88), TL (r = 0.86) and cellulose content (r = 0.70), but negatively correlated with ASL (r = -0.70). Similarly, for FM significant correlations with KL (r = 0.82), TL (r = 0. 81), and cellulose (r = 0.68) were observed. These findings have been well supported in the literature, where lignin content played a key role for a significant improvement in mechanical properties, and eventually enhanced the lodging resistance of crops [113]–[115]. Compared to lodging-resistant varieties, low lignin content was detected in lodging-type wheat, rice, corn, and miscanthus [100], [116]–[119]. Reductions in lignin content were also associated with reductions in FS and FM in poplar wood [120]. Cellulose constitutes the main backbone of the cell wall, and its content and structure contribute to the stiffness and strength of the cell wall. Stalk breaking resistance has been found to be positively correlated with the cellulose and lignin content of maize internodes [121]. Akira et al. [122] found a positive correlation between FS and cellulose content. Moreover,

significant correlation of FM with cellulose content (r =0.79) and lignin content (r = 0.47) has been reported in young bamboo [111]. On the other hand, bending properties were not significantly correlated with hemicellulose content, similar to the reports in bamboo [111]. The hemicellulose content was not significantly correlated with breaking force in rice, which is an important indicator of stem lodging [123]. Contrarily, bending strength was found to decrease with ASL content (r = -0.70) (Table 5.7). Nevertheless, no published data was found about the correlation of bending behavior with ASL content. The results demonstrated that rind biomechanical properties were strongly correlated with their chemical composition, and low content of lignin and cellulose results in weak stem strength and could easily cause stem lodging [46].

Table 5.7. Pearson's correlation coefficients between chemical composition and bending properties

	FM	KL	ASL	TL	Glucan	Hemicellulose
FS	0.96***	0.88***	-0.78***	0.86***	0.70***	-0.35
FM		0.82***	-0.70***	0.81**	0.68***	-0.25
KL			-0.76**	0.99***	0.67***	-0.30
ASL				-0.69***	-0.48**	0.57
TL					0.68***	-0.22
Glucan						-0.62

*Klason lignin (KL), acid soluble lignin (ASL), total lignin (TL) and cellulose; with flexural strength (FS) and flexural modulus (FM) at internodes in sorghum, ***, ** and * represent significant correlation respectively at $p < 0.001$, $p < 0.01$, and $p < 0.05$.*

5.5 Conclusion

The rind mechanical and viscoelastic properties of Della and RG sorghum stalk varieties grown in two different seasons have been evaluated using DMA. The three-point bending test results provided two useful quantities: the flexural modulus (FM) and the flexural strength (FS). The results showed that a significant reduction in FM and FS was associated with lignin and cellulose content reduction. Particularly, the FS and FM values of the RG2 variety were found to be significantly reduced and attributed to low lignin and cellulose contents. Acid soluble lignin was found to be negatively correlated whereas Klason lignin was positively correlated with biomechanical properties. However, hemicellulose was not shown to significantly influence mechanical properties. The combined influence of lignin and cellulose content shows the most significant effect on both the FM and FS. Furthermore, MFA was an important superstructural parameter highly influencing biomechanical property. This study further suggested that varieties with lower MFA, higher lignin, and cellulose accumulation can further be used for breeding to develop lodging resistance cultivars. DMA using a

3-point micro-bending fixture was shown to be a convenient and efficient tool for measuring the mechanical properties of crop stalk rind sections at a small scale.

5.6 References

[1] F. E. Gomez, J. E. Mullet, A. H. Muliana, K. J. Niklas, and W. L. Rooney, "The genetic architecture of biomechanical traits in sorghum," Crop Science, vol. 60, no. 1, pp. 82–99, Jan. 2020, doi: 10.1002/CSC2.20049.

[2] W. Wu and B. Ma, "A new method for assessing plant lodging and the impact of management options on lodging in canola crop production," Scientific Reports 2016 6:1, vol. 6, no. 1, pp. 1–17, Aug. 2016, doi: 10.1038/srep31890.

[3] L. Shah et al., "Improving Lodging Resistance: Using Wheat and Rice as Classical Examples," International Journal of Molecular Sciences, vol. 20, no. 17, Sep. 2019, doi: 10.3390/IJMS20174211.

[4] N. Shah, M. Tanveer, A. ur Rehman, S. A. Anjum, J. Iqbal, and R. Ahmad, "Lodging stress in cereal—effects and management: an overview," Environmental Science and Pollution Research, vol. 24, no. 6, pp. 5222–5237, Feb. 2017, doi: 10.1007/S11356-016-8237-1/FIGURES/1.

[5] H. Hu et al., "QTL mapping of stalk bending strength in a recombinant inbred line maize population," Theoretical and Applied Genetics, vol. 126, no. 9, pp. 2257–2266, Sep. 2013, doi: 10.1007/S00122-013-2132-7/TABLES/3.

[6] V. Brulé, A. Rafsanjani, D. Pasini, and T. L. Western, "Hierarchies of plant stiffness," Plant Science, vol. 250, pp. 79–96, Sep. 2016, doi: 10.1016/J.PLANTSCI.2016.06.002.

[7] T. Speck and I. Burgert, "Plant Stems: Functional Design and Mechanics," Annual Review of Materials Research, vol. 41, pp. 169–193, Jul. 2011, doi: 10.1146/ANNUREV-MATSCI-062910-100425.

[8] M. Bayable et al., "Biomechanical Properties and Agro-Morphological Traits for Improved Lodging Resistance in Ethiopian Teff (Eragrostis tef (Zucc.) Trottor) Accessions," Agronomy 2020, Vol. 10, Page 1012, vol. 10, no. 7, p. 1012, Jul. 2020, doi: 10.3390/AGRONOMY10071012.

[9] R. Khobra, S. Sareen, B. K. Meena, A. Kumar, V. Tiwari, and G. P. Singh, "Exploring the traits for lodging tolerance in wheat genotypes: a review," Physiology and Molecular Biology of Plants, vol. 25, no. 3, p. 589, May 2019, doi: 10.1007/S12298-018-0629-X.

[10] N. Shah et al., "Combating Dual Challenges in Maize Under High Planting Density: Stem Lodging and Kernel Abortion," Frontiers in Plant Science, vol. 12, p. 2216, Nov. 2021, doi: 10.3389/FPLS.2021.699085/BIBTEX.

[11] E. Kong et al., "Anatomical and chemical characteristics associated with lodging resistance in wheat," The Crop Journal, vol. 1, no. 1, pp. 43–49, Oct. 2013, doi: 10.1016/J.CJ.2013.07.012.

[12] A. Kokubo, S. Kuraishi, and N. Sakurai, "Culm Strength of Barley Correlation Among Maximum Bending Stress, Cell Wall Dimensions, and Cellulose Content," Plant Physiology, vol. 91, no. 3, pp. 876–882, Nov. 1989, doi: 10.1104/PP.91.3.876.

[13] R. Zhong and Z. H. Ye, "Secondary Cell Walls: Biosynthesis, Patterned Deposition and Transcriptional Regulation," Plant and Cell Physiology, vol. 56, no. 2, pp. 195–214, Feb. 2015, doi: 10.1093/PCP/PCU140.

[14] Shah D, T. P. S. Reynolds, and M. H. Ramage, "The strength of plants: Theory and experimental methods to measure the mechanical properties of stems," Journal of Experimental Botany, vol. 68, no. 16, pp. 4497–4516, Oct. 2017, doi: 10.1093/jxb/erx245.

[15] S.-M. Yang, L. XIE, S.-L. ZHENG, J. LI, and J.-C. YUAN, "Effects of Nitrogen Rate and Transplanting Density on Physical and Chemical Characteristics and Lodging Resistance of Culms in Hybrid Rice," ACTA AGRONOMICA SINICA, vol. 35, no. 1, pp. 93–103, Mar. 2009, doi: 10.3724/SP.J.1006.2009.00093.

[16] S. Lee et al., "Time-dependent mechanical behavior of sweet sorghum stems," Journal of the Mechanical Behavior of Biomedical Materials, vol. 106, p. 103731, Jun. 2020, doi: 10.1016/J.JMBBM.2020.103731.

[17] F. E. Gomez, A. H. Muliana, K. J. Niklas, and W. L. Rooney, “Identifying Morphological and Mechanical Traits Associated with Stem Lodging in Bioenergy Sorghum (Sorghum bicolor),” Bioenergy Research, vol. 10, no. 3, pp. 635–647, Sep. 2017, doi: 10.1007/S12155-017-9826-7/FIGURES/9.

[18] D. J. Cosgrove and M. C. Jarvis, “Comparative structure and biomechanics of plant primary and secondary cell walls,” Frontiers in Plant Science, vol. 3, no. AUG, p. 204, Aug. 2012, doi: 10.3389/FPLS.2012.00204/BIBTEX.

[19] W. Wu and B. Ma, “The mechanical roles of the clasping leaf sheath in cereals: Two case studies from oat and wheat plants,” Journal of Agronomy and Crop Science, vol. 206, no. 1, pp. 118–129, Feb. 2020, doi: 10.1111/JAC.12362.

[20] M. S. Zuber, T. R. Colbert, and L. L. Darrah, “Effect of Recurrent Selection for Crushing Strength on Several Stalk Components in Maize,” Crop Science, vol. 20, no. 6, pp. 711–717, Nov. 1980, doi: 10.2135/CROPSCI1980.0011183X002000060009X.

[21] J. A. Peiffer, S. A. Flint-Garcia, N. De Leon, M. D. McMullen, S. M. Kaeppler, and E. S. Buckler, “The Genetic Architecture of Maize Stalk Strength,” PLOS ONE, vol. 8, no. 6, p. e67066, Jun. 2013, doi: 10.1371/JOURNAL.PONE.0067066.

[22] X. Arzola-Villegas, R. Lakes, N. Z. Plaza, and J. E. Jakes, “Wood Moisture-Induced Swelling at the Cellular Scale—Ab Intra,” Forests 2019, Vol. 10, Page 996, vol. 10, no. 11, p. 996, Nov. 2019, doi: 10.3390/F10110996.

[23] Lyu J, Peng Hui, Cao JinZhen, Jiang JiaLi, Zhao RongJun, and Gao YuLei, “Application of dynamic mechanical analysis in wood science research.,” Journal of Forestry Engineering, vol. 3, no. 5, pp. 1–11, 2018.

[24] J. H. Chen, N. Zhao, N. Fu, D. Li, L. J. Wang, and X. D. Chen, “Mechanical Properties of Hulless Barley Stem with Different Moisture Contents,” International Journal of Food Engineering, vol. 15, no. 1–2, Feb. 2019, doi: 10.1515/IJFE-2018-0033/MACHINEREADABLECITATION/RIS.

[25] Q. Xu and B. Engquist, “A mathematical model for fitting and predicting relaxation modulus and simulating viscoelastic responses,” Proceedings of the Royal Society A: Mathematical, Physical and Engineering Sciences, vol. 474, no. 2213, May 2018, doi: 10.1098/RSPA.2017.0540.

[26] J. Simsiriwong, R. W. Sullivan, and H. H. Hilton, “Viscoelastic creep compliance using prony series and spectrum function approach,” Conference Proceedings of the Society for Experimental Mechanics Series, vol. 2, pp. 149–160, 2013, doi: 10.1007/978-1-4614-4241-7_21/COVER.

[27] Schöning and G. Johansson, “Absorptiometric determination of acid-soluble lignin in semichemical bisulfite pulps and in some woods and plants | Semantic Scholar,” Svensk Papperstidning-nordisk Cellulosa, vol. 68, pp. 607–613, 1965.

[28] E. Mengistie, A. M. Alayat, F. Sotoudehnia, N. Bokros, S. DeBolt, and A. G. McDonald, “Evaluation of Cell Wall Chemistry of della and Its Mutant Sweet Sorghum Stalks,” Journal of Agricultural and Food Chemistry, vol. 70, no. 5, pp. 1689–1703, Feb. 2022, doi: 10.1021/ACS.JAFC.1C07176/ASSET/IMAGES/LARGE/JF1C07176_0010.JPEG.

[29] Yamamoto, T. Okuyama, and Masato Yoshida, “Method of determining the mean microfibril angle of wood over a wide range by the improved Cave’s method,” Journal of the Japan Wood Research Society, vol. 39, pp. 375–381, 1993.

[30] I. D. Cave, “Theory of X-ray measurement of microfibril angle in wood,” Wood Science and Technology 1997 31:3, vol. 31, no. 3, pp. 143–152, 1997, doi: 10.1007/BF00705881.

[31] O. Faix, D. Meier, and I. Fortmann, “Thermal degradation products of wood,” Holz als Roh- und Werkstoff 1990 48:9, vol. 48, no. 9, pp. 351–354, 1990, doi: 10.1007/BF02639897.

[32] D. Meier and O. Faix, “Pyrolysis-Gas Chromatography-Mass Spectrometry,” in Methods in Lignin Chemistry, Springer, Berlin, Heidelberg, 1992, pp. 177–199. doi: 10.1007/978-3-642-74065-7_13.

[33] F. Lu and J. Ralph, “Derivatization Followed by Reductive Cleavage (DFRC Method), a New Method for Lignin Analysis: Protocol for Analysis of DFRC Monomers,” Journal of Agricultural and Food Chemistry, vol. 45, no. 7, pp. 2590–2592, 1997, doi: 10.1021/JF970258H/ASSET/IMAGES/LARGE/JF970258HF00002.JPEG.

[34] F. Lu and J. Ralph, “The DFRC Method for Lignin Analysis. 2. Monomers from Isolated Lignins,” Journal of Agricultural and Food Chemistry, vol. 46, no. 2, pp. 547–552, 1998, doi: 10.1021/JF970676M/ASSET/IMAGES/LARGE/JF970676MF00003.JPEG.

[35] L. Erndwein, D. D. Cook, D. J. Robertson, and E. E. Sparks, “Field-based mechanical phenotyping of cereal crops to assess lodging resistance,” Applications in Plant Sciences, vol. 8, no. 8, p. e11382, Aug. 2020, doi: 10.1002/APS3.11382.

[36] J. E. Winandy and R. M. Rowell, “The Chemistry of Wood Strength,” in The Chemistry of Solid Wood, vol. 207, Advances in Chemistry, 1984, pp. 211–255. doi: 10.1021/BA-1984-0207.CH005.

[37] C. J. Stubbs, Y. A. Oduntan, T. R. Keep, S. D. Noble, and D. J. Robertson, “The effect of plant weight on estimations of stalk lodging resistance,” Plant Methods, vol. 16, no. 1, pp. 1–18, Sep. 2020, doi: 10.1186/s13007-020-00670-w.

[38] N. Martin-Nelson, B. Sutherland, M. Yancey, C. S. Liao, C. J. Stubbs, and D. D. Cook, “Axial variation in flexural stiffness of plant stem segments: measurement methods and the influence of measurement uncertainty,” Plant Methods, vol. 17, no. 1, pp. 1–11, Dec. 2021, doi: 10.1186/S13007-021-00793-8/FIGURES/9.

[39] T. Ookawa et al., “Biomass production and lodging resistance in ‘Leaf Star’, a new long-culm rice forage cultivar,” Plant Production Science, vol. 13, no. 1, pp. 58–66, Dec. 2009, doi: 10.1626/PPS.13.58.

[40] M. Li et al., “Physical fractionation of sweet sorghum and forage/energy sorghum for optimal processing in a biorefinery,” Industrial Crops and Products, vol. 124, pp. 607–616, Nov. 2018, doi: 10.1016/J.INDCROP.2018.07.002.

[41] F. E. Gomez, A. H. Muliana, and W. L. Rooney, “Predicting Stem Strength in Diverse Bioenergy Sorghum Genotypes,” Crop Science, vol. 58, no. 2, pp. 739–751, Mar. 2018, doi: 10.2135/CROPSCI2017.09.0588.

[42] C. T. Wright, P. A. Pryfogle, N. A. Stevens, E. D. Steffler, J. R. Hess, and T. H. Ulrich, “Biomechanics of wheat/barley straw and corn stover,” Applied Biochemistry and Biotechnology - Part A Enzyme Engineering and Biotechnology, vol. 121, no. 1–3, pp. 5–19, 2005, doi: 10.1007/978-1-59259-991-2_2/COVER.

[43] D. J. Robertson, S. Y. Lee, M. Julias, and D. D. Cook, “Maize Stalk Lodging: Flexural Stiffness Predicts Strength,” Crop Science, vol. 56, no. 4, pp. 1711–1718, Jul. 2016, doi: 10.2135/CROPSCI2015.11.0665.

[44] L. Zhang, Z. Yang, Q. Zhang, and H. Guo, “Tensile properties of maize stalk rind,” BioResources, vol. 11, no. 3, pp. 6151–6161, 2016, doi: 10.15376/BIORES.11.3.6151-6161.

[45] Y. Xu, J. Li, Z. Xin, S. R. Bean, M. Tilley, and D. Wang, “Water-soluble sugars of pedigreed sorghum mutant stalks and their recovery after pretreatment,” Applied Sciences (Switzerland), vol. 10, no. 16, Aug. 2020, doi: 10.3390/APP10165472.

[46] R. S. Sekhon, C. N. Joyner, A. J. Ackerman, C. S. McMahan, D. D. Cook, and D. J. Robertson, “Stalk Bending Strength is Strongly Associated with Maize Stalk Lodging Incidence Across Multiple Environments,” Field Crops Research, vol. 249, Apr. 2020, doi: 10.1016/J.FCR.2020.107737.

[47] H. A. Esechie, J. W. Maranville, and W. M. Ross, “Relationship of Stalk Morphology and Chemical Composition to Lodging Resistance in Sorghum,” Crop Science, vol. 17, no. 4, pp. 609–612, Jul. 1977.

[48] S. L. Hansen et al., “Mechanical Properties of Plant Cell Walls Probed by Relaxation Spectra,” Plant Physiology, vol. 155, no. 1, pp. 246–258, Jan. 2011, doi: 10.1104/PP.110.166629.

[49] T. Zhan, J. Jiang, J. Lu, and H. Peng, “Dynamic viscoelastic properties of Chinese fir under cyclical relative humidity variation,” Journal of Wood Science, vol. 61, no. 5, pp. 465–473, Oct. 2015, doi: 10.1007/S10086-015-1491-X/TABLES/3.

[50] C. Czibula, T. Seidlhofer, C. Ganser, U. Hirn, and C. Teichert, “Longitudinal and transverse low frequency viscoelastic characterization of wood pulp fibers at different relative humidity,” Materialia, vol. 16, p. 101094, May 2021, doi: 10.1016/J.MTLA.2021.101094.

[51] J. E. Jakes, “Mechanism for Diffusion through Secondary Cell Walls in Lignocellulosic Biomass,” Journal of Physical Chemistry B, vol. 123, no. 19, pp. 4333–4339, May 2019, doi: 10.1021/ACS.JPCB.9B01430/ASSET/IMAGES/MEDIUM/JP-2019-014304_M001.GIF.

[52] S. Zauscher, D. F. Caulfield, and A. H. Nissan, “The influence of water on the elastic modulus of paper Part 1: Extension of the H-Bond theory,” 1996.

[53] Y. Meng, Y. Xia, T. M. Young, Z. Cai, and S. Wang, “Viscoelasticity of wood cell walls with different moisture content as measured by nanoindentation,” RSC Advances, vol. 5, no. 59, pp. 47538–47547, May 2015, doi: 10.1039/C5RA05822H.

[54] C. Birkinshaw, M. Buggy, and G. G. Henn, “Dynamic mechanical analysis of wood,” Journal of Materials Science Letters 1986 5:9, vol. 5, no. 9, pp. 898–900, Sep. 1986, doi: 10.1007/BF01729266.

[55] A. Kaboorani and P. Blanchet, “Determining the linear viscoelastic region of sugar maple wood by dynamic mechanical analysis,” BioResources, vol. 9, no. 3, pp. 4392–4409, 2014, doi: 10.15376/BIORES.9.3.4392-4409.

[56] T. Zhang, S. L. Bai, Y. F. Zhang, and B. Thibaut, “Viscoelastic properties of wood materials characterized by nanoindentation experiments,” Wood Science and Technology, vol. 46, no. 5, pp. 1003–1016, Sep. 2012, doi: 10.1007/S00226-011-0458-3/FIGURES/10.

[57] L. Kong, Z. Zhao, Z. He, and S. Yi, “Effects of steaming treatment on crystallinity and glass transition temperature of Eucalyptuses grandis × E. urophylla,” Results in Physics, vol. 7, pp. 914–919, Jan. 2017, doi: 10.1016/J.RINP.2017.02.017.

[58] G. Wan, T. Frazier, J. Jorgensen, B. Zhao, and C. E. Frazier, “Rheology of transgenic switchgrass reveals practical aspects of biomass processing,” Biotechnology for Biofuels, vol. 11, no. 1, pp. 1–10, Mar. 2018, doi: 10.1186/S13068-018-1056-5/TABLES/4.

[59] M. Cristea, D. Ionita, and M. M. Iftime, “Dynamic Mechanical Analysis Investigations of PLA-Based Renewable Materials: How Are They Useful?,” Materials 2020, Vol. 13, Page 5302, vol. 13, no. 22, p. 5302, Nov. 2020, doi: 10.3390/MA13225302.

[60] B. Horvath, P. Peralta, C. Frazier, and I. Peszlen, “Thermal softening of transgenic aspen,” BioResources, vol. 6, no. 2, pp. 2125–2134, 2011.

[61] W. Stelte, C. Clemons, J. K. Holm, J. Ahrenfeldt, U. B. Henriksen, and A. R. Sanadi, “Thermal transitions of the amorphous polymers in wheat straw,” Industrial Crops and Products, vol. 34, no. 1, pp. 1053–1056, Jul. 2011, doi: 10.1016/J.INDCROP.2011.03.014.

[62] A. M. Olsson and L. Salmén, “The effect of lignin composition on the viscoelastic properties of wood,” Nordic Pulp and Paper Research Journal, vol. 12, no. 3, pp. 140–144, Aug. 1997, doi: 10.3183/NPPRJ-1997-12-03-P140-144/HTML.

[63] S. Chowdhury and C. E. Frazier, “Thermorheological complexity and fragility in plasticized lignocellulose,” Biomacromolecules, vol. 14, no. 4, pp. 1166–1173, Apr. 2013, doi: 10.1021/bm400080f/suppl_file/bm400080f_si_001.pdf.

[64] Z. Börcsök and Z. Pásztory, “The role of lignin in wood working processes using elevated temperatures: an abbreviated literature survey,” European Journal of Wood and Wood Products 2020 79:3, vol. 79, no. 3, pp. 511–526, Dec. 2020, doi: 10.1007/S00107-020-01637-3.

[65] S. Chowdhury, J. Fabiyi, and C. E. Frazier, “Advancing the dynamic mechanical analysis of biomass: Comparison of tensile-torsion and compressive-torsion wood DMA,” Holzforschung, vol. 64, no. 6, pp. 747–756.

[66] P. J. Harris and B. A. Stone, “Chemistry and Molecular Organization of Plant Cell Walls,” Biomass Recalcitrance: Deconstructing the Plant Cell Wall for Bioenergy, pp. 61–93, Mar. 2009, doi: 10.1002/9781444305418.CH4.

[67] J. C. Roland, D. Reis, B. Vian, and S. Roy, “The helicoidal plant cell wall as a performing cellulose-based composite,” Biology of the Cell, vol. 67, no. 2, pp. 209–220, Jan. 1989, doi: 10.1111/j.1768-322X.1989.tb00864.x.

[68] C. M. Hayot, E. Forouzesh, A. Goel, Z. Avramova, and J. A. Turner, “Viscoelastic properties of cell walls of single living plant cells determined by dynamic nanoindentation,” Journal of Experimental Botany, vol. 63, no. 7, pp. 2525–2540, Apr. 2012, doi: 10.1093/JXB/ERR428.

[69] L. Chen, N. Liao, L. Xing, and L. Han, “Description of Wheat Straw Relaxation Behavior Based on a Fractional-Order Constitutive Model,” Agronomy Journal, vol. 105, no. 1, pp. 134–142, Jan. 2013, doi: 10.2134/AGRONJ2012.0190.

[70] Hu Jian-Jun, Lei Ting-Zhou, Xu Guang-Yin, Shen Sheng-Qiang, and Liu Jun-Wei, “Experimental study of stress relaxation in the process of cold molding with straw :: BioResources,” BioResources, vol. 4, no. 3, pp. 1158–1167, 2009.

[71] H. L. Liu, W. D. Yu, and H. B. Jin, “Modeling the stress-relaxation behavior of wool fibers,” Journal of Applied Polymer Science, vol. 110, no. 4, pp. 2078–2084, Nov. 2008, doi: 10.1002/APP.28764.

[72] C. A. Tweedie and K. J. Van Vliet, “Contact creep compliance of viscoelastic materials via nanoindentation,” Journal of Materials Research 2006 21:6, vol. 21, no. 6, pp. 1576–1589, Jun. 2006, doi: 10.1557/JMR.2006.0197.

[73] Y. D. Zhu, N. Fu, D. Li, L. J. Wang, and X. D. Chen, “Physical and Viscoelastic Properties of Different Moisture Content Highland Barley Kernels,” International Journal of Food Engineering, vol. 13, no. 12, Dec. 2017, doi: 10.1515/IJFE-2017-0186/MACHINEREADABLECITATION/RIS.

[74] F. William, L. J. S., and O. Kasif, “Nonlinear Creep at Constant Stress and Relaxation at Constant Strain,” in Creep and Relaxation of Nonlinear Viscoelastic Materials, vol. 18, no. C, North-Holland, 1976, pp. 176–219. doi: 10.1016/B978-0-7204-2369-3.50011-4.

[75] H. L. Ornaghi, J. H. S. Almeida, F. M. Monticeli, and R. M. Neves, “Stress relaxation, creep, and recovery of carbon fiber non-crimp fabric composites,” Composites Part C: Open Access, vol. 3, p. 100051, Nov. 2020, doi: 10.1016/J.JCOMC.2020.100051.

[76] C. R. Siviour and J. L. Jordan, “High Strain Rate Mechanics of Polymers: A Review,” Journal of Dynamic Behavior of Materials 2016 2:1, vol. 2, no. 1, pp. 15–32, Jan. 2016, doi: 10.1007/S40870-016-0052-8.

[77] D. Roylance, “Engineering Viscoelasticity ,” 2001.

[78] M. Poletto, A. J. Zattera, and R. M. C. Santana, “Structural differences between wood species: Evidence from chemical composition, FTIR spectroscopy, and thermogravimetric analysis,” Journal of Applied Polymer Science, vol. 126, no. S1, pp. E337–E344, Oct. 2012, doi: 10.1002/APP.36991.

[79] G. E. Acquah, B. K. Via, O. O. Fasina, and L. G. Eckhardt, “Rapid Quantitative Analysis of Forest Biomass Using Fourier Transform Infrared Spectroscopy and Partial Least Squares Regression,” Journal of Analytical Methods in Chemistry, vol. 2016, 2016, doi: 10.1155/2016/1839598.

[80] O. Faix, “Classification of Lignins from Different Botanical Origins by FT-IR Spectroscopy,” Holzforschung, vol. 45, no. s1, pp. 21–28, Jan. 1991, doi: 10.1515/HFSG.1991.45.S1.21/MACHINEREADABLECITATION/RIS.

[81] A. Isogai and M. Usuda, “Crystallinity Indexes of Cellulosic Materials,” Sen’i Gakkaishi, vol. 46, no. 8, pp. 324–329, Aug. 1990, doi: 10.2115/FIBER.46.8_324.

[82] S. Park, J. O. Baker, M. E. Himmel, P. A. Parilla, and D. K. Johnson, “Cellulose crystallinity index: Measurement techniques and their impact on interpreting cellulase performance,” Biotechnology for Biofuels, vol. 3, no. 1, pp. 1–10, May 2010, doi: 10.1186/1754-6834-3-10/TABLES/2.

[83] C. Zhao, Q. Shao, Z. Ma, B. Li, and X. Zhao, “Physical and chemical characterizations of corn stalk resulting from hydrogen peroxide presoaking prior to ammonia fiber expansion pretreatment,” Industrial Crops and Products, vol. 83, pp. 86–93, May 2016, doi: 10.1016/J.INDCROP.2015.12.018.

[84] J. P. Vandenbrink, R. N. Hilten, K. C. Das, A. H. Paterson, and F. A. Feltus, “Analysis of crystallinity index and hydrolysis rates in the bioenergy crop Sorghum bicolor,” Bioenergy Research, vol. 5, no. 2, pp. 387–397, Jun. 2012, doi: 10.1007/S12155-011-9146-2/TABLES/3.

[85] N. Reddy and Y. Yang, “Structure and properties of natural cellulose fibers obtained from sorghum leaves and stems,” Journal of Agricultural and Food Chemistry, vol. 55, no. 14, pp. 5569–5574, Jul. 2007, doi: 10.1021/JF0707379/ASSET/IMAGES/LARGE/JF0707379F00006.JPEG.

[86] R. Dungani, M. Karina, Subyakto, A. Sulaeman, D. Hermawan, and A. Hadiyane, “Agricultural waste fibers towards sustainability and advanced utilization: A review,” Asian Journal of Plant Sciences, vol. 15, no. 1–2, pp. 42–55, 2016, doi: 10.3923/AJPS.2016.42.55.

[87] N. Venkateshwaran, A. Elayaperumal, and G. K. Sathiya, “Prediction of tensile properties of hybrid-natural fiber composites,” Composites Part B: Engineering, vol. 43, no. 2, pp. 793–796, Mar. 2012, doi: 10.1016/J.COMPOSITESB.2011.08.023.

[88] C. Driemeier, W. D. Santos, and M. S. Buckeridge, “Cellulose crystals in fibrovascular bundles of sugarcane culms: Orientation, size, distortion, and variability,” Cellulose, vol. 19, no. 5, pp. 1507–1515, Oct. 2012, doi: 10.1007/S10570-012-9743-Z/FIGURES/7.

[89] T. A. Tabet and F. A. Aziz, “Cellulose Microfibril Angle in Wood and Its Dynamic Mechanical Significance,” Cellulose - Fundamental Aspects, Aug. 2013, doi: 10.5772/51105.

[90] J. R. Barnett and V. A. Bonham, “Cellulose microfibril angle in the cell wall of wood fibres,” Biological reviews of the Cambridge Philosophical Society, vol. 79, no. 2, pp. 461–472, May 2004, doi: 10.1017/s1464793103006377.

[91] M. J. Rosado et al., “Differences in the content, composition and structure of the lignins from rind and pith of papyrus (Cyperus papyrus L.) culms,” Industrial Crops and Products, vol. 174, p. 114226, Dec. 2021, doi: 10.1016/J.INDCROP.2021.114226.

[92] A. Sequeiros and J. Labidi, “Characterization and determination of the S/G ratio via Py-GC/MS of agricultural and industrial residues,” Industrial Crops and Products, vol. 97, pp. 469–476, Mar. 2017, doi: 10.1016/J.INDCROP.2016.12.056.

[93] C. Torri, A. Adamiano, D. Fabbri, C. Lindfors, A. Monti, and A. Oasmaa, “Comparative analysis of pyrolysate from herbaceous and woody energy crops by Py-GC with atomic emission and mass spectrometric detection,” Journal of Analytical and Applied Pyrolysis, vol. 88, no. 2, pp. 175–180, Jul. 2010, doi: 10.1016/J.JAAP.2010.04.003.

[94] X. Li et al., “Downregulation of caffeoyl-CoA O-methyltransferase (CCoAOMT) by RNA interference leads to reduced lignin production in maize straw,” Genetics and Molecular Biology, vol. 36, no. 4, pp. 540–546, 2013, doi: 10.1590/S1415-47572013005000039.

[95] K. E. Achyuthan et al., “Supramolecular Self-Assembled Chaos: Polyphenolic Lignin’s Barrier to Cost-Effective Lignocellulosic Biofuels,” Molecules, vol. 15, no. 12, pp. 8641–8688, Dec. 2010, doi: 10.3390/MOLECULES15118641.

[96] S. R. Verma and U. N. Dwivedi, “Lignin genetic engineering for improvement of wood quality: Applications in paper and textile industries, fodder and bioenergy production,” South African Journal of Botany, vol. 91, pp. 107–125, Mar. 2014, doi: 10.1016/j.sajb.2014.01.002.

[97] A. Ziebell et al., “Increase in 4-coumaryl alcohol units during lignification in alfalfa (Medicago sativa) alters the extractability and molecular weight of lignin,” Journal of Biological Chemistry, vol. 285, no. 50, pp. 38961–38968, Dec. 2010, doi: 10.1074/jbc.M110.137315.

[98] I. Cesarino, P. Araújo, A. P. Domingues, and P. Mazzafera, “An overview of lignin metabolism and its effect on biomass recalcitrance,” Revista Brasileira de Botanica, vol. 35, no. 4, pp. 303–311, 2012, doi: 10.1590/S0100-84042012000400003.

[99] J. L. Ferrer, M. B. Austin, C. Stewart, and J. P. Noel, “Structure and function of enzymes involved in the biosynthesis of phenylpropanoids,” Plant Physiology and Biochemistry, vol. 46, no. 3, pp. 356–370, Mar. 2008, doi: 10.1016/j.plaphy.2007.12.009.

[100] D. Hu et al., “The lignin synthesis related genes and lodging resistance of Fagopyrum esculentum,” Biologia Plantarum 2017 61:1, vol. 61, no. 1, pp. 138–146, Nov. 2016, doi: 10.1007/S10535-016-0685-4.

[101] L. Wei et al., “Genetic and transcriptomic analyses of lignin- and lodging-related traits in Brassica napus,” Theoretical and Applied Genetics, vol. 9, no. 130, pp. 1961–1973, Sep. 2017, doi: 10.1007/S00122-017-2937-X.

[102] F. Li et al., “High-level hemicellulosic arabinose predominately affects lignocellulose crystallinity for genetically enhancing both plant lodging resistance and biomass enzymatic digestibility in rice mutants,” Plant Biotechnology Journal, vol. 13, no. 4, pp. 514–525, May 2015, doi: 10.1111/pbi.12276.

[103] Y. Luo et al., “Regulation of lignin composition by nitrogen rate and density and its relationship with stem mechanical strength of wheat,” Field Crops Research, vol. 241, p. 107572, Sep. 2019, doi: 10.1016/J.FCR.2019.107572.

[104] J. Rencoret et al., “Lignin Composition and Structure in Young versus Adult Eucalyptus globulus Plants,” Plant Physiology, vol. 155, no. 2, pp. 667–682, Feb. 2011, doi: 10.1104/PP.110.167254.

[105] M. Li, Y. Pu, and J. Ragauskas, “Current understanding of the correlation of lignin structure with biomass recalcitrance,” Frontiers in Chemistry, vol. 4, no. NOV. 2016. doi: 10.3389/fchem.2016.00045.

[106] A. Manga-Robles et al., “Elucidating compositional factors of maize cell walls contributing to stalk strength and lodging resistance,” Plant Science, vol. 307, p. 110882, Jun. 2021, doi: 10.1016/j.plantsci.2021.110882.

[107] J. C. Del Río, J. Rencoret, P. Prinsen, Á. T. Martínez, J. Ralph, and A. Gutiérrez, “Structural characterization of wheat straw lignin as revealed by analytical pyrolysis, 2D-NMR, and reductive cleavage methods,” Journal of Agricultural and Food Chemistry, vol. 60, no. 23, pp. 5922–5935, Jun. 2012, doi: 10.1021/jf301002n.

[108] J. Huang, W. Liu, F. Zhou, and Y. Peng, “Effect of multiscale structural parameters on the mechanical properties of rice stems,” Journal of the Mechanical Behavior of Biomedical Materials, vol. 82, pp. 239–247, Jun. 2018, doi: Effect of multiscale structural parameters on the mechanical properties of rice stems.

[109] L. A. Rivera-Burgos, J. J. Volenec, and G. Ejeta, “Biomass and Bioenergy Potential of Brown Midrib Sweet Sorghum Germplasm,” Frontiers in Plant Science, vol. 10, p. 1142, Sep. 2019, doi: 10.3389/FPLS.2019.01142/BIBTEX.

[110] M. Genet et al., “The Influence of Cellulose Content on Tensile Strength in Tree Roots,” Plant and Soil 2005 278:1, vol. 278, no. 1, pp. 1–9, 2005, doi: 10.1007/S11104-005-8768-6.

[111] L. A. Sánchez-Echeverri, G. Aita, D. Robert, and M. E. Rodriguez Garcia, "Correlation between chemical compounds and mechanical response in culms of two different ages of Guadua angustifolia Kunth," Madera y Bosques, vol. 20, no. 2, pp. 87–94, Jun. 2014, doi: 10.21829/MYB.2014.202166.

[112] L. Wu et al., "Shading contributes to the reduction of stem mechanical strength by decreasing cell wall synthesis in japonica rice (Oryza sativa L.)," Frontiers in Plant Science, vol. 8, p. 881, May 2017, doi: 10.3389/FPLS.2017.00881/BIBTEX.

[113] D. Peng et al., "Lodging resistance of winter wheat (Triticum aestivum L.): Lignin accumulation and its related enzymes activities due to the application of paclobutrazol or gibberellin acid," Field Crops Research, vol. 157, pp. 1–7, Feb. 2014, doi: 10.1016/j.fcr.2013.11.015.

[114] S. R. Turner and C. R. Somerville, "Collapsed xylem phenotype of Arabidopsis identifies mutants deficient in cellulose deposition in the secondary cell wall.," The Plant Cell, vol. 9, no. 5, pp. 689–701, May 1997, doi: 10.1105/TPC.9.5.689.

[115] X.-G. Chen et al., "Relationship between Lignin Metabolism and Lodging Resistance in Wheat," ACTA AGRONOMICA SINICA, vol. 37, no. 9, pp. 1616–1622, Dec. 2011, doi: 10.3724/SP.J.1006.2011.01616.

[116] E. Hondroyianni, D. K. Papakosta, A. A. Gagianas, and K. A. Tsatsarelis, "Corn stalk traits related to lodging resistance in two soils of differing salinity," Maydica, vol. 45, no. 2, pp. 125–133, 2000.

[117] K. Kaack, K. U. Schwarz, and P. E. Brander, "Variation in morphology, anatomy and chemistry of stems of Miscanthus genotypes differing in mechanical properties," Industrial Crops and Products, vol. 17, no. 2, pp. 131–142, Mar. 2003, doi: 10.1016/S0926-6690(02)00093-6.

[118] A. Okuno et al., "New Approach to Increasing Rice Lodging Resistance and Biomass Yield Through the Use of High Gibberellin Producing Varieties," PLOS ONE, vol. 9, no. 2, p. e86870, Feb. 2014, doi: 10.1371/JOURNAL.PONE.0086870.

[119] F.-Z. Wei, "Effects of Nitrogenous Fertilizer Application Model on Culm Lodging Re-sistance in Winter Wheat," ACTA AGRONOMICA SINICA, vol. 34, no. 6, pp. 1080–1085, Jun. 2008, doi: 10.3724/SP.J.1006.2008.01080.

[120] S. L. Voelker, B. Lachenbruch, F. C. Meinzer, and S. H. Strauss, "Reduced wood stiffness and strength, and altered stem form, in young antisense 4CL transgenic poplars with reduced lignin contents," New Phytologist, vol. 189, no. 4, pp. 1096–1109, Mar. 2011, doi: 10.1111/j.1469-8137.2010.03572.x Key.

[121] Y. Zhang et al., "Ethephon Improved Stalk Strength of Maize (Zea Mays L.) Mainly through Altering Internode Morphological Traits to Modulate Mechanical Properties under Field Conditions," Agronomy 2019, Vol. 9, Page 186, vol. 9, no. 4, p. 186, Apr. 2019, doi: 10.3390/AGRONOMY9040186.

[122] K. Akira, K. S, and S. N, "Culm strength of barley : correlation among maximum bending stress, cell wall dimensions, and cellulose content," Plant physiology, vol. 91, no. 3, pp. 876–882, Nov. 1989.

[123] S. Liu, Y. Huang, H. Xu, M. Zhao, Q. Xu, and F. Li, "Genetic enhancement of lodging resistance in rice due to the key cell wall polymer lignin, which affects stem characteristics," Breeding Science, vol. 68, no. 5, p. 508, 2018, doi: 10.1270/jsbbs.18050.

Chapter 6: Microstructural Evaluation of Sorghum Stalks

6.1 Abstract

Advancements in genetic manipulation, through breeding or genetic engineering, have made it possible to modify the biomechanical properties of crops. However, such modifications can considerably modify crops' biomechanical behavior and their susceptibility to lodging. Therefore, there is a growing interest in evaluation of the changes in the microstructure for understanding the biomechanical properties of mutated crop plant structures. X-ray tomography, scanning electron microscope (SEM) and nanoindentation was performed on sorghum stalks. The X-ray tomography revealed the variation in the varieties in terms of distribution and location of vascular bundles across the rinds and pith. The SEM micrographs demonstrated the reduction of density of vascular bundles in RG1, which might compromise its biomechanical property. Nanoindentation elastic modulus and hardness at the secondary cell walls and corner compound middle lamella was not significantly different except between RG2 and D2. The results suggested that density of structural-supporting tissues might have dominant influence on the biomechanical properties than the micro-scale cellular micro-mechanics.

6.2 Introduction

Stalk strength is one of the sorghum's most important agronomic traits directly related to yield [1]. The strength of a stalk is controlled by the morphological (e.g. plant height, ear height, stalk diameter, and internode plumpness) and cell wall structural components such as cellulose and lignin contents and structures [2]. The biomechanical bending strength of the basal internodes of stalks plays an essential role in lodging resistance. Stalk bending strength has been used to assess and quantify lodging resistance in crops [3], [4]. The sorghum stem is consisting of different tissues and cell types, namely vascular bundles, sclerenchyma, chlorenchyma, parenchyma, and the epidermis [5]. Most of the small vascular bundles and sclerenchyma are in the outer layer of the stalk/rind whereas the pith, which consists of most of the volume of the stalk and is located at the inner part, mainly consists of parenchyma with large vascular bundles [2], [6]. One of the primary factors that distinguish stalk tissues from one another is the thickness and localization of the cell walls of a given cell type or tissue [2].

Genomic developments have made it possible to modify the biomechanical characteristics of crops, which creates plethora of agricultural and forestry applications including optimized degradation of crop residues to biofuels [7] [8], breeding high yield and lodging resistant crop species [9], and the design of engineered plants with functional properties for sustainable construction [10]. Genetic

modifications, however, have the potential to drastically modify crops' biomechanical behavior and their vulnerability to lodging. Therefore, there is a growing interest in evaluation of the changes in the microstructure for understanding the biomechanical behavior of the mutated crop plant structures [11].

Stems can be considered as a multiscale composite structure, with sclerenchyma fibers embedded in a matrix of parenchyma cells and the fibers themselves being multilayered composites made of cellulose fibrils [12], [13]. As many of the parameters regulating stem mechanics are based on its architecture, which can be represented at both the microstructure and macrostructure scales, understanding the stem architecture and its relationship to biomechanical properties is essential. To explain the observed biomechanical property variations, these factors must be taken into consideration. In addition, knowledge of the stem structural hierarchy may be useful in inferring material properties (at the tissue and cell wall level) from measured properties of the stem structure [13]. Plant materials organize themselves hierarchically across multiple scales ranging from base constituents (lignin, cellulose, and hemicellulose), cells, tissue, organ, and whole plant [14]. At the microstructure scale, stems consist of three primary tissue: (1) dermal tissue as a protective surface layer; (2) ground tissue, which typically makes up the largest fraction of a stem's volume, used for photosynthesis, storage, and support; and (3) vascular tissue for water and nutrient transport, but also structural support [15]. Each tissue type is composed of various cell types, with the structure of the cells having evolved for specific functions [13].

The primary cell wall of parenchyma cells in the ground tissue is soft, thin, and flexible and often lignin deficient and contains low content of cellulose fibrils [13], [16] . Collenchyma cells in the ground tissue have unevenly thickened primary cell walls with higher cellulose content, and therefore can offer some rigidity to young stems [17]. Specialized sclerenchyma fiber cells, which are predominantly found in vascular tissue and in ground tissue in limited quantity, serve as the primary structure-supporting cells. These cells have strong secondary cell walls that are rich in lignin and cellulose as well as primary cell walls. Secondary cell walls in vascular cells provide substantial structural [18]. Therefore, the stem's biomechanical properties represent the combination of characteristics contributed by the different tissues and scales [13]. Hence, a complex interaction of morphological and compositional features across different length ranges determines the stiffness and strength characteristics of crops. These factors contribute to the morphology of crops, and thus biomechanical properties. This complex interdependency makes it difficult to determine the contribution of each individual parameter and component to the mechanical properties [11].

Therefore, characterization and evaluation of the hierarchical microstructures across all the scales are crucial to understanding its influence on the biomechanical and lodging properties of stalks.

The sorghum stalks are made up of a pithy core (mainly parenchyma, but also some collenchyma and vascular bundles) and a denser outer shell or rind (composed of sclerenchyma, vascular bundles, and collenchyma)[5], [13], [19]. A three-point bending test study [20] on the separated outer tissues and inner core of the herbaceous grass showed that the outer strengthening tissues (made up of collenchyma, parenchyma, and sclerenchyma) had an elastic modulus and strength approximately four times higher than the core tissues (phloem, xylem, interfascicular parenchyma, and pith). Furthermore, another study [21] also demonstrated that mature stem epidermis (including the underlying layer of collenchyma cells) accounts as much as 50% overall stem bending stiffness. All these studies revealed that collenchyma and sclerenchyma tissues are the principal structure supporting cells against bending loads [13]. Stems are described as fiber-reinforced composites [12]. At the cellular level, thin sclerenchyma with thick cell walls and low microfibril angle are found in the matrix of shorter and softer parenchyma, whereas in the secondary cell walls, cellulose fibrils are in the matrix of other lignin and hemicellulose [13]. The parenchymatous core cells are like foam cores in sandwich-structured composites and provide resistance to buckling of the stem. Similar to the mechanics of fiber-reinforced composites, vascular tissue bundles , including fibers and tracheids, serve as the main load-bearing components in stems, and the stem biomechanical properties are mainly determined by the characteristics of vascular bundles and their differential distribution across the stem [12], [13]. This study aimed at identifying the microstructural traits underlying the variation in the biomechanical strength of sorghum stems.

6.3 Materials and Methods

6.3.1 Sample preparation and X-ray microtomography (micro-CT)

For the experiment, the sorghum stalks of different varieties approximately 14 mm long and diameter of D1 (16.3 mm), RG1(8.7 mm), D1 (18.1 mm) and RG2 (21.4 mm) were prepared. The samples were glued on top of each other on pad (Figure 6.1). For X-ray microtomography, the samples were transferred to sample holders consisting of polystyrene with diameter of 26 mm. X-ray microtomography was carried out using a desktop SkyScan 1275 µCT scanner (Bruker, Kontich, Belgium) at source tube voltage of 45 kV microfocus X-ray and a beam source current of 62 µA. The tomography experiments were performed with an effective pixel size of 15 µm, and samples were projected at 360^{o} round with rotation step of 0.1^{o} and an exposure time of 115 s. Data processing and reconstruction was performed in an automated fashion Bruker SkyScan 1275 and NRecon software (version 1.7.4.6), respectively.

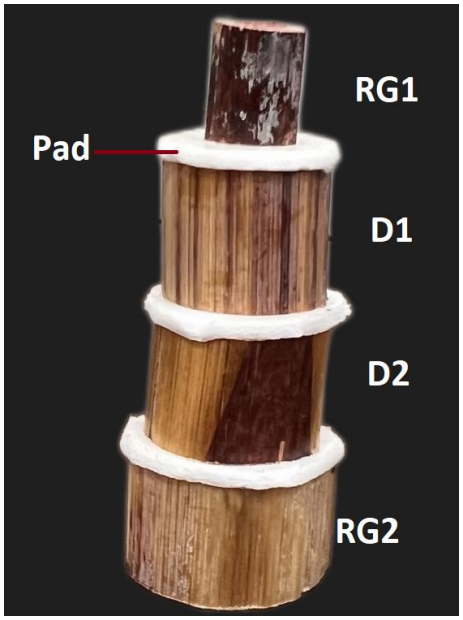

Figure 6.1. Specimen preparation for the X-ray tomography for Della 1 (D1), RG1, Della 2 (D2), and RG2.

6.3.2 Scanning Electron Microscopy (SEM)

The microstructure of sorghum stalks at the internodes was characterized by scanning electron microscopy of rind thin sections. Thin sections of rinds of about 1 mm were manually prepared by using a razor blade. Scanning microscopy (Leo Gemini field emission SEM) was performed on tissues samples, which were sputter-coated with gold. The accelerating voltage was 5 kV.

6.3.3 Nanoindentation

A specimen for nanoindentation was prepared from transverse cross-section of sorghum stalk. The method is based on the works of Jakes and Stone [22]. The specimen was prepared from the rind under ambient conditions. The transverse side of a defect-free 5-mm cube was bonded with a thin layer of 5-min epoxy to the face of an 8-mm-diameter steel cylinder with 10 mm length, in which the cylinder was fit into a trimming block of a Sorvall (Norwalk,CT, USA) MT-2 ultramicrotome. The exposed transverse surface was then carefully shaped into a blunt wedge geometry using disposable hand razors. The top ridge of the wedge was approximately 0.5 mm long and positioned along the radial direction. The cylinder was fit into the chuck of the ultramicrotome in such a way that that the length of the wedge tip was parallel to the diamond knife (A 45^{o} Micro Star Technologies, Huntsville, TX, USA) edge. Approximately 1µm-thick sections were removed from the tip of the wedge until an area of about 0.2 by 0.6 mm was prepared. Final sectioning was done by removing a few 200-nm-thick sections. Nanoindentation was performed by Bruker-Hysitron TI 900 TriboIndenter equipped with a Berkovich probe. The relative humidity was maintained at 35 %, and nanoindentation

biomechanical properties (elastic modulus and hardness) were determined based on literature [22]. Nanoindentation was performed on the vascular bundles.

6.4 Results and discussion

6.4.1 Microstructure analysis of maize stalk using µ-CT

Visualization of the cross-sectional images obtained from the CT scanner and the analysis of the resulting tomographic reconstructions revealed clear differences in image contrast between different sample areas, which were imputable to the signal intensity difference detected among different types of tissues. Analysis of samples at different regions revealed variations in the density attributed to various anatomical features. The microtomographic constructions show a high level of anatomical structural detail, especially from larger vessels such as the vascular bundles. Due to the differences in the features, stalks showed different X-ray absorption properties. The *XY* tomographic slice image of the samples is shown (Figure 6.2). The images revealed two different zones: the thinner dense peripheral zone with concentrated grey dots (fibers, and vascular bundles) and the larger volume with dark parts (pith), demonstrating cross-sectional variation of absorption of X-Ray intensity. The darker regions represented low densities, while bright regions correspond to high densities[23]. The cross-sectional imaging showed that vascular bundles were clearly distributed more intensively in the rind but dispersedly in the pith center.

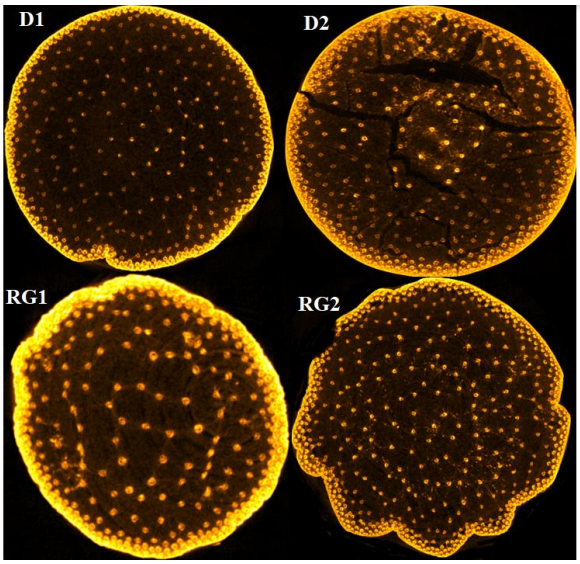

Figure 6.2. Cross section (slice) through the three-dimensional x-ray microtomography images for samples D1, RG1, D2, and RG2.

The micro-CT scan result (Figure 6.3) revealed that distinct patterns of vascular bundles are found in the rind, especially in D2. In addition to the vascular bundles, the presence of smaller, but dense fibers/white dots in D2, could be reinforcing entities to bolster its strength.

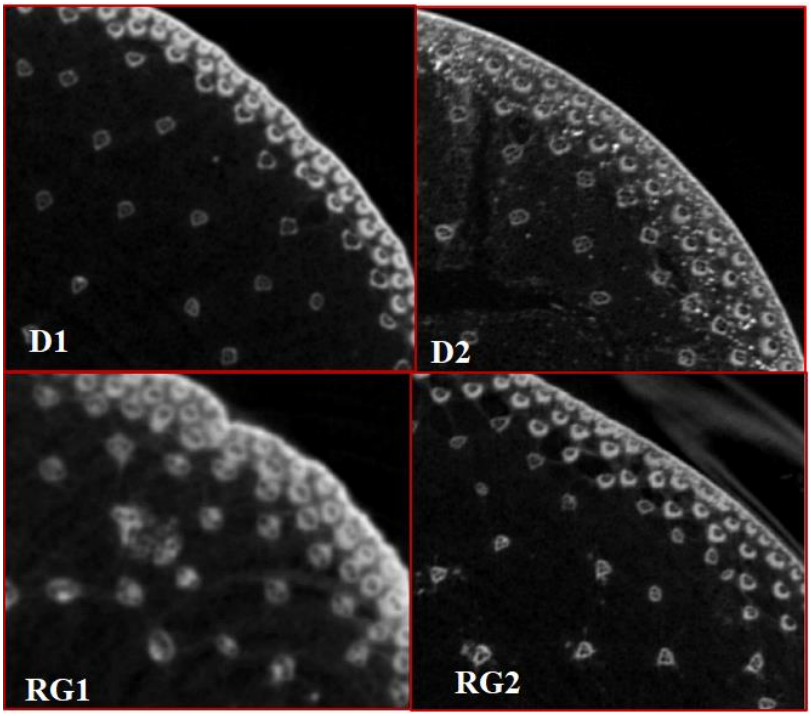

Figure 6.3. A closer comparison of x-ray microtomography gray-scale images for D1, RG1, D2 and RG2 at the third internode.

Tomographic reconstruction of projection images provides with a 3D map of X-ray absorption and its projection image is shown (Figure 6.4). The reconstructed sections from four separate tomographic datasets of sorghum stalk reveal the density variation of rinds and the pith. Internal damage on D2 was clearly observed. It suggests that selecting lodging based on biomechanical phenotyping might lead to unrealistic classification of varieties.

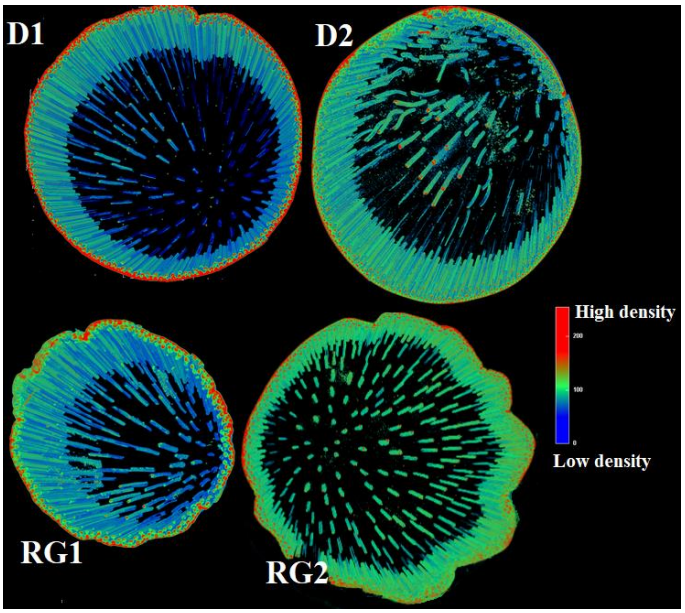

Figure 6.4. Tomographic reconstruction of projection images provides a 3D map of X-ray absorption and its projection image for D1, RG1, D2 and RG2 sorghum stalks.

6.4.2 SEM microstructures

The biomechanical behavior of the stalk rinds could be related to the architecture of the stem. Reduction in the biomechanical strength of rinds of stalks may reflect alterations in cell wall structure. Thus, the microstructure of the cross-sections from the internodes of the two different lines was investigated using SEM. Figure 6.5 SEM of sclerenchyma cells (SC), vascular bundles (VB) and parenchyma cells (PC) in the transverse section of the sorghum internode. The cross-sections at internodes showed that vascular bundles were embedded in a matrix of parenchyma cells/matrix surrounded by a ring of sclerenchyma cells.

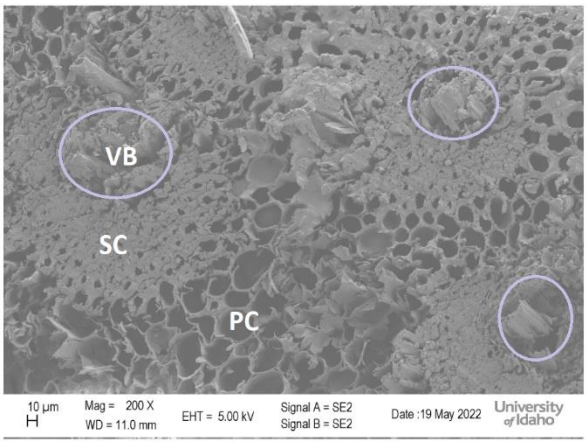

Figure 6.5. Scanning electron micrographs (SEM) of sclerenchyma cells (SC), vascular bundles (VB) and parenchyma cells (PC) in the transverse section of the sorghum internode. Scale is 10 µm.

Figure 6.6 shows the comparison of SEM micrographs of the cross-section of rinds in D1, RG1, D2 and RG2. SEM (Figure 6.6) observations revealed that the Della-type variety consists of more vascular bundles than RG variety. Particularly in RG1, the number of observed vascular bundles were small compared to other samples. Layers of cells, especially those around the peripheral vascular tissues and under the epidermal layer in culms, provide mechanical support for the plants [24]. The vascular bundle consists of protoxylem vessels, metaxylem vessels, phloem tissue, and the vascular bundle sheath [2]. Xylem and phloem of vascular bundles are responsible for the transportation of nutrients and water into the plant and are supported by sclerenchyma fiber sheath. The parenchyma cells consist of thin cell walls and exhibit polyhedral geometry while the sclerenchyma fibers are long hollow tubes with thick cell walls oriented in the stem direction [11]. A three-point test on rinds revealed that flexural modulus and flexural strength of RG1was the lowest among all samples. Literatures [20], [21] showed that collenchyma and sclerenchyma tissues are the principal structure supporting cells against bending loads. Thus, SEM micrographs suggest that the low density of sclerenchyma cells in RG could compromise its biomechanical strength. On the other hand, higher density of vascular bundles in the other samples could influence their biomechanical properties. Enhanced stalk bending resistance of Maize has been related to the thickening of the cell walls and decreases in the area of the vascular bundles [2]. Furthermore, density of vascular bundles has increased the bending and lodging resistance [23].

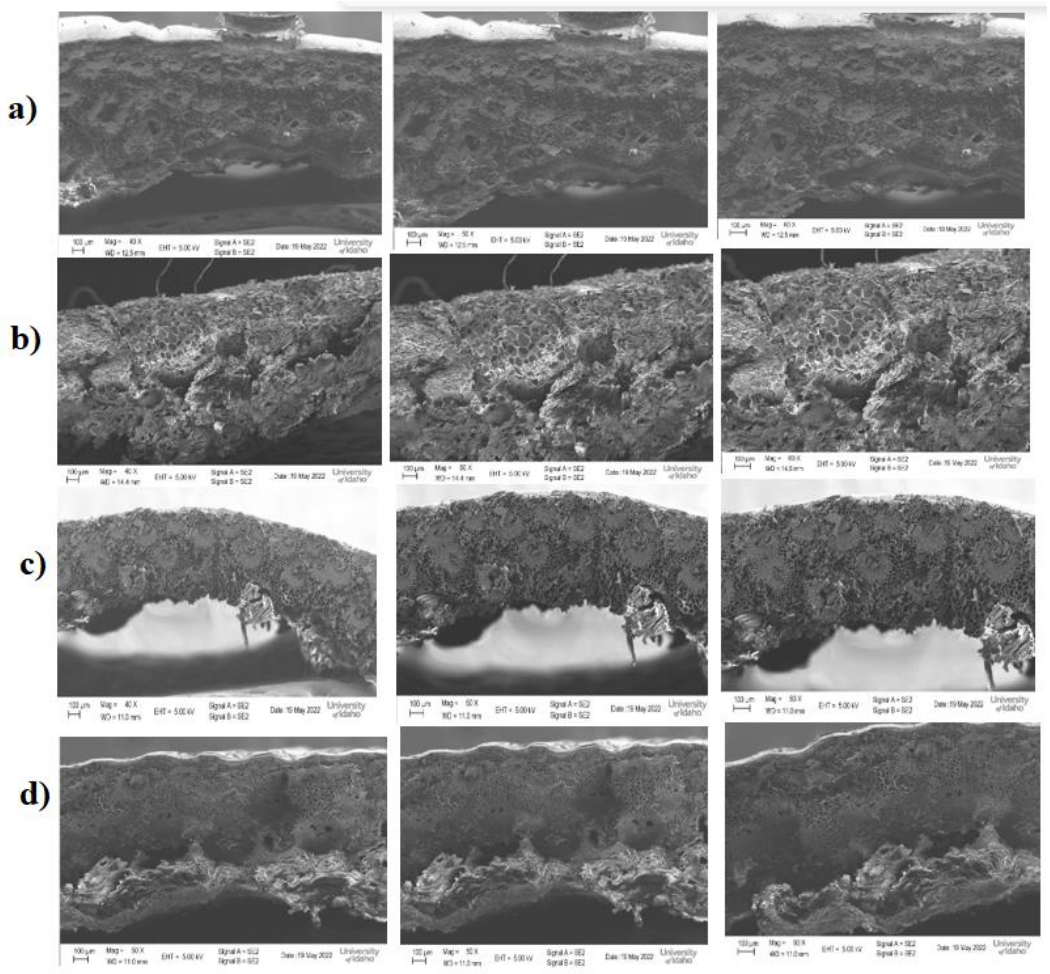

Figure 6.6. Scanning Electron Micrographs showing images of rinds taking from internode 3 at 40X, 50X, and 60X magnification (From left to right). a) D1, b) RG1, c) D2 and d) RG2. Scale bar is 100 µm..

6.4.3 Nanoindentation

Nanoindentation was performed on rinds of sorghum to measure the *in-situ* biomechanical properties at micro-scales. The multiload nanoindentations were measured on the secondary cell wall layers (SCW) and compound corner middle lamellae (CCML) (Figure 6.7).

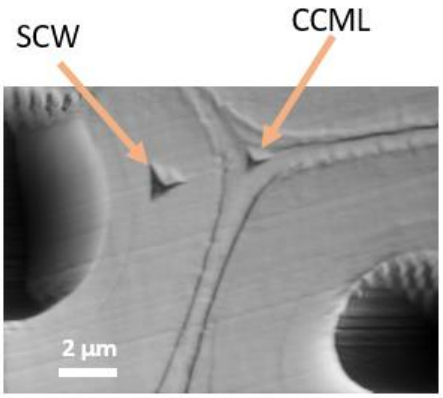

Figure 6.7. Scanning probe microscopy image of nanoindentations placed in the secondary cell wall (SCW) and compound corner middle lamella (CCML) of fibers in the vascular bundle.

The elastic modulus (EM) quantifies a material's stiffness or resistance to elastic (recoverable) deformation under stress, while hardness of the materials quantifies a material's resistance to plastic or permanent deformations [22]. The elastic modulus (EM) and hardness (H) results are determined from internode 3 at both SCW and CCML and summarized (Figure 6.8). The result revealed that the EM of SCW was found significantly higher than the EM of CCML in all samples, which was expected. The average EM of D1, RG1, D2 and RG2 at the SCW was found to be about 13.8 GPa, 16.8 GPa, 17.1 GPa and 17.5 GPa, respectively. ANOVA analysis of EM at the SCW showed that, except RG2 and D1, all samples were not significantly different. However, RG2 of SCW was 26.7% stiffer than D1. The EM of all samples at the CCML was detected as 5.1 GPa, 8.1 GPa, 6.6 GPa and 7.6 GPa respectively for D1, RG1, D2 and RG2. A similar trend was detected at CCML, where the EM of RG2 was found to be 47% stiffer than D1, while the variation in D2, RG1 and RG2 was not significant. Previous DMA three-point bending test revealed that flexural modulus and flexural strength of rinds was significantly different in the order of D2 > RG2 > D1 > RG1. Thus, the nanoindentation test at both SCW and CCML agrees with DMA test of RG2 and D1, both methods signifying that RG2 is stiffer than D1 at both cellular and macroscopic stem level. On the other hand, unlike the DMA three-point test, the similarity of EM at both SCW and CCML for RG1, D2 and RG2 suggests that the macrostructural behaviors at the stem could be governed by density than cellular biomechanics. A study by Fournier et al.[25] showed that density is positively correlated with both the stiffness and strength biomechanical properties. The density of a stem increases with the solid fraction (i.e. a larger proportion of thicker cells with secondary growth), as well as cellulose content and cellulose crystallinity [26].

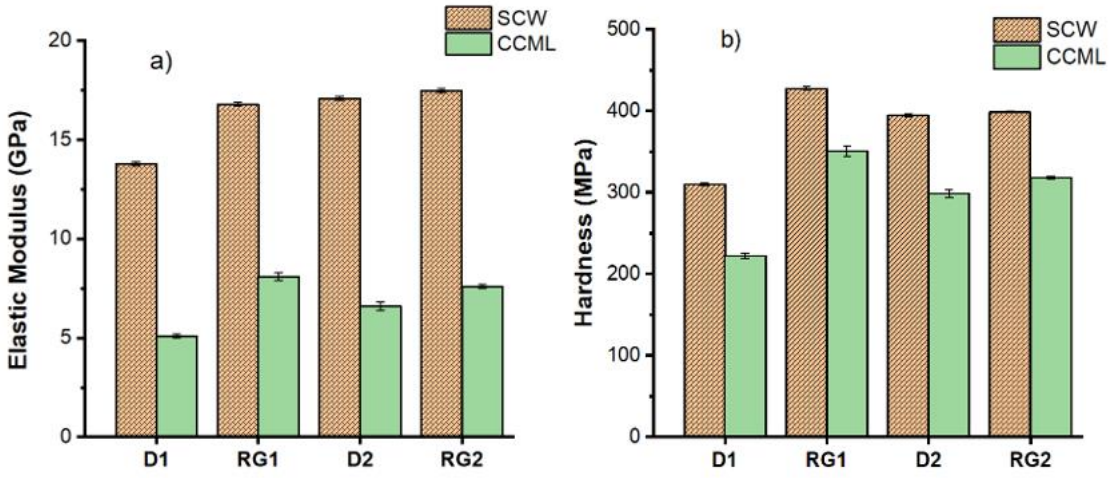

Figure 6.8. Mechanical properties of sorghum stalks measured by nanoindentation at the secondary cell walls (SCW) and compound corner middle lamella (CCML). a) Elastic modulus (GPa) and, b) hardness (MPa). Each result is based on the averages of two different specimens with similar conditions and properties. Errors are standard errors.

On the other hand, the average hardness at SCW was found to be 310 MPa, 428 MPa, 395 MPa and 399 MPa respectively for D1, RG1, D2 and RG2. Similarly, the average values of H at the CCML were D1 (222 MPa), RG1 (351 MPa), D2 (299 MPa) and RG2 (318 MPa). The ANOVA analysis at both SCW and CCML demonstrated that D1 is significantly less stiff than D2, RG1, and RG2, while the variation between D2, RG1 and RG2 was not notable. An average nanoindentation elastic modulus and hardness for Pine wood at SCW was reported to be 15.7 GPA, and 379 MPa. For CCML the same study reported a value of 4.9 GPa and 291 MPa, respectively for EM and H [22]. The findings closely agree with our result for the sorghum stalk, which suggests that the contribution of cellular mechanics to the macrostructure stem level could be minimal.

6.5 Correlation of Nanoindentation with Compositions

The correlation of the nanoindentation properties (EM, H) at the SC and CCML with compositional attributes was performed and given (Table 6.1). It was found that the composition was not correlated with nanoindentation properties. Meanwhile, elastic modulus and hardness at CCML, and hardness at both SCW and CCML was found correlated (Table 6.1). Literature on wood showed that a significant negative correlation between MFA, elastic modulus and hardness was detected [27]. Besides, the same study revealed positive correlation between elastic modulus and hardness with cellulose and lignin contents. Generation of significant amount of nanoindentation data is suggested for future correlation analysis.

Table 6.1. Correlation coefficients between composition and nanoindentation.

	EMM	**HS**	**HM**	**H**	**G**	**S**	**S/G**	**MFA**	**Gluc.**	**Xylan**
EMS	0.84	0.90	0.87	-0.03	-0.08	0.35	0.92	-0.36	0.06	0.63
EMM		0.95	0.98*	0.43	-0.53	-0.06	0.95	0.19	-0.36	0.36
HS			0.99*	0.40	-0.5	-0.08	0.89	0.04	-0.37	0.63
HM				0.46	-0.56	-0.12	0.91	0.15	-0.42	0.51

*EMM: elastic modulus at CCML; EMS: elastic modulus at SCW; HS: hardness at the SCW, HM: hardness at CCML; Gluc.: glucan; H: p-hydroxyphenyl; G: guaiacyl; S: syringyl; S/G: syringyl-to-guaiacyl ratio and * represents $p<0.05$*

6.6 Conclusion

Microstructural characterization (X-ray tomography and scanning electron microscope) and nanoindentation was performed on the sorghum stalks. Different features of the rind, pith, including the distribution and location of vascular bundles have been observed. SEM images revealed that RG1 was detected as vascular bundle deficient, while X-ray tomography images showed relatively higher density of vascular bundles. The nanoindentation, which was performed on single vascular bundles detected no significant biomechanical variation between RG1, D2 and RG2 at cellular levels. However, the elastic modulus and hardness of D1 was found to be significantly less than RG2 at both SCW and CCML.

6.7 References

[1] D. J. Robertson, Z. W. Brenton, S. Kresovich, and D. D. Cook, “Maize lodging resistance: Stalk architecture is a stronger predictor of stalk bending strength than chemical composition,” Biosyst. Eng., vol. 219, pp. 124–134, Jul. 2022, doi: 10.1016/J.BIOSYSTEMSENG.2022.04.010.

[2] Y. Li, G. Huang, Y. Guo, Y. Zhou, and L. Duan, “Coronatine Enhances Stalk Bending Resistance of Maize, Thickens the Cell Wall and decreases the Area of the Vascular Bundles,” Agron. 2020, Vol. 10, Page 807, vol. 10, no. 6, p. 807, Jun. 2020, doi: 10.3390/AGRONOMY10060807.

[3] R. S. Sekhon, C. N. Joyner, A. J. Ackerman, C. S. McMahan, D. D. Cook, and D. J. Robertson, “Stalk Bending Strength is Strongly Associated with Maize Stalk Lodging Incidence Across Multiple Environments,” F. Crop. Res., vol. 249, Apr. 2020, doi: 10.1016/J.FCR.2020.107737.

[4] D. Xiang et al., “Relationship between stem characteristics and lodging resistance of Tartary buckwheat (Fagopyrum tataricum),” Plant Prod. Sci., vol. 22, no. 2, 2019, doi: 10.1080/1343943X.2019.1577143.

[5] M. Li et al., “Physical fractionation of sweet sorghum and forage/energy sorghum for optimal processing in a biorefinery,” Ind. Crops Prod., vol. 124, pp. 607–616, Nov. 2018, doi: 10.1016/J.INDCROP.2018.07.002.

[6] D. A. Matos, I. P. Whitney, M. J. Harrington, and S. P. Hazen, “Cell Walls and the Developmental Anatomy of the Brachypodium distachyon Stem Internode,” PLoS One, vol. 8, no. 11, p. 80640, 2013, doi: 10.1371/journal.pone.0080640.

[7] M. C. McCann, M. S. Buckeridge, and N. C. Carpita, “Plants and BioEnergy,” Plants and BioEnergy, pp. 1–289, Jan. 2014, doi: 10.1007/978-1-4614-9329-7/COVER.

[8] V. Brulé, A. Rafsanjani, D. Pasini, and T. L. Western, “Hierarchies of plant stiffness,” Plant Sci., vol. 250, pp. 79–96, Sep. 2016, doi: 10.1016/J.PLANTSCI.2016.06.002.

[9] P. M. Berry et al., “Understanding and Reducing Lodging in Cereals,” Adv. Agron., vol. 84, pp. 217–271, 2004, doi: 10.1016/S0065-2113(04)84005-7.

[10] S. Schleicher, J. Lienhard, S. Poppinga, T. Speck, and J. Knippers, “A methodology for transferring principles of plant movements to elastic systems in architecture,” Comput. Des., vol. 60, pp. 105–117, Mar. 2015, doi: 10.1016/J.CAD.2014.01.005.

[11] T. Gangwar, D. J. Heuschele, G. Annor, A. Fok, K. P. Smith, and D. Schillinger, “Multiscale characterization and micromechanical modeling of crop stem materials,” Biomech. Model. Mechanobiol., vol. 20, no. 1, p. 69, Feb. 2021, doi: 10.1007/S10237-020-01369-6.

[12] L. J. Gibson, “The hierarchical structure and mechanics of plant materials,” J. R. Soc. Interface, vol. 9, no. 76, pp. 2749–2766, Nov. 2012, doi: 10.1098/rsif.2012.0341.

[13] Shah D, T. P. S. Reynolds, and M. H. Ramage, “The strength of plants: Theory and experimental methods to measure the mechanical properties of stems,” J. Exp. Bot., vol. 68, no. 16, pp. 4497–4516, Oct. 2017, doi: 10.1093/jxb/erx245.

[14] U. G. K. Wegst, H. Bai, E. Saiz, A. P. Tomsia, and R. O. Ritchie, “Bioinspired structural materials,” Nat. Mater. 2014 141, vol. 14, no. 1, pp. 23–36, Oct. 2014, doi: 10.1038/nmat4089.

[15] T. Speck and I. Burgert, “Plant Stems: Functional Design and Mechanics,” Annu. Rev. Mater. Res., vol. 41, pp. 169–193, Jul. 2011, doi: 10.1146/ANNUREV-MATSCI-062910-100425.

[16] M. C. Jarvis and M. C. McCann, “Macromolecular biophysics of the plant cell wall: Concepts and methodology,” Plant Physiol. Biochem., vol. 38, no. 1–2, pp. 1–13, Jan. 2000, doi: 10.1016/S0981-9428(00)00172-8.

[17] O. Leroux, “Collenchyma: a versatile mechanical tissue with dynamic cell walls,” Ann. Bot., vol. 110, no. 6, pp. 1083–1098, Nov. 2012, doi: 10.1093/AOB/MCS186.

[18] R. Zhong and Z. H. Ye, “Secondary Cell Walls: Biosynthesis, Patterned Deposition and Transcriptional Regulation,” Plant Cell Physiol., vol. 56, no. 2, pp. 195–214, Feb. 2015, doi: 10.1093/PCP/PCU140.

[19] M.-L. Lemloh et al., “Structure-property relationships in mechanically stimulated Sorghum bicolor stalks,” Bioinspired Mater., vol. 1, no. 1, Oct. 2014, doi: 10.2478/BIMA-2014-0001.

[20] L. Köhler and H. C. Spatz, “Micromechanics of plant tissues beyond the linear-elastic range,” Planta 2002 2151, vol. 215, no. 1, pp. 33–40, 2002, doi: 10.1007/S00425-001-0718-9.

[21] C. B. Beck, “The epidermis,” An Introd. to Plant Struct. Dev., pp. 138–153, Jun. 2005, doi: 10.1017/CBO9781139165365.009.

[22] J. E. Jakes and D. S. Stone, “Best Practices for Quasistatic Berkovich Nanoindentation of Wood Cell Walls,” For. 2021, Vol. 12, Page 1696, vol. 12, no. 12, p. 1696, Dec. 2021, doi: 10.3390/F12121696.

[23] J. Du et al., “Micron-scale phenotyping quantification and three-dimensional microstructure reconstruction of vascular bundles within maize stalks based on micro-CT scanning,” Funct. Plant Biol., vol. 44, no. 1, pp. 10–22, 2016, doi: 10.1071/FP16117.

[24] Y. Li et al., “BRITTLE CULM1, Which Encodes a COBRA-Like Protein, Affects the Mechanical Properties of Rice Plants,” Plant Cell, vol. 15, no. 9, p. 2020, Sep. 2003, doi: 10.1105/TPC.011775.

[25] M. Fournier, J. Dlouhá, G. Jaouen, and T. Almeras, “Integrative biomechanics for tree ecology: beyond wood density and strength,” J. Exp. Bot., vol. 64, no. 15, pp. 4793–4815, Nov. 2013, doi: 10.1093/JXB/ERT279.

[26] D. U. Shah, “Developing plant fibre composites for structural applications by optimising composite parameters: a critical review,” J. Mater. Sci. 2013 4818, vol. 48, no. 18, pp. 6083–6107, Jun. 2013, doi: 10.1007/S10853-013-7458-7.

[27] E. Xi, “Dynamic relationship between mechanical properties and chemical composition distribution of wood cell walls,” Wood Res., vol. 63, no. 2, 2018.

Chapter 7: Conclusion

7.1 Summary

The biomechanical strength and structural rigidity of stalks are critical determinants of stalk lodging resistance. From the structural constituents of the stalk, the rind provides the principal structure supporting cells against tension and bending loads. In this work, for understanding the relationship between the biomechanical properties and /or lodging behavior and the compositional attributes, two sorghum varieties, Della (D) and its mutant (*REDforGREEN,* RG) grown in 2018 (D1 and RG1) and 2019 (D2 and RG2) was evaluated. The composition of the whole stalk was evaluated comprehensively by employing GCMS, FTIR, HPLC, Py-GCMS, TGA, XRD, and 2D ^{1}H-^{13}C NMR. X-ray tomography, scanning electron microscope, and nanoindentation were also applied for investigating microstructural and micro-scale mechanics. Compositional, microstructural, and supramolecular variations in the cell wall polymers of Della and RG were detected, attributed to changes in lignin, cellulose, and hemicellulose contents and structures. Furthermore, the biomechanical and viscoelastic behavior of the rind from the internodes was investigated by three-point micro-bending tests using a dynamic mechanical analysis (DMA). In addition, the microfibril angle (MFA) of the S2 cell wall was determined using XRD. The finding revealed that the biomechanical behavior of the Della varieties was stiffer than their respective mutant RG. The lignin content, cellulose content, and MFA were found key cell wall parameters positively correlated with the biomechanical strength and /or stalk lodging of the stalks. The Guaiacyl and *p*-hydroxyphenyl units of lignin were found respectively, positively, and negatively correlated with biomechanical properties. Genetic modification of cell walls and breeding have been proposed and implemented as a mechanism to tailor cell wall biomechanics. Thus, the findings could be implemented or can be used as a base for developing lodging-resistant varieties.

7.2 Recommendations and future works

Developing lodging-resistant and high-yielding crops is challenging and requires a comprehensive understanding of the biochemical and physiological pathways behind the development of stronger sorghum phenotypes. However, the molecular mechanisms of plant lodging resistance remain largely uninvestigated. Lodging-inducing factors such as meteorological, pathological/biological, nutrient levels, the morphological, anatomical, and biochemical composition of the cell walls, and the interactions of all these factors make lodging one of the complex multi-scale phenomena in the sphere of agronomy. Thus, lodging cannot simply be assayed by one single or few factors due to the complex and still unknown interactions between these parameters. The complexity of the plant cell wall and the exact effects of its polymers on crop lodging resistance remain subtle. However, genetic analysis

combined with compositional and environmental factors could help to better understand lodging traits. In addition, water is an important component in determining the viscoelastic and biomechanical properties of biological samples. Structural changes are followed by loss of water. Cell wall polymeric components behavior at natural wet conditions and ‘dry’ and /or artificial “wet” conditions could vary significantly, and lead to virtually different experimentations.

The concept “structure determines the properties” can be applied to the lodging susceptibility of sorghum to investigate the structure-property relationships of the stalks and develop governing models and principles. Hence for future developments, the integration and analysis of a large amount of data using different machine learning algorithms could assist in developing more complex models and predicting the behavior of lodging. In this context, different imaging techniques of cell walls, and an understanding of structural features at the cellular level might be essential to acquire the underlying mechanisms of lodging at the molecular level. As one of the most complex natural nanostructures, employing all technological advancements can be an effective way of understanding the cell wall component interactions and their effect on the lodging mechanism.

Future research in the following directions is recommended.

- Development of predicting spectroscopic techniques for rapid on-field compositional analysis, such as using near-infrared (NIR) spectroscopy, to replace traditional wet chemical techniques and be able to correlate the compositional data with biomechanical properties produced in the field. These techniques could help to predict the composition of biomass and significantly decrease the time and cost required for routine wet-chemical-based biomass compositional analyses.
- Applying the materials science principles and application of rigorous non-destructive advanced imaging and characterization techniques for an understanding of structural features at the molecular level to acquire the underlying mechanisms of lodging. The study of cell walls and their correlation with macrostructure stalk level biomechanical behavior and structure-property-agricultural performance relationships would help to understand the roles of lignin, cellulose, and hemicelluloses for stalk cell wall micromechanics and identify mechanisms responsible for lodging.
- Application of machine learning algorithms for future developments and analysis of data, which could assist in developing complex models for predicting the behavior of lodging.

Appendix A: Stalk Extractives Content and Fatty Acid Concentrations

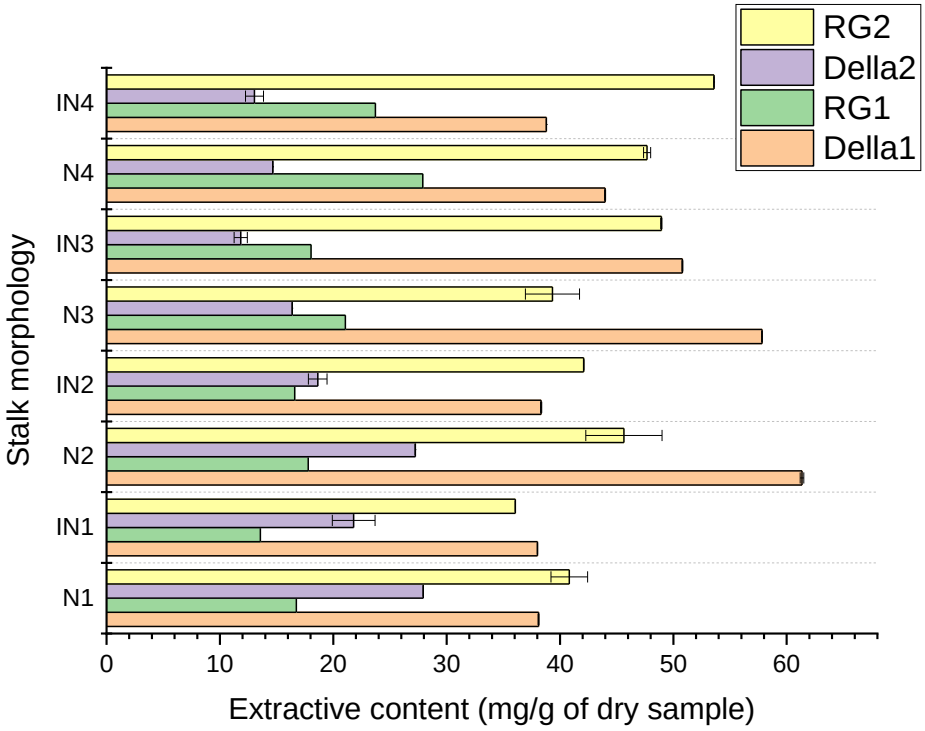

Figure A1 Extractive content (mg/g of dry sample) for Della1, RG1, Della2 and RG2 at internodes and nodes

Table A1 Fatty acid concentrations of DCM extracts from Della1, RG1, Della2 and RG2 at nodes and internodes (in mg/g of extract) determined by GCMS as FAME derivatives

Fatty Acid	M^+ (m/z)	RT(min)	Stalks	Internodes				Nodes			
				IN1	IN2	IN3	IN4	N1	N2	N3	N4
Lauric Acid	214	24.2	Della1	1.4±0.1	9.6±0.6	9.9±0.0	3.4±0.1	16.7±1.8	7.0±0.3	2.5±0.0	1.3±0.0
			RG1	0.3± 0.0	0.4± 0.1	0.5± 0.1	0.4± 0.1	0.8±0.0	0.8±0.1	1.4±0.0	1.5±0.3
			Della2	6.1±0.7	25.9±5.7	42.8±2.1	5.2±0.3	1.4±0.2	1.4±0.0	1.9±0.0	7.3±1.7
			RG2	0.3±0.0	0.3±0.0	0.6±0.0	0.3±0.0	0.2±0.1	0.3±0.0	17.0±1.4	4.6±0.5
Azelaic Acid	216	24.3	Della1	1.5±0.2	3.9±0.3	3.9±0.1	4.0±0.2	2.5±0.1	3.0±0.2	5.7±0.1	5.2±0.1
			RG1	1.1±0.1	0.8±0.0	0.4±0.0	0.2±0.0	0.7±0.0	1.0±0.0	0.9±0.1	2.2±0.1
			Della2	1.1±0.3	-	1.7±0.3	0.4±0.0	0.2±0.0	0.1±0.0	-	-
			RG2	0.6±0.0	0.4±0.0	1.4±0.1	0.3±0.1	2.9±0.6	2.2±0.0	1.0±0.1	0.3±0.1
Myristic Acid	242	28.7	Della1	2.16±0.1	1.2±0.3	2.0±0.0	1.5±0.1	2.5±0.1	1.1±0.0	2.4±0.0	2.8±0.0
			RG1	1.2± 0.1	1.2± 0.1	1.3± 0.1	1.2± 0.1	0.6±0.0	0.6±0.0	1.3±0.1	1.0±0.0
			Della2	8.6±1.0	9.5±4.7	11.1±0.4	7.0±0.5	4.6±0.6	3.9±0.0	12.8±0.0	7.5±1.9
			RG2	0.6±0.0	0.8±0.0	1.4±0.0	0.9±0.1	8.5±0.7	4.7±0.0	2.7±0.0	0.3±0.0
Palmitoleic Acid	268	32.4	Della1	3.7±0.1	2.8±1.5	4.6±0.1	3.3±0.1	6.2±1.0	5.0±1.2	11.4±0.2	14.9±0.1
			RG1	6.5±0.3	5.9±0.4	3.9±0.2	2.3±0.3	4.6±0.1	2.8±0.3	4.2±0.2	3.6±0.1
			Della2	11.5±1.7	12.5±0.9	21.4±0.8	15.2±1.0	8.2±1.0	7.8±2.6	9.6±0.4	9.8±8±2.4
			RG2	1.2±0.1	1.6±0.0	2.5±0.0	0.9±0.1	12.4±2.1	13.6±0.1	4.6±1.4	1.6±0.0
Palmitic Acid	270	32.8	Della1	50.3±0.4	50.6±6.2	63.1±0.7	53.3±1.6	85.6±0.3	41.2±3.8	80.5±0.6	80.5±1.0
			RG1	61.5± 0.7	62.4±0.7	64.7±0.7	62.4± 0.7	66.8±0.7	56.1±5.8	114.6±3.3	90.2±0.1
			Della2	113.4±12.4	94.9±4.1	150.4±7.0	90.0±4.5	110.5±1.8	64.0±0.1	121.5±1.3	138.8±15.2
			RG2	78.1±4.7	63.0.2±1.6	73.3±3.4	79.9±3.3	130.9±14.6	77.3±0.1	29.8±4.4	76.9±10.7
Linoleic Acid	294	34.7	Della1	116.7±11.6	91.1±7.0	94.0±0.6	64.3±3.1	211.3±5.2	100.3±12.9	170.6±1.4	136.7±0.7
			RG1	47.7± 2.3	48.4± 2.3	50.1± 2.4	48.4± 2.3	39.4±2.2	23.5±2.2	57.3±3.4	84.2±1.0
			Della2	144.9±17.6	146.8±0.7	164.3±2.8	118.2±3.7	174.2±2.9	128.1±0.8	151.1±0.5	237.0±19.2
			RG2	104.6±2.3	84.2±6.4	80.1±1.3	104.9±2.2	177.5±19.0	109.3±0.7	58.3±4.4	136.3±9.6
Oleic Acid	296	36.1	Della1	151.4±19.3	146.3±10.0	167.3±1.7	139.4±1.2	246.8±6.6	168±1.4	295.0±6.6	292.7±0.4
			RG1	159.4± 0.4	161.7± 0.4	167.6± 0.3	161.7± 0.4	104.0±1.3	129.6±15.1	245.4±12.6	225.4±2.0
			Della2	454.6±17.4	390.0±1.5	477.5±11.7	295.2±10.4	265.3±1.0	292.3±2.7	598.3±3.6	536.6±29.4
			RG2	351.9±9.3	233.3±10.8	232.8±5.7	264.9±6.7	395.1±6.8	353.0±3.3	144.8±14.6	448.7±15.8
Stearic Acid	298	36.6	Della1	10.0±0.7	12.7±1.9	10.0±0.1	8.5±0.2	19.5±1.6	10.1±0.1	16.0±0.2	14.0±0.6
			RG1	21.3± 1.2	21.6± 1.2	22.4±1.3	21.6± 1.2	10.0±0.4	9.2±0.8	18.3±1.8	18.1±0.4
			Della2	25.8±6.5	18.0±9.5	31.3±0.8	19.4±1.8	22.9±1.4	17.5±0.2	36.9±2.3	28.8±8.6
			RG2	24.6±1.1	15.1±1.8	15.2±0.4	17.2±1.4	39.4±0.0	21.2±0.2	12.1±1.1	18.1±3.2
Eicosanoic acid	326	40.0	Della1	11.4±0.3	7.9±2.1	10.7±0.4	6.7±0.2	14.9±1.8	6.7±0.3	7.7±0.0	12.5±0.6
			RG1	5.4± 0.9	5.5± 0.9	5.7± 0.9	5.5± 0.9	2.3±0.4	2.3±0.2	5.6±0.5	6.1±0.1
			Della2	24.4±3.1	15.9±3.0	24.6±0.7	12.0±0.5	9.1±0.6	6.4±0.2	33.8±0.5	12.7±4.3
			RG2	16.4±1.7	10.6±0.9	12.0±0.3	10.6±0.5	14.7±2.3	7.7±0.3	3.4±0.4	8.0±1.8

Appendix B: Stalk Compositional Data

Table B1. FTIR Assignments for main functional groups in sorghum stalk biomass assigned based on the literature [44] [46,47].

Wavenumbers (cm^{-1})	Assignments	Descriptions
3360	O─H stretching	O–H in cellulose, hemicellulose, and lignin (phenolic and CH_2OH)
2920;2850	C─H stretching	Asymmetric and symmetric stretching respectively in aromatic methoxy groups, CH_3 and CH_2 groups of the side chains of lignin and aliphatic waxes.
1735	C═O	Unconjugated carbonyl stretching in ketones, aldehydes, and ester groups.
1630	C═O	Conjugated carbonyl-carboxyl stretching from ketone groups.
1605-1600	C═C +C═O	Aromatic skeleton vibrations in S and G lignin, coupled with C═O stretch
1520-1505	C═C	Aromatic skeletal vibrations of S and G
1460	C─H	Asymmetric bending of CH_2 in cellulose, and CH_3 in methoxy (CH_3–O) and hemicelluloses (CH_3─(C═O) ─).
1425-1430	C═C+C─H	Aromatic skeletal vibrations combined with C─H in plane deformation
1370-1375	C─H	C─H bending of CH_3 in cellulose and hemicelluloses, and phenolic O─H
1325	Aromatic ring	Syringyl ring breathing with CO stretching
1235-1245	C═O, C─O, C─C	C─C, C─O and C═O stretching in Guaiacyl
1160-1170	C═O	Typical for HGS type lignin; C═O stretching from conjugated ketone, and ester groups
1120	C─H	Aromatic C─H bending in-plane (typical for S units)
1034	C─H, C–O–C	Aromatic C–H in-plane deformation from guaiacyl lignin and C–O–C glycosidic linkage from hemicellulose and cellulose
835	C─H	C─H out of plane in position 2 and 6 of syringyl and in all positions of hydroxyphenyl lignin

Table B2. Identification and relative abundance (%) of main pyrolysates from internodes of D1, RG1, D2, and RG2 sorghum stalks

RT	Compound	MW	Formula	D1-IN	RG1-IN	D2-IN	RG2-IN
1.43	**Carbon dioxide**	44	CO_2	9.78±1.27	16.55±5.97	14.04±0.04	17.24±2.03
1.64	**Methyl glyoxal**	72	$C_3H_4O_2$	4.43±1.43	5.22±1.22	9.05±0.24	6.36±0.65
2.07	**Acetic acid**	60	$C_2H_4O_2$	12.21±0.52	4.52±1.38	16.79±1.43	15.99±0.50
2.42	**1-hydroxy-2-Propanone**	74	$C_3H_6O_2$	8.53±0.21	-	8.54±0.68	5.31±0.66
2.57	**2(3H)-Furanone, dihydro-4-hydroxy-**	102	$C_4H_6O_3$	1.23±0.09	1.71±0.33	0.80±0.06	-
2.80	**Acetoin**	88	$C_4H_8O_2$	-	-	-	3.81±0.05
3.36	**Butanal, 3-hydroxy-**	88	$C_4H_8O_2$	0.44±0.03	0.47±0.09	0.88±0.00	1.19±0.18
3.58	**2-Butanone, 1-(acetyloxy)-**	130	$C_6H_{10}O_3$	2.16±0.26	-	3.64±0.18	4.36±0.12
3.8	**Succindialdehyde**	86	$C_4H_6O_2$	3.81±1.65	2.91±1.28	5.81±0.51	5.18±0.26
4.71	**Furfural**	96	$C_5H_4O_2$	3.80±0.26	2.49±0.73	2.49±0.01	1.74±0.17
5.23	**2-Hexanone, 3-methyl-**	114	$C_7H_{14}O$	1.12±0.54	-	1.40±0.11	1.28±0.12
5.44	**2-Propanone, 1-(acetyloxy)-**	116	$C_5H_8O_3$	1.20±0.45	-	1.64±0.16	0.97±0.24
5.83	**4-Cyclopentene-1,3-dione**	96	$C_5H_4O_2$	0.44±0.18	-	0.59±0.07	0.42±0.04
6.32	**2-Cyclopenten-1-one, 2-methyl-**	96	C_6H_8O	0.35±0.16	-	0.66±0.04	0.58±0.01
6.44	**Ethanone, 1-(2-furanyl)-**	110	$C_6H_6O_2$	0.31±0.16	-	0.22±0.43	0.13±0.02
6.63	**2(5H)-Furanone**	84	$C_4H_4O_2$	0.98±0.30	2.37±0.51	1.21±0.07	1.66±0.05
6.82	**1,2-Cyclopentanedione**	98	$C_5H_6O_2$	2.45±0.61	3.84±1.21	3.18±0.41	2.33±0.40
7.22	**2(5H)-Furanone, 5-methyl-**	98	$C_5H_6O_2$	-	-	0.17±0.01	0.13±0.01
7.85	**2,5-Furandione, dihydro-3-methylene-**	112	$C_5H_4O_3$	1.16±0.48	-	1.42±0.09	0.95±0.09
8.26	**Phenol**	94	C_6H_6O	2.66±0.60	3.95±1.95	1.76±0.03	1.43±0.01
8.79	**3,4-Dihydro-2-methoxy-2H-pyran**	114	$C_6H_{10}O_2$	0.37±0.03	-	0.76±0.00	1.16±0.07
9.57	**3-Methyl-1,2-cyclopentanedione**	112	$C_6H_8O_2$	2.12±0.56	2.49±0.73	1.74±0.09	1.35±0.14
9.89	**2,3-Dimethyl-2-cyclopenten-1-one**	110	$C_7H_{10}O$	0.31±0.16	-	0.24±0.01	0.15±0.01
10.3	**Phenol, 3-methyl-**	108	C_7H_8O	0.87±0.21	-	0.54±0.05	0.54±0.16
11.0	**p-Cresol**	108	C_7H_8O	1.54±0.32	2.05±0.52	0.85±0.00	0.63±0.06
11.2	**Furyl hydroxymethyl ketone**	126	$C_6H_6O_3$	0.21±0.03	-	-	0.22±0.05
11.3	**Phenol, 2-methoxy-**	124	$C_7H_8O_2$	1.30±0.42	1.21±0.74	1.10±0.18	1.00±0.01
11.7	**Cyclopropyl carbinol**	72	C_4H_8O	0.18±0.08	2.50±0.30	-	-
12.2	**4-Pentylcyclohexanone**	168	$C_{11}H_{20}O$	0.48±0.14	0.41±0.08	-	-
12.3	**2-Cyclopenten-1-one, 3-ethyl-2-hydroxy-**	126	$C_7H_{10}O_2$	-	0.47±0.18	0.34±0.01	0.69±0.10
12.6	**2,4(3H,5H)-Furandione, 3-methyl-**	114	$C_5H_6O_3$	0.21±0.02	1.09±0.16	-	-
13.0	**Phenol, 2,3-dimethyl-**	122	$C_8H_{10}O$	0.46±0.14	-	0.37±0.06	0.19±0.04
13.5	**Phenol, 4-ethyl-**	122	$C_8H_{10}O$	1.86±0.28	2.28±1.01	1.43±0.20	0.92±0.39
14.3	**Creosol**	138	$C_8H_{10}O_2$	-0.47±0.12	-	0.49±0.04	0.63±0.14
14.6	**Catechol**	110	$C_6H_6O_2$	2.36±0.43	2.45±1.03	-	-
14.9	**1,4:3,6-Dianhydro-α-d-glucopyranose**	144	$C_6H_8O_4$	-	1.26±0.10	-	-
15.0	**4-vinylphenol**	120	C_8H_8O	10.02±0.91	18.10±0.36	11.39±1.96	14.5±1.06
16.2	**5-Hydroxymethylfurfural**	126	$C_6H_6O_3$	1.45±0.27	2.95±0.98	-	-
16.7	**Phenol, 4-ethyl-2-methoxy-**	152	$C_9H_{12}O_2$	0.25±0.03	-	0.38±0.06	0.2±0.06
16.9	**p-Isobutylbenzaldehyde**	162	$C_{11}H_{14}O$	0.13±0.02	-	-	0.25±0.03
17.8	***4-Vinyl guaiacol***	150	$C_9H_{10}O_2$	2.07±0.27	4.05±0.74	2.76±0.48	2.68±0.63
18.7	***4-vinylsyringol***	154	$C_8H_{10}O_3$	1.45±0.35	2.82±0.89	1.68±0.17	1.44±0.14
20.0	**Benzaldehyde, 3-hydroxy-4-methoxy-**	152	$C_8H_8O_3$	0.27±0.04	0.60±0.01	-	0.12±0.07
20.1	**Phenol, 4-methoxy-3-(methoxymethyl)-**	168	$C_9H_{12}O_3$	-	0.54±0.20	-	-
21.2	**Phenol, 2-methoxy-4-(1-propenyl)-**	164	$C_{10}H_{12}O_2$	0.86±0.12	0.81±0.20	0.76±0.02	1.01±0.22
22.0	**Benzene, 3-ethyl-1,2,4,5-tetramethyl-**	162	$C_{12}H_{18}$	-	0.48±0.07	-	0.25±0.16
22.2	**5-Hepten-3-yn-2-ol, 6-methyl-5-(1-methylethyl)-**	166	$C_{11}H_{18}O$	0.14±0.03	1.20±0.39	-	-
24.1	**Phenol, 4-ethenyl-2,6-dimethoxy-**	180	$C_{10}H_{12}O_3$	0.91±0.13	1.83±0.57	0.10±0.00	0.67±0.06
25.0	**Phenol, 2,6-dimethoxy-4-(2-propenyl)-**	194	$C_{11}H_{14}O_3$	-	0.31±0.06	0.04±0.00	-
26.3	**Benzaldehyde, 4-hydroxy-3,5-dimethoxy-**	182	$C_9H_{10}O_4$	0.14±0.04	0.31±0.00	-	-
26.7	**2-Allyl-1,4-dimethoxy-3-methylbenzene**	192	$C_{12}H_{16}O_2$	0.25±0.02	0.95±0.30	-	-
27.2	**(E)-2,6-Dimethoxy-4-(prop-1-en-1-yl) phenol**	194	$C_{11}H_{14}O_3$	0.28±0.03	1.60±0.23	-	-

Table B3. Compounds identified and relative abundance (Area %) of pyrolysates from nodes of D1, RG1, D2 and RG2 stalks

RT	Compound	MW	Formula	D1-N	RG1-N	D2-N	RG2-N
1.43	**Carbon dioxide**	44	CO_2	12.59±0.22	13.05±1.57	17.18±1.42	16.55±0.29
1.64	**Methyl glyoxal**	72	$C_3H_4O_2$	7.51±1.2	4.90±0.18	7.35±0.53	7.01±0.48
2.07	**Acetic acid**	60	$C_2H_4O_2$	13.35±3.71	4.56±0.91	13.65±0.45	16.76±0.76
2.42	**1-hydroxy-2-Propanone**	74	$C_3H_6O_2$	10.06±2.0	-	8.27±1.98	7.50±0.76
2.57	**2(3H)-Furanone, dihydro-4-hydroxy-**	102	$C_4H_6O_3$	1.06±0.03	1.94±0.16	0.75±0.16	-
2.80	**Acetoin**	88	$C_4H_8O_2$	1.56±0.78	-	-	1.89±0.35
3.36	**Butanal, 3-hydroxy-**	88	$C_4H_8O_2$	1.50±0.04	0.38±0.05	0.99±0.22	1.61±0.00
3.58	**2-Butanone, 1-(acetyloxy)-**	130	$C_6H_{10}O_3$	3.42±1.15	-	3.18±0.79	4.15±0.48
3.8	**Succindialdehyde**	86	$C_4H_6O_2$	4.73±1.85	7.78±1.28	6.40±2.38	4.94±0.0.65
4.71	**Furfural**	96	$C_5H_4O_2$	3.40±0.97	-	2.66±0.89	2.04±0.01
5.23	**2-Hexanone, 3-methyl-**	114	$C_7H_{14}O$	1.62±0.60	-	-	1.30±0.13
5.44	**2-Propanone, 1-(acetyloxy)-**	116	$C_5H_8O_3$	2.10±0.38	-	1.58±0.41	1.57±0.24
5.83	**4-Cyclopentene-1,3-dione**	96	$C_5H_4O_2$	0.11±0.00	-	0.48±0.09	0.97±0.24
6.32	**2-Cyclopenten-1-one, 2-methyl-**	96	C_6H_8O	0.72±0.06	-	0.72±0.20	0.42±0.04
6.44	**Ethanone, 1-(2-furanyl)-**	110	$C_6H_6O_2$	0.19±0.00	-	0.22±0.06	0.28±0.07
6.63	**2(5H)-Furanone**	84	$C_4H_4O_2$	1.16±0.38	3.67±0.13	1.09±0.11	1.51±0.08
6.82	**1,2-Cyclopentanedione**	98	$C_5H_6O_2$	2.21±0.37	3.84±1.21	2.86±0.34	2.49±0.74
7.22	**2(5H)-Furanone, 5-methyl-**	98	$C_5H_6O_2$	0.14±0.02	-	0.19±0.07	0.5±0.06
7.32	**2,5-Furandione, dihydro-3-methylene-**	112	$C_5H_4O_3$	0.12±0.05	-	0.92±0.06	0.19±0.07
8.26	**Phenol**	94	C_6H_6O	1.91±0.24	5.05±0.35	2.12±0.50	1.82±0.30
8.79	**3,4-Dihydro-2-methoxy-2H-pyran**	114	$C_6H_{10}O_2$	0.53±0.23	-	0.76±0.08	1.09±0.21
9.57	**3-Methyl-1,2-cyclopentanedione**	112	$C_6H_8O_2$	1.78±0.27	2.87±0.25	2.08±0.68	-
9.89	**2,3-Dimethyl-2-cyclopenten-1-one**	110	$C_7H_{10}O$	0.26±0.04	-	0.34±0.09	-
10.3	**Phenol, 3-methyl-**	108	C_7H_8O	0.75±0.14	-	0.77±0.33	-
10.88	**p-Cresol**	108	C_7H_8O	1.03±0.27	1.39±1.06	1.05±0.00	-
11.2	**Furyl hydroxymethyl ketone**	126	$C_6H_6O_3$	0.19±0.06	-	-	0.29±0.06
11.33	**Phenol, 2-methoxy-**	124	$C_7H_8O_2$	0.94±0.22	2.16±0.74	1.49±0.0.31	1.05±0.24
11.68	**Cyclopropyl carbinol**	72	C_4H_8O	0.68±0.07	2.83±0.07	-	-
12.18	**2-Cyclopenten-1-one, 3-ethyl-2-hydroxy-**	126	$C_7H_{10}O_2$	0.15±0.02	0.53±0.03	0.51±0.19	-
12.55	**2,4(3H,5H)-Furandione, 3-methyl-**	114	$C_5H_6O_3$	0.19±0.05	1.41±0.01	-	-
12.96	**Phenol, 2,3-dimethyl-**	122	$C_8H_{10}O$	0.34±0.07	-	0.55±0.27	-
13.49	**Phenol, 4-ethyl-**	122	$C_8H_{10}O$	1.26±0.26	1.67±0.00	1.58±0.76	1.01±0.15
14.28	**Creosol**	138	$C_8H_{10}O_2$	0.50±0.11	-	0.57±0.12	0.40±0.06
14.57	**Catechol**	110	$C_6H_6O_2$	-	2.41±0.03	-	-
14.93	**1,4:3,6-Dianhydro-α-d-glucopyranose**	144	$C_6H_8O_4$	0.51±0.16	1.06±0.00	-	-
15.0	**4-vinylphenol**	120	C_8H_8O	7.5±0.71	19.41±1.49	11.68±1.06	11.90±0.29
16.24	**5-Hydroxymethylfurfural**	126	$C_6H_6O_3$	0.73±0.09	2.3±0.0.0	-	-
16.67	**Phenol, 4-ethyl-2-methoxy-**	152	$C_9H_{12}O_2$	0.30±0.03	-	0.36±0.11	0.23±0.04
16.92	**p-Isobutylbenzaldehyde**	162	$C_{11}H_{14}O$	0.31±0.09	-	-	0.42±0.06
17.64	***4-Vinylguaiacol***	150	$C_9H_{10}O_2$	2.01±0.30	2.88±0.74	3.28±0.92	2.56±0.03
18.69	***4-vinylsyringol***	154	$C_8H_{10}O_3$	1.14±0.16	2.89±0.35	1.79±0.20	1.95±0.18
20.06	**Benzaldehyde, 3-hydroxy-4-methoxy-**	152	$C_8H_8O_3$	0.13±0.04	0.66±0.01	-	-
20.5	**Phenol, 4-methoxy-3-(methoxymethyl)-**	168	$C_9H_{12}O_3$	-	0.63±0.00	-	-
20.1	**Phenol, 2-methoxy-4-(1-propenyl)-**	164	$C_{10}H_{12}O_2$	0.70±0.01	0.83±0.20	0.63±0.02	1.05±0.21
22.02	**Benzene, 3-ethyl-1,2,4,5-tetramethyl-**	162	$C_{12}H_{18}$	0.38±0.02	0.35±0.07		0.15±0.03
22.18	**5-Hepten-3-yn-2-ol, 6-methyl-5-(1-methylethyl)-**	166	$C_{11}H_{18}O$	0.13±0.04	0.98±0.10	0.54±0.00	0.33±0.17
22.2	**Pentadecane**	212	$C_{15}H_{32}$	0.12±0.01	0.68±0.07	0.18±0.00	0.10±0.03
23.97	**Phenol, 4-ethenyl-2,6-dimethoxy-**	180	$C_{10}H_{12}O_3$	0.68±0.18	2.17±0.19	0.23±0.01	-
24.9	**Phenol, 2,6-dimethoxy-4-(2-propenyl)-**	194	$C_{11}H_{14}O_3$	0.13±0.09	0.41±0.03	0.03±0.00	-
26.34	**Benzaldehyde, 4-hydroxy-3,5-dimethoxy-**	182	$C_9H_{10}O_4$	0.14±0.05	0.30±0.00	0.18±0.09	0.06±0.01
26.72	**2-Allyl-1,4-dimethoxy-3-methylbenzene**	192	$C_{12}H_{16}O_2$	-	0.22±0.04	-	-
27.19	**(E)-2,6-Dimethoxy-4-(prop-1-en-1-yl) phenol**	194	$C_{11}H_{14}O_3$	0.07±0.00	1.71±0.13	-	-

Table B4. HSQC assignments of sorghum stalk whole-cell wall in DMSO-d6/pyridine-d_5 solvent

Label	δC/δH (ppm)	Assignment
	Linkages	
OMe	55.69/3.68	C–H in methoxyl (–OCH3)
β-O-4 (Aγ)	60.95/3.57	Cγ/Hγ in G type β–O–4 units
Cγ	61.71/4.16	Cγ/Hγ cinnamyl alcohol end group
Aγ'	63.04/3.94	Cγ/Hγ in γ-acylated β–O–4
F'	66.63/4.48	Cγ/Hγ in cinnamyl acetate
Bγ	68.14/3.71	Cγ/Hγ in β-β′ (resinol) substructures (B)
$Xylp_{(5)}$	63.12/3.27	C_5/H_5 in (1→4)-β-D-xylopyranoside
-	67.74/3.74	C_5/H_5 in (1,4)-β-D- xylopyranoside (NR)
Aα	72.23/4.96	Cα/Hα in β–O–4 substructures
$Xylp_{(2)}$	72.83/3.16	C_2/H_2 in (1→4)-β-D-xylopyranoside
$Xylp_{(3)}$	74.04/3.35	C_3/H_3 in (1→4)-β-D-xylopyranoside
$Xylp_{(4)}$	75.51/3.63	C_4/H_4 in (1→4)-β-D-xylopyranoside
2-*O*-Ac-β-D-Xyl*p*	73.51/4.61	C_2/H_2 in 2-O-acetyl-β-D-xylopyranoside
-	73.79/3.38	C_5/H_5 in (1,4)-α-D-glucopyranoside
-	74.65/3.05	C_3/H_3 in 3-O-acetyl-β-D-xylopyranoside
3-*O*-Ac- β -D-Xyl*p*	75.00/4.91	C_3/H_3 in 3-O-acetyl-β-D-xylopyranoside
-	75.00/3.03	Unknown polysaccharide
$Xylp_{(4,NR)}$	76.82/3.22	C_4/H_4 in (1→4)-β-D-xylopyranoside for non-reducing end
(1,3)-α-L-Araf	80.81/3.86	C_2–H_2 in (1,3)-α-L-arabinofuranoside
(1,2)-α-L-Araf	81.73/3.69	C_2–H_2 in (1,2)-α-L-arabinofuranoside
(1,3)-α-L-Araf	82.69/3.96	C_2–H_2 in (1,3)-α-L-arabinofuranoside
$A–S_β$	86.21/4.20	$C_β$-$H_β$ in β–O–4 linked to S unit
	Anomeric Region	
-	91.83/5.30	Unknown Anomeric
$αGlu_{(R)}$	92.38/5.06	(1→4)-α-D- glucopyranoside (R)
$αGal_{(R)}$	93.29/5.04	(1→4)- α -D-galactopyranoside (R)
$βX_{(R)}$	96.66/4.42	(1→4)-β-D-xylopyranoside (R)
$βX_{(R)}$	97.10/4.40	(1→4)-β-D-xylopyranoside (R)
-	97.48/5.26	4-*O*-methyl-α-D-glucuronic acid
-	98.32/4.81	2-*O*- acetylated- mannopyranoside
G	99.38/3.67	Unknown polysaccharide
X2	99.32/4.63	2-O-acetylated-β-D-xylopyranoside

Table B4 (continued).

R	**100.13/5.20**	**α-L-Fucopyranoside**
-	100.72/5.12	α-L-Fucopyranoside
X3	101.56/4.38	3-O-acetylated-β-D-xylopyranoside
βGlu	103.01/4.30	(1→4)-β-D-glucopyranoside
H	103.26/3.67	Unknown polysaccharide
Araf	107.17/5.41	α-L-arabinofuranoside
	Aromatic Region	
$S_{2/6}$	103.48/6.75	$C_{2,6}/H_{2,6}$ in syringyl units (S)
$S'_{2/6}$	104.12/7.43	$C_{2/6}/H_{2/6}$ in oxidized syringyl (S') units at C_{α}=O
G_2	110.07/6.98	C_2/H_2 in guaiacyl units
FA2	110.91/7.07	C_2/H_2 in ferulate
***p*CA_8**	113.54/6.31	C_8/H_8 in *p*-coumaric acid
G_5	114.59/6.79	$C_{5/}H_5$ in guaiacyl units
FA_8	115.19/6.5	C_8/H_8 in ferulate
***p*$CA_{3/5}$**	115.46/6.78	$C_{3/5}/H_{3/5}$ in *p*-coumaric acid
G_6	119.09/6.86	$C_{6/}H_6$ in guaiacyl units
$H_{2/6}$	127.92/7.26	$C_{2/6}/H_{2/6}$ in *p*-hydroxyphenyl (H) units
	&129.02/7.27	
***p*$CA_{2/6}$**	129.84/7.48	$C_{2/6}/H_{2/6}$ *p*-coumaric acid
***p*CA_{α}/FA_{α}**	144.27/7.42	Cα/Hα in *p*-coumaric acid (*p*-CA) or Ferulate (FA)

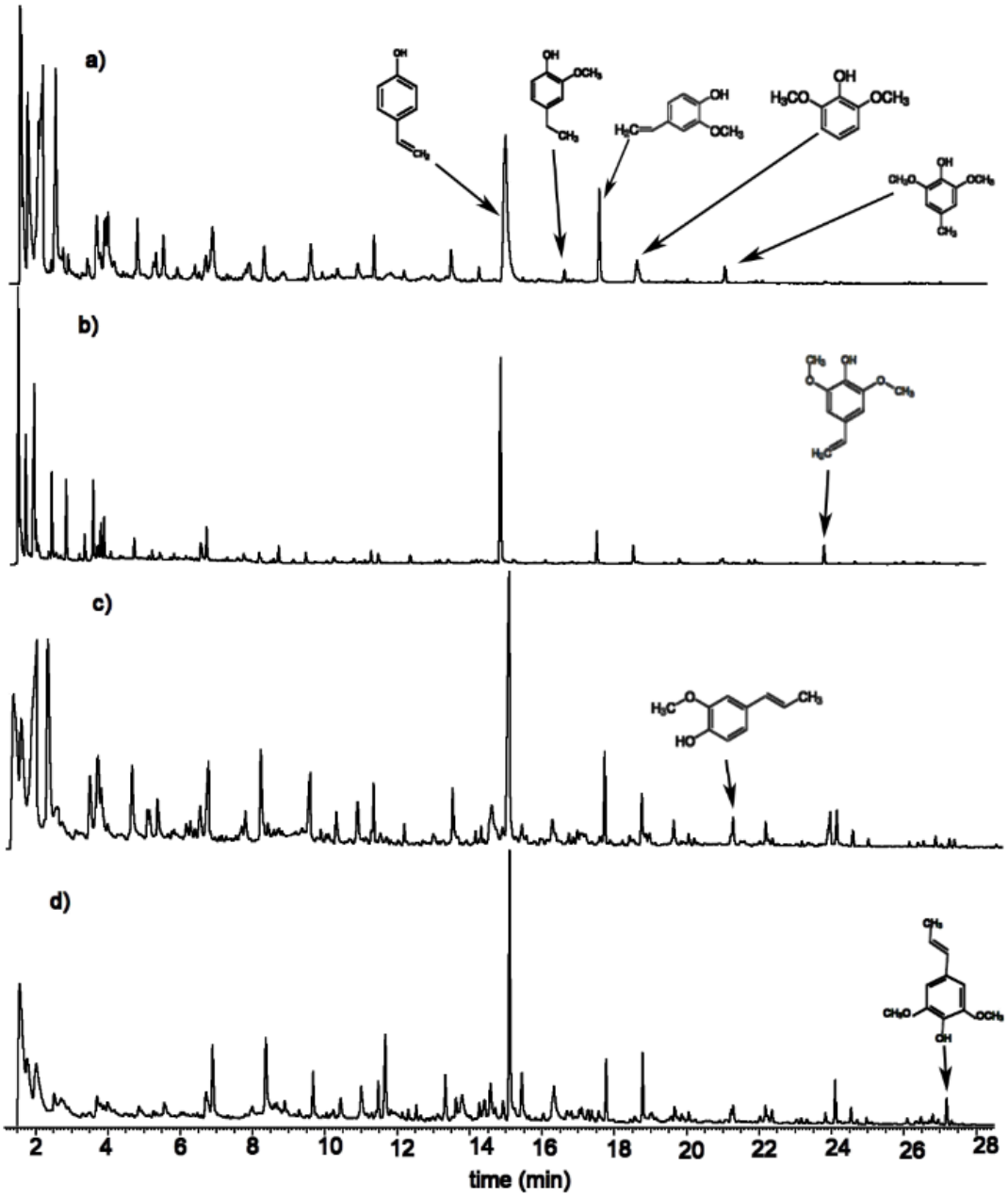

Figure B1. GCMS Pyrogram of Sorghum stalks (a) D2-IN, (b) RG2-IN, (c) D1-IN, and (d) RG1-IN.

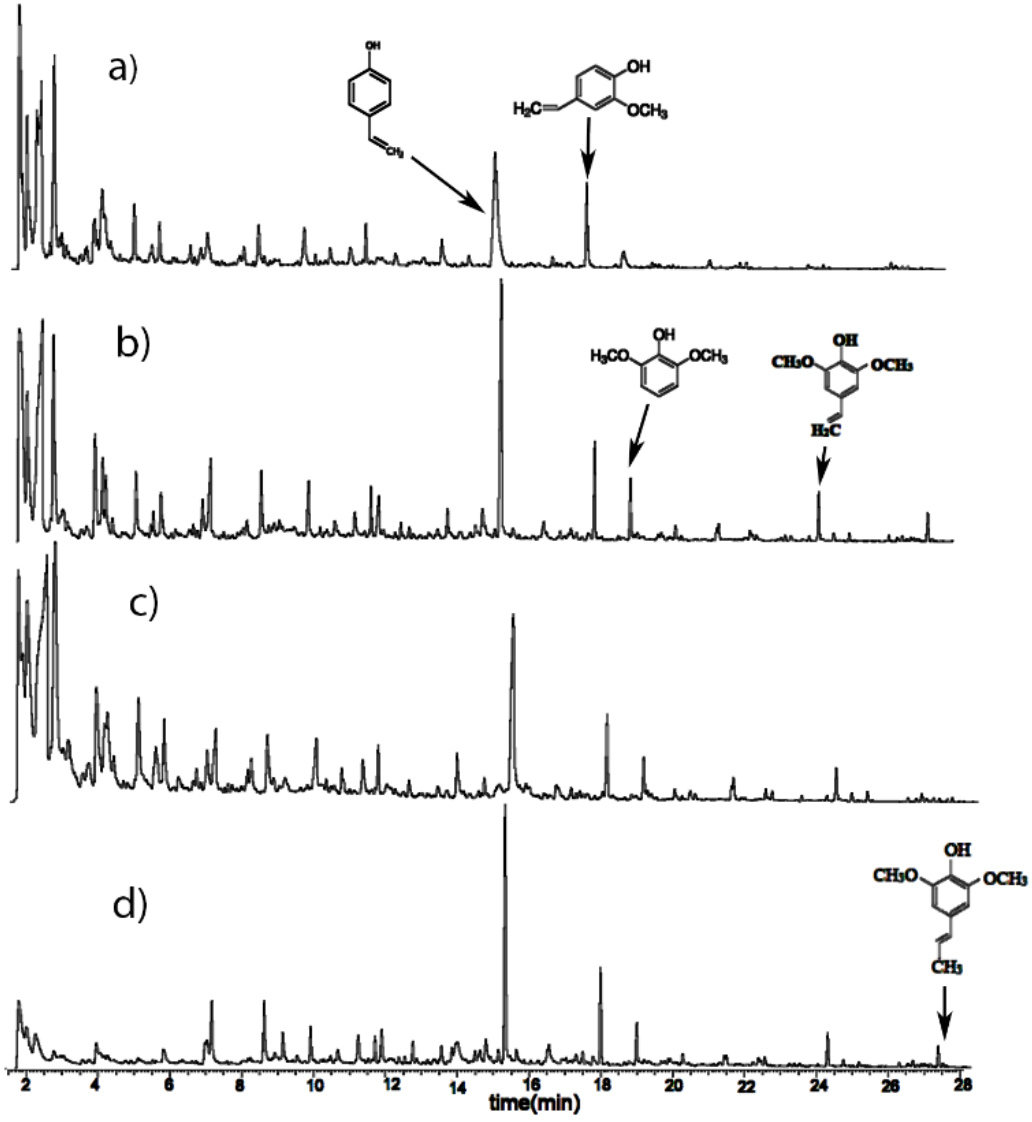

Figure B2. Py-GCMS Pyrogram of Sorghum stalks (a) D2-N, (b) RG2-N, (c) D1-N, (d) RG1-N

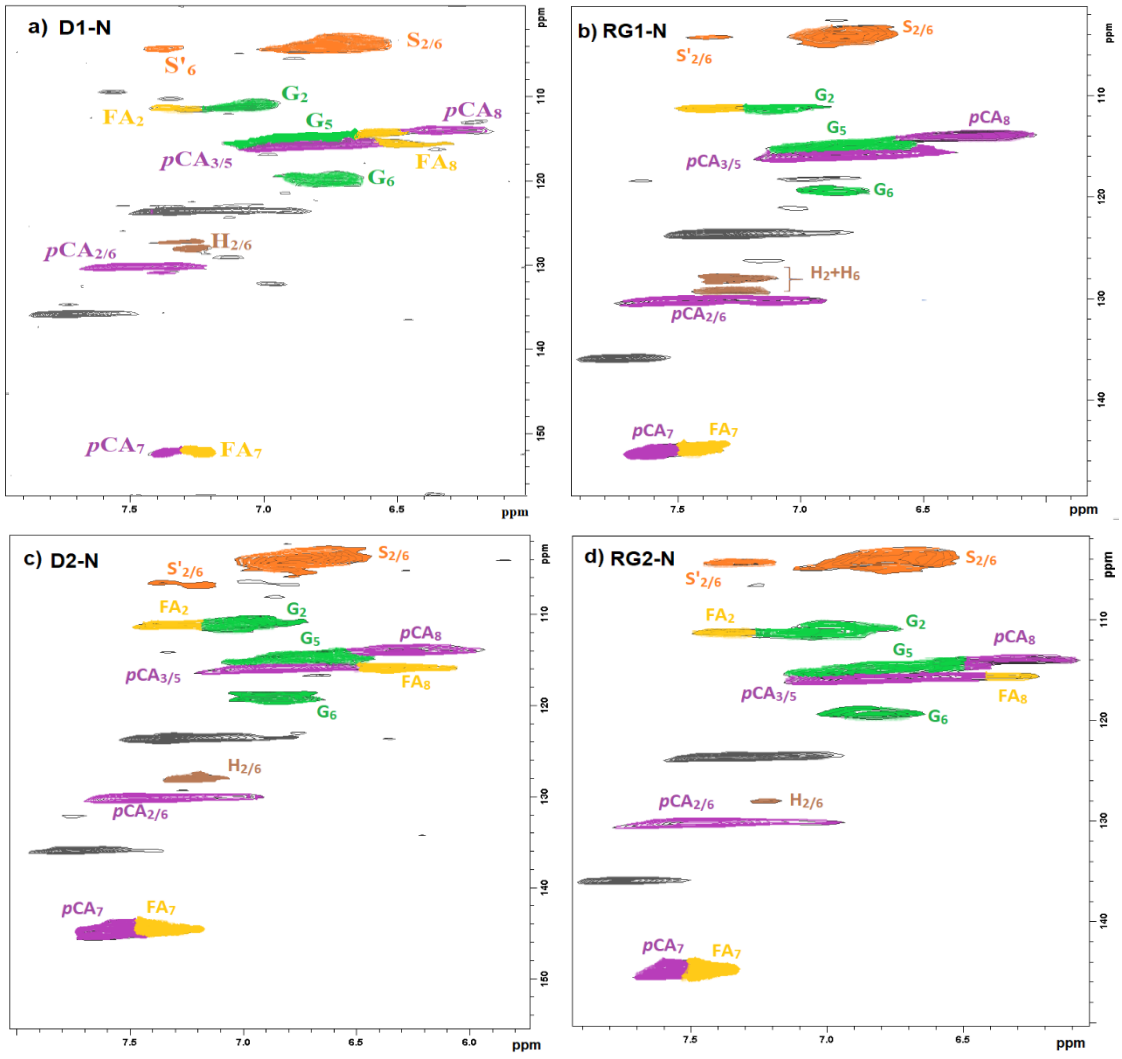

Figure B3. HSQC of sorghum whole-cell wall gels in DMSO-d_6/pyridine-d5 (4:1) solvent in the aromatic region at nodes (N) (a) D1-N, (b) RG1-N, (c) D2-N, (d) RG2-N. The signals in black/grey correspond to pyridine d_5.

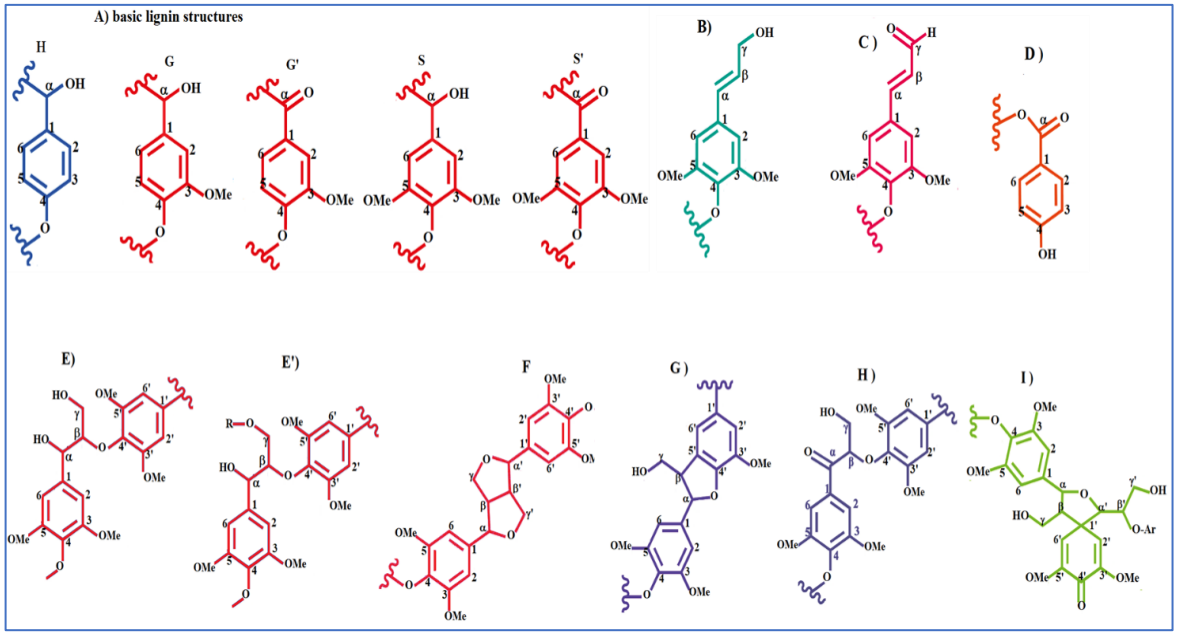

Figure B4. (A) basic lignin structures: H- p-hydroxyphenyl units; G-guaiacyl units; G'-oxidized guaiacyl units with α-ketone; S- syringyl units; S'- oxidized syringyl units with a Cα ketone. (B) p-hydroxycinnamyl alcohol end groups; (C) Cinnamaldehyde end-groups; (D) p-hydroxybenzoate substructures; (E) Aryl-ether (β-O-4') linkages with a free OH at the γ-carbon; (E') Aryl-ether (β-O-4') linkages acylated at γ-carbon; (F) Resinol substructures formed by β-β', α-O-γ', and γ-O-α' linkages; (G) Phenylcoumaran substructures formed by β–5' and α–O–4' linkages; (H) Cα-oxidized β-O-4' substructures; (I) Spirodienone substructures formed by β-1' and α-O-α' linkages;

Appendix C: Rind Compositional and Rheological Data

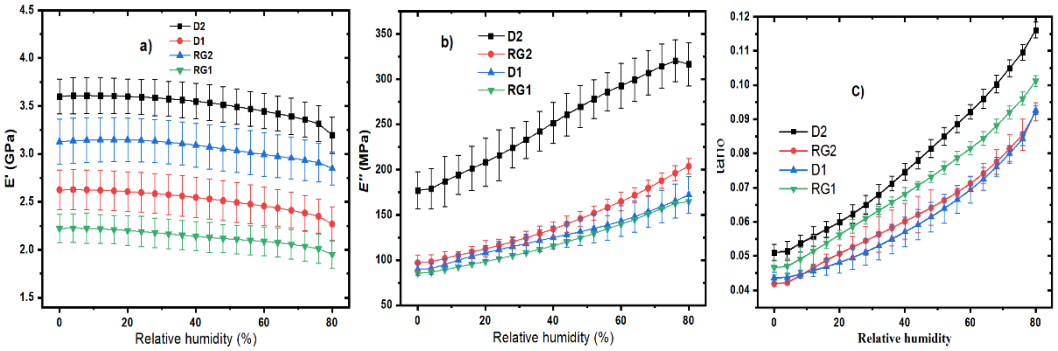

Figure C1. Effect of relative humidity on the rheological properties. a) Storage modulus (*E′*), b) loss modulus (*E″*), and c) damping factor (*tan δ*) as a function of relative humidity (RH) for sorghum stalk rinds from Della and RG varieties (whiskers represent the standard error mean)

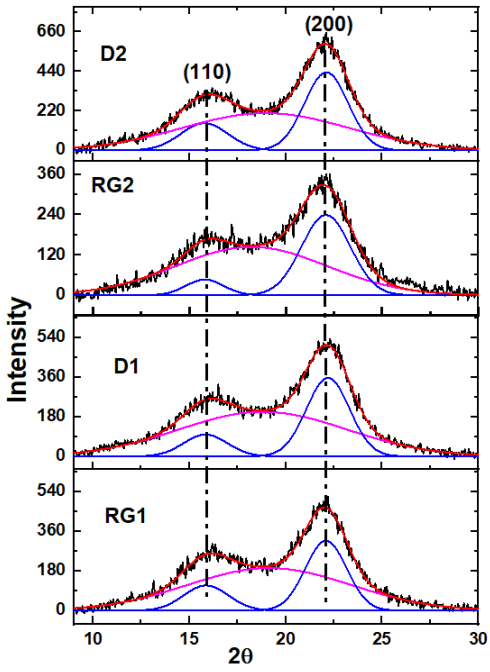

Figure C2. XRD diffractograms sorghum rinds from D2, RG2, D1 and RG1

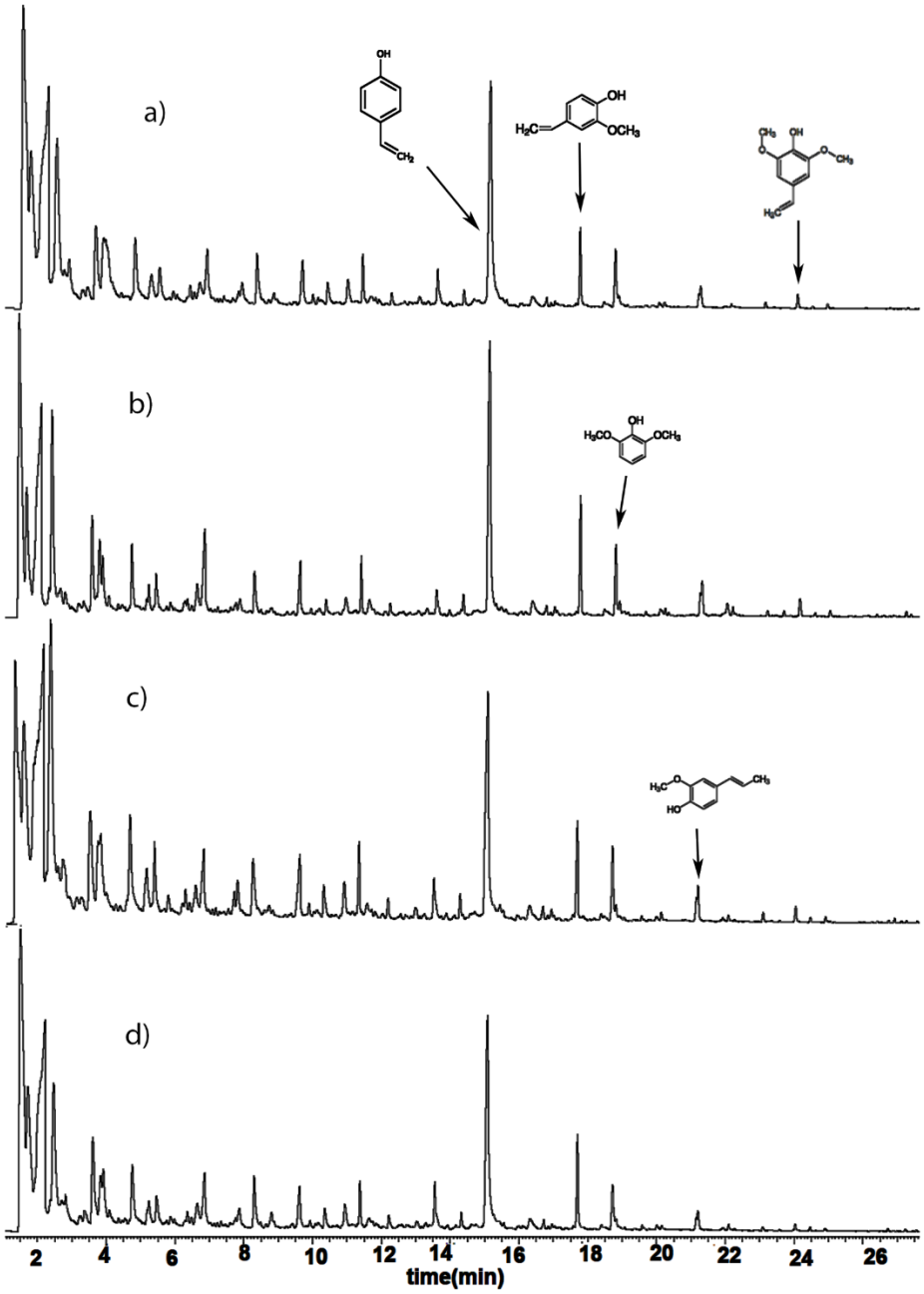

Figure C3. Py-GCMS pyrograms of rinds from a) D2, b) RG2, c) D1 and d) RG1

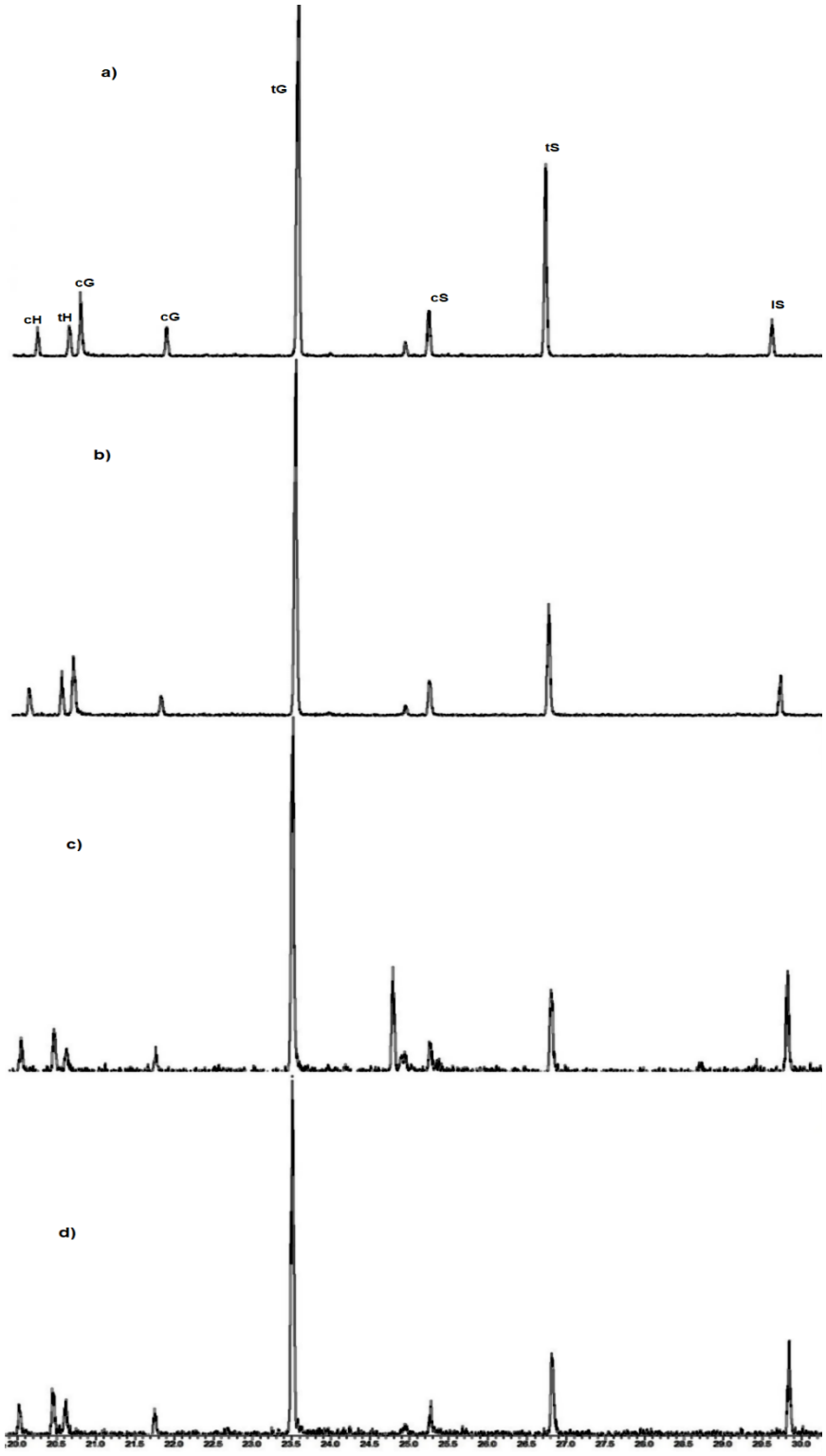

Figure C4.Chromatograms (GC-TIC) of the DFRC degradation products from the MWL isolated from sorghum stalks of: (a) D2, b) RG2, c) D1 and d) RG1. The monomers cH, tH, cG, tG, cS, represents cis- and trans- *p*-hydroxyphenyl, guaiacyl and syringyl

Table C1. FTIR Assignments for functional groups in sorghum rinds of WT1, RG1, WT2 and RG2 assigned based on (Faix 1991; Mengistie et al. 2022)

Wavenumbers (cm^{-1})	Assignments
3340	O–H stretching from cellulose, hemicellulose, and lignin (phenolic and CH_2OH)
2900;2853	Asymmetric and symmetric C─H stretching respectively; from OCH_3 & CH_3 and CH_2 groups of the side chains of lignin and aliphatic waxes.
1730	Unconjugated C═O stretching in ketones, aldehydes, and ester groups.
1630	Conjugated carbonyl-carboxyl stretching from ketone groups
1605-1600	C=C vibrations in S and G lignin, coupled with C═O stretch
1520-1510	Aromatic skeletal (C═C) vibrations of S and G
1460	Asymmetric bending of C─H from CH_2 in cellulose, CH_3 in CH_3O and hemicelluloses (CH_3-(C=O)-)
1425-1430	Skeletal vibrations (C=C) coupled with C─H in plane deformation
1375	C─H bending of CH_3 in cellulose and hemicelluloses
1325	Syringyl ring breathing with C─O stretching
1235	C─C, C─O and C═O stretching in Guacyl
1160	Typical for HGS; C═O stretching from conjugated ketone and ester groups
1120	Aromatic C─H bending in-plane (typical for S units)
1035	Mainly C–O–C glycosidic linkage from hemicellulose and cellulose
898	C–H deformation in cellulose
865	Aromatic out-of-plane deformation vibration in G
835	C-H out-of-plane in position 2 and 6 of S, and in all positions of H units
820	Aromatic out-of-plane deformation vibration in S

Table C2. Pyrolysis products identified in the rinds of D2, RG2, D1 and RG1 sorghum variety

RT	Compound	MW	Formula	D2	RG2	D1	RG1
1.43	Carbon dioxide	44	CO_2	19.29±1.61	14.90±0.78	12.86±1.50	17.42±0.97
1.72	Methyl glyoxal	72	$C_3H_4O_2$	8.04±0.24	6.53±0.15	9.28±0.345	7.55±0.60
2.24	Acetic acid	60	$C_2H_4O_2$	15.23±1.13	13.49±1.01	12.21±0.52	15.67±0.56
2.49	1-hydroxy-2-Propanone	74	$C_3H_6O_2$	7.54±0.07	6.96±0.04	9.96±0.62	7.33±0.28
2.84	Dianhydromannitol	146	$C_6H_{10}O_4$	1.29±0.04	0.88±0.11	1.01±0.11	0.75±0.19
3.21	Butanal, 3-hydroxy-	88	$C_4H_8O_2$	0.44±0.04	0.34±0.01	0.4±0.04	0.39±0.01
3.36	3-Cyclopentene-1,2-diol, cis-	100	$C_5H_8O_2$	0.48±0.01	0.42±0.01	0.45±0.01	0.73±0.02
3.61	2-Butanone, 1-(acetyloxy)-	130	$C_6H_{10}O_3$	2.39±0.26	2.93±0.06	3.07±0.18	2.89±0.03
3.84	Succindialdehyde	86	$C_4H_6O_2$	4.21±0.04	4.18±0.07	3.88±0.4	4.18±0.06
4.76	Furfural	96	$C_5H_4O_2$	2.54±0.01	2.45±0.04	2.43±0.41	2.55±0.01
5.23	2-Furanmethanol	98	$C_5H_6O_2$	1.11±0.02	1.02±0.02	1.35±0.02	1.02±0.01
5.44	2-Propanone, 1-(acetyloxy)-	116	$C_5H_8O_3$	1.33±0.07	1.23±0.02	1.64±0.04	1.34±0.01
5.83	Cyclohexanone, 3-hydroxy-	114	$C_6H_{10}O_2$	0.26±0.01	0.38±0.01	0.44±0.06	0.26±0.03
6.32	2-Cyclopenten-1-one, 2-methyl-	96	C_6H_8O	0.56±0.01	0.68±0.01	0.54±0.06	0.72±0.08
6.47	Ethanone, 1-(2-furanyl)-	110	$C_6H_6O_2$	0.15±0.01	0.14±0.00	0.14±0.03	0.21±0.00
6.63	Dihydropyran	84	C_5H_8O	0.91±0.04	1.11±0.00	0.92±0.07	1.00±0.04
6.86	1,2-Cyclopentanedione	98	$C_5H_6O_2$	2.14±0.11	2.66±0.01	1.86±0.09	2.43±0.06
7.85	2-Furancarboxaldehyde, 5-methyl-	110	$C_6H_6O_2$	0.94±0.07	0.67±0.01	0.91±0.04	0.71±0.04
8.26	Phenol	94	C_6H_6O	1.79±0.01	1.67±0.01	1.75±0.01	1.98±0.08
8.79	3,4-Dihydro-2-methoxy-2H-pyran	114	$C_6H_{10}O_2$	0.41±0.10	0.40±0.01	0.28±0.00	0.36±0.00
9.57	3-Methyl-1,2-cyclopentanedione	112	$C_6H_8O_2$	1.69±0.19	1.66±0.01	1.7±0.01	1.85±0.13
9.89	2,3-Dimethyl-2-cyclopenten-1-one	110	$C_7H_{10}O$	0.30±0.02	0.25±0.01	0.27±0.05	0.24±0.00
10.4	Phenol, 3-methyl-	108	C_7H_8O	0.75±0.01	0.62±0.02	0.76±0.02	0.69±0.04
10.9	Phenol, 3-methyl-	108	C_7H_8O	1.00±0.04	0.89±0.09	1.089±0.04	1.05±0.05
11.4	Phenol, 2-methoxy-	124	$C_7H_8O_2$	1.04±0.01	1.28±0.04	1.18±0.03	1.20±0.02
11.7	Cyclopropyl carbinol	72	C_4H_8O	0.14±0.00	0.825±0.02	0.22±0.11	0.61±0.04
12.2	2-Cyclopenten-1-one, 3-ethyl-2-hydroxy-	126	$C_7H_{10}O_2$	0.32±0.02	0.32±0.01	0.36±0.00	0.47±0.04
13.0	Phenol, 2,5-dimethyl-	122	$C_8H_{10}O$	0.31±0.03	0.29±0.00	0.33±0.03	0.31±0.00
13.5	Phenol, 4-ethyl-	122	$C_8H_{10}O$	1.27±0.1	1.65±0.35	1.47±0.25	1.35±0.07
14.3	Creosol	138	$C_8H_{10}O_2$	0.43±0.06	0.68±0.06	0.49±0.01	0.52±0.04
15.0	4-vinylphenol	120	C_8H_8O	9.74±0.1	10.73±0.06	8.08±0.62	11.50±0.04
16.3	1,2-Benzenediol, 3-methoxy-	140	$C_7H_8O_3$	0.85±0.02	0.74±0.04	1.45±0.27	2.95±0.98
16.7	Phenol, 4-ethyl-2-methoxy-	152	$C_9H_{12}O_2$	0.22±0.01	0.30±0.02	0.24±0.01	0.25±0.01
16.9	p-Isobutylbenzaldehyde	162	$C_{11}H_{14}O$	0.26±0.04	0.31±0.00	0.26±0.00	0.26±0.03
17.7	2-Methoxy-4-vinylphenol	150	$C_9H_{10}O_2$	1.82±0.00	2.70±0.16	1.90±0.05	2.57±0.04
18.7	Phenol, 2,6-dimethoxy-	154	$C_8H_{10}O_3$	1.82±0.05	2.23±0.05	1.68±0.08	2.12±0.11
20.0	Benzaldehyde, 3-hydroxy-4-methoxy-	152	$C_8H_8O_3$	0.13±0.01	0.20±0.02	0.16±0.05	0.05±0.00
20.1	Phenol, 4-methoxy-3-(methoxymethyl)-	168	$C_9H_{12}O_3$	0.20±.06	0.21±0.00	0.88±0.04	0.16±0.00
21.2	Phenol, 2-methoxy-4-(1-propenyl)-	164	$C_{10}H_{12}O_2$	0.84±0.08	1.36±0.00	0.86±0.05	0.99±0.08
22.0	Benzene, 3-ethyl-1,2,4,5-tetramethyl-	162	$C_{12}H_{18}$	0.21±0.1	0.25±0.03	0.25±0.03	0.08±0.00
23.0	2,5-Dimethoxybenzoic acid	182	$C_9H_{10}O_4$	0.19±0.02	0.21±0.01	0.16±0.00	0.08±0.00
24.0	Phenol, 4-ethenyl-2,6-dimethoxy-	180	$C_{10}H_{12}O_3$	0.60±0.07	0.53±0.03	0.61±0.10	0.20±0.11
24.8	Phenol, 2,6-dimethoxy-4-(2-propenyl)-	194	$C_{11}H_{14}O_3$	0.14±0.03	0.14±0.01	0.13±0.02	0.08±0.01
26.2	Benzaldehyde, 4-hydroxy-3,5-dimethoxy-	182	$C_9H_{10}O_4$	-	0.07±0.01	-	-
27.0	(E)-2,6-Dimethoxy-4-(prop-1-en-1-yl) phenol	194	$C_{11}H_{14}O_3$	-	0.27±0.16	-	-
27.8	Benzaldehyde, 2,3,4-trimethoxy-	196	$C_{10}H_{12}O_4$	-	0.185±0.08	-	-

Note: RT=retention time (min); MW= Molecular weight, the errors are standard error from duplicates